Warwick Manufacturing Group

University of Warwick

Fast Charging Strategies in Lithium-ion Batteries -

Detection and Control of Lithium Plating

Innovation Report

Submitted in Partial Fulfilment of the Requirements of the Academic Degree

Doctor of Engineering (EngD)

Author:	Upender Rao Koleti
Registration Number:	1691913
Academic supervisors:	Prof. James Marco
Industrial sup e:	Dr Truong Quang Dinh
Industrial supervisors:	
Industrial supervisors:	Dr Jabez Dhinagar
Industrial supervisors	TVS Motor Company Limited, India

Coventry (United Kingdom), September 30, 2020

Declaration of authorship

I hereby confirm that this innovation report is presented following academic rules and ethical conduct and that it has been written and compiled by myself and has not been submitted anywhere else. The composition of the report is my work except where explicitly stated.

Coventry (United Kingdom), September 30, 2020

_____

Upender Rao Koleti

Abstract

The fast charging of lithium-ion (Li-ion) batteries is required as one means of reinforcing consumer acceptance of future electric vehicle (EV) technology. However, the useful life of a Li-ion battery is known to be closely related to the magnitude of applied current, the state of charge (SOC) range over which the current is applied and the temperature of the battery during the charging period. Lithium plating on the negative electrode (NE) is known to be one of the major ageing mechanisms associated with fast charging. Therefore, an optimal charging profile that avoids or minimizes lithium plating is necessary for Li-ion batteries to achieve fast charging while simultaneously maintaining a longer cycle life. The use of model-based lithium plating control techniques that employ electrochemical models is complex to deploy and still face significant challenges in their implementation. The aim of this research therefore primarily focuses on experimental approaches to detect lithium plating and to derive fast-charge protocols that avoid or minimize the occurrence of lithium plating.

Within this Engineering Doctorate Portfolio, lithium plating detection techniques and their application to control lithium plating are investigated. The contribution of this research is to provide knowledge that may underpin future fast charging algorithms for integration with a Battery Management System (BMS). This has been achieved through five related studies.

The experimental approaches such as neutron diffraction and voltage relaxation profiles (VRP) detect lithium plating based on the influence of lithium plating on the electrode lithiation levels and the cell terminal voltage. In this research, experimental evidence that establishes the influence of the CV phase of charging on the lithium plating detection ability (study 1) is presented for the first time. Further, in this study, it is identified that the VRP method that infers the occurrence of lithium plating using a two-stage voltage relaxation can false detect in some charge events because of the NE phase changes. A procedure to differentiate the plating induced two-stage recovery is suggested.

In study 2, a closed-loop control scheme is developed to derive a multi-stage charge profile for offline and online use with the support of existing approaches of lithium plating detection where the terminating voltage of the first stage CC is adjusted based on the occurrence of lithium plating. The Online approach bases on the improved and validated VRP method suitable for low-temperature applications. The second one utilizes the Coulombic efficiency method that is intended for identifying an offline charge profile. Although the developed charge profiles have improved the battery life compared to a standard CC-CV charge profile, many limitations are identified. One of them is their inability to detect and control lithium plating within a charging event.

In study 3, a detailed quantification of plating induced battery degradation modes in terms of Loss of lithium inventory (LLI) and loss of active material (LAM) at the electrodes is undertaken. The results in this work highlight that lithium plating results in significant LAM at the NE in addition to the LLI. This helps to improve our understanding of lithium plating and its effect on battery degradation.

In Study 4, a new approach to detect lithium plating while the battery is still undergoing charge is proposed and validated at near operating conditions (temperatures between 10 to 30 ^{o}C and Charge rates from 0.25 to 1.25C). Impact of lithium plating as a side reaction on the high-frequency impedance of the battery is utilized to identify the onset of plating with the proposed impedance tracking procedure. The new method is then utilised to develop two different charge control strategies- online and offline (study 5). Experimental validation of these charging approaches while cycling the cells has shown significant cycle life improvement (> 80%) at the cost of up to 20% increased charging time. The results indicate that both of these approaches can be improved to extend battery life further. Future work in this direction is outlined.

The primary area of novelty within this research is to detect the onset of lithium plating in-situ and control the charge current accordingly to minimize lithium plating. EV manufacturers to derive an optimal charging strategy can utilize the findings from this research.

Contents

List of Figures

List of tables

List of abbreviations

Ah	Ampere Hour
BMS	Battery Management System
CC	Constant Current
CE	Coulombic Efficiency
CC-CV	Constant Current Constant Voltage
CTL	Charge Transfer Limitations
CV	Constant Voltage
DV	Differential Voltage
EIS	Electrochemical Impedance Spectroscopy
EoC	End of Charge
EoD	End of Discharge
EV	Electric Vehicle
GITT	*Galvanostatic Intermittent Titration Technique*
IR	Innovation Report
IT	Impedance Tracking
LAM	Loss of Active Material
LIB	Lithium Ion Battery
LLI	Loss of Lithium Inventory
NE	Negative Electrode
NEP	Negative Electrode Potential
NCA	Lithium Nickel Cobalt Aluminium Oxide
NMR	Nuclear Magnetic Resonance
OCV	Open Circuit Voltage
OEM	Original Equipment Manufacturer
PE	Positive Electrode
SDL	Solid Diffusion limitations
SEI	Solid Electrolyte Interphase
SOC	State of Charge
SOH	State of Health
VRP	Voltage Relaxation Profiles

1 Introduction

1.1 Motivation for the Research

The transport sector is one of the major contributors to rising environmental pollution levels in Indian cities as India experiences increasing urbanization [1, 2]. To reduce pollution levels, the Indian government like many other countries worldwide is imposing stringent emission norms [3]. Therefore, the Indian automotive sector is under pressure to lessen exhaust emissions without a significant drop in performance and cost escalation.

Electric vehicles (EVs) that use a battery and electric motor in their power train offer near-zero emissions and is a promising alternative technology to meet ever-rising emission norms. Therefore, automotive original equipment manufacturers (OEMs) including TVS motor company ltd. in India have chosen to support the government initiative by taking up EV development activities. Currently, EV market share in India is less than 1% of the total passenger vehicle sales [4]. The Cost of the EV technology, battery life (3-8 years) and long charging time (> 1 h) are major limiting factors for EV penetration given that customers expect the performance of EVs to match with the conventional internal combustion engine (ICE) vehicles [5, 6]. For example, Tata Nexon car in its EV form is circa 40% more expensive than its petrol version [7]. Falling battery prices ($400/kWh in 2015 to $150/kWh in 2020 [8]) when coupled with the lower running cost of the EVs, it is expected that the lifetime cost of the EVs will reach comparable levels to that of conventional internal combustion engine (ICE) vehicles by 2030. Besides, support from the Indian government for the EVs in terms of reduced taxes and investments in charging infrastructure may further help reduce the overall cost of the EVs [9].

Charging the battery takes longer time (1 to 8 h) compared to a mere few minutes of refuelling a conventional ICE vehicle and represents a significant barrier to consumer acceptance [10]. The Tata Nexon EV that provides a driving range of 190 miles takes approximately 2 to 8 h to fully charge its battery (capacity: 30.2 kWh). Long charging time coupled with the limited drive range leads to the fear of running out of charge (referred to as range anxiety), particularly when covering long distances which may limit the EV penetration significantly. According to the U.S. Advanced Battery Consortium (USABC), the long-term goal for fast charging is to return 40% of the state of charge (SOC) of the battery within 15 minutes [6]. Although there exist no set standards for charging speed, to make the EVs attractive, it is essential to improve the charging speed.

Although lithium-ion battery (LIB) that use graphite as the negative electrode (NE) is most preferred compared to batteries with other types of NE materials (see Table 1.1) [11, 12], they need to be charged with relatively lower charge rates to maximize their life as charging time and battery life are closely related [13, 14]. Taking in consideration the end of life (EoL) value defined by Tata is 8 years [15], Tata would need to replace the battery packs with new ones within its warranty period or reduce warranty period if they allow higher charge currents that keep the charging time under one 1 h. The price of a battery pack for the Tata EV is known to be in the order of £7000 each [16]. Therefore, extending the battery life while improving the charging speed is vital for automotive OEMs to ensure a commercially viable business strategy.

Table 1.1: Comparison of different NE materials

NE material	Energy density (mAh/g)	Volume expansion in charge (%)	Cost	Lifetime
Graphite [2, 17]	372	10	Low	Medium
$Li_4Ti_5O_{12}$ [18, 19]	175	0.1	High	High
Silicon [11]	3580	400	Low	Low

The limiting factor for improving the charging speed comes in the form of lithium metal depositions or lithium plating, an unwanted side reaction at the NE. During charge, lithium ions move from the positive electrode (PE) to the NE. While lithium ions intercalate into the NE, the NE potential (NEP) of the battery drops and comes closer to the Li/Li^+ reference potential [20, 21]. When coupled with the potential drops due to internal kinetics such as charge transfer limitations (CTL) at the electrode surface and solid diffusion limitations (SDL) in the electrodes, the NEP may decrease below the Li/Li+ reference potential [20, 22]. Potential drops at the NE can increase because of the high charge currents and reduced kinetics due to low ambient temperatures [23]. Once the NEP drops below the Li+ reference, lithium plating on the NE begins in addition to the usual intercalation [24, 25]. Figure 1.1 shows the NEP in charge with the conventional constant current followed by the constant voltage (CC-CV) profile. In the initial phase of the charging, as shown in the figure, the total charge is utilized in lithiating the NE as long as the NEP is maintained above the reference. Once the NEP is dropped below the Li+ reference, the charge is split into the lithiation of the NE and lithium plating over the NE. In addition to the operating conditions, loss of active material (LAM) at the NE particularly in a delithiated state due to usual degradation induced by cycling (charge/discharge events) can oversaturate the NE that lead to lithium metal depositions as the NE cannot absorb more incoming lithium from the positive electrode (PE) [26]. The active material of an electrode that is lost is no longer available for the lithiation due to loss of electrical contact with its current collector and particle cracking or blocking of active sites by layers formed out of side reactions. Mechanical stresses induced

by usual lithiation/delithiation of the electrodes, corrosion of the current collectors and decomposition of the binder that keeps the active material in contact with the current collector are known to result in LAM [27].

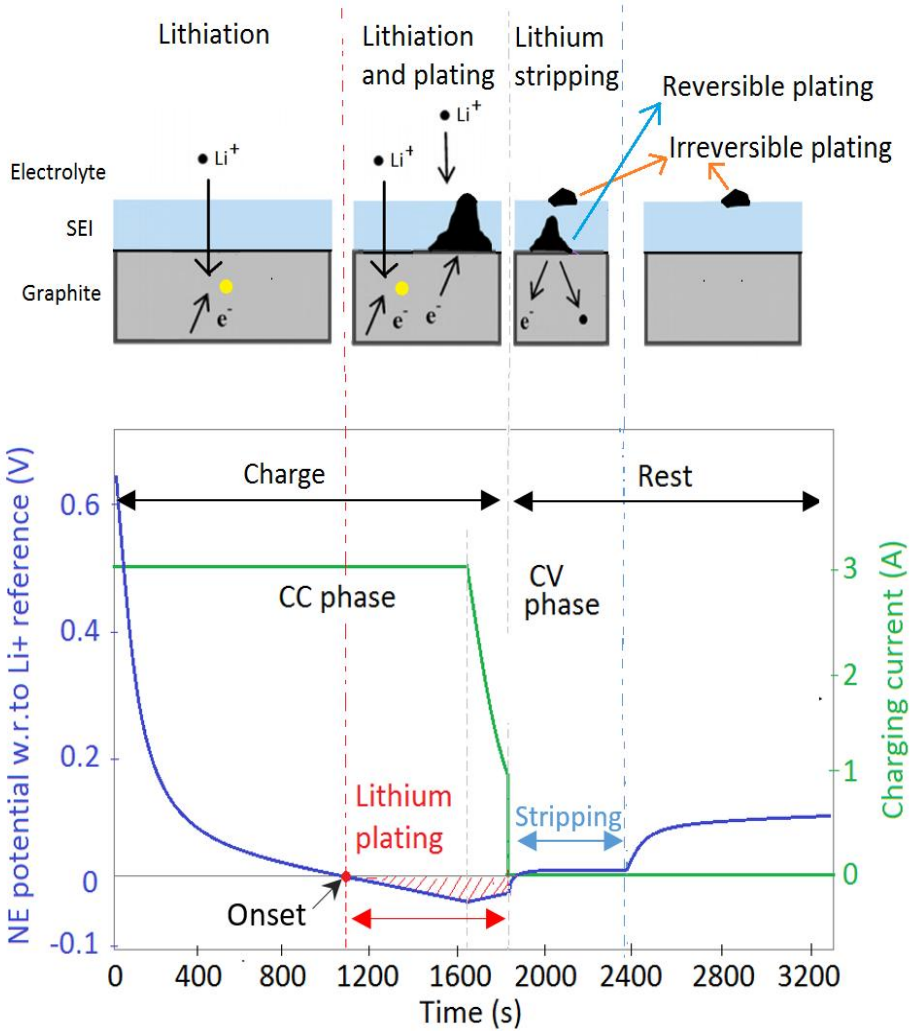

Figure 1.1: An illustration of lithium plating and stripping over the NE and its link to the NEP and charge current

Lithium metal deposited over the negative electrode surface during charge is not completely lost. The metal, which is in contact with the electrode starts oxidising once the electrode potential becomes positive and returns to the electrode [13, 28]. The reversible reactions are typically referred to as lithium stripping. As shown in Figure 1.1, in rest condition after the charge is terminated, lithium stripping begins as soon as the NEP becomes positive. In the process of stripping, some of the plated metal is irreversibly lost due to the loss of electrical contact with the electrode as shown in Figure 1.1. Thus, plated lithium is categorized into reversible plating and irreversible plating. The irreversible part of the lithium metal depositions, therefore, results in loss of lithium inventory (LLI) [2]. With LLI, cyclable lithium between the electrodes reduces. Side reactions that lead to the formation of solid electrolyte interface (SEI) layer over the NE and decomposition reactions at the electrode-electrolyte

surface are some other ageing mechanisms that lead to the LLI. Besides the LLI from the irreversible plating, the lithium depositions that may grow through the SEI layer resulting in its damage, and thus further growth of the layer that consumes additional lithium in the process [29, 30]. As a result, reduced cyclable lithium due to lithium plating results in battery capacity loss.

To avoid or reduce lithium plating, detecting the onset of lithium plating or monitoring the NEP during charge is essential [5, 17]. Charging at a high current until the onset of plating and then controlling the charge current such that the NEP is maintained above the Li+ reference can increase the charging speed while minimizing the onset of lithium plating. Based on the examples reported in [6, 23], it can be concluded that understanding and mitigating battery degradation under fast charging is essential to minimise its adverse effects on battery life and performance. Further, lithium plating favourable conditions change in a battery over its lifetime [31, 32]. Therefore, any charging strategy developed needs to adapt to battery operating conditions. In line with this, the scope of this research is to detect and control the occurrence of lithium plating to provide an optimal charging strategy that minimizes the charging time while extending the battery life for future EV applications.

1.2 The Sponsoring Company and their Relevance to the direction of the Research

The direction of the research was considered from the perspective of TVS Motor Company Ltd, the sponsoring company. TVS is a two and three-wheeler automotive company in India with sales in over 60 countries and is the fifth largest 2-wheeler manufacturer in the world in terms of sales volume [33]. TVS focuses on the design, development, manufacture and sale of bikes and three-wheelers.

Like many of their competitors (Hero, Honda and Bajaj), TVS has been adopting a vehicle electrification strategy to meet automotive regulations (e.g., Indian emission regulation Bharat Stage six or BSVI [3]). As evidence, TVS has launched an electric scooter (TVS iQube) in January 2020 with a driving range of 70 km [34]. When compared to the petrol-powered TVS scooter derivative (Model: Jupiter), as shown in Table 1.2, TVS iQube costs a further 50%, offers less driving range and needs a longer refill time. The driving range that can be increased by raising the battery capacity is limited to avoid the further rise of iQube cost. The other option to minimize the range anxiety is to increase the charging speed so that the scooter is charged as quickly as possible. Since high charge rates are known to accelerate battery degradation, a charge rate of C/4 is employed for the iQube that takes approximately 4 h to

fully charge the battery. Submission 1 provides more details about TVS and its plans and needs for EV development.

Table 1.2: Comparison of TVS's EV product with its ICE based product

Vehicle type	Model name	Drive range (km)	Refill time (minutes)	On-road price in ₹	Life expectancy
Petrol scooter	Jupiter	300	< 2	82700	15 years
Electric scooter	iQube	70	> 240	122000	3-8 years for battery

To minimize range anxiety with minimal impact on the pricing and battery warranty period, TVS understands the need for developing charging strategies. In this aspect, when this doctorate was commissioned in 2016, TVS aimed to improve their knowledge and expertise in the following topics:

- Impact of fast charging on battery performance and lifetime.
- Non-invasive detection of side reactions/lithium plating associated with fast charging.
- Development of fast charging algorithms for the BMS.
- Assessment of fast charging strategies in terms of charging speed and battery life.

Based on the findings, this project proposes a systematic procedure to develop fast-charging strategies while meeting the objectives set by TVS as follows.

- Literature review to understand the state of the art of the selected topic (Chapter 2)
- Improve the existing non-invasive lithium plating detection methods (chapter 3)
- Develop optimal fast-charging strategies implementable in BMS using the existing non-invasive techniques (Chapter 4)
- Study the fast charging impact on battery degradation (Chapter 5)
- Explore a new method of lithium plating detection to identify the onset of plating within a charging event non-invasively (Chapter 6)
- Develop improved charging strategies with the new detection method (Chapter 7)

The impact of this research on TVS activities is given in Chapter 8. The results are also applicable to other applications and organisations that use Li-ion battery. As evidence, part of the work performed here has been recognised through journal publications [35-38].

1.3 Research areas and Aims

The research objective of this Innovation Report (IR) is to minimize the degradation associated the fast charging within the context of a real-time embedded control application such as BMS to improve the performance of future EV. Following on from the literature review conducted in Chapter 2 and the challenges faced by the sponsoring company (refer to Section 1.2), fast charging is studied within three research areas as summarized in Figure 1.2 and detailed in the following sections.

1. **Understanding the influence of lithium plating on battery degradation**: It is well known that lithium

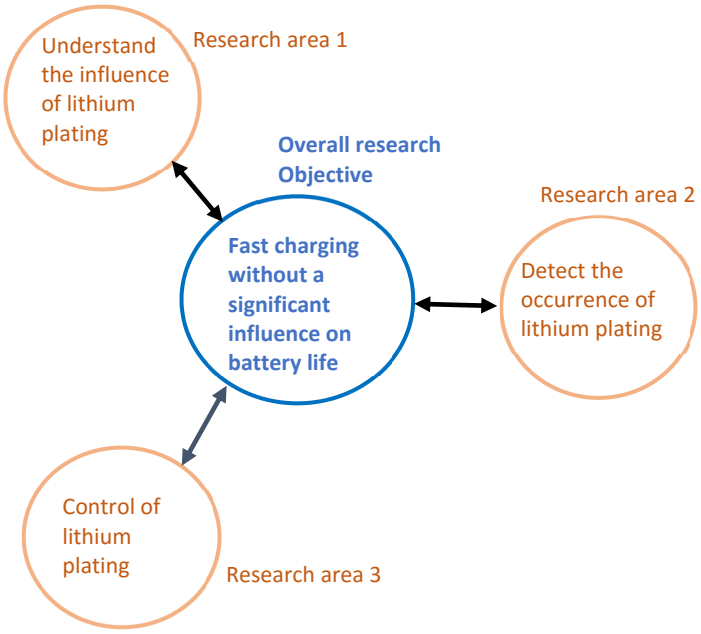

Figure 1.2: Research objective and relevant research areas in fast charging strategies

plating results in capacity fade. However, it is not clear yet the underlying degradation modes (LLI or LAM or a combination of them) of lithium plating as both LAM and LLI lead to capacity fade. Therefore, understanding the influence of lithium plating is key to develop lifetime charging strategies. Section 2.2 explains in detail lithium plating influence on battery performance and life.

2. **Detection of lithium plating in fast charging**: to control lithium plating, its detection is essential. Besides, as battery degradation modifies its internal kinetics, and thus lithium plating tendency over different cycles, it is important to keep track of lithium plating during the battery's lifetime. Therefore, lithium plating detection in real-time applications is essential to improve charging strategies. Section 2.3 details the existing approach of lithium plating detection and its method, limitations and scope for improvement.

3. **Control of lithium plating in fast charging**: to achieve maximum possible charging speed while minimizing the battery degradation, the NEP needs to be maintained at the Li+ reference potential as

detailed in Section 2.4. This is achieved by controlling the charge current and by tracking the NEP or detecting the onset of lithium plating. A charging strategy that aims to control lithium plating needs to adapt to battery operating condition such as operating temperature and ageing level as they modify the lithium plating tendency. Therefore, fast charging strategies implementable in real-time applications are key to extend battery life for future battery designs. Section 2.4 explains in detail the existing fast charging strategies and their limitations and defines further work.

1.4 Scope of the IR

The scope of this thesis is to study the degradation associated with fast charging and provide solutions that detect and control lithium plating within the context of real-time implementation in EVs. Since lithium plating is a severe ageing mechanism experienced by the graphite electrodes during fast charging, the findings in this study are limited to Li-ion batteries that employ graphite as the NE.

Although research into Li-ion battery involves many disciplines such as physics, chemistry or engineering whose knowledge is essential, the research undertaken in this doctorate focuses on the engineering domain of fast charging strategies. Therefore, identifying and quantifying ageing mechanisms associated with the fast charging at material, physical and chemical level is not undertaken in this study. The research presented in this work covers the implementation, validation of the concepts proposed. However, it does not cover an exhaustive analysis of the optimization of the developed algorithms and implementation in an EV BMS. Additional information regarding areas of further work within the scope of this research is given for each respective study (refer to Limitations and Further Work sections) and in Section 7.5.

1.5 Structure of the Portfolio

This IR is structured to follow the studies and investigations conducted as part of the EngD that are reported through a series of research submissions.

As described in Section 1.2, the research within this EngD is focused on three key subject areas to understand and limit the degradation associated with fast charging. As shown in Figure 1.2, These areas are 1. Understanding the influence of lithium plating on battery degradation; 2. Detection of lithium plating occurrence; and 3. Control of lithium plating. A critical review of the literature covering three research areas (Chapter 2) is presented largely in the Submissions 1 and introduction sections of the remaining submissions. The study covering Research area 2 is undertaken at two different levels. First, validation and improvement of an existing non-invasive detection method (Chapter 3) are performed as presented in Submission 2 and 5, respectively. While investigating new

approaches to lithium plating detection, the early part of this study is focused on existing detection approaches. Second, a new method of plating detection is proposed and validated (Chapter 6) as reported in Submission 6. Similarly, research area 2 is executed at two different stages. First, the improved non-invasive detection method is employed to develop a charging strategy (Chapter 4) as presented in Submission 3. Next, two different charging strategies to reduce lithium plating using the new detection method are derived and evaluated (Chapter 7) as detailed in Submission 7. Besides, the experimental data gathered in Submission 3 is further used in Submission 4 to study the degradation modes of lithium plating (Chapter 5). Although each research area covers a different topic, they are still related to each other under the theme of lithium plating. Table 1.3 presents the IR structure that summarizes the studies undertaken and their corresponding research submissions and papers in each research area.

Table 1.3: Submissions and publications related to the IR structure

Research Area	**Study**	**Chapter in this IR**		**Studied in Submission**		**Published in**
		Literature review	Study	Literature review	Study	
Influence of lithium plating on battery degradation	Quantify the degradation of Li-ion battery aged under fast charge cycle regime	2	5	1, 4	4	[36]
Detection of lithium plating	Study the influence of constant voltage (CV) phase and graphite phase changes on the detection sensitivity of the VRP method	2	3	1, 2, 5	2, 5	[37]
	Investigate and develop a new method of plating detection suitable for BMS use	2	6	1, 6	6	[35]
Control of lithium plating	Develop optimal charging strategies utilizing the existing detection methods	2	4	1, 3	3	[38]
	Utilize the new online method of lithium plating detection for plating control	2	7	1, 7	7	Submitted [39]

In addition to the IR that is derived from the submissions, a personal portfolio that presents all assignments from the six MSc modules undertaken, published journals and conference papers from this research project is included. The personal portfolio presents a summary of the primary competencies gained or enhanced through the activities and research undertaken with the EngD. The IR structure along with the personal portfolio is summarized in Figure 1.3.

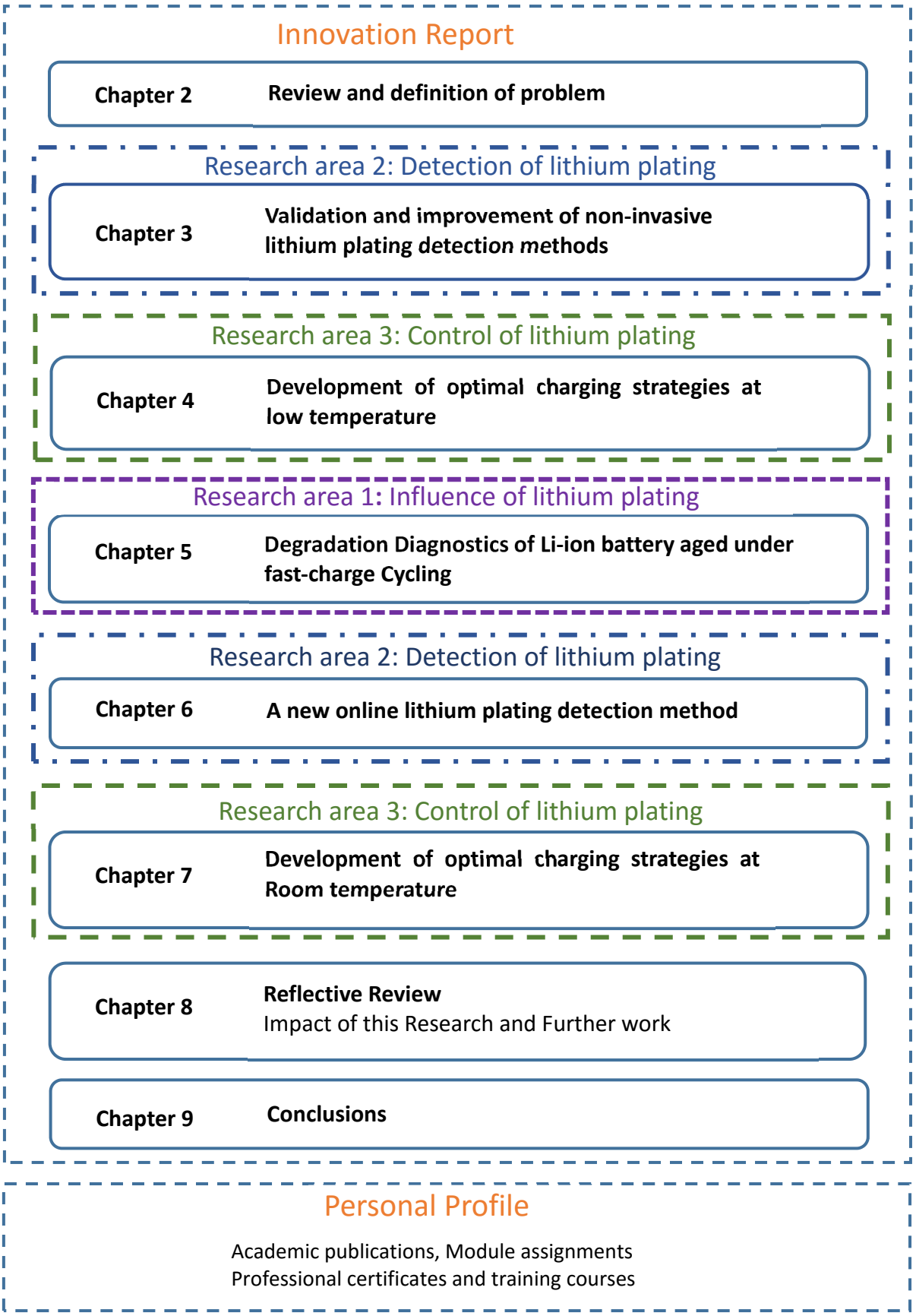

Figure 1.3: Portfolio Structure

1.6 Structure of the Innovation Report

This IR presents the research undertaken and demonstrates the connection between projects that have all contributed to the objectives of the EngD. As the chronological order of the Submissions is different from the structure of this IR, it is recommended that the portfolio supporting this research is reviewed in the sequence defined in Figure 1.3.

Chapter 2 critically reviews the current state of the art covering previous studies that have investigated three research areas: 1. Detection of lithium plating occurrence; 2. Control of lithium plating; and 3. Understanding the influence of lithium plating on battery degradation. After studying the main findings and identifying knowledge gaps in each research area, research objectives are determined. To meet these objectives, multiple research studies are undertaken within this EngD.

Chapter 3 investigates a procedure to improve the lithium plating detection sensitivity of non-invasive methods. The impact of the CV phase charging on the plating detection is established. An approach to identify the charge cut-off current in the CV phase that allows improved detection ability is presented. It is shown that lithium-plating occurrence can be incorrectly assumed while using post-charge voltage relaxation profiles as graphite phase changes and lithium-stripping reactions produce a similar influence on the voltage profiles. A procedure to identify the lithium plating induced phase changes is developed.

Chapter 4 utilizes the improved detection method presented in Chapter 3 for identifying the onset of plating and developing a novel three-stage charge profile. Its effectiveness on the charging speed and battery lifetime during cycle ageing are evaluated along with a conventional constant current followed by a constant voltage (CC-CV) profile and a charge profile derived based on the Coulombic efficiency. Performance of these profiles along with their limitations is detailed in this chapter. It is understood that the inability to detect the onset of plating within a charging event is limiting their effectiveness.

Chapter 5 quantifies the degradation modes of cell aged in fast-charge cycling to study the influence of lithium plating on battery degradation. For this, a new procedure to quantify the degradation modes is proposed using the open-circuit voltage (OCV) profiles of electrodes and cell. The procedure when applied to the cells aged in fast charge cycling indicates significant levels of LAM at the NE in addition to LLI.

Chapter 6 presents a proposed new method to identify the onset of plating within a charging event. The influence of lithium plating as a side reaction on the value of cell impedance allows detecting the onset of plating. The impedance profile is tracked by inducing a current disturbance and monitoring

its impact on the voltage once in every 1% capacity increase during charge. Once plating onsets, the impedance profile starts to deviate from its usual plating free profile. Validation at different temperatures and C-rates confirms its superiority over the existing methods.

Chapter 7 utilizes the developed detection method to derive charge profiles at 20 ^{o}C in Offline and Online modes. A multi-state constant current (CC) profile beginning with 1.5C drops to 0.5C in steps of 0.25C where the detection of plating onset defines the transition to the next CC stage. A pre characterization procedure is followed to identify the cell voltages corresponding to these transitions in the offline mode while the online one tracks the impedance during charge and identifies the transition. Evaluation of the derived charge profiles during cycle ageing indicate significant improvement in cycling life and scope for further improvement of the charging strategies.

Because of the research carried out within this EngD, several innovations are realised. For each innovation achieved, the academic contribution and benefits to the sponsoring company are described in Chapter 8. The first author publication of four Journal (three Q1) papers [35-38] reflects the contribution to academia. Besides, one Q1 journal publication was submitted to the editor by the time this thesis was submitted. The benefit to the sponsoring company is evidenced by the significant contribution to the research objectives regarding fast charge strategies (refer to Section 1.3). Chapter 8 also discusses the limitations and areas of further work concerning the development of optimal charging strategies and implementation of the findings presented. Finally, Chapter 9 presents a summary and the overall conclusions of this research work undertaken in this EngD.

2 Literature Review

2.1 Introduction

Chapter 1 places this IR in context, presenting the key research challenges regarding the fast charging of Li-ion batteries for EV applications. This Chapter aims to translate the research challenges faced by academia and industry in the selected areas into research questions. For each research question within the context of fast charging, an extensive literature review is conducted. Further details of this literature review can be found in individual submissions to the EngD portfolio [40-46] and journal publications [35-38]. From the knowledge gaps identified for each research question, research objectives are defined. These objectives determine the research work undertaken within this EngD.

2.2 Research area 1: Battery degradation during fast charging

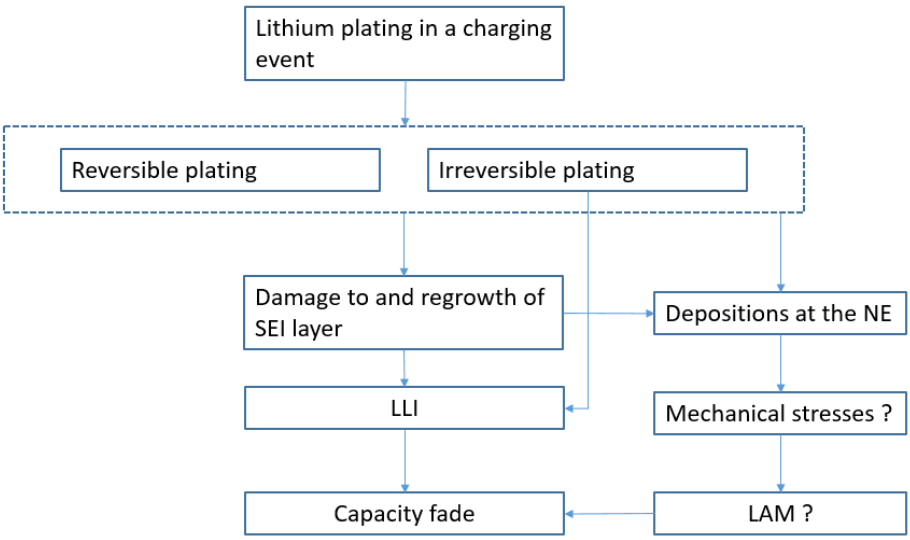

Figure 2.1: Influence of lithium plating on battery degradation

It is well understood how operating conditions of the battery such as charge current, ambient temperature and ageing condition influence the negative electrode potential (NEP) and thus lithium plating [17, 25]. On the other hand, although it is known that lithium plating leads to capacity fade, the exact underlying degradation happening to the battery under the influence of lithium plating is not clear. The capacity fade observed at the cell level can result from impedance rise, loss of lithium inventory (LLI) and loss of active material (LAM) at the electrodes or a combination of them [27, 47]. However, the influence of the impedance change on the capacity estimation can be reduced by performing the capacity tests at low C-rates or including the CV toward the end of discharge. Since

capacity tests are performed with CV throughout the experimental work in this research, capacity fade analysis is limited to LAM and LLI as shown in Figure 2.1.

The irreversible plating that reacts with the electrolyte or become electrically isolated from the electrode, leading to a reduction of cyclable lithium between the electrodes and thus LLI. Besides, lithium depositions on the NE can grow through the SEI layer, and thus damage to the SEI layer, which leads to regrowth of the SEI layer [2]. Since the SEI layer growth consumes a portion of cyclable lithium [48, 49], this further increases the LLI.

In addition to the LLI, lithium plating may also induce LAM. As discussed within [24], lithium plating increases the volume expansion of the cell. The study proved theoretically and experimentally that plated lithium occupies nearly four times more volume than the volume expansion experienced by the graphite for the same amount of lithium intercalation. Besides, the SEI growth due to its damage inflicted by lithium plating can increase its depositions and thus volume expansion locally [50]. This volume expansion may add to the usual volume changes experienced during cycling, and thus raising mechanical stresses. As discussed within [51], these mechanical stresses may contribute to active material cracks at the electrode, leading to a LAM at the electrodes – another contributor to capacity fade.

Increased mechanical stresses or LAM due to lithium plating if confirmed may indicate that higher volume-occupying depositions from previous lithium plating can continue to cause mechanical stresses locally and produce long-lasting negative impacts on battery life. Given all this, it is important to study and quantify the degradation modes (LLI and LAM) in batteries affected by lithium plating. Additionally, this information will help underpin the design of charge strategies for the older batteries that might have experienced lithium plating in their first use. From this, a research question is formulated:

Research question 1: Can the degradation modes that underpin lithium plating be quantified so that the impact of lithium plating on the battery is understood better and controlled?

It is believed that detailed quantification of plating induced battery degradation modes in terms of LLI, LAM at the positive electrode (LAM_{PE}) and LAM at the negative electrode (LAM_{NE}) would improve our understanding of lithium plating and its effect on battery degradation. To study battery degradation, many researchers use differential voltage (DV) curves (dV/dQ) and incremental capacity (IC) curves (dQ/dV), where dQ stands for the incremental capacity while dV defines for the differential voltage calculated from the battery OCV. By comparing the IC or DV curves of a cell at two different ageing states, the degradation modes of the battery can be inferred [52, 53].

The majority of the studies that use IC or DV curves are focused on studying the degradation modes in cells that are in either calendar or cycle ageing where the operating conditions such as temperature and charge currents are kept within the manufacturer recommended levels [50, 54]. The degradation modes identified under these ageing conditions cannot be attributed largely to lithium plating as the charge currents are not raised or temperatures are not dropped beyond the recommended limits that could not make lithium plating as a significant ageing mechanism. However, two different studies applied IC and DV analysis to the cycle aged cells where the lithium-plating occurrence is reported. As discussed within [26], IC and DV curves were employed to understand the reason for lithium plating occurrence in the later part of cycle ageing. Through the analysis, the paper reports large levels of LAM at the NE in delithiated state (LAM_{deNE}) is leading to saturation of NE lithiation and thus lithium plating. The second one, as reported by [31], used IC and DV curves to identify the underlying causes that gradually reduced lithium plating with the increasing cycle number while cycling at -22 ^{o}C. According to the authors, increasing LLI levels through cycles could reduce lithium plating. They hypothesised that the lithiation level of the NE toward the end of charging reduces or high state of charge (SOC) region of the NE where its potential gets closer to the Li+ reference is not accessible anymore with increasing LLI. However, the study is not extended further to look into the other degradation mode, LAM. Therefore, to quantify the degradation modes of lithium plating, a separate study is required.

From the interpretations of the IC or DV curves using the cell level OCV vs Capacity profiles, it is difficult to quantify the changes that are occurring to each electrode since both the electrodes contribute to the features in the cell OCV profile [55]. To overcome this issue, a degradation diagnostic technique using the electrode OCV profile was suggested by Birkl et al. [27]. Degradation within the battery modifies the lithiation levels and their offsets at the end of charge (EoC) and End of discharge (EoD). The degradation modes are then calculated using these levels. However, the quantification method used within [55] can be simplified to reduce the complexity using the electrode lithiation levels rather than their offsets at the EoC and EoD. Based on these knowledge gaps, the following research objective is defined for the research question 1:

Research Objective: Develop a simplified degradation mode quantification procedure and identify the degradation modes of Li-ion battery aged under fast charge cycling.

The research work undertaken to meet this objective is reported in Chapter 5 in this IR and presented in detail in Submission 4.

2.3 Research area 2: Detection of lithium plating occurrence

To understand the operating conditions that lead to and control lithium plating, it is essential to detect the occurrence of plating. The literature review concerning lithium-plating detection is done in three stages. First, the desired characteristics of a lithium plating detection method are presented. Next, the methods suggested in the literature are reviewed. Finally, the research objectives for further improvements in plating detection are defined.

Lithium plating, as mentioned in [24] and as illustrated in Figure 1.1, starts at some point during charging when the NEP gets below the Li+ reference potential. The degradation caused by lithium plating in the previous charging event modifies the cell kinetics such as diffusion in the electrodes, which change the plating onset point, and lithium plating amounts in the next charging event. Depending on the operating conditions and cell construction, the plating tendency can increase or decrease [26, 31]. For example, dominant levels of LAM at the NE can increase the plating tendency as this leads to the saturation of NE lithiation [26] while higher levels of LLI due to SEI growth can lead to the opposite behaviour as it reduces the NE lithiation level [31]. Therefore, a selected charge profile that avoids lithium plating in a new cell does not guarantee the absence of plating through the cycles. As a result, to track this changing behaviour with cycling, it is essential to detect the occurrence in real-time. The following characteristics are therefore desirable for a lithium plating detection method:

- Shall identify the cell voltage or SOC level at which lithium plating commences.
- Shall be able to track the lithium plating occurrence cycle by cycle
- Shall be suitable for implementation in BMS with minimal impact on its hardware, volume and cost

These learnings rise the following research question:

Research question 2: Is it possible to detect the occurrence and onset of lithium plating in real-time applications in a non-invasive manner?

The occurrence of lithium plating affects the battery in different ways. The irreversible part of lithium plating leads to metal depositions while the reversible part influences the electrode lithiation levels, cell voltage or impedance. Besides, battery capacity drop and volume expansion are observed under the influence of lithium plating. Therefore, monitoring these changes allow the detection of lithium plating. Multiple detection methods are suggested in the literature that can be broadly categorized as two different types based on the approach they employ to infer/detect the occurrence of lithium plating:

- Invasive techniques
- Non-invasive techniques

The Non-invasive approaches can be further divided into three sub-categories:

- NEP based
- Reversible lithium plating based
- Impact of lithium plating based

Each of these categories is presented within the context of real-time use in the following sections.

2.3.1 Invasive methods

The invasive techniques such as Nuclear Magnetic Resonance (NMR) [56], Inductively Coupled Plasma Optical Emission Spectrometry (ICP-OES) [57] and visual inspection of electrodes [20, 58] are used to either quantify or confirm the metal depositions present in a cell that has experienced lithium plating previously. Lithium plating is known to occur non-uniformly over the NE surface because of the non-homogeneities in cell construction such as different electrode particle sizes, their distribution and varying compression levels during calendaring [59, 60]. Visual inspection of the electrodes confirms this localized plating tendency [20, 58]. Although the invasive methods provide definitive confirmation of lithium plating occurrence and help in validating the non-invasive methods of plating detection, they pose many limitations for detection and control of lithium plating or for developing fast charging strategies. First, these methods only rely on the occurrence of irreversible plating. Second, it cannot relate the identified lithium metal depositions to individual cycles. Third, these methods fail to identify the SOC level or cell voltage corresponding to the lithium-plating onset within a charging event. Finally, the need for cell dismantling makes them unsuitable for BMS application. Therefore, the application of these approaches is largely limited to confirm the occurrence or to validate the non-invasive methods that detect lithium plating indirectly [2, 24].

2.3.2 Non-invasive methods – NEP

The onset of lithium plating is inferred when the measured or estimated NEP gets below the Li+ reference [10, 17]. NEP is estimated by electrochemical battery modelling where the NEP is described by a set of partial differential equations (PDEs) based on the physical and electrochemical properties of the battery constituents such as the electrodes and electrolyte. Common model formulations include the pseudo two dimensional (P2D) model [61], the single-particle model (SPM) [62] and the single-particle model with electrolyte (SPMe) [63]. Lithium concentration gradients in the electrode and the electrolyte, charge transfer limitations (CTL) at the electrode-

electrolyte interface, etc. that govern the behaviour of the NEP are considered. However, the main concern of this kind of method is the model parameterisation and implementation in real-time applications due to its complex structure and equations. Besides, the physical and electrochemical properties change as battery ages and thus the magnitude of the potential drop at the NE [31], because of several degradation mechanisms such as electrolyte decomposition [64], active material cracking [65], loss of lithium and porosity reduction due to previously deposited lithium metal layers [66], etc. These effects along with the non-homogeneities in cell construction further compound the significant research challenge of extending these models to take account of the different degradation modes and to accurately represent battery [26, 67].

Conversely, the NEP measurement directly in a commercial cell is not possible, as they do not come with a reference electrode (RE). The RE that has a stable and known potential allows measuring both NE and PE potentials directly. As an alternative, to study the NEP during charge in a laboratory setup, a reconstructed three-electrode cell using the electrodes harvested from a commercial cell and lithium as a RE is used in [5]. Nevertheless, this modification could add large uncertainties to the electrode potential behaviour (depending on the modifying process), leading to difficulties in monitoring the NEP accurately. First, the separation of electrodes from the commercial cell could increase the electrode impedance. Particularly, the process of clearing electrode material from one side of the current collector can modify the electrode properties such as its porosity and conductivity. Second, the use of a different electrolyte could change the internal kinetics, and thus, the potential drops within the cell. As shown in [5], the voltage dynamics of the reconstructed cell were significantly different from those of the commercial cell during the high-current (1C) charge. Therefore, the results obtained from the reconstructed cell cannot be directly applied to the commercial variant from which it is derived. Besides, this method cannot be used in real-time applications to monitor the NEP as battery ages because existing commercial cells do not have the third (lithium reference) electrode.

The NEP based plating detection methods pose a further challenge as there is no clarity within the literature whether all or only a portion of potential drops at the NE causes plating. Generally, the NEP (measured between the separator and current collector) includes potential drops due to multiple phenomena such as concentration gradients in the electrolyte, SEI layer, CTL, SDL in the bulk electrode, and the Ohmic resistance in the current collector in addition to the OCV of the electrode. In electrochemical models [17, 61], potential drops due to CTL, SEI and SDL from the OCV of the NE were considered for plating reactions. On the other hand, experimental based plating control studies [5, 68] considered the entire drop between the current collector and the separator. Although the non-

invasive methods can be validated using the invasive approaches [10, 17], it is difficult to verify the onset of lithium plating and thus the NEP influence on plating as none of the existing approaches of detection could identify the onset of plating during charge.

2.3.3 Non-invasive methods – Impact of lithium plating

Plating detection at cell level using the non-invasive methods captures the average behaviour or influence of the non-uniform lithium metal depositions over the NE [26]. Influence of lithium plating on the cell capacity and volume is utilized to detect plating non-invasively. Reduced Coulombic efficiency while cycling at high C-rates or low temperatures may indicate the occurrences of lithium plating indirectly [69, 70]. Here, Coulombic efficiency is the ratio of charge output compared to the charge input. However, the need for high precision measurement of Coulombic efficiency (<0.01%) limits its implementation in a typical BMS [71]. Besides, as changes to the Coulombic efficiency can occur due to any ageing mechanism or combination of different ageing mechanisms, it is difficult to attribute the reduction to lithium plating alone [70]. Tracking volume changes allow detecting the presence of lithium plating [24] as plated lithium occupies circa four times more volume than the volume expansion experienced by the graphite when lithiated with the same amount of lithium. Detection of lithium plating by tracking the changes in cell dimensions (< 1 µm) is difficult in practical application.

2.3.4 Non-invasive methods - reversible plating

Reversible plating based methods assume significance in lithium plating studies given their ability to track lithium plating cycle by cycle [26, 72]. A set of non-invasive methods such as tomography and electrochemical impedance spectroscopy (EIS) rely on observable features introduced by reversible lithium plating that occurs in the cell immediately after charging. The rise in the electrode lithiation level indicates the amount of lithium returned and can be measured by neutron diffraction-based Tomography techniques [73]. While lithium stripping influences the evolution of impedance spectra during the post-charge relaxation is identified by the EIS method [74]. However, these methods cannot be applied within a practical battery because of the measuring mechanism required.

Alternatively, the influence of reversible plating on the cell voltage can also be used to detect lithium plating. This is done by monitoring the cell voltage in two different battery conditions: under a low c-rate discharge and in the rest state. In the first approach referred to as differential voltage curves (DVC) method, a high voltage plateau due to reversible plating during a low c-rate (< C/10) discharge is observed for plating detection [26, 74]. Reversible part of the plated lithium while contributing to the load current produces a higher voltage plateau compared to the usual delithiation of the graphite

electrode. The second approach based on a cell voltage relaxation profile (VRP) observed in a post-charge rest period [28, 74]. Once the charge is terminated, the NEP starts to transition to a positive OCV level. Once the NEP becomes positive, lithium stripping begins. As long as stripping lasts, the NEP will remain constant close to the Li+ reference level (see **Error! Reference source not found.**). The voltage relaxation experienced by the NE and observed at the battery terminals continues after the completion of lithium stripping. This reaction manifests as a change to the single-stage relaxation profile within the cell terminal voltage, in which a two-stage voltage relaxation can be observed. This unique feature of the cell terminal voltage during the relaxation period is used to infer the presence of lithium stripping reactions. The VRP method is presented in detail in Chapter 3 with the support of experimental data collected at the electrode and cell level. However, lithium plating can be incorrectly assumed if the 2-stage voltage relaxation originates from a different phenomenon. As discussed within [2, 20], the NE could exhibit multiple phase changes in its OCV profiles. While charging, the NE experiences lithium concentration gradients within its particles and these differences come down during the post-charge rest (the lithium concentration at the NE particle surface gradually drops to the average particle concentration). This phenomenon could lead to a phase change at the NE and thus 2-stage recovery, causing difficulties in lithium plating detection using the 2-stage voltage relaxation profile. In addition, for both DVC and VRP methods, a reduced amount of lithium plating and increased lithium stripping rate at high temperatures [2, 24] limit the ability to detect reversible plating when compared to low temperatures (<10 ^{o}C).

Further to the limitations of each method, the CV phase of charging may influence the detection sensitivity of the non-invasive techniques that are based on reversible plating. The NEP reaches a minimum at the end of the CC phase and starts increasing during the CV phase [22, 75]. A low current cut-off value, in the order of 0.1C, leads to a prolonged CV phase, and the negative potential has a higher chance of becoming positive before the CV phase ends. As a consequence, a portion of the plated lithium reverses in the CV phase itself, which will reduce the amount of reversible plating for detection during the relaxation stage after the CV phase. Petzl et al. have mentioned such an issue in their plating studies [76]. It was shown that the total estimated plating values went up until a certain SOC level and then came down with a further rise of SOC. According to the authors, lithium stripping in the CV phase is the cause. Therefore, for plating detection improvement, it is important to study the CV phase influence on lithium plating detection.

2.3.5. Summary and research objective

Real-time lithium plating detection is needed to maximise the charging performance throughout the battery life as plating behaviour changes with ageing and operating conditions. Table 2.1 presents the

summary of the lithium plating detection methods and Submission 1 provides a detailed review of these methods. The invasive approaches are not suitable for BMS use as they need cell dismantling. When it comes to non-invasive methods, the VRP and DVC methods may be implemented within a BMS given their dependency on current and voltage measurements alone. Since there exist many limitations in detecting lithium plating for both these methods (see Table 2.1) and none of the existing methods could detect the onset of lithium plating within a charging event, the research work relevant to detection is proposed in two stages. First, to improve an existing approach that is implementable in real-time use. Between the VRP and DVC approaches, a requirement of simple rest period (up to 1 h) provides an advantage to the VRP method when compared to the DVC method that needs a low C-rate discharge within the context of real-time implementation. As mentioned earlier, understanding the impact of the CV phase charging on the plating detection sensitivity and avoiding the misdetection due to graphite phase changes can improve the efficacy of the VRP method. Therefore, the research objective concerning lithium-plating detection for the existing approaches is defined as:

Research Objective 2: Investigate the impact of the CV phase of charging and graphite phase changes on the VRP method and improve its detection sensitivity.

The research work undertaken to meet this objective is reported in Chapter 3 in this IR and presented in detail in Submissions 2 and 5.

Second, develop a new method of lithium plating detection. As existing methods fail to detect the onset of plating within a charging event and face limitations in detecting lower levels of plating occurrence (<2.5%) [28], a new method of plating detection is required for early detection and control for BMS use. Therefore, the research objective concerning a new approach of lithium plating detection is defined as:

Research Objective 3: Research and develop a new approach to lithium plating detection that is implementable in real-time use and can identify the onset of plating within a charging event

The research work undertaken to meet this objective is reported in Chapter 6 in this IR and presented in detail within Submission 6.

Table 2.1: Summary of li-ion plating detection methods within the context of possible BMS deployment

Category		Method	Advantages/Disadvantages	BMS use
Invasive		NMR [56], ICP-OES [57] and Electrodes inspection [20, 58]	Provides definitive confirmation of lithium plating occurrence Not Suitable for monitoring lithium plating cycle by cycle Fails to detect the onset of plating within a charging event	No (Cell dismantling limits their BMS use)
Non-invasive	Tracking the NEP	Electrochemical model [56, 75]	Provides theoretical guidance Accuracy and model complexity are concerns Model adaptability to ageing is difficult Not possible to validate the identified onset of plating	No (Model complexity limits its BMS use)
		Insertion of RE or reconstruction of 3 electrode cell [5]	Insertion process, materials used can influence the NEP measurement Not suitable for real-time use Not possible to validate the identified onset of plating	No (Commercial cells do not come with the RE)
	Reversible plating	Tomography [73]	Tomography: Quantifies reversible plating cycle by cycle CV phase of charging influences the detection Fails to detect lower levels (< 2.5%) Fails to detect the onset of plating within a charging event Tomography: Not accessible even for researchers VRP: Long rest (> 1 h) is required after the charge DVC: Low C-rate discharge is required	No (Instrumentation required limits its BMS use)
		EIS [74]		No (Instrumentation required limits its BMS use)
		VRP [28, 74]		Yes (it requires monitoring of cell voltage and current)
		DVC [26, 74]		Yes (it requires monitoring of cell voltage and current)
	Impact of lithium plating	Coulombic efficiency [69]	High accuracy (<0.01%) is required Full charge/discharge is required Fails to detect the onset of plating within a charging event	No (High measurement accuracy and full charge/discharge need limit its BMS use)
		Volume expansion [24]	Measurement of 1 µm thickness changes is required Fails to detect the onset of plating within a charging event	No (Instrumentation required limits its BMS use)

2.4 Research area 3: Lithium plating control approaches

Use of higher charge currents to reduce the charging time can negatively influence the battery lifetime [70]. It is well understood that lithium plating is a major ageing mechanism while charging at high C-rates or low temperatures. Besides, many researchers have reported that conditions favouring lithium-plating change as battery undergo degradation [26, 31]. Therefore, charging strategies that aim to eliminate/reduce lithium plating shall adapt to battery ageing. While developing a charging strategy, the following attributes of a charging profile are desirable:

- Reduced charging time
- No accelerated degradation or minimize lithium plating due to the charging profile
- Adaptation of the charging profile to the operating conditions and battery ageing

These learnings rise the following research question:

Research question 3: Is it possible to develop a real-time implementable charging strategy that minimizes charging time while avoiding lithium plating?

Multiple fast charge profiles are suggested in the literature that can be broadly divided into three categories as:

- The standard CC-CV protocol
- Use of two or more CC stages in place of the single CC stage used in the CC-CV
- A more dynamic charge profile.

While utilizing these charging strategies for real-time use, either online or offline implementation is considered. In the online implementation [17], the charging profile is identified in real-time according to the operating conditions such as temperature and battery ageing level. An algorithm is developed and written to the electronic control module such as the BMS to define the self-regulating charge current so that the NEP is maintained above the Li+ reference or lithium plating is avoided. The advantage with the online mode is the charging profile can adapt to the operating conditions. On the other hand, in the Offline mode, a pre characterisation procedure is employed to identify the charge profile [5]. Depending upon the EV usage patterns, battery ageing and its internal potential drops can be different in different EVs [77]. Therefore, while using pre-identified charge profiles, multiple combinations of operating conditions such as different temperatures and ageing levels need to be considered to have a charge profile for each combination. This process requires numerous testing that may be difficult in practice. However, due to multiple challenges posed by the online strategies as

detailed in the following sections, offline implementation is still of great importance. Therefore, both online and offline charging strategies suggested in the literature are reviewed within the context of their implementation to define the research objective.

2.4.1 The standard CC-CV protocol

With the standard CC-CV charge profile, use of a high C-rate to reduce charging time can induce lithium plating while a low C-rate application can avoid plating but can result in longer charging time [23]. Therefore, identification of a maximum C-rate that avoid lithium plating is essential. Figure 2.2 shows an illustration of how C-rate influences NEP. At a low C-rate of 0.1C, the NEP is sufficiently maintained above the reference value. In the case of 1C, the NEP has become negative after the charge is initiated. On the other hand, at 0.5C, the NEP is just reached 0 V by the end of CC stage and started to rise as current reduces in the CV phase indicating the optimum C-rate for the CC-CV profile.

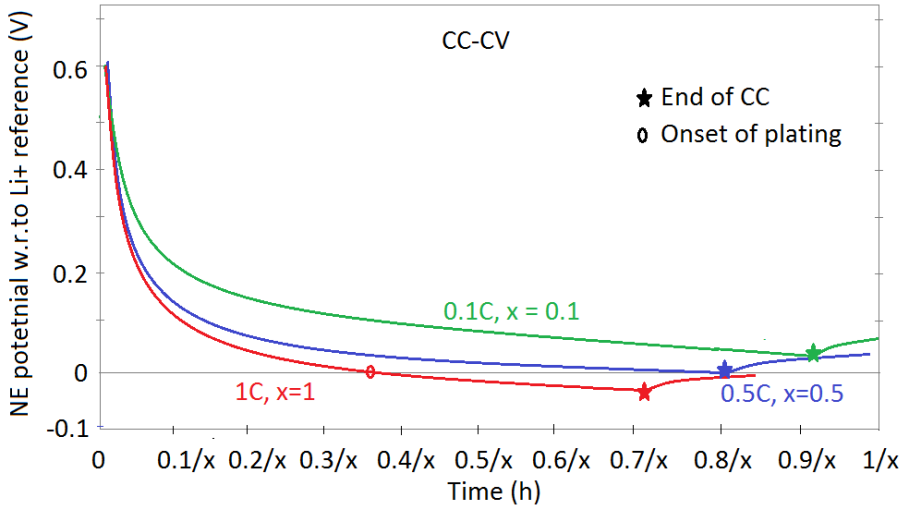

Figure 2.2: Illustration of the NEP at different C-rates of the CC-CV charge profile. Here, x indicates the C-rate.

Through usual cycling of cells at different C-rates of charging and frequent capacity estimation tests, it is possible to identify the C-rate that provides a maximum number of charge/discharge cycles before the cells lose specified capacity loss such as a loss of 20% capacity [10, 14]. However, battery life tests need excessive testing time depending upon the charge/discharge rates and the battery degradation rate.

Alternatively, to identify the optimum C-rate for the CC-CV profile within a few cycles, the CE method is suggested [70]. Charge rates higher than the optimum level lead to lithium plating and thus a drop in the Coulombic efficiency. By obtaining the CE values of cells cycling at different charge C-rates, the optimum C-rate that produces maximum Coulombic efficiency can be selected. This approach tries to minimize the capacity fade arising from different ageing mechanisms present under the selected

operating conditions. Prolonged charging time at low C-rates increases the amount of SEI growth in a cycle while a higher C-rate leads to lithium plating [69]. Therefore, the CE approach identifies the charge C-rate that minimises the overall capacity fade not limiting to lithium plating.

Since the capacity drop in a few cycles is typically small in Li-ion batteries and to be able to observe the minute differences between these capacity changes at different C-rates, the capacity measurement accuracy (>0.01%) needs to be high when using this approach [71]. A full charge and discharge are required to identify the capacity. As a result, implementation of the CE within the BMS for online identification of the C-rate is limited. Yet, this approach is useful for offline implementation with the pre-identified optimum C-rates at different temperatures for a new cell. However, to adapt to battery ageing, it is difficult to perform off-line characterization at regular intervals because of numerous tests that need to cover various C-rates and temperatures. Further, a common offline profile identified for one particular usage pattern may not be suitable for other usage patterns of the EVs. Therefore, each EV specific offline characterization during its lifetime is difficult considering the test requirements.

2.4.2 Multi-stage CC protocol

As mentioned in the previous section, the NEP reach Li+ reference value at the end of the CC stage or when the cell voltage rise to 4.2 V while using the optimum C-rate in the standard CC-CV profile. Use of a high C-rate compared to the optimum C-rate in the early part of the charging until the NEP reach Li+ reference or the onset of lithium plating and then reducing the charge current to keep the NEP above the reference can improve the charging speed [5]. The simplest form of this approach is replacing the single-stage CC with a two-stage CC profile. Figure 2.3a shows the illustration of the NEP and charge currents for a two-stage CC in place of the usual single stage CC. At the second stage CC, the NEP rises initially from the Li+ reference and then begins to reduce [5]. Further optimisation of this approach is to introduce multi-stage CC as shown in Figure 2.3b to keep the NEP as close as possible to the reference value. The charge rates are dropped stepwise in the multi-stage CC profile [78].

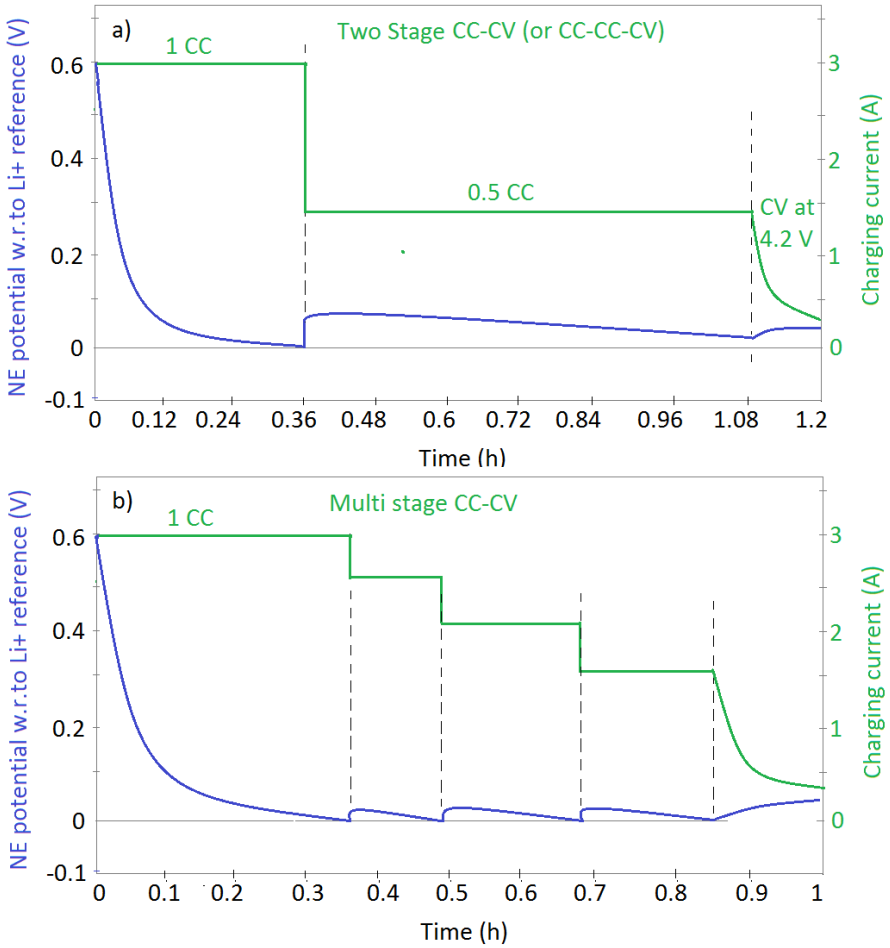

Figure 2.3: Illustration of the NEP while using a) 2-stage and b) multi-stage CC profile.

In a study by Thomas et al., a two-stage CC-CC (0.5C-0.2C) charging profile was developed to maintain the NEP above the Li+ reference voltage [5]. Here, the charging current was kept at 0.5C until the cell voltage reached a level (tagged as V_{tc}) at which the NEP dropped below the reference with the high charging current (0.5C) and then the charge current was reduced to 0.2C. To monitor the NEP behaviour, the authors reconstructed manually a three-electrode cell by adding a lithium reference electrode. With the monitored NEP, the V_{tc} is identified for a new cell. Since cell to cell variations such as capacity and impedance differences within a set of new cells are expected to be low compared to aged cells [79], the results obtained using the harvested electrodes from one new cell can apply to other new cells. However, this may not be the case with the aged cells as these differences can be significantly higher within the cells in an EV or between the cells in different EVs. Besides, the need for a reconstructed cell to identify the CC-CC profile could add large uncertainties to the electrode potential behaviour, leading to difficulties in the identification of V_{tc} accurately as described in Section 2.3.2. Therefore, this approach is not suitable for adapting the charging profile to the ageing conditions.

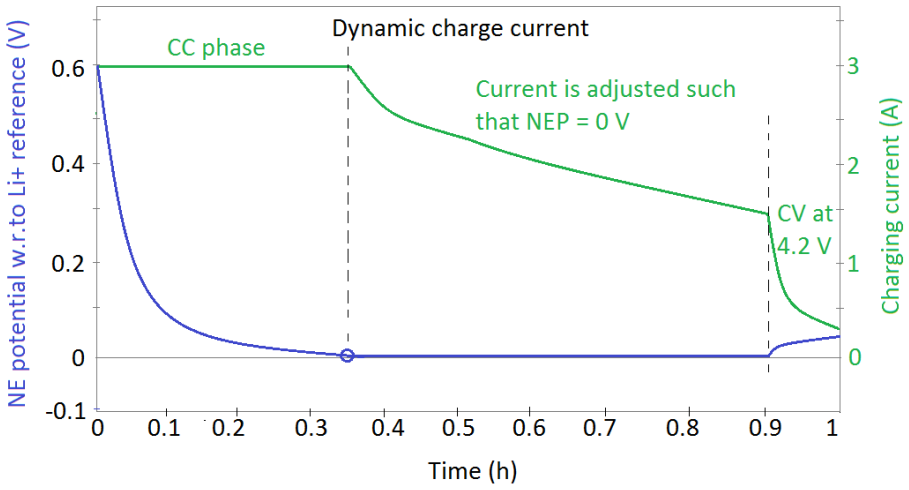

Figure 2.4: Illustration of the NEP with the dynamic charge profile that keeps the NEP at the Li+ reference

2.4.3 Optimum charge protocol

The optimum charge profile is the one that keeps the NEP at the reference voltage during charging [13, 17]. This can be achieved by applying a dynamic charge current profile. Figure 2.4 shows the illustration of the NEP with the dynamic charge current profile. To be able to manage the NEP with feedback control, it needs to be either estimated or measured. To measure the NEP directly on a cell, a RE is required as it allows monitoring of each electrode's potential [80]. To the best knowledge of the author, none of the commercially available Li-ion cells is provided with this additional electrode and therefore it is not possible to acquire and control the NEP directly online. On the other hand, an offline profile may be developed by modifying the commercial new cells in the laboratory setup. However, the RE insertion procedure, long-term stability of the material used for the RE and disturbance to the ionic flow due to the RE still pose many challenges to the RE based studies [81]. Besides, the NEP measured with the RE may not reflect the actual potential that causes plating as described in section 2.3.4. Therefore, isolating the processes that do not influence lithium plating from the NEP is another major challenge for RE based studies.

Alternatively, electrochemical models can be employed within the off-line simulation to quantify the NEP and identify the charge current profile that keeps the NEP at the Li+ reference value. However, model accuracy in estimating the NEP is still a major concern in utilizing them [82]. On the other hand, online use of these models for estimating the NEP and controlling the charge current in real-time face further challenges such as computationally efficiency and model adaption to battery ageing [32] as mentioned in Section 2.3.2.

2.4.4 Other charge profiles

As an alternative to the previously mentioned approaches, researchers have proposed intuitive charge profiles such as Multi-step charging [83], Boost charging [10], Pulse charging [84] and dynamic charging [23] profiles. These approaches use basic knowledge about conditions favouring lithium plating. For example, compared to low temperatures, charging at higher temperatures can reduce the chances of NEP getting below the reference because of reduced potential drops or improved kinetics. Similarly, it is known that compared to the lower SOC range, vulnerability to lithium plating at a higher SOC band is high as NEP drops with increasing SOC level. Utilizing this information, the Boost charging approach proposes high C-rate application at lower SOC levels that raise the battery temperature and then use of a lower C-rate charge in the higher SOC band [10]. Raised temperature coupled with the lower C-rate in the later part of charging may reduce or avoid lithium plating. On similar lines, pulse charging [84] is suggested based on the understanding that intermittent interruption of charge current can reduce the concentration gradients in the electrodes and thus, potential drops at the electrodes.

Although some of these charging profiles have shown improvements in battery life extension, they cannot optimize the charging process due to a lack of underpinning knowledge regarding the potentials and the potential drops at the negative electrode which are responsible for lithium plating occurrence [10, 23]. Moreover, these offline charge profiles suggested for new cells do not adapt to battery ageing.

2.4.5 Summary and Research objective

Table 2.2 presents a summary of the charging strategies often cited in the literature. The NEP based approaches such as the electrochemical model or the RE could optimize the charging profile. However, there exist many challenges in their online or offline application. On the other hand, the intuitive charge profiles may not optimise the charge profile as they lack theoretical guidance. While the CE approach enables the selection of optimum CC-CV profile for offline selection and it is not suitable for online implementation due to the need for measurement accuracy. To improve the charging speed compared to the optimum CC-CV profile, a multi-stage CC profile is suggested with the reconstructed cells. Nevertheless, the offline procedure followed in the reconstruction of cells can influence the charge profile selection. Therefore, a more practical approach to derive a dynamic or multi-stage CC charge profile is missing.

Table 2.2: Comparison of different charging strategies within the context of their EV application

Category	**Methodology**	**Primary advantages and limitations**	**Online use**	**Offline use (For new cell)**
CC-CV	Coulombic efficiency [70]	Helps to identify the optimum C-rate for the CC-CV profile It may be used for developing multi-stage CC to further improve the charge profile Difficult to adapt to cell ageing	No	Yes
Multi-stage CC	Reconstructed three-electrode cell [5]	Method affects the accuracy Not suitable for aged cells	No	Yes
Dynamic charge profile	Electrochemical model [17]	Can provide an optimum charge profile Implementation and adapting to battery ageing is difficult.	No	
	Reference electrode (RE) [81]	Can provide an optimum charge profile Process of insertion and material used for the RE influence results Not suitable for real-time use	No	Yes
Intuitive charge profiles	Boost charging [10] Pulse charging [84]	Simple to develop Cant optimize charge profile Do not take battery ageing into account	No	Yes

Not limiting to the identification of optimum C-rate for the CC-CV profile, the CE approach may be used to improve the charging speed further by keeping the NEP closer to the Li/Li+ reference for the larger part of the charging. This may be achieved by replacing the single-stage CC with a two-stage CC similar to the one developed with the reconstructed three-electrode cell. For the first stage CC, identifying the cell voltage level (or the V_{tc}) that corresponds to the NEP reaching Li+ reference voltage using the CE approach is possible. Therefore, a procedure to improve the charging speed using the CE approach needs to be developed for offline use.

Along with the development of an offline charging profile, in the same study, the derivation of an online charge profile using a non-invasive plating detection technique is explored. Since the VRP method is implementable in BMS and works at low temperatures (< 25^{o}C) as discussed in Section 2.3.4, it can be used to derive the online profile for low-temperature applications. In the two-stage CC charge profile, the V_{tc} is identified by tracking the lithium plating using the VRP method. Therefore, the first

research objective in the third research area is to develop multi-stage CC profiles for offline and online use with the help of CE and the VRP approaches, respectively.

Research Objective 4: Develop a systematic procedure to identify multi-stage CC charge profiles using the CE and VRP approaches and verify their performance

The research work undertaken to meet this objective is reported in Chapter 4 in this IR and presented in detail in Submission 2 and 5.

In addition to the development of offline and low-temperature specific online charging profile, a more practical approach to suit different temperatures and ageing levels for online implementation is needed. Research objective 3 aims to develop a new method of lithium plating detection suitable for different operating conditions and online implementation. The developed method will then be utilized in developing an online charging strategy that shall adapt to varying temperatures and battery ageing level. Therefore, the second objective of lithium-plating control is to develop an online implementable charging strategy.

Research objective 5: Develop an optimal charging strategy that can be implemented in online mode

The research work undertaken to meet this objective is reported in Chapter 7 in this IR and presented in detail in Submission 7.

2.5 Conclusions

Chapter 1 outlines that the development of Li-ion batteries plays an important role in future vehicle electrification. Fast charging in Li-ion batteries is a key research area for industry and academia because it has a direct impact on the charging time and battery life. From this, the scope of this thesis is focused on three research areas. These areas are:

1. Understanding the influence of lithium plating on battery degradation;

2. Detection of lithium plating occurrence and

3. Control of lithium plating.

For these research areas, three further research questions are formulated as detailed in this Chapter. For each research question, a review of the most relevant literature leads to 5 research objectives to be addressed. Figure 2.5 summarizes the relationship between each research area and research question.

Understanding the influence of lithium plating on battery degradation (research area 1) will be useful in devising fast-charging strategies. It is known that lithium plating affects the cycle life negatively, performance, and safety of Li-ion batteries. Loss of cyclable lithium or LLI to lithium plating is believed to be the major degradation mode. However, the literature review suggests that lithium plating may raise volume expansion that could lead to active material cracking or LAM. The presence of high volume-occupying lithium metal depositions can have long-lasting negative impacts on the battery capacity. Quantifying the degradation modes of lithium plating in terms of LLI and LAM can help understand whether LAM is rising in the presence of lithium plating. Knowledge about the short-term and long-term impacts of lithium plating on battery degradation is essential to develop charging strategies that provide a trade-off between the charging speed and battery life. None of the reviewed studies attempted to understand and quantify the degradation modes of lithium plating. From this, the research objective is to study the influence of lithium plating by quantifying the degradation modes of a Li-ion battery in fast-charge cycle ageing.

The detection of lithium plating occurrence (research area 2) is essential to study the operating conditions that potentially cause lithium plating. The invasive methods that confirm the presence of metal depositions need cell dismantling which limits their application in online use. Further, they are not suitable for studying the lithium-plating tendency cycle by cycle. On the other hand, the non-invasive approaches that detect the presence of lithium plating after a charging event are completed. Their dependency on reversible lithium plating indicates that the CV phase of charging can influence their detection sensitivity. Improving the methods that allow tracking lithium plating cycle by cycle is essential to study lithium plating at different ageing levels. Among them, the VRP approach may be useful in cycle ageing studies as it relies on the cell voltage measurements in the post-charge rest period. Therefore, the first research objective concerning the detection of lithium plating is to develop a systematic procedure to improve the non-invasive methods as they facilitate tracking plating cycle by cycle.

Further, the review of existing lithium plating methods indicates two major drawbacks when it comes to their real-time use for fast charge development. First, these methods fail to detect lower levels of lithium plating (< 2.5%) that occurs while charging at high temperatures (>20 ^{o}C) or low C-rates (< manufacturer-recommended C-rate limit). Second, none of these methods can detect the onset of lithium plating during charging. This suggests that a new lithium plating method is required to help its improved detection and control. Therefore, the second research objective regarding lithium-plating detection is to investigate and develop a new detection method to suit practical conditions.

Development of fast charging strategies that avoid or reduce lithium plating (research area 3) is required to maximise battery performance. Review of charging strategies that aim to minimize lithium plating and maximise the charging speed suggest that an optimum charge profile keeps the NEP at the Li+ reference value for longer. Achieving this in practice has many limitations as the implementation of electrochemical models or the inclusion of RE in real-time applications is difficult. Alternatively, the most optimum C-rate for the standard CC-CV profile can be identified using the CE method for a new cell. However, the offline charge profile can be improved by replacing the single-stage CC with a two-stage CC. Besides, the non-invasive detection methods can be studied for online implementation, as there exists no online implementable charging strategy that adapts to ageing conditions. Therefore, the first research objective concerning the control of lithium plating is to develop optimal charging strategies with the Coulombic efficiency and the VRP methods.

Further, given there exist many difficulties in the online implementation of the CE approach or application of the VRP method at room temperatures, an online implementable charging strategy suitable for near-operating conditions is required. A new method of plating detection suitable for real-time use once developed will be utilized for charge control. Therefore, the second research objective regarding the development of charging strategies is to develop optimal online charging strategies at room temperatures.

In summary, the literature review presented in this Chapter has identified the research areas, which require further attention in terms of understanding, detecting and controlling lithium plating in Li-ion batteries for EV applications. The identified research objectives in this Chapter directs the work presented in the rest of the thesis.

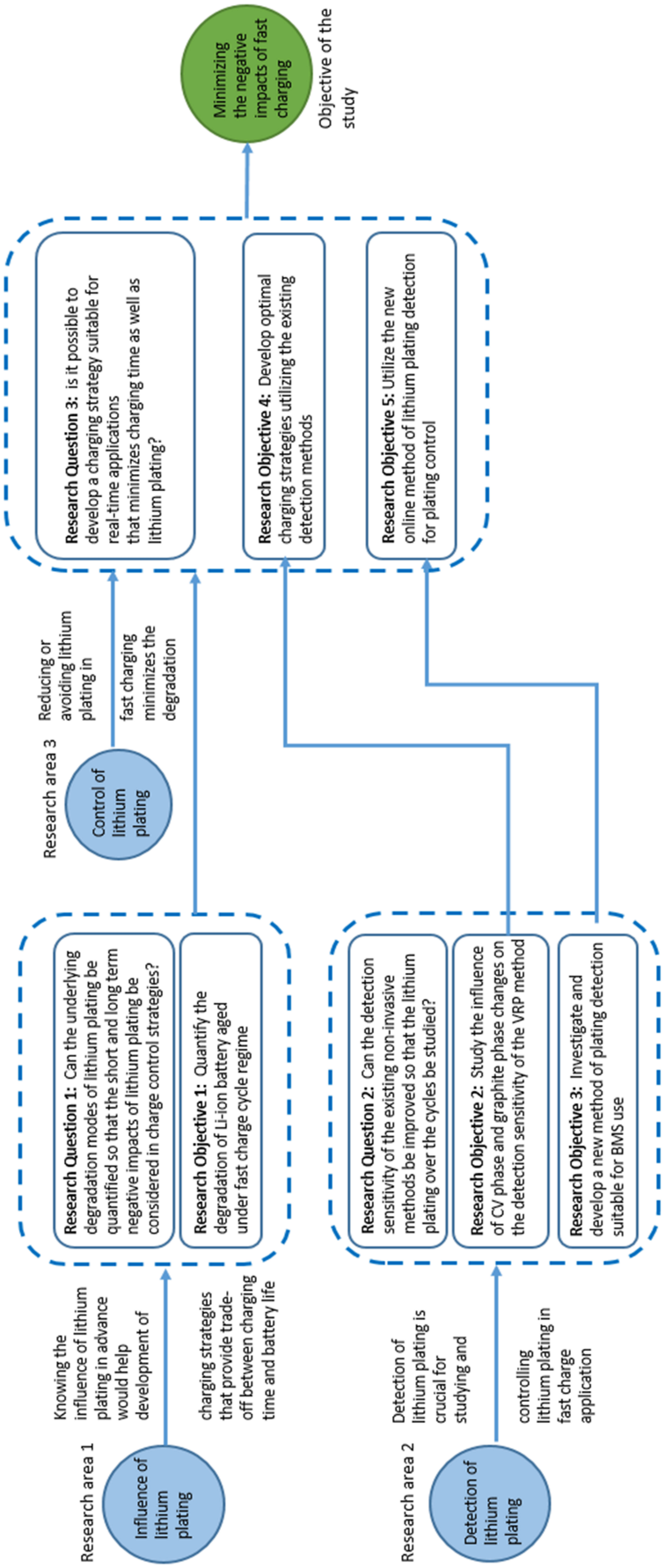

Figure 2.5: Relationship between different research questions and research objectives

3 Study 1- Improvement of lithium plating detection sensitivity in Li-ion batteries

3.1 Introduction

To ensure fast charging without accelerated battery degradation, lithium plating needs to be diagnosed along with battery operation since operating conditions including the ageing levels influence lithium plating tendency [31, 52]. As detailed in Chapter 2, the non-invasive approaches that are based on reversible lithium plating allow studying lithium plating cycle by cycle [26]. Although these methods face challenges in detecting lithium plating levels lower than 2.5% [28], they may be suitable for controlling lithium plating at low temperatures such as below 10 ^{o}C where lithium-plating levels are expected to be higher and the lithium-stripping rate is lower compared to charging at room temperature [28, 76]. These approaches allow validation of any new method of lithium plating detection non-invasively as discussed in Chapter 6. However, as discussed in Section 2.3, these methods can be improved further to improve their ability to detect lithium plating to meet objective 2. The constant voltage (CV) phase of charging can influence the detection ability of these methods if lithium stripping begins in the CV phase itself. In the first part of this study, an experiment-based approach is proposed to identify the optimal charge cut-off current during the CV phase that allows the total amount of reversible lithium plating available for stripping and thus for detection in the post-charge conditions.

Among the non-invasive approaches, the voltage relaxation profiles (VRP) approach is deemed to be suitable for BMS applications because the cell voltage tracked during the post-charge relaxation enables the detection of lithium plating. As discussed in Section 2.3.4 and presented in Section 3.3 in detail, a two-stage voltage relaxation produced by lithium stripping after completion of a charging event is used to infer the occurrence of lithium plating within that charging event. However, lithium plating can be detected incorrectly if graphite experiences phase changes during the relaxation and produce a similar two-stage voltage relaxation. Lithiation level of the electrode and its potentials in the 2-stage relaxation at half-cell level are studied in the second part of this study to develop a systematic procedure to distinguish the plating-induced phase change from the graphite phase changes at the cell level.

The remainder of this chapter is divided into two sub-studies. The first one as described in Section 3.3 analyses how the graphite phase changes impact on the 2-stage voltage relaxation and proposes ways

to distinguish the plating induced 2-stage recovery from it experimentally. A step-by-step procedure that utilizes voltage levels during the relaxation and electrode lithiation levels towards the end charging to identify the plating induced two-stage recovery is presented. The second study presented in Section 3.4 deals with the CV influence on the detection of lithium plating. An experimental procedure to identify the cut-off current in the CV phase that avoids lithium stripping in the charge is detailed. The application and limitations of the study within the context of BMS are discussed in Sections 3.5 and 3.6, respectively. The main conclusions of this study are presented in Section 3.7.

3.2 Objectives of this study

The main objective of this study is:

- To improve the sensitivity of the non-invasive detection methods by studying the CV cut-off current impact on plating detection
- To study and distinguish two-stage recoveries occurring due to lithium plating and graphite phase changes.

The half-cell level studies look into the processes between the separator and the current collector that contribute to lithium plating experimentally and theoretically. Such analysis is utilized in the process of developing a new method of lithium plating discussed in Chapter 6.

3.3 Influence of graphite phase changes

A phase change introduced by the lithium stripping at the graphite electrode produces a two-stage voltage relaxation at the electrode and cell level that allow detecting lithium plating [28, 74]. However, usual phase changes of the graphite electrode may produce a similar two-stage recovery and thus affect the detection ability. Therefore, to develop a procedure to identify the source of the two-stage recovery at the cell level, it is essential to study the graphite electrode potentials. To monitor the NEP, its phase changes of the OCV profile and post-charge relaxation behaviour, half-cells are prepared in a coin cell (2032) format. These half-cells with graphite as the working electrode and lithium foil as counter electrode allow monitoring the graphite potential or the NEP against the Li/Li+ reference during its lithiation or delithiation. Experimental work, results and a procedure to identify the plating induced two-stage relaxation are detailed in the following sections.

3.3.1 Experimental

3.3.1.1 Half-cells preparation

The objective of the experiments is to monitor the NEP using graphite half-cells to study the correlation between lithium plating and the NEP. Each of the electrochemical half-cells used in this work is assembled in a 2032 coin cell housing as per [85] using a graphite electrode (Ø 14.8 mm), a lithium foil (Ø 14.8 mm, 0.38 mm thickness) as the counter electrode, a trilayer separator (Ø 19 mm and 25 µm thickness, Celgard® 2325) filled with 100 µL of LP50 (1 M $LiPF_6$ solved in EC: EMC with 3:7 volume ratios) as the electrolyte. The graphite electrodes are manufactured in the lab from a slurry coated onto a copper (as current collector) sheet. The slurry is prepared using graphite (SFG-6, TIMCAL C-NERGY), carbon conductive additive (C45, TIMCAL C-NERGY), and binder (CMC and SBR with 1:1 weight ratio) with a weight ratio of 91:5:4 respectively. To estimate the half-cell capacity, the active mass of the graphite in the electrode is calculated by subtracting the measured mass of the copper current collector from the measured mass of the electrode (graphite coated current collector). The half-cells are estimated to have an average 4.18 mAh capacity based on the average 11.2 (± 0.33) mg graphite calculated from the eight half-cells prepared [11]. This estimated capacity is used for setting the initial charge/discharge currents to measure the actual capacity.

3.3.1.2 Half-cell test setup

To support tests on the half-cells, BioLogic VMP-3 potentiostats are employed. Cell voltage and current are recorded on the half-cells and the specification and parameter setting for the proposed test plan are listed in Table 3.1. Since the potential of the graphite half-cells can reduce gradually from a positive to a negative level with respect to Li reference while charging, the voltage range of the potentiostats is set to -1 to +1 V.

Table 3.1: Measurement parameters and their range and accuracies

Measuring parameter	Use range	Accuracy	Resolution	Sampling time
Voltage	-1 to 1 V	+/- 1 mV	5 µV	1 s
Current	+10 to -10 mA	+/- 0.02%	1 nA	1 s

To control the environmental temperature during the experiments, the cells are placed inside a thermal chamber (Lucky Reptile Herp Nursery II -incubator). As the maximum dissipating power of the cell is less than 4.5 mW (4.5 mA or 1C current at a maximum voltage of 1 V) during charging or discharging, the temperature of the coin cell is assumed to be similar to the set environment temperature.

3.3.1.3 Test procedure

As detailed in Table 3.2, the half-cells have undergone preconditioning (to stabilize their energy capacity), OCV (to observe the graphite phase changes) and plating tests in sequence. This section presents the test procedure.

Table 3.2: Test plan at the half-cell level

Step. no	Sub-step no	Exp. Setup	Current rate	limits
Pre-conditioning	1.1	Equilibrate at 25°C	-	t>4 h
	1.2	Constant current charge	0.25C	V<0 V
	1.3	Constant voltage charge	variable	I<1/40C, V=0 V
	1.4	Rest	-	t>1 h
	1.5	Constant current discharge	0.25C	V>1 V
	1.6	Constant voltage discharge	variable	I<1/40C, V=1 V
	1.7	Rest	-	t>1 h
	1.8	Repeat steps 1.2 to 1.7	-	Cycle number <6
OCV measurement	2.1	Partial constant current charge	1/40C	$\Delta Q > Q_{nom}/120$
	2.2	Voltage relaxation	-	t>1 h
	2.3	Repeat steps 2.1 & 2.2 until V limit reached	-	V<0 V
Plating tests	3.1	Equilibrate at 10°C	t>4h	
	3.2	Constant current discharge	0.25C	V>1 V
	3.3	Constant voltage discharge	variable	I<1/40C, V=1 V
	3.4	Rest	-	t>1 h
	3.5	Constant current charge	1C	SOC_f > x Cycle number 1: x=20% Cycle number 2: x=30% Cycle number 3: x=40% Cycle number 4: x=50% Cycle number 5: x=60% cycle number 6: x=70% cycle number 7: x=80% cycle number 8: x=90%
	3.6	Rest	-	t>4 h
	3.7	Repeat steps 3.2 to 3.6	-	Cycle number > 8

Generally, side reactions between the electrolyte and graphite electrode that form the SEI layer over the graphite electrode [29] leads to cell capacity reduction. The decomposition reaction slows down within the first few cycles as the thickness of the passivating SEI layer increases. Consequently, it slows down the growth rate of the SEI layer and thus the capacity reduction. Besides, electrode material wetting with the electrolyte improves significantly within the first few cycles that could affect the capacity delivered [86]. To eliminate the unwanted influence of SEI layer growth and the wetting on the OCV measurement, all the cells are firstly preconditioned by cycling them six times at 25°C and 0.25C using CC-CV protocol for both discharge (or delithiation) and charge (or lithiation) [54]. Step 1

in Table 3.2 presents the preconditioning test procedure. Once the pre-conditioning tests are completed, the cells are ready for the OCV measurement.

Cell OCV measurement is necessary to capture the graphite phase transitions [21]. The cells are delithiated to 1 V at 0.25C using CC-CV discharge profile and rested for one hour before the OCV measurements are obtained on the following charge. At room temperature, the OCV of the NE is measured during charge as per the test plan presented in Table 3.2 (Step 2). To capture true OCV over the potential range of the cells between 1 and 0 V, the half-cells are charged incrementally, in steps of 1/120 of the nominal capacity ($\Delta Q = Q_{max}/120$), by applying small currents (1/40C) and subsequently allowing the cell voltage to relax for one hour as discussed within [85]. Here, Q_{max} of the cell refers to the maximum capacity delivered in the preceding discharge event. Higher the number of steps or OCV profile data points, the more accurate the OCV profile. Similarly, lower the C-rate current, lower the potential drops to relax in the rest period. The OCV measurements are recorded at the end of each rest period. This kind of OCV measurement is referred to as the galvanostatic intermittent titration technique (GITT) [85]. Since the minimum OCV of the graphite is zero and the capacity levels are significantly low for the potentials higher than 1 V, the normalized charge capacity or the state of charge (SOC) between the voltage levels of 1 and 0 V can be expressed as the lithiation level of the electrode from 0 to 1 [27].

After the OCV experiments, the half-cells are charged at 1C and 5 ^{o}C to study the NEP under lithium plating. During charging, due to the lack of access to lithium ions directly to all the graphite crystals (especially those at the centre of the particles), the graphite particle experiences higher levels of lithiation at the surface compared to the inner crystals within the particle [87]. Since the particle's surface is in electrical contact with the current collector, the surface potential of the particle represents the electrode potential while in charge and this potential is lower than the average electrode particle potential or the electrode OCV [56, 88]. Diffusion of the lithium from the boundary graphite crystals to the inner crystals continues even after the termination of charge because of the concentration gradients. This results in a reduction of lithiation level at the particle surface in the post-charge relaxation, and thus electrode potential rises following the OCV vs lithiation profile. Since the OCV profile of the graphite electrode consists of multiple plateaus and transitions [21], there is a potential for a 2-stage voltage relaxation during the post-charge rest period as discussed in section 3.3.2. This, therefore, could lead to the wrong detection of lithium plating since the VRP method attributes the 2-stage recovery to lithium plating.

To monitor the NEP relaxation trends when charged to different SOC levels, the cells are charged at 5 ^{o}C and 1C current from 0 % SOC to different SOC set-points (denoted as $SOC_{f,}$ ranging from 20 to 90%)

in sequence as shown in Step 3 of Table 3.2. The selected low temperature combined with the high C-rate of charge current increases the concentration gradients in the electrode and could potentially provoke plating in some cases where SOC_f levels are relatively high [56]. Before every charging event; first, the cells are discharged to 1 V using CC-CV discharge profile (0.25C at the CC and 1/40C cut-off current at the CV) and rested for one. Next, for the i^{th} cycle, the cells are charged from 0% SOC to a level of x_i% SOC and then allowed to rest for four hours to monitor the voltage relaxation. This procedure is then repeated and each time the SOC_f is increased by 10% until it reached 90%.

3.3.2 Results and Discussions

3.3.2.1 Capacity stabilization in pre-conditioning tests

Through the pre-conditioning tests (as discussed in Section 3.3.1), capacity changes of the half-cells are more than 1% in the first cycle and reduced with increasing cycle number. Three half-cells with the lowest capacity fade rates after the sixth cycles (below 0.5%) are selected for the OCV measurement and plating tests. Table 3.3 presents the measured capacities and capacity fade rates of these cells at the end of the pre-conditioning procedure.

Table 3.3: Capacity levels and drops of the selected half-cells at the end of the pre-conditioning test

Cell number	Capacity at 6^{th} Cycle	ΔQ in the sixth cycle
1	4.03 mAh	0.021 mAh
2	4.21 mAh	0.019 mAh
3	3.95 mAh	0.015 mAh

3.3.2.2 OCV profile measurement

Figure 3.1a shows voltage and OCV points measured on cell number one (following the GITT test for OCV as discussed in Section 3.3.1) for a given charge current profile shown in Figure 3.1b. The OCV profile as a function of SOC for this cell is constructed as illustrated in Figure 3.1c by normalising the charged capacity between 0 and 100%.

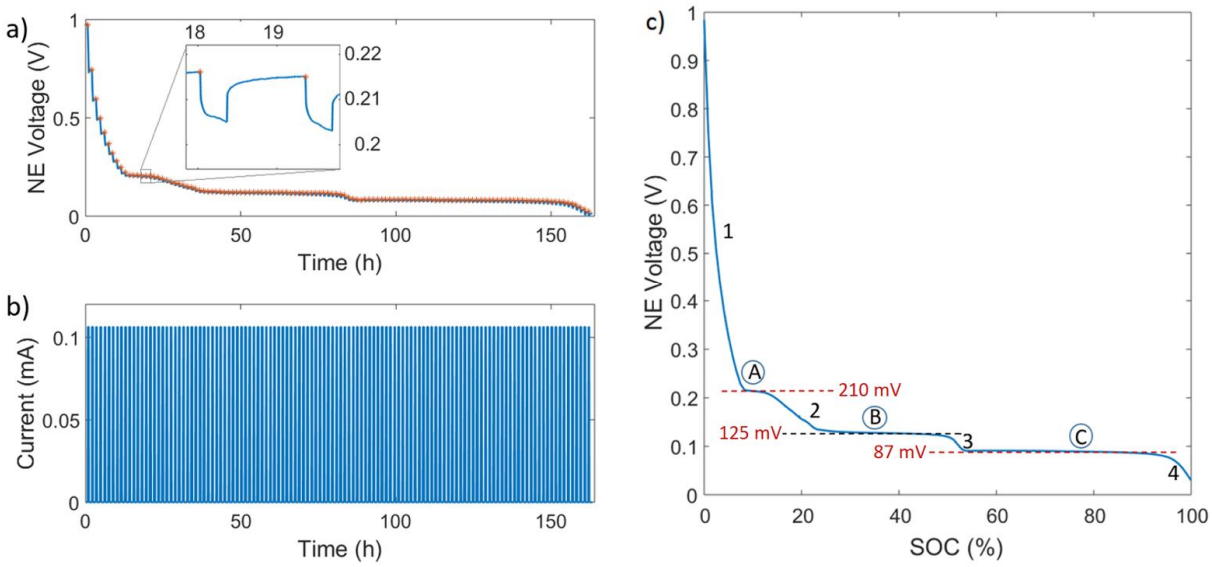

Figure 3.1: OCV measurement by incremental charge (or lithiation) and subsequent relaxation on cell one: a) cell voltage (line) and OCV measurements (markers), recorded at the end of each relaxation period, b) Incremental discharge current and c) OCV as a function

As seen from Figure 3.1c, with the lithiation of NE, there are three obvious voltage plateaus (denoted as A, B and C), and four transitions (marked as 1, 2, 3 and 4) in the OCV profile. On the plateaus, near to the voltage levels of 210, 125 and 87 mV, the OCV gradients are in turn 1.6, 0.4 and 0.2 mV per 1% SOC change. Meanwhile, in the transition regions between the voltage levels of 200-130, 116-94 and 78-20 mV, the OCV drop rates are high at 8.4, 6 and 7.9 mV per 1% SOC change, respectively. One potential reason for this phenomenon could be the graphite phase changes. The coexistence of two lithiated graphite phases such as Li_xC_6 and Li_xC_{12} could lead to the nearly flat voltage regions with a low OCV gradient while the single-phase such as Li_xC_6 could lead to the transient regions with high OCV gradient [20]. Irrespective of the reasons for the features in the OCV profile, during the relaxation, if the electrode lithiation at the surface drops from one voltage plateau to another (for example, C to B or B to A), a 2-stage potential recovery can be observed in the full-cell voltage profile.

3.3.2.3 Two-stage voltage relaxation for plating detection in half-cells

Figure 3.2a and Figure 3.2b display the charge currents and electrode potentials respectively, during the charge and relaxation periods (following the different SOC_f set-points, Section 3.3.1.3) while Figure 3.3a shows only the potentials in relaxation zones in all the test cases for a half-cell. As seen from Figure 3.3a, the voltage relaxation behaviour of the cell with the $SOC_f \geq 50\%$ is in a 2-stage recovery where the voltage recovered quickly at the beginning and then became quite stable before recovering again until reaching a constant level. For example, in the case of 80% SOC_f, the cell voltage increased from its initial level of -180 mV to 22 mV within the first 100 s and then mostly stayed constant at circa 27 mV for the next 3000 s. After this, the voltage increase continued considerably to 80 mV in less

than 2000 s to reach a final level of 85 mV by the end of a 4 hours relaxation period. Conversely, the voltage relaxation profiles of the cell with the SOC_f < 40% are with a single-stage where the voltage recovery speed is monotonously reducing. For the case with SOC_f of 40%, the cell voltage recovery profile stayed between the single and two-stage form. To demonstrate recovery phases of the tested cells, the cell voltage in the relaxation period is differentiated (dv/dt) and plotted as shown in Figure 3.3b. For the cases with $SOC_f \geq 40\%$, the voltage differential shows peaks and valleys presenting a 2-stage recovery that indicates the lithium-plating occurrence according to the VRP method. However as discussed earlier, phase changes of the graphite could also cause a 2-stage recovery profile.

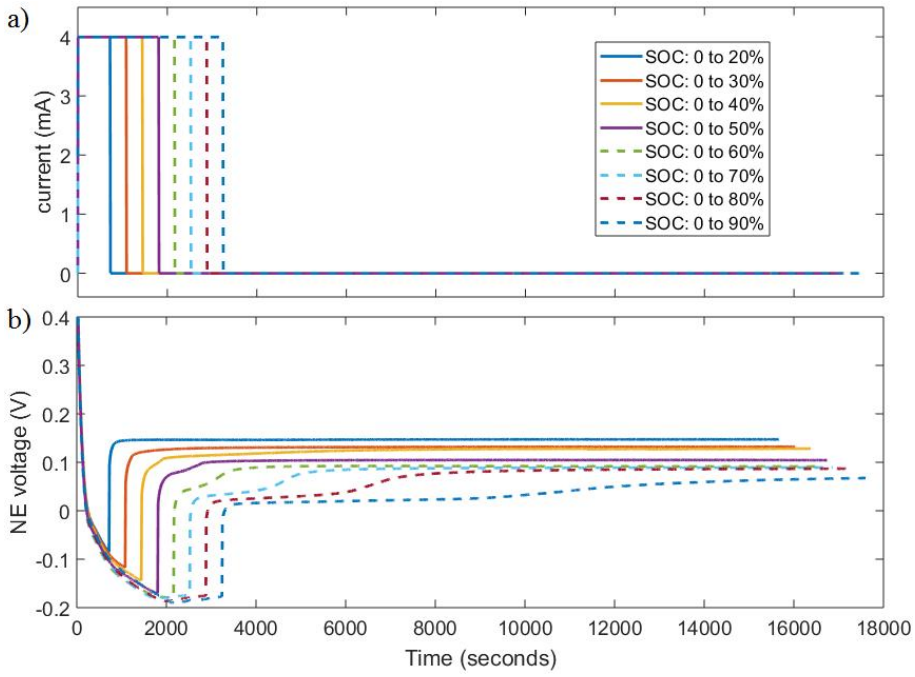

Figure 3.2: Fast charge profiles when charged to different SOC levels on half-cell one: a) Charge current and b) NEP over time.

To help identify the source of the 2-stage recovery, the NEP monitored in the relaxation period is analysed. As further discussed in Section 3.3.2.5, after 10 s into the relaxation, except the potential drops due to diffusion limitations in the electrode rest other potential drops between the separator and the current collector recover by that time. Therefore, the NEP measured after 10 s of relaxation could be used to track the particle surface. Here, the lithiation level of the particle surface drops with the diffusion of lithium from the surface to the inside until there exists a lithium concentration difference within the particle. Therefore, the electrode potential increases with the decrease of lithiation level at the particle surface. In the case of lithium plating, the drop in the lithiation level at the surface slows down in the initial period of relaxation and thus the potential change because of the incoming lithium from the reversible lithium plating. On the other hand, in the absence of plating, the

NEP can still produce a 2-stage recovery when the lithiation level of the particle surface drops from one voltage plateau to another due to lithium concentration differences within the electrode. Since graphite has a specific voltage level in each plateau region (as seen from Figure 3.1c, voltage ranges of plateau zones A, B and C are observed within 206 to 220, 122 to 132, and 79 to 94 mV, respectively), the voltage levels of the plateaus in the 2-stage relaxation shall indicate whether it is due to graphite phase changes. To identify the plateau voltage level in a 2-stage relaxation, the voltage differential (dv/dt) is plotted against the measured voltage as shown in Figure 3.3c. Here, the vertical dotted lines indicate the voltage level at which the differential attained a local minimum because of the voltage plateau in the middle of relaxation as seen in Figure 3.3a. For example, the voltage level in the plateau region is about 27 mV in the case of SOC_f = 80%.

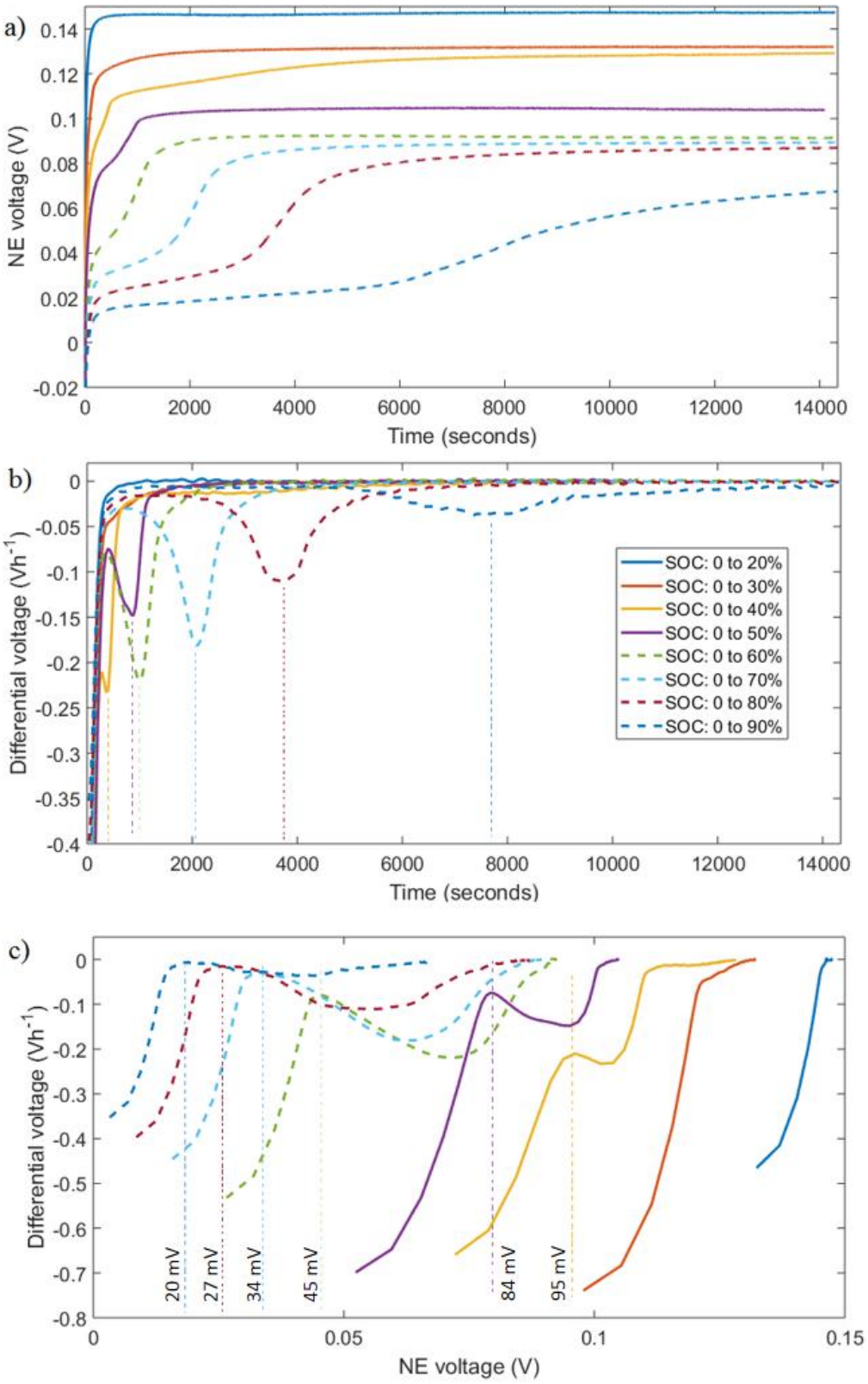

Figure 3.3: a) Voltage during the 4-h rest period displayed over time for different final SOC levels. b) Differential voltage during the 4-h rest period displayed over time for different final SOC levels. c) Differential voltage during the 4-h rest period displayed over the NEP measured for different final SOC levels. Vertical markers in differential curves indicate the plateau regions of 2-stage relaxation

As depicted in Figure 3.3c, for the cases with $SOC_f \geq 60\%$, the voltage plateau levels were below 46 mV, and less than the last voltage plateau of the graphite OCV profile (within range of 79 to 94 mV, Figure 3.1c). This indicates that there is a new voltage plateau caused by lithium plating. On the other hand, for the cases with SOC_f of 50% and 40%, the voltage plateaus levels were in turn 84 and 95 mV (in Figure 3.3c). In these cases, the voltage plateaus could be due to the graphite phase change (zone C in Figure 3.1c) or plating or their combination.

In addition to the potentials, the charge level of the NE as well supports the observed 2-stage recovery link to the lithium plating for the cases of $SOC_f \geq 60\%$. As shown in Figure 3.4, the last voltage plateau of the graphite, C, begins from the SOC level of circa 57%. In a case where the NE is charged to an average lithiation level of 57% or higher, a drop of lithium concentration at the particle surface from a higher level to the average lithiation level does not produce a step increase in the voltage (see Figure 3.4) after the initial recovery and thus does not produce a 2-stage recovery. As a result, for the cases with $SOC_f > 57\%$, the 2-stage recovery is not expected from graphite phase changes.

The results, therefore, highlight that the VRP method could only effectively detect lithium plating when the electrode lithiation level is above 57%. This observation is useful for plating studies since the majority of the plating studies are performed at low temperatures or at higher C-rates where charge levels at the end of charging will be lower than 100% SOC due to increased potential drops. To confirm lithium-plating detection using the VRP method, the average NE lithiation at the end of charging must be higher than the 57% level. This applies to plating studies performed on half-cells as those examined in this study and full-cells as it is typically performed on a commercial cell. To identify the lithiation level of NE at the end of a charging event at the full-cell level to confirm the plating occurrence using the VRP method, the following procedure is suggested in this work.

3.3.2.4 Lithium plating detection at the full cell level

To facilitate practical application, it is desirable to identify the phase transitions (and thus the lithiation level) of the NE at full cell level without the need for constructing half-cells. First, graphite phase transitions could be identified using its dV/dQ curve at the half-cell level as shown in Figure 3.4. The OCV profile vs charge capacity measured on a half-cell is used for the derivation of dV/dQ. Looking at this dV/dQ curve, two-phase transitions occur between voltage plateaus. The first transition with a peak marked as N1 between the voltage plateaus A and B, is at circa 16% SOC while the second one whose peak marked as N2 between the voltage plateaus B and C is at circa 53% SOC.

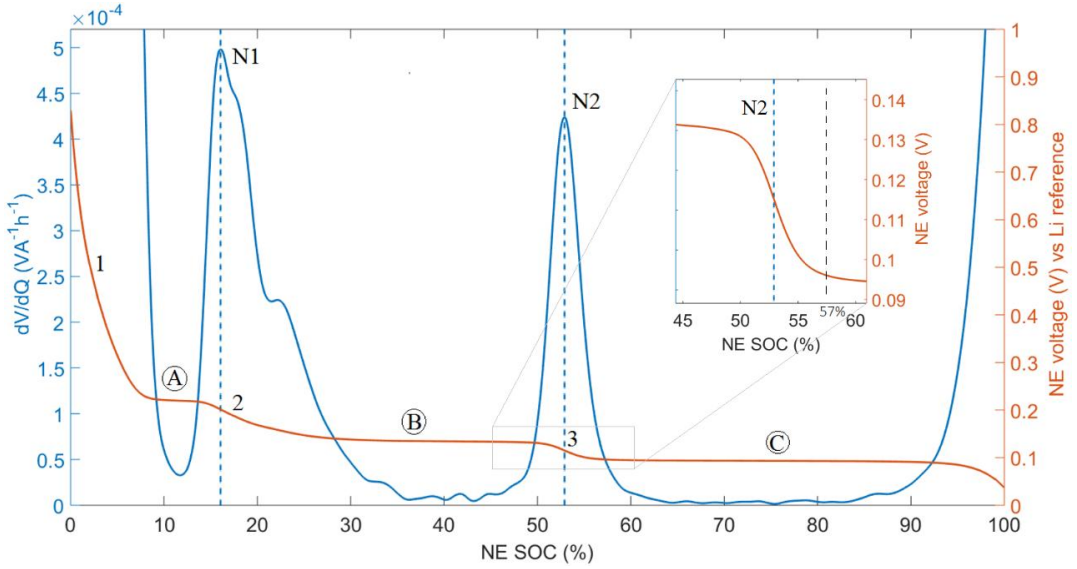

Figure 3.4: OCV and DV curves of a half-cell (graphite electrode) as a function of SOC. The last plateau begins at circa 57% SOC level as shown in the inset.

The next step is to obtain the NE lithiation level from the full cell-level test data. In commercial cells (or full cells) where NEP cannot be monitored directly, it is necessary to confirm that the NE is charged beyond the critical level (57% lithiation level, see inset in Figure 3.4) to attribute the observed 2-stage recovery to lithium plating. As discussed within [21, 26, 89] covering NCA, NMC and LFP chemistry cells, phase transitions of the NE (N1 and N2) can be identified using full cell dV/dQ curves based on the OCV profile captured at room temperature. To utilize the previously proposed dV/dQ curves for the plating studies, this study suggests the following approach. First, prior to fast charging experiments, dV/dQ analysis on the OCV curve at the full-cell level shall be performed to identify the transitions N1 and N2 and their corresponding charge levels. Next, with the measured capacity levels between the peaks N1 and N2 that correspond to the NE lithiation levels of 16 and 53% respectively, the critical charge capacity required to lithiated the NE to the level of 57% shall be calculated using the linear relationship between the NE lithiation level and its capacity. Finally, to attribute any 2-stage recovery observed during the post-charge relaxation to lithium plating, the full-cell needs to be checked whether it has been charged beyond the critical charge level. Application of this approach at the full cell level is presented in Section 3.4.2.

3.3.2.5 NE potential influence on lithium plating

In all the test cases (Step 3 in Table 3.2), the NEP is found with potentials below the Li reference as shown in Figure 3.2b. However, the 2-stage voltage relaxation phenomenon is not detected in all the test cases as indicated in Figure 3.3a. When the half-cell is charged to 20% SOC, the electrode potential towards the end of charge is -86 mV and the voltage recovery curve in the rest period is in a single stage (Figure 3.2b). This shows that the NEP potential below the reference during the charge

does not always lead to lithium plating and could be influenced by a subset of the voltage drops occurring between the separator and the current collector.

To identify the voltage drops that influence plating, the schematic of the graphite electrode between the separator and the current collector as presented in Figure 3.5a is analysed. Lithium ions moving through the separator towards the working electrode cross the electrolyte and the SEI layer leading to potential drops V_{EL} and V_{SEI} due to their impedances represented by Z_{EL} and Z_{SEI} respectively. While lithium ions entering the electrode whose surface potential is represented by $V_{NE,S}$ they face additional potential drop (V_{CTL}) due to the CTL at the electrode interface. The impedance due to CTL is identified by Z_{CTL}. On the other side, electrons, before combining with the lithium ions in the electrode, pass through the current collector and the conductive network in the electrode whose combined impedance is referred by Z_{Ω} and cause a potential drop (V_{Ω}). As discussed within [90], the NEP can be represented by

$$NEP = V_{NE,S} - V_{CTL} - V_{SEI} - V_{El} - V_{\Omega} \quad (3.1)$$

$$where\ V_{NE,S} = V_{NE,OCV} - V_{SDL} \quad (3.2)$$

Here, $V_{NE,S}$ is the surface potential of the electrode; $V_{NE,OCV}$ is the electrode OCV; and V_{SDL} is the potential difference between them that represent the potential drop in the electrode due to its SDL whose impedance is identified by Z_{SDL}. As shown in Figure 3.5a, the total charge current (i_t) contributes to the intercalation current (i_{in}) if there is no lithium plating.

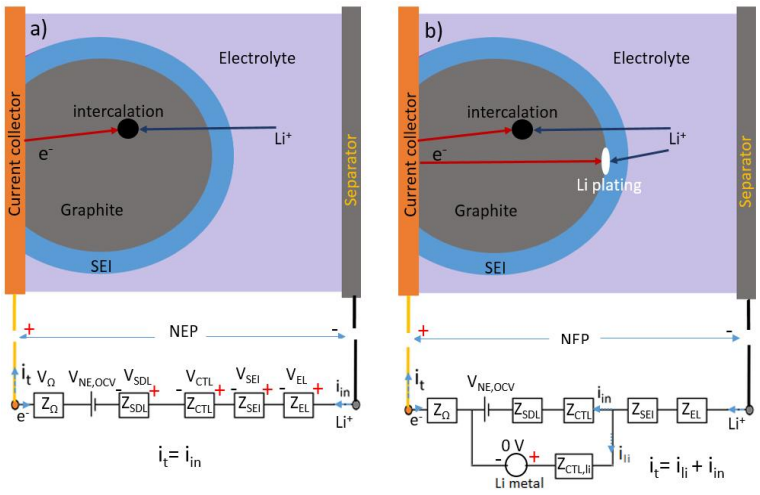

Figure 3.5: Schematic representation of charge flow and potential drops between the separator and the current collector in two scenarios: a) Prior to plating with 100% charge current contributing to graphite intercalation and b) during plating where charge current is split into interaction current and plating current

In the case of charging with the existence of lithium-plating as shown in Figure 3.5b, the total charge current (i_t) is split into the intercalation current (i_{in}) and lithium plating current (i_{li}). As discussed within

[56, 75], lithium metal deposits over the NE surface which lies between the SEI layer and the electrode (Figure 3.5b). Therefore, lithium ions after crossing the SEI layer divide into intercalating ions that enter the electrode and plating ions that cause lithium metal depositions over the electrode surface. On the other side, electrons after passing through the current collector split where one portion enters the electrode for intercalation (intercalating current) and the rest contributes to lithium plating (plating current). As a result, the total current both in electronic and ionic movement splits only at the electrode interface. According to the Kirchhoff's voltage law [91], the current splitting between the branches of a parallel network is independent of the potential drops occurring outside this parallel branch. From this understanding, the current distribution between the intercalation and lithium plating does not depend on the voltage drops V_{SEI}, V_{El} and V_{cu}. Therefore, lithium plating depends on the potential drops due to $\mathrm{Z_{SDL}}$ and $\mathrm{Z_{CTL}}$ and occurs when:

$$V_{NE,S} - V_{CTL} < 0 \text{ (or equivalently)} \quad V_{NE,OCV} - V_{SDL} - V_{CTL} < 0 \qquad (3.3)$$

During lithium plating, as discussed within [56], the plating current faces a potential drop ($\mathrm{V_{CTL,li}}$) due to the CTL at the interface whose impedance is denoted by $Z_{CTL,li}$ similar to the intercalating current. Unlike the graphite electrode that is intercalated with lithium in its structure, lithium plating does not exhibit solid diffusion limitations or concentration differences because of its metallic form. Lithium depositions are at the same potential as the electrode surface since they are deposited over the electrode. Therefore, the total current split into intercalation and plating currents is governed by the following condition:

$$\begin{gathered} V_{NE,OCV} - V_{SDL} - V_{CTL} = -V_{CTL,li} \\ \text{(or equivalently)} \quad V_{NE,OCV} - i_{in} * Z_{SDL} - i_{in} * Z_{CTL} = -i_{li} * Z_{CTL,li} \end{gathered} \qquad (3.4)$$

In the case of charging up to 20% SOC (Figure 3.2b), although the NEP is sufficiently below the reference, non-detection of plating suggests that $\mathrm{V_{NE,OCV} - V_{SDL} - V_{CTL}}$ is higher than the Li reference potential throughout the charging in this case. Therefore, the experimental results backed by the theoretical understanding supports that the NEP measured between the separator and the collector cannot be directly related to lithium plating. Since the electrode OCV along with the diffusion limitations in the electrode and interfacial drops at the electrode interface ($\mathrm{V_{NE,OCV}}$, $\mathrm{V_{SDL}}$ and $\mathrm{V_{CTL}}$) are influencing the favourable condition for lithium plating as shown in equation (3.3), considering them instead of the NEP measured between the separator and the current collector in plating mitigation studies will help in improving the plating control strategies. This finding applies to the charge control methods that employ an RE in commercial cells or a reconstructed cell. Besides, since potential drops or impedance due to CTL and SDL are largely influencing the plating tendency and the

corresponding impedance is getting affected after the onset of plating (see Figure 3.5b), it may be possible to identify the onset of lithium plating by tracking the impedance at the electrode surface during charge. Study 4 presented in Chapter 6 tracks the changes in impedance of the CTL from the cell impedance to investigate a new method of lithium plating detection.

3.4 Influence of CV phase

As mentioned earlier, lithium plating starts reversing once the NEP becomes positive. This can occur in the CV phase of charging if the cut-off current is sufficiently small [76]. Figure 3.6 illustrates the NEP during charge and the $I_{critical}$ where the NEP regains positive levels. Identifying the $I_{critical}$ and terminating the charge at the $I_{critical}$ will provide an improved scope to observe the total reversible plating in the post-charge relaxation and thus improving the sensitivity of plating detection. Experimental work, results and a procedure to identify the $I_{critical}$ are detailed in the following sections.

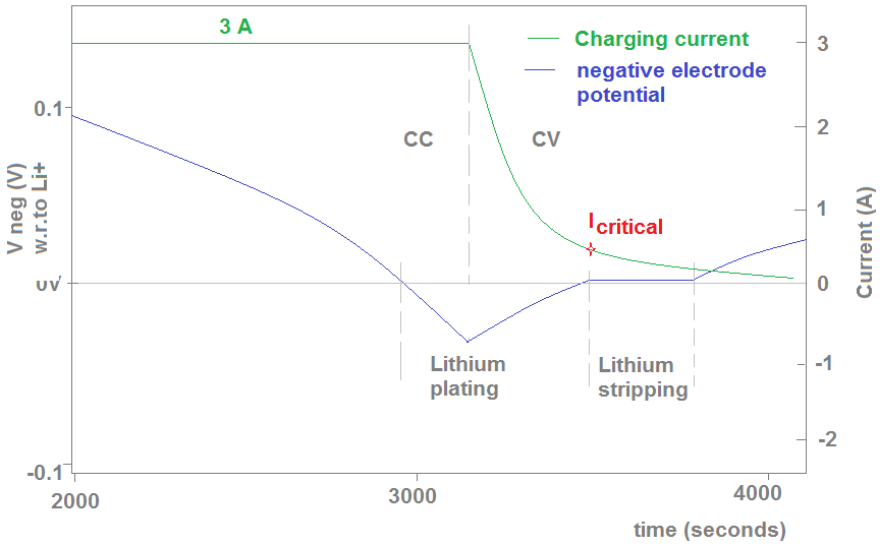

Figure 3.6: An illustration of plating and stripping and their link to charge current in CCCV profile [5, 76]

3.4.1 Experimental

3.4.1.1 Test procedure

Since the NEP cannot be monitored in a commercial cell, identification of the $I_{critical}$ using the VRP method is proposed here. Charge terminating current levels higher than the $I_{critical}$ reduce the amount of lithium plating and thus the lithium stripping level in the post-charge relaxation. On the other hand, CV cut-off currents lower than the $I_{critical}$ do not influence lithium-plating amount. However, it can reduce the lithium available for stripping in the post-charge relaxation as stripping begins in the CV phase itself. Therefore, to avoid lithium stripping in the CV phase and to detect the total amount in the post-charge relaxation, it is necessary to terminate the charge in the CV phase with a cut-off

current higher than the $I_{critical.}$ To identify the $I_{critical}$, experiments are conducted on a commercially available (Panasonic BD) 18650-type cell. The NE material is graphite and the PE material is $LiNiCoAlO_2$, known as NCA. Product specifications given by the manufacturer show that these cells have a rated capacity of 3 Ah between 2.5 and 4.2V. It is noteworthy that the same type of cell is used throughout this EngD for consistency.

Since the amount of lithium plating in a charging event depends on the temperature, charge C-rate and ageing level [31, 52], the value of $I_{critical}$ may vary according to the operating conditions. Due to the test feasibility, this study focuses on identifying the $I_{critical}$ at a selected temperature (5 ^{o}C) and C-rate (1C). These operating conditions are beyond the manufacturer recommended limits (charge temperature range: 10 to 45 ^{o}C; maximum charge C-rate: 0.5C) and therefore, could potentially cause lithium plating. Nine cells with different ageing levels are chosen from a group of 32 cells with unknown history by characterizing their capacity levels. Experiments on the nine cells are categorised into characterization tests and plating tests. A flowchart for the overall test plan is presented in Figure 3.7.

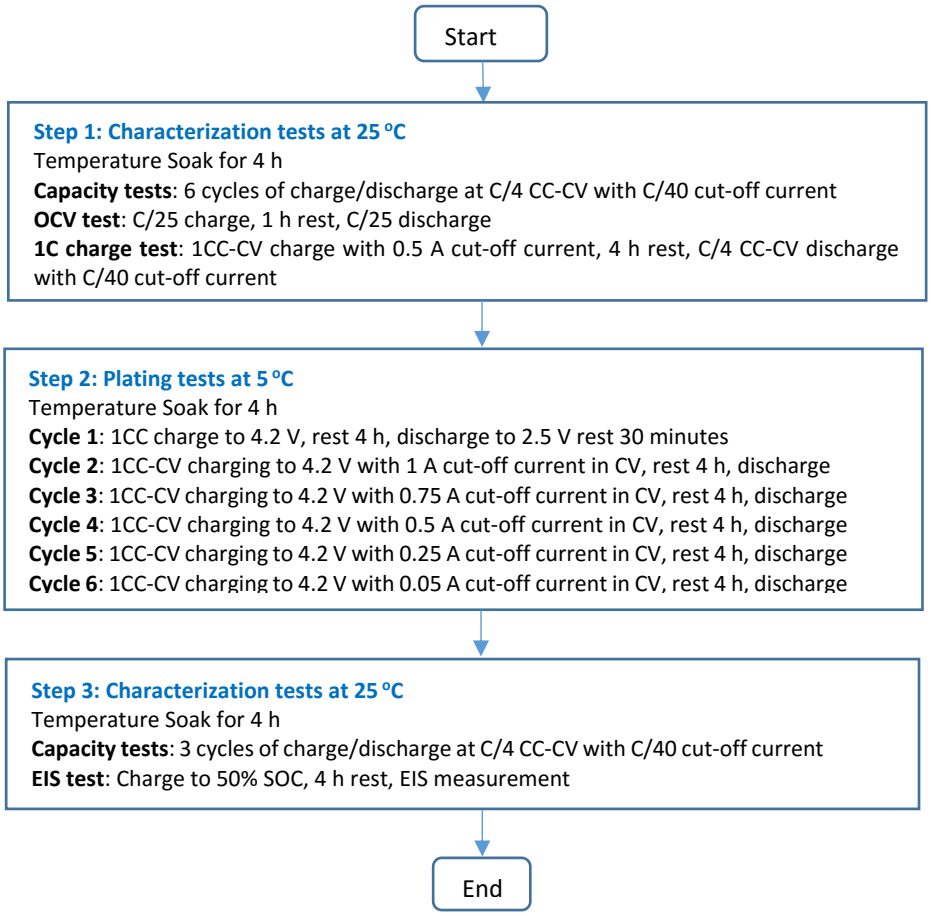

Figure 3.7: Flowchart of the experiments

The characterization tests at 25 °C prior to the plating tests (Step 1 of the flow chart shown in Figure 3.7) are performed in three stages. First, cells are subjected to six cycles with a CC-CV charge and discharge between 2.5V and 4.2V with a cut-off current of C/40 to precondition the cells as few of them can be unused previously and to measure their capacity. The CV during discharge in both preconditioning and capacity estimation tests is included in this work to alleviate the impact of impedance on the measured capacity of the cell. The kinetics of lithium exchange between the electrodes, and thus the impedance to the current flow in the battery varies according to the electrode's inhomogeneities [92], deactivation of electrode particles due to porosity reduction [66], anode overhang that is the excess area at the NE that does not face the cathode [93, 94] and battery degradation level [95]. As discussed within [92], using a CV discharge with a sufficiently low cut-off current can reduce the impedance effect on the battery capacity estimation. Once the pre-conditioning tests are completed, the cells are then deemed ready for fast charge experiments and further capacity characterisation.

The discharge capacity measured in the last preconditioning cycle is taken as the cell capacity before the plating experiments starts. Next, the cells are tested for OCV to identify the NE signatures N1 and N2 at the cell level. As discussed within [52], a pseudo-OCV profile that is the mean of voltage profiles

taken at C/25 charge and discharge enable the identification of electrode level signatures with sufficient accuracy. Therefore, the cells are subject to the low C-rate charge and discharge. Finally, the cells are charged at 1C to 4.2 V with a cut-off current of 0.5 A in the CV phase followed by a 4 h rest to verify whether lithium is detectable at room temperature (25 ^{o}C).

After the characterization tests, the cells are allowed to soak at 5 ^{o}C for 4 h before the lithium-plating experiments are performed. The fully discharged cells are then charged at 1C rate (or 3 A) in the CC phase but with different CV phase cut-off current (3, 1, 0.75, 0.5, 0.25 and 0.05 A) in each charging event as per the Step 2 in the flowchart in Figure 3.7. The purpose of this test is to identify the optimal cut-off current at which the plated lithium starts reversing or that allow detecting maximum lithium stripping amount in the post-charge rest period.

After the plating tests, the cells are once again tested for capacity at room temperature to measure the capacity drop during the experiments as shown in Step 3 of the flowchart in Figure 3.7.

3.4.1.2 Experimental setup

Figure 3.8a shows the experimental setup block diagram. To maintain a constant ambient temperature, the tests are performed inside a thermal chamber (Model: ESPEC PL-3KPH). The cells are placed on a Perspex plate fixture through which the cells are connected to a Bitrode cell cycler (Model: MCV 16-100-5). The Bitrode program running on a compatible computer controls this cycler. The supported program is capable of setting and monitoring charge/discharge, rest durations, voltage cut-off limits and chamber temperature. If the temperature exceeds 60°C or the voltage falls outside the desired operating range of 2.5 to 4.2 V, the Bitrode program automatically stops the test. The operating limits are set based on supplier recommendations. For the analysis, the Bitrode unit enables data records of the cell voltage and current within +\-5 mV and +\- 10 mA, respectively. Furthermore, a Bitrode probe using J-type thermocouples with an accuracy of ± 2.2°C is attached to the negative

tab of all the cells based on the accessibility to measure the cell surface temperature synchronously. The setting parameters for the proposed test plan using the Bitrode are listed in Table 3.4.

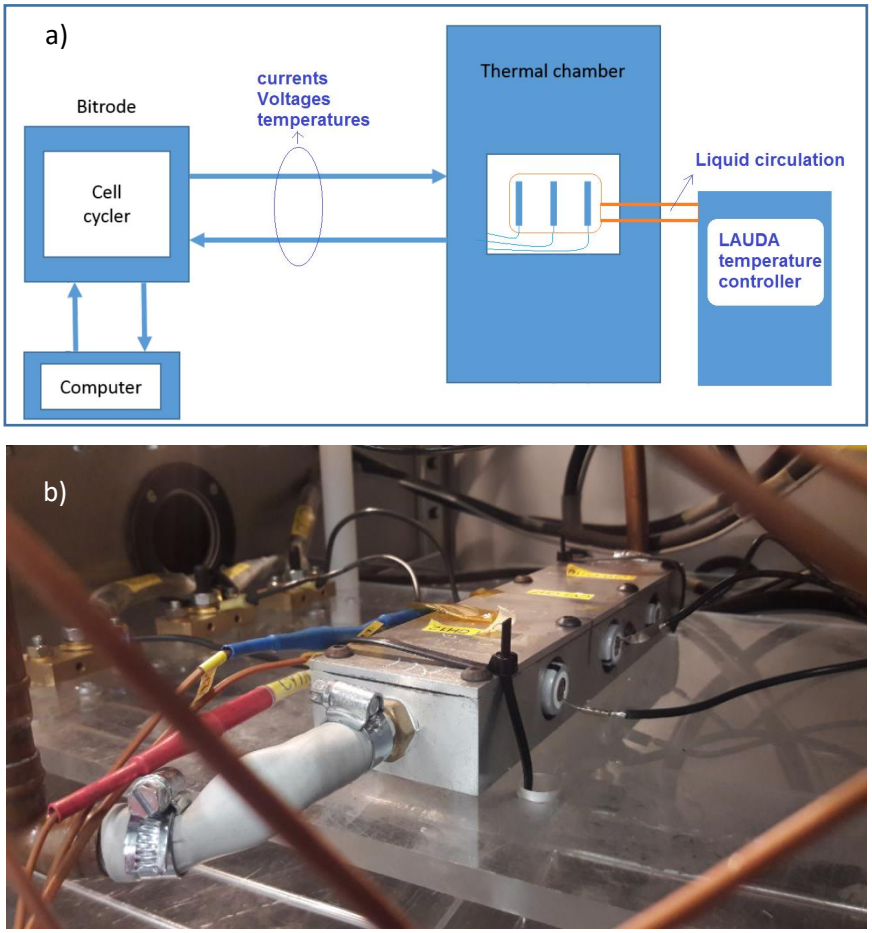

Figure 3.8: Experimental setup: a) Block diagram and b) active cooling mechanism

Table 3.4: Measurement parameters and their range and accuracies

Measuring parameter	Use range	accuracy	Resolution	Sampling time
Voltage	2.5 to 4.2 V	± 5 mV	1 mV	1 s
Current	+3 to -3 A	± 10 mA	1 mA	1 s
Temperature	0 to 30 °C	± 2.2 °C	0.5 °C	1 s

During operation, the temperature of the cells may rise even while remaining in the thermal-controlled chamber due to internal heat generation. Varying CV phase cut-off currents and different levels of ageing together may lead to large variations in temperatures across the cells [96]. This makes the comparison of reversible plating amounts difficult since lithium stripping rate depends on the temperature [76]. To keep the cell temperature as close as possible to the desired level, liquid cooling over the cell surface is applied using a LAUDA temperature Controller with +/- 0.01°C accuracy (Model: Proline RP 845 C) (see Figure 3.8b).

3.4.2 Results & Discussions

3.4.2.1 Cell characterization

The conditioning tests are undertaken at room temperature to stabilize the capacity of the cells. The results show that the discharge capacity is lower than the charge capacity in every cycle. By the sixth cycle, the magnitude of capacity change per cycle and the capacity difference between charge and discharge has reduced, indicating that the cells are asymptotically stable in terms of capacity retention with less than 0.03% change in capacity reduction per cycle. The value of cell capacities measured at the 6^{th} cycle is taken as the initial capacity of the respective cells. For completeness, Table 3.5 presents the actual values of capacity measured for each cell at the end of the 6^{th} conditioning cycle.

Table 3.5: Results in the cell characterization test

Cell number	**Capacity (Ah)**	**Capacity at N1 (C_{N1})**	**Capacity at N2 (C_{N2})**	**C_{TH} (Ah)**
1	3.13	0.30	1.61	1.75
2	3.09	0.29	1.58	1.72
3	3.06	0.29	1.62	1.76
4	2.97	0.32	1.55	1.68
5	2.96	0.28	1.57	1.71
6	2.95	0.35	1.62	1.76
7	2.88	0.31	1.61	1.75
8	2.71	0.31	1.53	1.66
9	2.52	0.35	1.57	1.70

In the OCV test, OCV vs capacity profiles are captured for the cells and dV/dQ is performed. Figure 3.9a and b show OCV profile and its differential for Cell number 4. As mentioned in Section 3.3.2, the

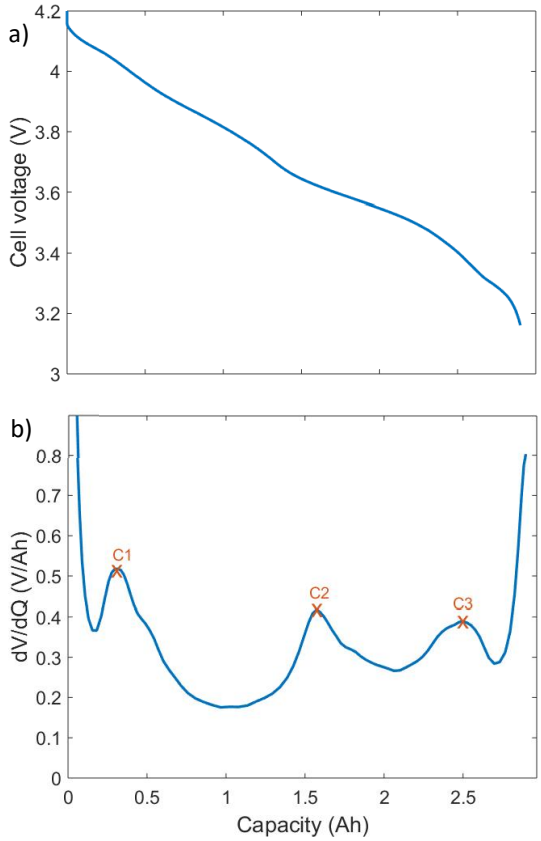

Figure 3.9: a) Pseudo OCV profile and b) its differential

two-stage relaxation observed in the post-charge relaxation does not originate from the graphite phase changes if the lithiation level of the NE rises beyond 57% at the EoC. Therefore, to confirm lithium-plating occurrence using the VRP approach, lithiation level of the NE needs to be identified. As discussed within [21, 50] and in Section 5.5, the NE signatures N1 and N2 correspond to the cell level dV/dQ signatures C1 and C2. Since N1 and N2 mark the graphite lithiation levels of 16 and 53%, respectively, cell capacity (referred to as C_{TH}) when graphite lithiation rises to 57% can be calculated as:

$$C_{TH} = C_{N2} + 4/(53 - 16) * (C_{N2} - C_{N1}) \quad (3.5)$$

where, C_{N1} and C_{N2} are the cell capacities at the signatures C1 and C2, respectively. Table 3.5 shows the C_{N1}, C_{N2} and C_{TH} for the nine cells. Two-stage voltage relaxation in cases where a cell is charged beyond its C_{TH} confirms the occurrence of lithium plating.

3.4.2.2 Detection of lithium plating

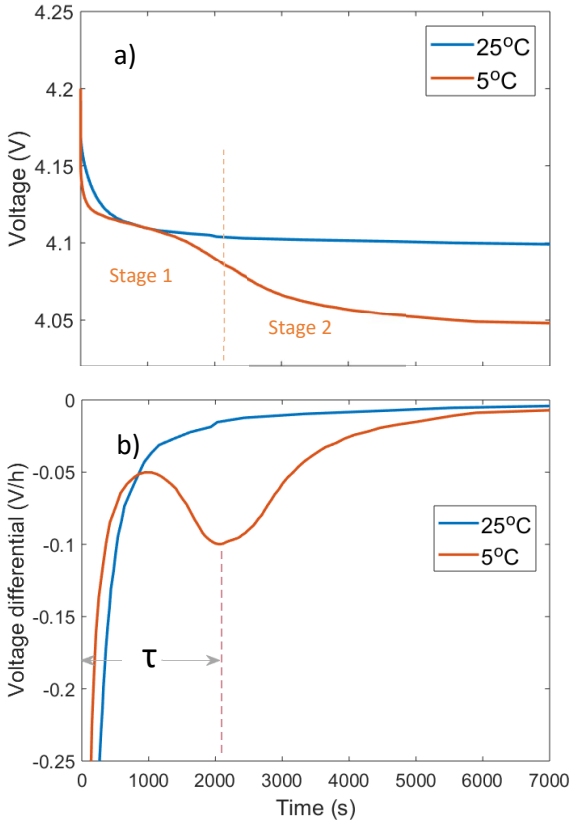

Figure 3.10: Voltage relaxation behaviour with and without lithium plating: a) Cell voltage and b) its differential

To create favourable conditions for lithium plating, cells are charged with 1CC-CV at 5°C. The post-charge cell voltage is monitored for four hours to observe the VRPs for plating detection. Figure 3.10a shows the voltage relaxation behaviour of cell number 4 in the post-charge rest at both 25°C and 5°C. The cell voltage is monotonically decreasing with time at room temperature. However, at the low temperature, the cell voltage is recovered in two stages which can originate from the graphite phase changes or lithium plating. Since the cell is charged beyond 2.4 Ah (> C_{TH}), this additional stage of recovery can be attributed to lithium plating as discussed in Section 3.3.

By the end of the first stage recovery, lithium stripping completes and cell voltage recovery accelerates once again. Since the stripping period is known to be proportional to the amount of reversible plating, the time point at which the second stage starts needs to be identified [28]. This is better captured by performing the rate of change profile, dv/dt, as depicted in Figure 3.10b. During lithium stripping, the slope of the dv/dt curve reaches minimum levels because of near to steady-state voltages and attains a maximum point thereafter at the end of reverse reactions [28, 74]. The stripping period (τ) which is approximately 2030 s as shown in the figure indicates that lithium stripping lasted over this period.

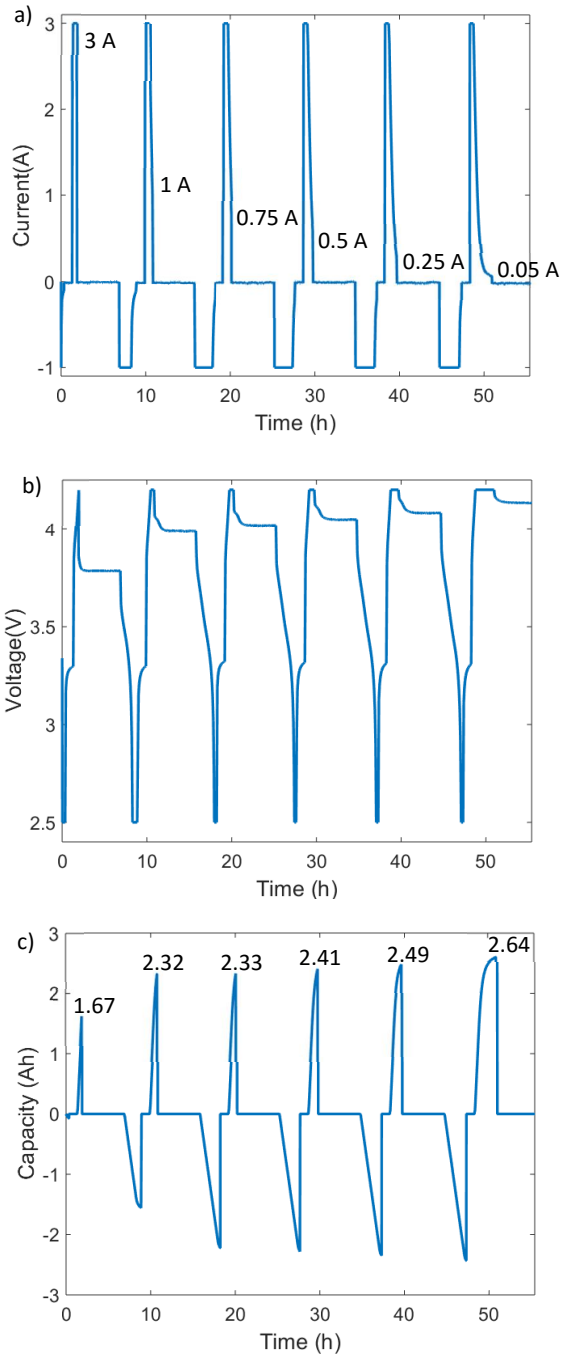

Figure 3.11: 1CC-CV charge with a) different cut-off currents in the CV phase and corresponding b) cell voltage and c) capacity profiles. Cut-off current levels and charge capacities are indicated in each case.

3.4.2.3 Identification of Cut-off current

At 5 °C, as shown in the flowchart presented in Figure 3.7, six test cases are performed in sequence on each cell. In each case, the cells are charged from the fully discharged state to a different CV cut-off current level as indicated in Figure 3.7 and then the cells are rested for four hours. After this, the cells are fully discharged to 2.5 V with a C/3 current until the cell reached 2.5 V for the next test case. Figure 3.11 shows the cell voltage, current and capacity profiles measured during these tests on cell 4 where positive levels of current indicate charging. Cell voltages in the post-charge relaxation and their

time differentials are shown in Figure 3.12 for the same cell. With the CV cut-off current reducing from 3 A (with CC alone) to 0.75 A, the stripping period has increased from 541 to 2253 s. Since stripping time (τ) is proportional to the amount of reversible lithium [28], increased stripping period suggests that the majority of lithium plating occurs in the CV phase compared to the CC phase. If the rate of reduction of the NEP towards the end of CC phase is higher than the recovery rate of the NEP in the CV phase, the NEP can be maintained below the Li+ reference for a longer period and thus larger levels of lithium plating in the CV phase compared to that of the CC phase.

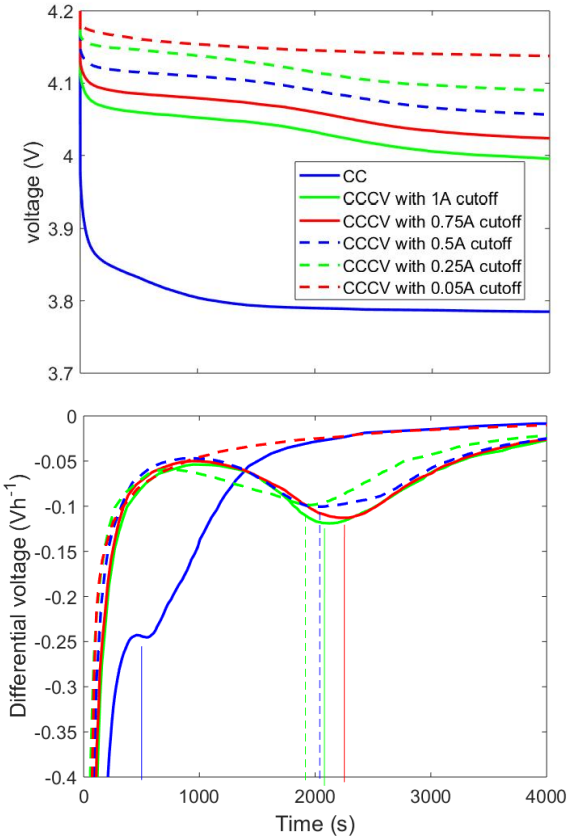

Figure 3.12: a) Voltages in rest and b) differential of them with different CV cut-off currents

Cut-off current levels below 0.75 A are seen with reduced stripping periods of 2170 and 1854 s for cut-off currents of 0.5 and 0.25 A, respectively compared to that of 0.75 A. As discussed within [28], longer the stripping period, higher the observable amount of reversible lithium plating. Therefore, detectable levels of reversible lithium plating are found to be reducing with the decreasing cut-off current level from 0.75 A, although the use of a lower cut-off current in the CV phase does not reduce the amount of lithium plating. Therefore, it can be concluded that $I_{critical}$ is circa 0.75 A for the cell. For a more precise critical current, the current step size in the test cases can be reduced further.

No two-stage recovery, and thus zero stripping period is observed when the cut-off current is further reduced to 50 mA as seen from Figure 3.12b. This indicates that lithium stripping that begins at circa

0.75 A is completed in the extended CV phase that is 6090 s longer than that of CV phase with 0.75 A cut-off level as seen from Figure 3.11a.

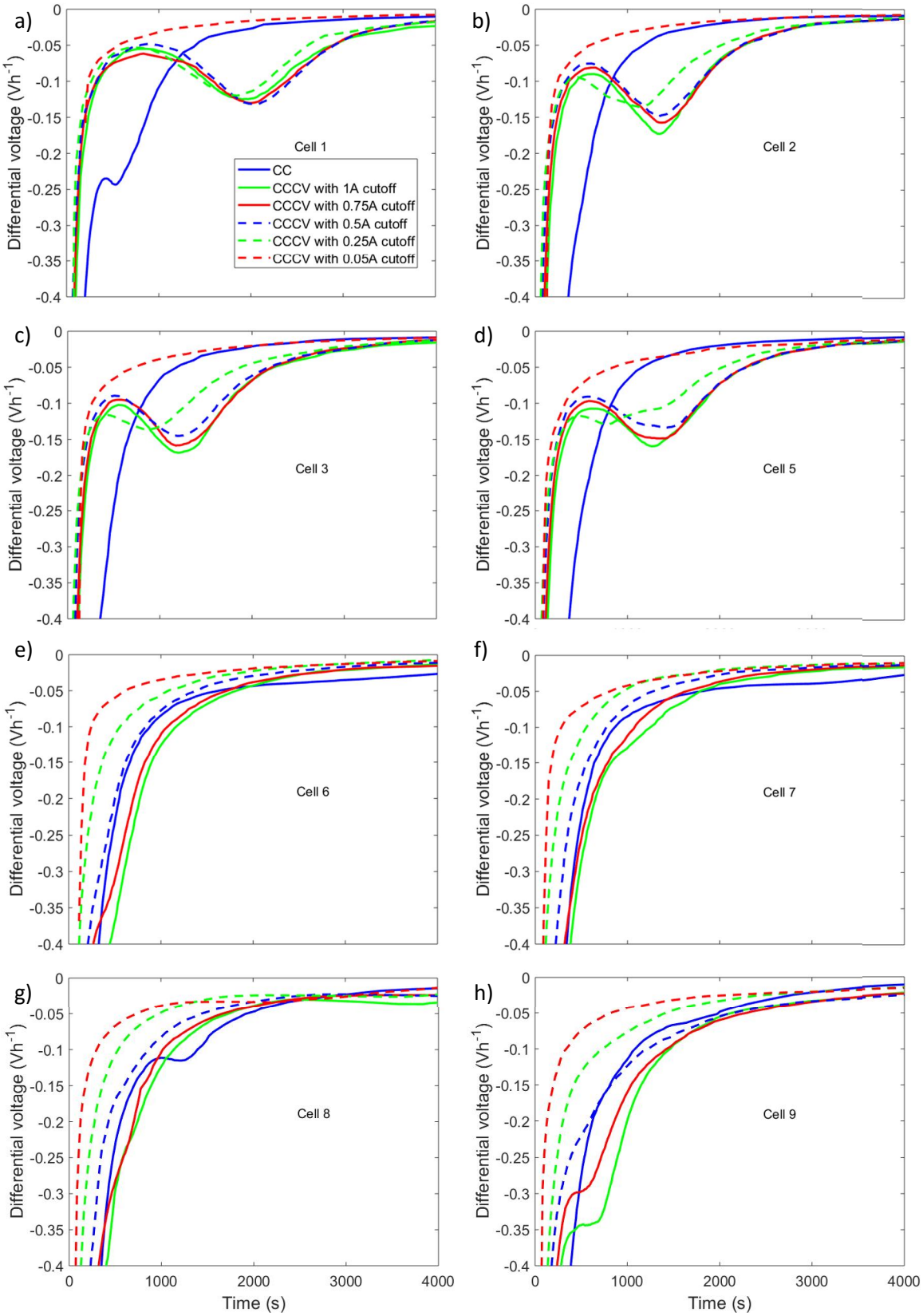

Figure 3.13: Voltage relaxation profiles and their differential for the other eight cells

3.4.2.4 Cut-off current variation with ageing

Figure 3.13 shows the voltage profiles and their differentials for the other eight cells with different CV cut-off currents. Two-stage relaxation is observed for cells numbered 1, 2, 3, 5 and 9 as shown in Figure 3.13 at some cut-off currents. As charge capacities of the cells are higher than their respective C_{TH} levels (see Table 3.6), all these cases indicate the presence of lithium plating.

Table 3.6: Cell charge capacities at different CV phase cut-off currents and capacity threshold (C_{TH}) to reach 57% lithiation of the graphite. The blue coloured date indicates the test cases with lithium plating

Cell number	C_{TH} (Ah)	C_{cc} (Ah)	C_{1A} (Ah)	$C_{0.75A}$ (Ah)	$C_{0.5A}$ (Ah)	$C_{0.25A}$ (Ah)	$C_{0.05A}$ (Ah)	Capacity drop (%)
1	1.75	**1.9**	**2.51**	**2.52**	**2.61**	**2.7**	2.85	3.5
2	1.72	1.73	**2.38**	**2.39**	**2.47**	**2.59**	2.73	2.6
3	1.76	1.68	**2.37**	**2.38**	**2.46**	**2.57**	2.72	2.5
4	1.66	**1.67**	**2.32**	**2.33**	**2.42**	**2.47**	2.61	9.3
5	1.71	1.57	**2.29**	**2.31**	**2.4**	**2.51**	2.65	1.3
6	1.76	1.3	1.99	2.24	2.37	2.55	2.71	0.7
7	1.75	1.26	2.17	2.22	2.36	2.54	2.67	0.35
8	1.66	0.9	2	2.08	2.23	2.41	2.57	0.3
9	1.7	0.7	**1.66**	**1.73**	1.85	2.01	2.15	7.5

On the other hand, two-stage voltage relaxation is not observed for the cells numbered 6 and 7 irrespective of the CV cut-off current (see Figure 3.13e and f). This indicates that either these cells have not experienced lithium plating or lithium-plating levels are below the detectable level (2.5%). While cell 8 is observed with a 2-stage relaxation for the CC case alone. However, the charge capacity of the cell, in this case, is found to be much lower than its C_{TH} (0.9 against 1.66 Ah, see Table 3.6). Therefore, it is difficult to confirm the occurrence of lithium plating as graphite phase changes can as well cause such a recovery. Besides, low capacity fade observed for these cells (numbered 6,7 and 8) when compared to other cells identified from the pre and post capacity tests (see Table 3.6) as well indicate they have experienced relatively low or no lithium plating at the 5 ^{o}C tests.

As seen in Table 3.7, $I_{critical}$ levels for the cells with different ageing levels are different. As cells undergo ageing, depending upon the degradation they encounter, their internal kinetics, and thus their lithium-plating tendency can vary. Therefore, the $I_{critical}$ level needs to be recalibrated as the cell ages to maximize the reversible lithium plating available for detection in post-charge conditions.

Table 3.7: Stripping periods with different cut-off currents. Case with the maximum stripping period is highlighted with blue colour for each cell.

Cell number	τ_{cc}	τ_{1A}	$\tau_{0.75A}$	$\tau_{0.5A}$	$\tau_{0.25A}$	$\tau_{0.05A}$
1	511	1823	1990	**2105**	1760	0
2	0	1351	**1428**	1353	1020	0
3	0	1201	1205	**1217**	870	0
4	541	2114	**2253**	2170	1854	0
5	0	740	1370	**1420**	1415	0
9	0	**655**	519	0	0	0

On the other hand, it is interesting to note that the range of the $I_{critical}$ lies between 0.5 and 1 A irrespective of the cell ageing condition at the selected temperature as seen in Table 3.7. This may indicate that use of 0.75 A as cut-off current may facilitate lithium plating detection over the cycles.

3.5 Implications for fast-charge strategies development

The results show that the improved and validated VRP method enhances the detection sensitivity and provides a definitive confirmation of lithium plating occurrence. However, it faces a challenge in detecting lithium plating when the stripping period is lower than circa 500 s (see Figure 3.13) potentially at high temperatures due to increased stripping rate or low lithium plating level as both the stages of recovery merge. Nevertheless, it is still useful for practical applications and research studies in the following aspects given there exists multiple challenges with the other approaches as highlighted in Table 2.1.

1. As EVs are expected to operate in a wide range of ambient temperatures (> 0 ^{o}C), it is essential to avoid lithium plating irrespective of the operating conditions [25, 78]. The improved method helps to study lithium plating in commercial cells and identifies a charge profile that minimizes lithium plating in batteries, particularly for low-temperature applications where lithium depositions can be higher than the minimum detectable level (2.5% of the cell capacity). Chapter 4 presents a procedure based on the VRP method to identify the optimal charge profile for the selected commercial cell.
2. Given its ability to detect lithium plating cycle-by-cycle and dependency on the cell voltage, the improved VRP method can be used to validate any future detection method non-invasively. Chapter 6 presents one such application for a new method proposed.

3.6 Limitations and future work

The half-cell level studies indicate that the two-stage relaxation infers the occurrence of lithium plating if the average lithiation of the NE at the EoC crosses 57%. On the other hand, it is difficult to identify the source of the two-stage recovery when the average lithiation is less than 57%. Therefore, the VRP method application shall be limited to charging events that lithiated the NE above 57%.

The $I_{critical}$ for the CV phase identified at a particular temperature can vary with temperature and C-rate as kinetics within the cell change. Therefore, to study the $I_{critical}$ at different temperatures and C-rate, a separate study is required. By identifying the $I_{critical}$ for cases where lithium plating levels are low, the VRP method may detect lithium plating even at room temperatures.

3.7 Conclusions

Non-invasive approaches of lithium plating detection assume significance as they allow detection cycle-by-cycle. To improve these methods as stated by objective 2 in Section 2.4, the study is conducted in two parts. First, the influence of the CV phase of charging on the detection ability of these methods is studied. The experimental results indicate that the CV phase cut-off current influences the accuracy of these methods. The reversible part of the plated lithium can start stripping in the CV phase if the cut-off current is too small, which reduces the detection sensitivity at the subsequent relaxation phase. Therefore, the charging process can be ended before the start of lithium stripping to improve the detection. The optimal cut-off current in the CV phase is identified experimentally to maximize the plating detection sensitivity.

Second, the influence of the graphite phase changes on the VRP approach is studied. The VRP method can be applied in real-time as it depends on the voltage profile obtained in the post-charge relaxation. A two-stage relaxation in the voltage profile is used to infer the presence of lithium plating in the previous charging event. The lithium plating studies with graphite half-cells give insights into the phase changes of the graphite electrode in the post-charge relaxation, its dependence on the electrode lithiation levels, and its possible impact on the reversible lithium plating detection using the VRP method. The careful examination on the interplay of these factors results in the inference that the 2-stage relaxation behaviour does not always come from the lithium plating. The required distinction between the graphite phase change and the plating induced phase change is established with the SOC (or lithiation) of the electrode. To identify the critical SOC level of the NE over which 2-stage relaxation does come from lithium plating, the cell level dV/dQ analysis is employed.

The improved and validated VRP method is useful for improving plating detection capability non-invasively and developing optimal fast charge profiles that improve the charging speed while reducing plating as demonstrated in Chapter 4.

4 Study 2- The Development of Optimal Charging Strategies

4.1 Introduction

Several studies have been reported within the literature the need to address the challenge of reducing lithium plating for lithium-ion batteries as detailed in Section 2.4. As electrochemical model-based approaches still face multiple research challenges in terms of their accuracy, implementation in a BMS and adaptability to battery degradation [26, 67], experimental means to identify a charge profile that minimizes the charging time and lithium plating, are of great interest [5, 10]. To meet research objective 4, two different approaches are proposed to develop optimal charging profiles for offline and online use using the existing methods of lithium plating detection.

The offline charging profile is derived using the CE method. The CE method can be employed to identify the optimum C-rate for the CC-CV profile [70]. However, the use of the optimum CC-CV charge profile does not minimize the charging time although it can avoid lithium plating as detailed in Section 2.4. To improve the charging speed further from the optimum CC-CV profile, the CC phase can be replaced by a multi-stage charge profile. A feasible solution is to (1) apply a high-rate CC charge until the cell terminal voltage has reached a pre-defined level (defined as $V_{HCC\text{-}end}$) lower than the full charge terminating voltage (V_f) and then, (2) reduce CC charge rate to reach the V_f. However, the selection of $V_{HCC\text{-}end}$ is critical since the use of a lower value for $V_{HCC\text{-}end}$ compared to the cell voltage (referred to as V_{tc}) at which the NEP drops below the reference prolongs the charging time unnecessarily, and a higher value fails to avoid lithium plating completely. Therefore, for the proper selection of $V_{HCC\text{-}end}$, it is necessary to identify V_{tc}. The occurrence of lithium plating is inferred by measuring the CE after every charge cycle to regulate the $V_{HCC\text{-}end}$ in such a way that it approaches the unknown V_{tc} where CE begins to drop as lithium plating begins to occur. The resulting $V_{HCC\text{-}end}$ is then used for cell optimal charging. The pre-identified charge profile using the CE approach can be applied to EV batteries.

The online charging profile that can adapt to battery ageing is derived using the VRP method. Given the high accuracy needs of the CE approach, its implementation for online use is limited. Therefore, a different approach implementable in a BMS to modify the charge profile according to the operating conditions is required. Within the non-invasive methods such as tomography [28], impedance spectroscopy [74], DVC [26, 76] and VRP [28, 74], the VRP has the potential for deployment within real-time charge control applications because it relies only on the cell terminal voltage measured in

post-charge relaxation. Therefore, the VRP method is proposed to identify the V_{tc} and thus to derive the two-stage CC charge profile. To facilitate comparison, results are presented for cells charged with the proposed charging profiles along with the traditional CC-CV charge profile.

This chapter is structured as follows. The research methodology associated with the development of modified charge control strategies underpinned by lithium plating detection and the CE is presented in Section 4.3. In Section 4.4, the experimental plan and experimental setup are introduced. Section 4.5 presents the experimental results that demonstrate the effectiveness of the new charge profiles when compared to conventional battery charge methods. The application and limitations of the study within the context of BMS operation are discussed in Sections 4.6 and 4.7, respectively. The main conclusions of this study are presented in Section 4.8.

4.2 Objectives of this study

The main objective of this study is:

- Develop a procedure to derive multi-stage charge profiles using the VRP and CE method
- Verify the performance of the proposed approaches in comparison to the standard CC-CV profile

4.3 Methodology

In this work, a three-stage (CC-CV-CC) charge protocol is derived to reduce lithium plating and therefore plating induced battery degradation while concurrently minimizing the charge profile impact on the charging time. Two methods are introduced that both employ the same three-stage, CC-CV-CC, charge profile. The primary difference between their implementation is the method used to regulate and optimize the terminating voltage level of the first stage CC, $V_{HCC\text{-}end}$. Detection of lithium plating and thus regulation of $V_{HCC\text{-}end}$ is achieved using either a measure of τ derived from the VRP method (discussed in Section 4.3.2) or from a direct estimate of CE per cycle defined as ΔSOH/cycle (discussed further in Section 4.3.3). Where the state of health (SOH) is defined as the ratio of the measured capacity vs the nominal value when the cell was new. Figure *4.1* shows a generalised block diagram representation for the proposed charge control strategy online implementation that would underpin its application within a BMS. Since a standard BMS monitors the cell voltage and tracks the SOH changes, both these approaches can be incorporated into the BMS that updates the charger with the latest $V_{HCC-end}$ for the next charge event. Development and Implementation of both the charge profiles are detailed in sections 4.3.2 and 4.3.3.

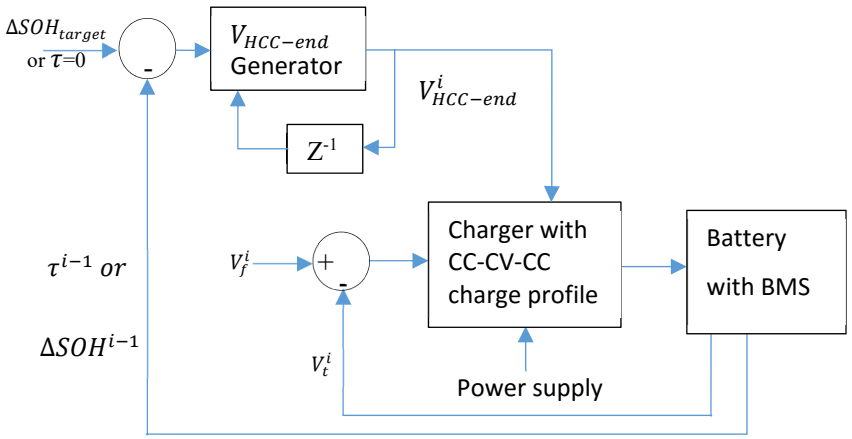

Figure 4.1: Online charging control proposition

4.3.1 CC-CV-CC Charge Profile Development

Figure 4.2 presents a comparison of the proposed CC-CV-CC protocol with the conventional CC-CV charge profile. In the CC-CV-CC profile, the first CC phase is applied until the cell voltage reaches V_{tc}. In this study, 1C charge rate is employed in the first CC stage. The CV phase is applied once the terminal voltage equals V_{tc} avoiding the NEP reducing below the reference value and therefore the onset of plating [5]. This is in contrast to the traditional CC-CV process in which the CC phase is maintained until, or close to 4.2V and the NEP reduces below the reference value at a time of 1800 s. The CV phase is maintained until the value of the charge rate falls to 0.25C. To avoid lithium plating and to improve charge time, the charge current in the third stage must be appropriately selected. From Chapter 3, for this cell, it was found that lithium plating was not detected with charge rates lower than 0.25C at ambient temperatures above 5°C and reversible plating detection ability was maximum with a cut-off charge rate of 0.25C. As discussed in Chapter 3, lithium stripping begins in the CV phase itself if the CV cut-off charge rate is below 0.25C that reduce the stripping lithium amount in the rest period and thus, the detection ability of reversible plating using the VRP method comes down. Therefore, the CV phase is maintained until the charge rate reduces to 0.25C and then the constant 0.25C charge rate is maintained until the cell voltage measures 4.2 V. Hence, the proposed charge profile becomes 1C-CV-0.25C as shown in Figure 4.2.

It is noteworthy, that as discussed within [75], the value of V_{tc} will vary as the cell ages and other degradation mechanisms impact the overall capacity and impedance of the cell. As a result, the value of V_{tc} must be re-evaluated during the operational life of the battery.

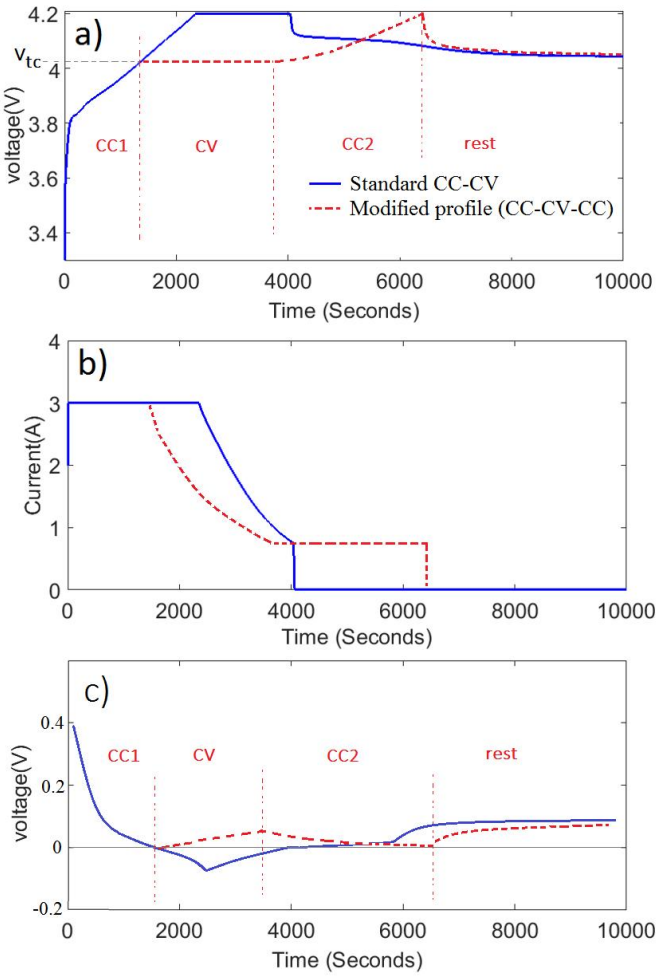

Figure 4.2: Proposed 3-stage and the conventional CC-CV charge protocol: a) cell voltage b) charge current and c) indicative negative electrode potential

4.3.2 Plating Detection-Based Charging Control Strategy

To identify the correct value of $V_{tc,}$ the VRP method is employed to detect the occurrence of reversible lithium plating within the proceeding charge event. Within the context of this experiment, V_{tc} is assumed to be unknown at the start. As a result, the CV phase voltage or the high rate first stage CC terminating voltage ($V_{HCC\text{-}end}$) can commence from a fixed value during the first cycle. In this study, $V_{HCC\text{-}end}$ for the first cycle is set to be 4.2 V. If lithium plating is detected after the first battery charge event it implies that the value of $V_{HCC\text{-}end}$ is greater than $V_{tc.}$ The value of $V_{HCC\text{-}end}$ is therefore reduced by an amount equal to ΔV for the next charge event. Conversely, in the case when lithium plating is not detected, $V_{HCC\text{-}end}$ can be increased by ΔV for the next charge cycle (while maintaining the upper and lower limits for cell voltage defined by the manufacturer). This adjustment to $V_{HCC\text{-}end}$ continues at

the end of each fast charge event until $V_{HCC\text{-}end}$ reaches the target value V_{tc} as depicted in Figure 4.3a. The selection of the voltage step size (ΔV) is detailed in the next section.

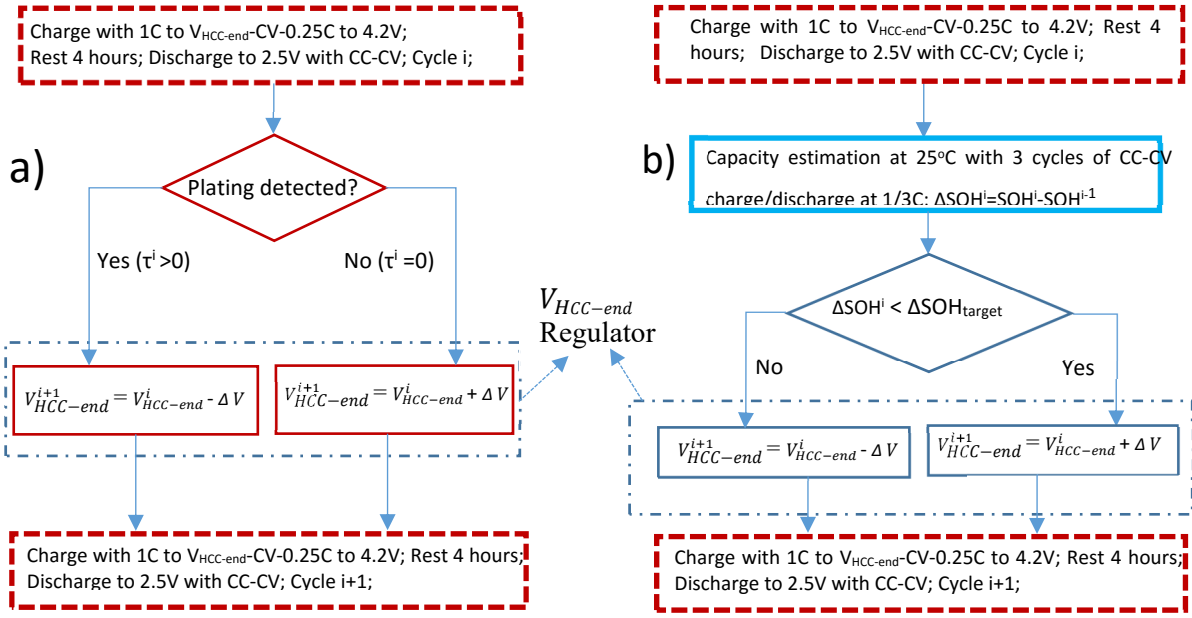

Figure 4.3: Flowchart for charging control using a) plating detection and b) CE

4.3.3 CE-Based Charge Control Strategy

In this technique, the value of $V_{HCC\text{-}end}$ is determined using the estimated capacity reduction per charge cycle to minimise battery degradation. It is noteworthy that this technique employs overall capacity fade as the control variable and therefore considers other battery degradation mechanisms that may occur, such as SEI formation, when the cell is under charge. To facilitate CE-based charge control, the target value of capacity reduction per cycle, defined as ΔSOH_{target} needs to be defined. Obviously, the lower the ΔSOH_{target} is set, then conceptually the longer the battery life, but with the implication that charge times will become excessively long. Generally, when lithium-ion cells are continually cycled at low charge/discharge rates (e.g. less than 0.25C) and ambient temperature, after the initial few cycles, the battery will exhibit an almost linear capacity fade [14] for much of its operational life. The ΔSOH_{target} can be defined based on this linear capacity reduction rate. The ΔSOH_{target} in this work is selected based on the previous low-temperature battery cycling results, reported within Chapter 3. A maximum of circa 10% capacity loss in ten cycles at 5°C and 1C charge/discharge rate with the CC-CV charging protocol is observed as shown in Table 3.6. This equates to a 1% ΔSOH per complete charge cycle. Therefore, by setting ΔSOH equal to 0.1%, the assumption is made that this would, in principle, extend the life of the cell by a factor of 10. On this basis, if the ΔSOH/cycle in the current cycle is higher than ΔSOH_{target}, $V_{HCC\text{-}end}$ is decreased by ΔV for the next cycle as depicted in Figure 4.3b. In this approach, an accurate estimate of ΔSOH and therefore cell capacity measurement is necessary. To measure a ΔSOH/cycle value of 0.1% with a relative error of ± 5%, the current

measurement accuracy must be in the order of ± 0.005%. An alternative approach is not to calculate ΔSOH after each charging event. For example, if the capacity is measured once in five charge cycles, a 0.5% ΔSOH change can be measured using a ± 0.025% accurate current sensor. This yields an average ΔSOH/cycle between 0.095 and 0.105% which meets the target requirement of 0.005% accuracy. However, the consequence of this hardware limitation is that $V_{HCC\text{-}end}$ is regulated only once in five cycles instead of cycle-by-cycle and therefore the cell may be subject to extended periods of degradation.

4.4 Experimental Approach

Three cells for each charge method (CC-CV; CC-CV-CC VRP based charge control and CC-CV-CC ΔSOH based charge control) are used. As shown in Table 4.1, nine cells are therefore employed during the experimentation to minimise the effects of cell-to-cell variations on the experimental results. For ease of reporting, the cells are classified as being within one of three groups: A, B or C with individual cell markings, for example, C_{A1}, C_{A2}, C_{A3} define the three cells within Group A.

Table 4.1: Test cases and cell requirements

Charge protocol	Cells used (group: cell marking)
Conventional CC-CV	Three new cells (A: C_{A1}, C_{A2}, C_{A3})
VRP based charging control	Three new cells (B: C_{B1}, C_{B2}, C_{B3})
CE or ΔSOH based charging control	Three new cells (C: C_{C1}, C_{C2}, C_{C3})

4.4.1 Experimental setup

All experiments are performed inside a thermal chamber (Model: ESPEC PL-3KPH), with the cells electrically loaded using a Maccor cell cycler (Model: Series 4000). The Maccor unit enables the measurement of the cell voltage and current with an accuracy of ± 1 mV and ± 0.6 mA respectively. In addition, K-type thermocouples with an accuracy of ± 1.5°C are attached to the negative tab of each cell to measure the cell surface temperature. The test parameters are summarised in Table 4.2.

Table 4.2: Measurement parameters and their range and accuracies

Measuring parameter	Measurement range	accuracy	Resolution	Sampling time
Voltage	2.5 to 4.2 V	+/- 1 mV	0.1 mV	0.1 s
Current	+3 to -3 A	+/- 0.02%	0.030 mA	0.1 s
Temperature	0 to 30 ^{o}C	+/- 1.5 ^{o}C	0.01 ^{o}C	1 s

Similar to Study 1, the cells are installed within a manifold and liquid surface cooling used to maintain cell temperature at the desired value using a LAUDA controller (Model: Proline RP 845 C) with the

ability to regulate temperature to an accuracy of ± 0.1 °C. As observed in this work, irrespective of the operating conditions, the surface temperature of these cells are maintained at the set temperature within ±0.5 °C with the active cooling mechanism.

4.4.2 Experimental Procedure

Figure 4.4 presents the procedure for cell experiments using the three different charge control strategies. The experiments comprised of three stages:

- Cell Pre-Conditioning,
- Fast Charge tests, and
- Capacity Characterization

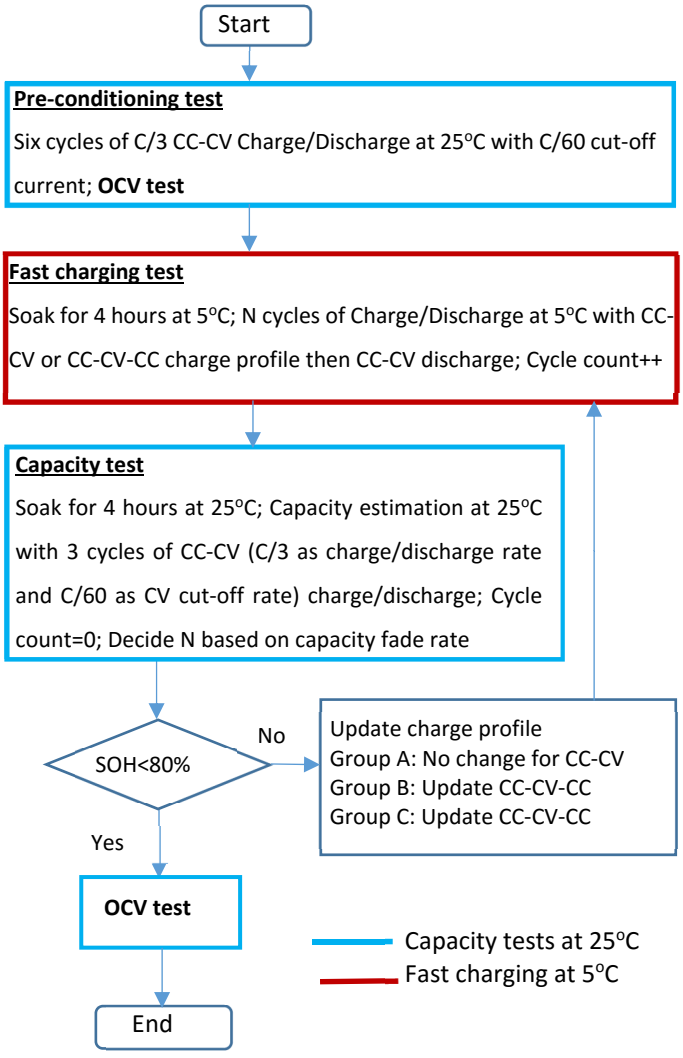

Figure 4.4: Procedure for experiments with cell charging

4.4.2.1 Cell Pre-Conditioning Tests

Side reactions between the electrolyte and electrode surface are known to form an SEI layer over the negative electrode which leads to cell capacity reduction as discussed in Section 3.3.1.3. The side reactions that lead to the SEI growth reduce within the first few cycles as the SEI thickness increases [29]. Consequently, this slows the growth rate of the SEI layer and thus the capacity reduction within the cell. To minimise the contribution of the SEI layer growth to the ΔSOH/cycle estimation, all nine cells irrespective of their charge protocol are cycled six times at 25 ^{o}C with CC-CV (CC charge/discharge rate of 1/3C and CV cut-off charge/discharge rate of C/60). The CV during discharge in both preconditioning and capacity estimation tests is included in this work to alleviate the impact of impedance on the measured capacity of the cell as detailed in Section 3.4.1.1. After the preconditioning tests, the cells are tested for OCV whose test procedure and application is detailed in Chapter 5. Once the pre-conditioning and OCV tests are completed, the cells are then deemed ready for fast charge experiments and further capacity characterisation.

4.4.2.2 Fast charging cycle tests

To provoke lithium plating and to enable its control, the cells are cycled at low temperature with high charge currents. The cells are allowed to soak for 4 hours at a temperature of 5 ^{o}C before performing the fast charging tests to ensure that they have reached thermal equilibrium. For all cells, a high charging current of 3 A (1C rate) is applied in the first CC phase and the charge is terminated when the cell voltage reached 4.2 V with 0.75 A (0.25C) current in the final stage. However, the current profile between these two values is varied based on the charge control strategy adopted.

- For the traditional CC-CV charge protocol; the 1C charge rate is applied until the cell voltage reached 4.2 V and then the CV phase was maintained at 4.2 V until the charge rate reduced to 0.25C.

- For the ΔSOH charge protocol; the 1C charge rate was applied during the first stage CC phase until the cell voltage reaches $V_{HCC\text{-}end.}$ CV charging was then maintained until the charge rate dropped to 0.25C. The 0.25C value was maintained until the cell voltage reached 4.2 V. Identification of $V_{HCC\text{-}end}$ was based on the method defined in Section 4.3.3.

- For the Plating Detection Charge Protocol; the same 1C charge rate was applied during the first stage CC phase until the cell voltage reached $V_{HCC\text{-}end.}$ CV charging is again maintained until the charge rate reduces to 0.25C. The 0.25C value is maintained until the cell voltage reached 4.2 V. However, the identification of $V_{HCC\text{-}end}$ is based on the VRP method described in Section 4.3.2.

For all conditions, once charging has ceased (cell voltage equal to 4.2 V with a 0.25C/h charge current), a rest period of 4 h is allowed to monitor cell voltage and temperature and to allow the cells to equilibrate. After 4 h, the cells were discharged to 2.5 V with CC-CV (using a CC discharge rate of C/3 and a CV cut-off discharge rate of C/20) to complete one fast charge cycle.

4.4.2.3 Capacity characterization tests

To support derivation of the ΔSOH cycle-based charge profile development, the fast charging profiles are interrupted and the temperature of the cells raised to 25 ^{o}C and left to rest for 4 hours. The number of fast-charge cycles (defined as N) between capacity tests is varied according to the measured rate of capacity fade. Adjustment of N helps in two ways. Firstly, a low value of N when the capacity fade rate is deemed to be high (e.g. greater than 0.5%) permits a faster intervention in the charge profile to reduce the magnitude of battery degradation. Secondly, a higher value for N when the capacity fade rate is slow (e.g. less than 0.1%) reduces the overall test period. As seen in Table 3.6, the rate of capacity reduction was comparatively high during the early cycles and then slowed as the level of battery degradation increases. Hence, for the first four fast-charging cycles, the capacity test is performed after each fast charge cycle (N=1). The capacity assessment is then undertaken every three cycles (from 5th to 13th fast charge cycles) and after six fast-charge cycles, from that point onwards. Table 4.3 summarises the frequency variation of capacity tests with cycle number during the ΔSOH cycle-based charge profile development.

Table 4.3: capacity test interruption to the fast charging cycles

The fast Charging cycle number	Capacity test frequency
1 to 4	After every fast charging cycle
5 to 13	Once per 3 fast charging cycles
14 to 52	Once per 6 fast charging cycles

To facilitate comparison, all capacity tests used a CC-CV profile with C/3 charge/discharge rate in the CC phase and a cut-off charge/discharge rate of C/60 in the CV phase at 4.2 V and 2.5 V for both charge and discharge respectively. Further, all the cells are tested for capacity at the same intervals of fast charging cycles for a better comparison of results since the capacity estimation procedure that interrupts the ageing tests has a significant influence on battery life [97].

In the capacity test, when the capacity retention level measured is found to be greater than 80% of the initial capacity for all cells, the cells are subject to a further set of fast-charging tests as shown in Figure 4.4. While the fast charge profile is unaltered for the cells loaded with the traditional CC-CV protocol, $V_{HCC\text{-}end}$ values are updated for the cells from sets B and C (from Table 4.3). As discussed, for

the cells from set B, the charge profile is updated based on the level of lithium plating detected in the last fast charging cycle. Here, the step-change (ΔV) was set to 100 mV in the initial cycles until lithium plating is detected and then it is reduced by 25 mV to further fine-tune the desired value of $V_{HCC\text{-}end}$. For cells from Set C, the charge profile is updated based on the capacity tests at 25 ^{o}C and the ΔV value is initially set to 50 mV until the ΔSOH/cycle reached the ΔSOH_{target} of 0.1% and then it is reduced to 25 mV to further fine-tune the transition point between the CC-CV phase of battery charging.

4.5 Results and discussions

4.5.1 Results

4.5.1.1 Conditioning Tests

The preconditioning tests are undertaken at ambient temperature to reduce the impact of the SEI layer growth rate on the fast charging experimental results. By the sixth cycle, the magnitude of capacity change per cycle is asymptotically stable in terms of capacity retention with less than 0.03% change in capacity reduction per cycle. The value of cell capacity measured at the 6th cycle is taken as the cell initial capacity prior to the fast-charge cycles. For completeness, Table 4.4 presents the actual values of capacity measured for each cell at the end of the 6th conditioning cycle.

Table 4.4: Measured nominal capacity values for each cell under test, after 6 conditioning cycles

Cell Identifier	**Capacity after 6th Conditioning cycle (Ah)**
C_{A1}, C_{A2}, C_{A2}	3.151, 3.171, 3.167
C_{B1}, C_{B2}, C_{B2}	3.182, 3.169, 3.172
C_{C1}, C_{C2}, C_{C3},	3.174, 3.191, 3.168

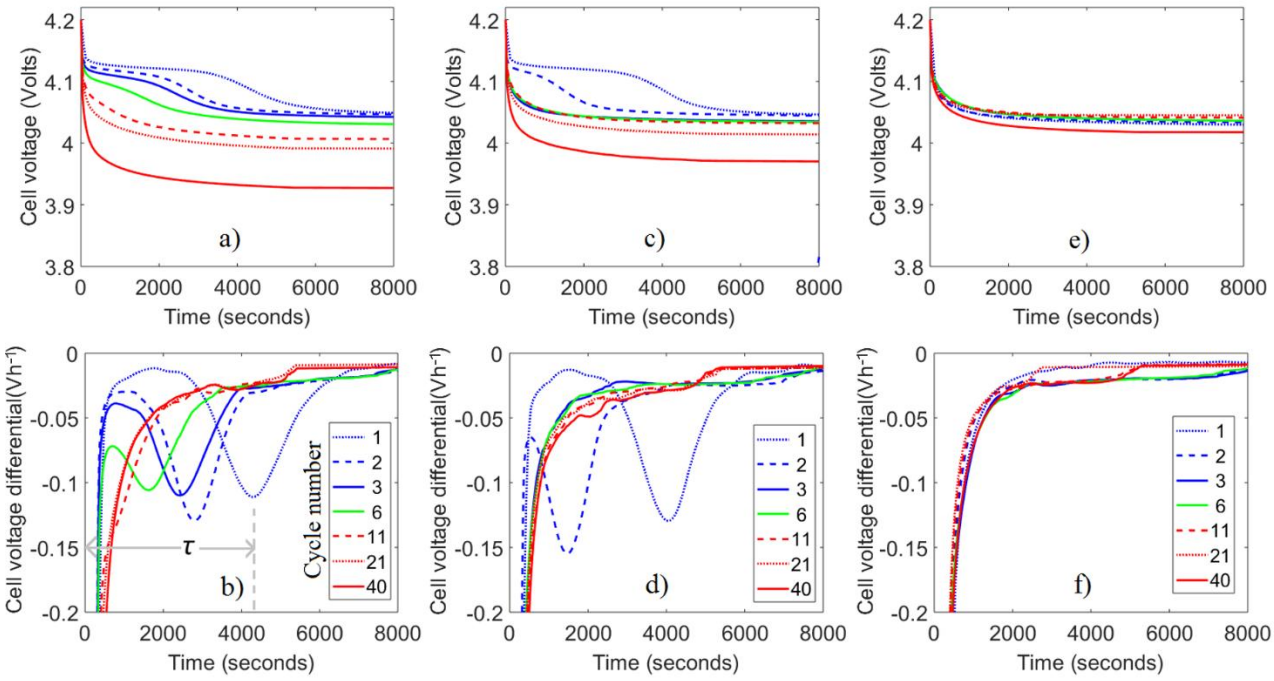

Figure 4.5: Reversible plating detection using cell voltage relaxation in rest period - Cells under CC-CV protocol a) cell voltage and b) its differential; Cells using plating detection-based charging protocol changing c) cell voltage and d) its differential; Cells using ΔSOH based charging protocol e) cell voltage and f) its differential at different fast charging cycles

4.5.1.2 Traditional CC-CV Charging Control

Set A cells are operated under the traditional CC-CV charge profile until they lost an average of 20% of their nominal capacity. In addition to capacity fade and charging time trends, these cells are also monitored for lithium plating occurrence using the VRP method with the help of a 4 h rest period at the end of every fast charge event. Figure 4.5a and Figure 4.5b present the post-charge voltage relaxation profiles and their differential respectively at different fast charging cycles. The onset of lithium plating can be observed and reversible plating decreasing with increasing cycle number. In the first cycle, the stripping period is found to be circa 4300 s, which reduced to 2800 s in the next charge cycle. Since, as discussed within [28], the stripping period is deemed to be in proportion to the amount of reversible plating, it can be assumed that reversible plating detection levels are equally reducing with cycle number. One possible reason is a loss of active lithium because of lithium plating can reduce the NE lithiation levels towards the end of a charge, and thus decreases lithium plating amounts with the increasing cycle number [26]. With further progress of fast charging cycles, no reversible plating is detected after the 11th fast charge cycle. To confirm the plating detection using the VRP method, one cell from each Set and one new cell for comparison are opened in an argon-filled glove box and the graphite electrodes are inspected visually for metallic depositions following a method described within [58]. Visible areas at the side edges of cell A are covered by silver colour depositions as shown in Figure 4.6a. These silver colour depositions are found to be lower for the Set B cell and much-

reduced levels for the Set C cell (see Figure 4.6b, c) compared to the Set A cell. Meanwhile, the graphite electrode of the new cell appears black as shown in Figure 4.6d, as is expected from a functional fully discharged graphite-based electrode. As discussed within [58], since the graphite electrode does not appear in silver colour at any of its lithiation levels, these depositions can be attributed to irreversible lithium plating. Therefore, cell A and cell C are exhibiting higher and smaller lithium metal depositions, respectively, which is in line with the lithium plating detection results using the VRP method as seen from Figure 4.5.

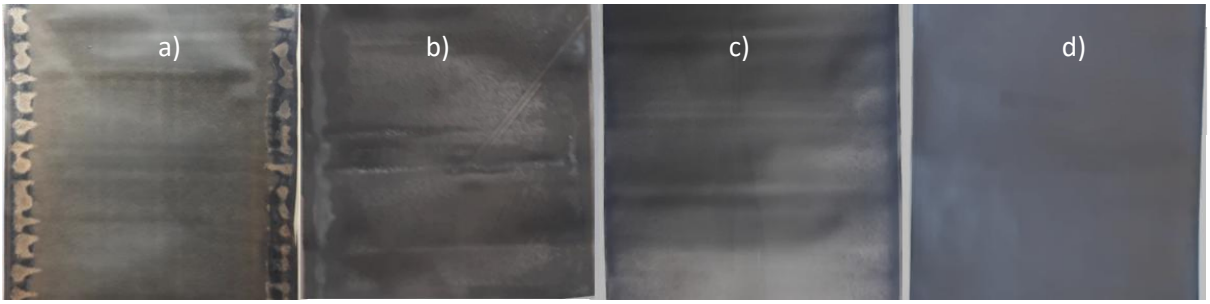

Figure 4.6: Photographs of graphite electrodes: a) Set A cell, b) Set B cell, c) Set C cell and d) new cell

4.5.1.3 Plating Detection-Based Charging Control

Similar to set A, in the first cycle where $V_{HCC\text{-}end}$ is predefined to 4.2 V, significant levels of lithium plating are observed using the VRP method in the cells contained within set B. Figure 4.5c, d shows the cell voltage and its differential respectively in the post-charge 4 h rest period. By employing the charge control method, $V_{HCC\text{-}end}$ is reduced to 4.1 V in the second cycle to reduce the level of plating occurring. Accordingly, the observed stripping period is reduced to 1250 s from 4100 s. Since lithium plating is still observed in this cycle, $V_{HCC\text{-}end}$ is further reduced by another 100 mV to 4.0 V for the third fast charge cycle. In the third cycle, no reversible plating is detected, indicating that V_{tc} is between 4.0 and 4.1 V. To further refine the estimate of the critical voltage where the NEP reduces below the reference value, $V_{HCC\text{-}end}$ is increased over the next fast-charge cycles in steps of 25 mV until the lithium plating is again detected. However, for these results plating is not identified in any subsequent fast charge cycle. This resulted in the rise of $V_{HCC\text{-}end}$ back to 4.2V. The drop in reversible plating detection levels with cycle number indicates that the reversible plating is either reducing or becoming too difficult to detect using the VRP method. The possible reasons for the detection failure using the VRP approach are further discussed in Section 4.7.2.

4.5.1.4 ΔSOH Based Charging Control

The CC-CV-CC charge protocol is applied for the ΔSOH-based charging control with the $V_{HCC\text{-}end}$ initially set to 3.9 V in the first cycle. Since the first four cycles are found with ΔSOH/cycle values lower than 0.1%, $V_{HCC\text{-}end}$ is increased in four steps from 3.9 V in the first cycle to 4.025 V in the fourth cycle as

shown in Figure 4.7. A further increase of $V_{HCC\text{-}end}$ to 4.05 V in the next three cycles (cycle 5, 6, 7) resulted in a rise of ΔSOH/cycle to circa 0.25%. To reduce the capacity reduction per cycle, $V_{HCC\text{-}end}$ is subsequently decreased to 4.025 V for the eighth cycle. This reduced the ΔSOH/cycle level to below the ΔSOH_{target} (0.1%). From this point, any rise of $V_{HCC\text{-}end}$ from 4.025 to 4.05 V consistently resulted in a ΔSOH/cycle value above the threshold of 0.1%. Figure 4.7 shows the variation of $V_{HCC\text{-}end}$ and capacity fade rate with cycle number. A $V_{HCC\text{-}end}$ value of 4.025 is seen as the optimum value to maintain the ΔSOH/cycle lower than 0.1%. The result also shows that reversible lithium plating is not observed (as per Figure 4.5e and Figure 4.5f) for the cells under this charging control strategy during any fast charge cycle. One reason for this may be because of the lower initial starting voltage of 3.9 V that is employed to transition the charging profile between the CC-CV phases.

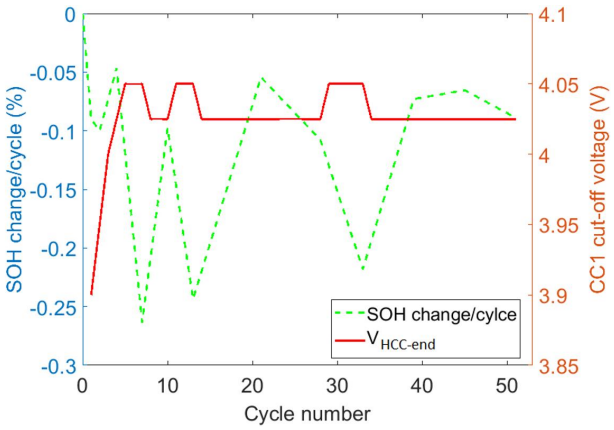

Figure 4.7: First stage CC end voltage and capacity fade with the cycle number for the ΔSOH based charge profile

4.5.1.5 Comparison of Results between the Three Charging Profiles

Figure 4.8 compares the performance of the cell sets (A, B and C) for the different fast charge strategies. The discussion is focused on the rate of capacity reduction due to fast charging each cell, the value of $V_{HCC\text{-}end}$ and the corresponding charge time.

a) Capacity Fade Analysis

From Figure 4.8a, it can be seen that battery life could be extended by employing the proposed fast charge control techniques. By using the plating detection-based method, the cells lost an average of 11% capacity compared to an average of 20% reduction for cells using the traditional CC-CV protocol. The reason for the large capacity reduction for the CC-CV charge protocol is the existence of lithium plating observed in the first ten cycles (see Figure 4.5b) and potential secondary effects of lithium plating accelerating the formation of SEI growth and changing the porosity in the electrode [66]. This is in contrast to the cells charged using the CC-CV-CC profile with the transition between the CC and CV phase governed by the plating detection-based control. The results show that reversible lithium

plating is only found in the first two fast charge cycles. This reaffirms the findings from [98] and the literature contained within [58, 99] that higher levels of plating lead to increased levels of capacity reduction and therefore must be avoided to prolong battery life.

With the ΔSOH-based charge strategy, the level of capacity reduction is further reduced for cells from set C, when compared to set A and B. The cells with the ΔSOH-based control lost only an average of 6% capacity after 52 cycles, compared to an average of 11% capacity reduction from set B cells. The reason for this is the maximum operated voltage in the ΔSOH-based control, $V_{HCC\text{-}end}$, is only 4.05 V. Low values of $V_{HCC\text{-}end}$ can benefit the cell in two ways. First, terminating the high CC stage at a lower cell voltage level can reduce or avoid lithium plating since the probability of occurrence of lithium-plating is higher at higher SOC or higher cell voltage levels [5, 6]. The experimental results show that reversible plating is not observed for the cells using the ΔSOH-based control method, which means that either lithium plating is completely avoided or reversible plating is below the detectable level using this technique. Besides, it can be hypothesised that the low level of $V_{HCC\text{-}end}$ voltage below 4.05 V could reduce other ageing mechanisms such as SEI growth or cycle induced mechanical stresses within the cell. Section 4.6 discusses these factors further within the context of overall battery degradation.

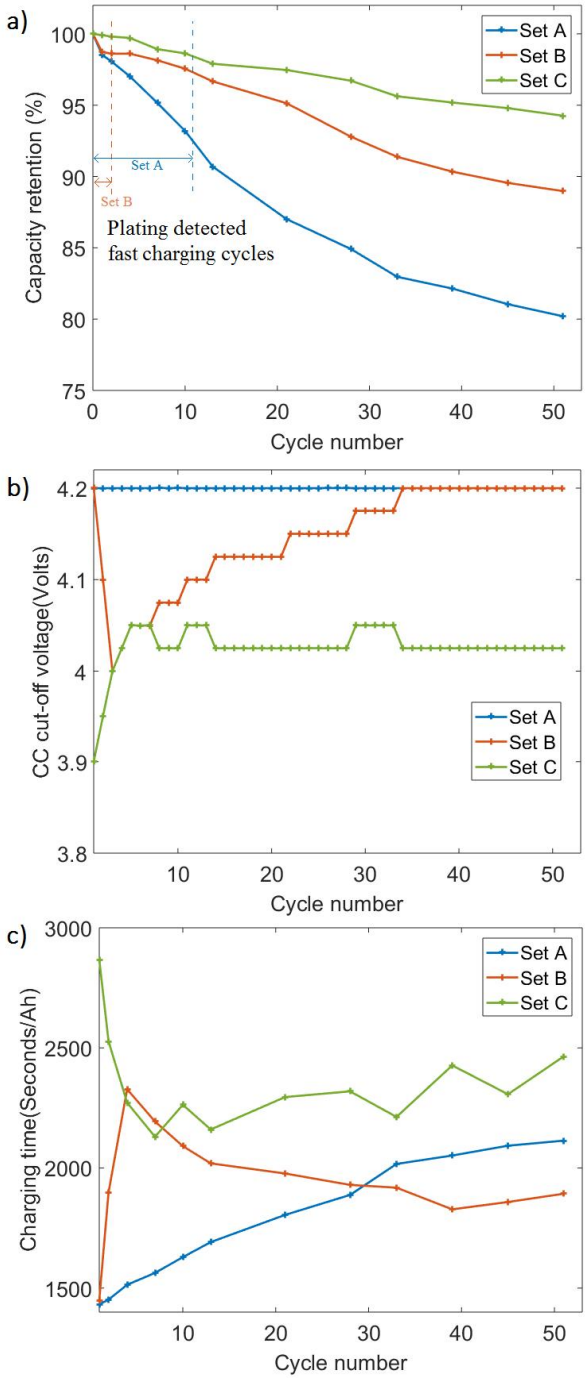

Figure 4.8: Comparison of the average cell performance using different charging control strategies: a) Charge retention, b) first stage CC end voltage value and c) charge time as a function of cycle number

Cells observed with lithium plating in the early cycles continued to lose higher levels of capacity in the later cycles where plating is not detected. For the cells from set A charged using the CC-CV profile, lithium plating is observed to occur until the fast charge cycle number 10 (Figure 4.5b). During the next 42 cycles, these cells lost 11% capacity where lithium plating is not detected (Figure 4.8a), which equates to an average capacity loss per cycle of 0.162%. Similar results are observed for the cells from set B that used the plating detection control method. For this case, lithium plating is not observed

after the first 2 cycles (Figure 4.5d). The cells proceeded to lose 9.2% capacity in the next 50 cycles where plating is not detected (Figure 4.8a), i.e. 0.184% loss per cycle. Conversely, lithium plating is never observed for the cells from set C that employed the ΔSOH control technique. For these cells only a 5.9% capacity reduction throughout the 52-cycles of fast charging (Figure 4.8a), i.e. 0.113% per cycle is experienced. This implies that the previous exposure to lithium plating for the cells may have a long-term negative impact on battery life and therefore cell SOH. As discussed in section 4.6, several possible reasons for this include: 1) the deposited lithium metals from the previous plating events may cause further battery degradation; or 2) the ability to detect lithium plating may be reducing with ongoing battery degradation, which fails to detect the occurrence of plating.

b) Charge Time Analysis

From Figure 4.8c, the cell charging time is normalised for improved ease of comparison. The normalized charging time is defined as the charging time per ampere-hour (time/Ah). From Figure 4.8c, the following observations can be made:

- The value of charging time is highly dependent on the duration of the first stage CC phase during fast charging when the charging current is high. Figure 4.8c shows the charging time variations over each cycle of the three charge profiles. For newer cells, the higher the $V_{HCC\text{-}end}$ threshold is, the longer the duration of the first stage CC phase is. As a result, the charging time overall is lower. For example, to charge one Ah capacity, the cells in set A ($V_{HCC\text{-}end}$ = 4.2 V) took only 1420 s while the cells in set C ($V_{HCC\text{-}end}$ = 3.9 V) took 2860 s, an increase of just over 100%.
- The impact of $V_{HCC\text{-}end}$ on the overall charge time could reduce with the value of capacity reduction. As seen in Figure 4.8c, the charging time for cells from set C, using ΔSOH based control protocol is 100% higher than the CC-CV protocol at the start of experimentation. This is improved to a value circa 20% higher than the CC-CV protocol towards the end of experimentation.
- More noticeably, it is found that plating-based charge control (set B cells) experienced an improvement in both charging time and battery life when compared to cells charged with the traditional CC-CV profile. Figure 8c shows that the value of charge time varied from 50% higher after the fifth cycle to 15% lower for the 50^{th} cycle. The key crossover point is the 30^{th} fast-charge cycle. This observation is highly significant because it implies that over time, the modified charging approach simultaneously yields reduced battery charge times and extends battery life. The reason for this is that the increased impedance associated with battery degradation reduces the CC phase charge time because of the increased potential drop. As a result, the charging speed of the CC-CV profile with the highest levels of degradation is significantly reduced in the end and the charging time difference between the CC-CV and proposed new charge profiles was reduced.

4.5.2 Discussion of Results

4.5.2.1 Large Reversible Plating Levels

As shown in [28], the minimum threshold for reversible plating detection for the selected cell at 0°C was around 2.5% of the nominal capacity using the VRP method. According to the authors, observable features from the cell terminal voltage are not identifiable when the reversible plating levels are lower than 2.5% [28]. This threshold level can increase with increasing ambient temperature because of the reverse reactions rate rise or the stripping time may reduce [76]. From Section 4.5.1.2, in the first cycle of set A test results, reversible plating was observed with a stripping period of circa 4300 s (Figure 4.5). The minimum stripping period identified from the results was about 800 s that was found after the 10^{th} cycle.

If an assumption is made that the 800 s stripping time corresponds to a reversible plating level at 2.5% of the charged capacity, as identified within [15], then the 4300 s stripping time found for the first cycle implies that circa 13.4% of the charged capacity could form part of the reversible plated lithium. From the experimental results shown in Figure 4.8a, the cells lost about 1.5% capacity after the first cycle. This further implies that irreversible plating was no more than 1.5% of the charged capacity. Therefore, the ratio between reversible and irreversible plating may be estimated as being 13.4%:1.5% or 8.96:1. This simplified analysis reinforces our assumption and that previously made within [26, 72] that lithium plating is largely reversible within new cells when they are charged.

4.5.2.2 Adaptive Charge Control

Unlike previous studies which derived the charging strategy off-line [5, 6], both the proposed methods of fast-charge control can be adapted to online use with the ability to adapt their behaviour as the overall degradation of the cell changes. This is because the identification of $V_{HCC\text{-}end}$ is based on the latest battery operation information and requires simply measurements of current and cell terminal voltage. As can be seen from Figure 4.5d and Figure 4.8b, $V_{HCC\text{-}end}$ for the plating control strategy reduced when the reversible plating is detected and then increased after the onset of reversible plating is no longer observed. This shows that lithium plating detection-based control has the potential to develop into an adaptive charge control strategy that can adjust the battery charging approach based on the real-time working conditions experienced by the cell. Similarly, the ΔSOH-based control approach relies on the measurement of the capacity fade of the current cycle to regulate the $V_{HCC\text{-}end}$ to control the capacity fade rate and therefore can also adapt to the battery ageing within a real-time control application.

4.6 Implications for fast-charge strategies development

Both the proposed non-destructive approaches are valuable in devising offline charge profiles for EV applications to avoid the onset of lithium plating. The research within this study focuses on a specific case where the charge rate and temperature were set to 1C and 5^{o}C respectively. This same methodology and test procedure can be more generalized to other working conditions to identify the optimal V_{tc} at the end of the first CC stage. For the 2nd stage CC current, a plating sensitivity analysis as described in Section 3.4 is necessary to identify the corresponding current at each temperature and fast charge current value. Once the offline characterization is completed, this model can then be used in a real-time application where $V_{HCC\text{-}end}$ is selected according to the operating conditions. This can help avoid large levels of lithium plating in the initial few cycles (as observed in set B cells in this work during the optimization of $V_{HCC\text{-}end}$) and thus, can extend battery life further compared to the performance of set B cells.

To take account of the VRP method's insensitivity to low levels of plating (below 2.5% of plating as discussed in [28]), an additional safety margin while selecting the $V_{HCC\text{-}end}$ can be considered to further guarantee the plating free charging event. For example, fast charging can be terminated 25 mV below the identified $V_{HCC\text{-}end}$.

While using the ΔSOH-based method for the development of offline charge profiles, the impact of interruption frequency of capacity tests on the capacity fade rate of fast charging cycles needs to be considered. As discussed within [97], increased interruption of fast charging cycles for capacity tests reduces the capacity fade rate. Therefore, to avoid a significant drop in the SOH level while identifying the V_{tc} at a selected SOH level, the capacity estimation test can be performed after every fast charging cycle. Further, for a fair comparison of different fast charging algorithms, the fast charging tests shall be designed such that all the battery cells in different groups undergo the same frequency of capacity characterization tests.

4.7 Limitations and future work

4.7.1 Online implementation

The proposed methods are based on onboard measurable parameters and their rate of change measured in real-time applications and can be, this way, integrated into a BMS for the development of dynamic charge profiles. However, there exist challenges towards the online implementation of these techniques that must be addressed.

The ΔSOH based charge control strategy can be extended to different types of lithium-ion cells irrespective of their format and chemistries since it is based on a direct measure of capacity fade. However, use of such a technique in real-time applications, particularly in EVs is difficult because of the high-accurate current measurement and regular operation of full charge-discharge requirements to estimate the retained capacity within the cell accurately. Future development of battery research may lead to an accurate online battery capacity estimation method that can meet the requirement for the ΔSOH based charging control, but until then, it can be employed for offline profile development.

For the VRP based method, two major challenges need to be addressed. First, the detection sensitivity of plating can drop as the battery ages [73], and thus the VRP method can fail to detect the occurrence of plating. As evidenced by the continued capacity losses even after lithium plating becomes undetectable in Set A and Set B cells, there is a possibility of battery ageing influence on the VRP method. The detection sensitivity of reversible lithium plating is highest if charging is terminated as soon as the NEP regains to a positive level [76, 98]. As presented in Chapter 3.4, cells with different ageing levels are found with different optimal cut-off currents in the CV phase ($I_{critical}$). As the range of the $I_{critical}$ is observed to be within 1 and 0.5 A (see), a fixed level of 0.75 A as the $I_{critical}$ is employed in this study through the cycles. However, tracking the $I_{critical}$ as the battery ages and terminating the CV at that level can improve the detection sensitivity. Further work is therefore required to study the detection sensitivity of the VRP method for different cell ageing levels for real-time use. In addition, new approaches either through experimentation or modelling may be required to improve the detection sensitivity in such a manner that is transferable to different cell technologies.

Second, since the VRP method depends on the relaxation in post-charge conditions, a further study is necessary to fully understand the usage patterns in real-time that might affect the periods immediately after battery charge. For example, charging the battery in fast-charging stations may not allow the cell to undergo the required relaxation. However, the usual end of day charging at home may provide sufficient time (> 1 h) to observe the voltages in relaxation. Therefore, further study is required to combine offline and online charge control strategies based on the charging patterns observed in real-time use.

The VRP method faces a challenge in detecting lithium plating at room temperature or higher as the amount of lithium plating reduces and lithium-stripping rate rises with increasing temperature [100]. Therefore, further study is necessary to develop a different approach to detect and control the occurrence of lithium plating to suit the wide range of operating temperatures.

4.7.2 Long-lasting impact of lithium plating

Charging strategies that aim to reduce lithium plating may fail to limit the degradation rate if lithium metal depositions from previous lithium plating continue to impact the battery performance negatively. As explained in [24], the plated lithium occupies nearly four times more volume than intercalated lithium within the electrode. Therefore, this may cause additional LAM in the electrodes in both cells from sets A and B which experienced plating. Previous work [26] assumes that lithium plating caused only an LLI while LAM rate was assumed to be constant over cycle number. However, as discussed in [24] and evidenced by the continued capacity losses even after lithium plating becomes undetectable in Set A and Set B cells, there is a possibility of increased mechanical stresses during and after charge cycles where lithium plating has occurred. This could be another potential reason for the continued capacity losses even after lithium plating becomes undetectable in Set A and Set B cells. Alternatively, the capacity loss can continue to be high if the ability to detect lithium-plating drops with ageing. Therefore, further study is necessary to better understand the limitations of the charging control strategies and the VRP method within cells that have experienced lithium plating at some point during their operational life by quantifying the degradation modes using differential voltage (DV) curves [26, 27]. Further, DV analysis along with an assessment of Coulombic efficiency (CE) [69] may help to understand whether plating becomes increasingly irreversible as the battery ages. For example, capacity imbalances between the electrodes and lithiation level of the NE at the end of charge may indicate the occurrence of lithium plating [26]. Reduced Coulombic efficiency and non-detection of reversible plating under potential plating conditions may highlight large levels of irreversible plating.

4.8 Conclusions

To meet objective 2 as defined in Chapter 2, a multi-stage (CC-CV-CC) charge profile using the existing approaches of lithium plating detection is proposed. A simple reduction of the first stage CC terminating voltage level ($V_{HCC\text{-}end}$) from the V_f (or 4.2 V) can reduce lithium plating. However, to minimize the impact of the modified charge profile on the charging time while concurrently avoiding lithium plating, identification of V_{tc} (or $V_{HCC\text{-}end}$ selection) is required. The V_{tc} is identified in two different approaches in this study. In the first approach, the VRP-method of lithium-plating detection is used to identify the V_{tc} where the NEP reduces below the Li\Li$^+$ reference value and defines the condition for lithium plating to occur. Unlike previous research, this approach enabled the identification of V_{tc} directly on commercial cells without modifications being required. This potentially makes the technique more suitable for practical implementation. The second method studied how a

measure of CE or overall battery capacity reduction per cycle, ΔSOH, can be used to identify the V_{tc} to minimise battery degradation.

Performance of the proposed charge profiles in terms of charging speed and capacity fade rate is compared with the standard CC-CV profile. From the experimental results obtained for the commercial NCA cell at 5^{o}C and 1C charge current, significant lithium plating is observed within the cells charged using the CC-CV charge protocol. Accordingly, the cells are found to have lost 20% of their nominal energy capacity over the 52 fast charge cycles. On the other hand, the capacity fade of cells using the proposed charging strategies is significantly reduced compared to when charged using the conventional CC-CV approach by 45 and 70% respectively, while concurrently achieving a charge time reduction of up to 10%.

The proposed CE based approach can be used for identifying the offline charge profile for practical applications. While the approach based on the VRP method is suitable for identifying the V_{tc} and adapting it to battery ageing, particularly for low temperature (< 20 ^{o}C) applications as the method still face many challenges in detecting lithium plating at high temperatures.

5 Study 3- A study on the influence of lithium plating on battery degradation

5.1 Introduction

Understanding the influence of lithium plating on battery degradation (research area 1) is essential to derive optimal charging strategies. From the existing literature, as presented in Chapter 2, there has not yet been a study conducted to quantify the degradation modes under the influence of fast charging or lithium plating. To meet research objective 1 defined in Chapter 2, this study proposes a degradation modes quantification procedure and quantifies the degradation modes of lithium plating with the support of experiments conducted at half-cell and full-cell level. From the half-cells, OCV profiles of the electrodes are obtained. Based on this information and the cell-level OCV profile, the lithiation levels at the end of charge (EoC) and the end of discharge (EoD) of the NE and PE are identified [27]. A procedure to quantify the degradation modes of a cell is proposed with the support of the lithiation levels obtained for the cell before and after fast charge cycle ageing.

The remainder of this chapter is organized as follows. Section 5.3 discusses the experimental stage of this research and presents the data acquired. Section 5.4 presents the methodology in quantifying battery degradation modes. The degradation modes estimated under the fast charging regime are presented and analysed in Section 5.5 by applying the methodology to the data acquired in Section 5.3. The application and limitations of the study within the context of EV are discussed in Sections 5.6 and 5.7, respectively. Overall conclusions of this research are given in the final section.

5.2 Objectives of this study

To study the impact of plating induced degradation and to simplify the degradation quantification procedure, the following objectives are defined for this study:

- To improve the degradation diagnostics model presented in [27] to simplify the quantification procedure of LLI, LAM_{NE} and LAM_{PE}
- To identify the degradation modes of a commercial cell aged under a fast charge regime and analyse the underlying degradation mechanisms.

5.3 Experimental

To quantify the LAM and LLI, measurement of OCVs of the half-cells (electrodes) and the full-cells is required. The experiments are then categorized into full-cell level and half-cell level tests. Degradation analysis is performed on the cells used in study 2 (Chapter 4). For this, OCV profiles of the cells captured before and after their fast-charge cycling are utilized here. For the half-cells, OCV profiles of the electrodes are obtained with the help of harvested electrodes from a pristine full-cell. The detailed setup, experimental procedure and the results for each are presented in the following sections. The experimental data collected in this section is used for the degradation analysis presented in Sections 5.4 and 5.5.

5.3.1 Full-cell experiments

Two test cases Set A and Set C that detected with and without lithium plating (referrer to Section 4.5), respectively are considered for the degradation analysis. As part of the experimental work presented in Chapter 4, the cells are tested for OCV before and after the fast charge cycles.

The OCV tests are performed at room temperature (25^{o}C) on the full-cells using the test procedure presented in Table 5.1. The cells are charged to 4.2 V with CC-CV (C/10 C-rate in the CC and 50 mA cut-off current in the CV) charge profile and rested for four hours before the OCV measurements are obtained on the following discharge. To capture a true OCV over the entire capacity range of the cells, the full cells are discharged incrementally following the GITT procedure defined in Section 3.3, in steps of 1/120 of the nominal capacity ($Q = Q_{nom}/120$), by applying small currents (C/20) and subsequently allowing the cell voltage to relax for one hour between pulses [85]. Here, Q_{nom} of the cell refers to the maximum capacity when the battery is completely charged. The OCV measurements are recorded at the end of each rest period. Figure 5.1a and b show the cell voltage and its OCV measurements for the given discharge current profile. The OCV profile as a function of capacity is then constructed as illustrated in Figure 5.1c.

Table 5.1: Full cell test procedure

Test sequence	Step no	Exp. Setup	Current/ voltage	Control limits
OCV test	1	Soak to 25°C	-	t>4h
	2	Constant current charge	C/10 current	V>4.2 V
	3	Constant voltage charge	4.2 V	I<C/60
	4	Rest	-	t>4 h
	5	Partial constant current discharge	C/20 current	$\Delta Q > Q_{nom}/120$
	6	Rest	-	t>1 h
	7	Repeat steps 5 & 6 until V limit reached	-	V<2.5 V

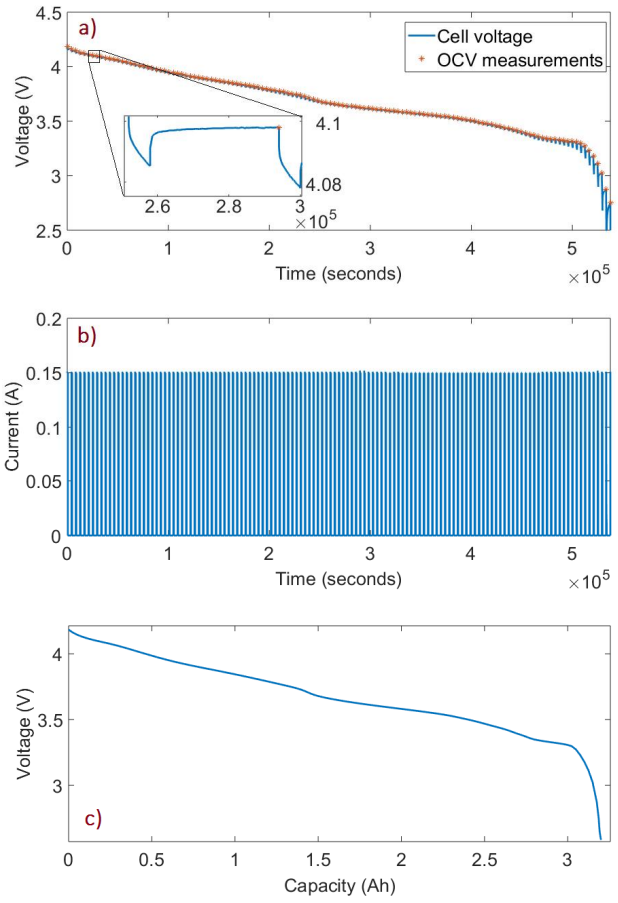

Figure 5.1: OCV measurement on cell A1 by incremental discharge and subsequent relaxation: a) Cell voltage and OCV measurements; b: Incremental discharge current; c: Cell OCV as a function of capacity.

Results of the ageing experiments from Chapter 4 as seen in Figure 4.5 and Figure 4.6 indicate that Cell A that lost 20% capacity is exhibiting at a much higher level of lithium plating compared to Cell C that lost 6% capacity in the same number of cycles. Further details for these cycle ageing tests can be found in Section 4.3. After the ageing tests, the cells are once again tested for the OCV profiles using the same procedure described in Table 5.1.

5.3.2 Half-cell experiments

To measure the OCV of each electrode, half-cells are prepared in a 2032 coin cell format using the electrode materials harvested from the fresh cell of the selected cell type. This new cell is fully discharged to 2.5 V with C/10 current. It is then opened in an argon atmosphere inside a closed glove box to access the jellyroll following the systematic procedure described in Figure 5.2. Next, the PE and NE samples (active material on the current collectors) are collected from the inner layers of the jellyroll since outer layers experience greater physical stresses during the cell opening process.

Six half-cell samples (03 NE-type units and 03 PE-type units) are prepared as described in [85] using a trilayer separator (Ø 19 mm and 25 µm thickness, Celgard® 2325) and LP50 (1 M $LiPF_6$ solved in EC: EMC with 3:7 volume ratios) electrolyte. The capacity of each cell is estimated based on the specific capacity of the electrode active material (PE: 180 ± 5 mAh/g, NE: 370 ± 5 mAh/g [11]) and its mass calculated from weights of the current collector with and without active material. The capacities of NE and PE half-cells are then theoretically found to be 7.5 ± 0.15 and 6.98 ± 0.16 mAh, respectively [11]. Based on these estimated capacities, the pre-conditioning test with C/10 charge/discharge currents is undertaken to measure the actual half-cell capacity.

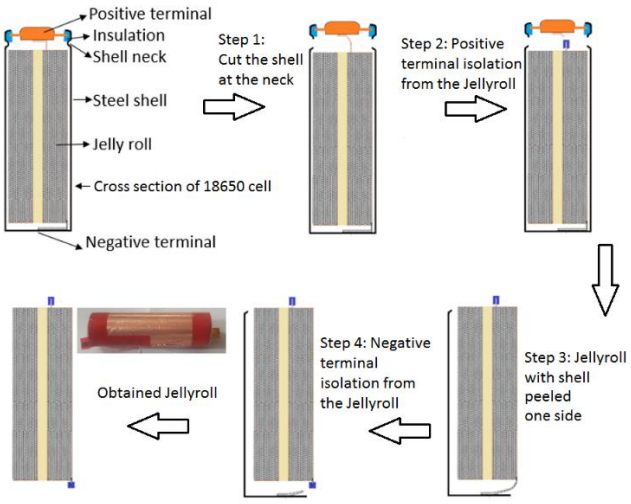

***Figure 5.2**: 18650 cell opening process illustration*

To support the half-cell OCV tests, Biologic BCS-805 potentiostats are employed and placed in a temperature-controlled room maintained at 25°C. The potential ranges for the tests are set to 0 to 1 V and 2.8 to 4.3 V, respectively. The selected voltage ranges can represent the full-cell OCV between 4.2 and 2.7 V [21] and could limit the electrode degradation during the OCV measurement [56, 101].

The half-cells are first pre-conditioned for 6 cycles with C/10 current prior to the OCV measurement. Figure 5.3 shows the voltage, current and capacity profiles of the NE in the preconditioning cycles. The result indicates that the PE half-cells are consistent with their delivered capacity with less than a 0.2% capacity fade/cycle. Conversely, the capacity change of NE half-cells is more than 0.5% in the first cycle and then reduced over the next cycles (below 0.2% in the sixth cycle). The average capacities delivered in the sixth preconditioning cycle by the NE and PE half-cells are measured to be 7.7 mAh and 7.1 mAh, respectively. A loading ration (LR = NE capacity/PE capacity = 7.7/7.1) of 1.08 indicates the NE half-cell has an 8% higher capacity than the PE half-cell [55].

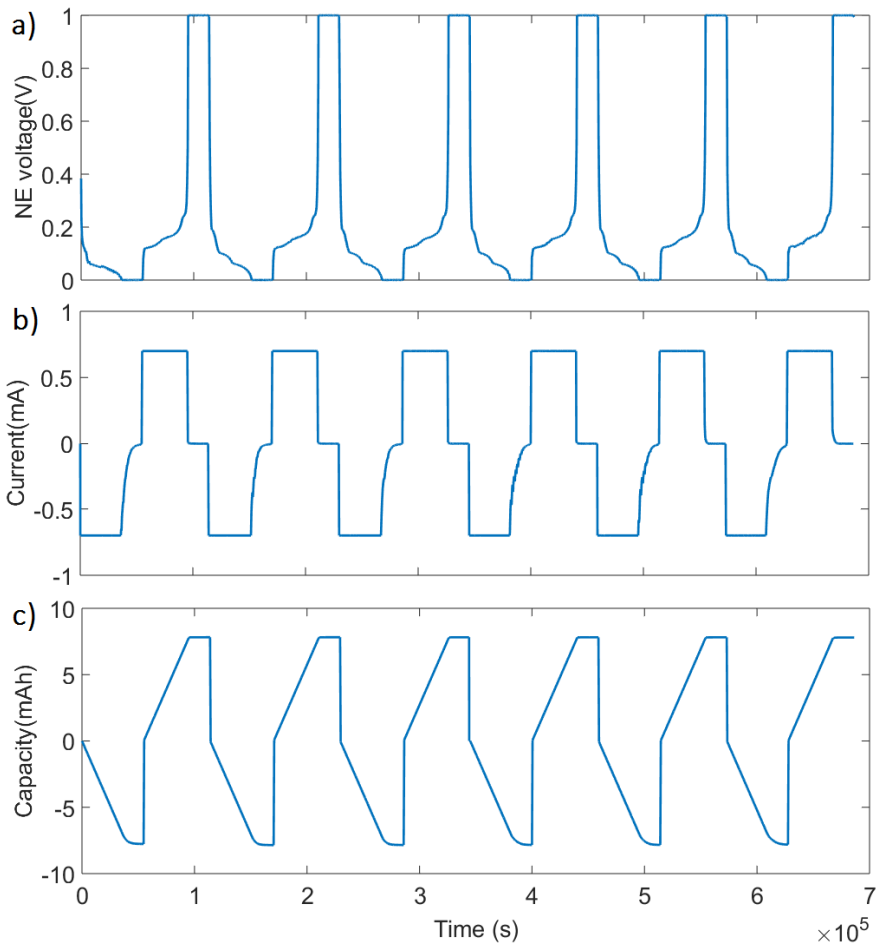

Figure 5.3: Half-cell preconditioning: a) voltage, b) current and c) capacity profiles measured on a NE half-cell. Positive currents and capacities indicate the discharge or delithiation of the electrode.

The half-cells were tested for OCV using the GITT procedure similar to the full-cell test procedure except for the voltage limits. For each NE or PE half-cell group, the root mean square error (RMSE) between any two OCV profiles measured is less than 1 mV. This confirms that the reliability of the OCV measurement method as well as the repeatability of the half-cell manufacturing process is acceptable. Figure 5.4 shows the OCV profiles as functions of normalized capacities delivered by the NE half-cells (between 0.03 and 0.8 V) and PE half-cells (between 4.3 and 3.35 V).

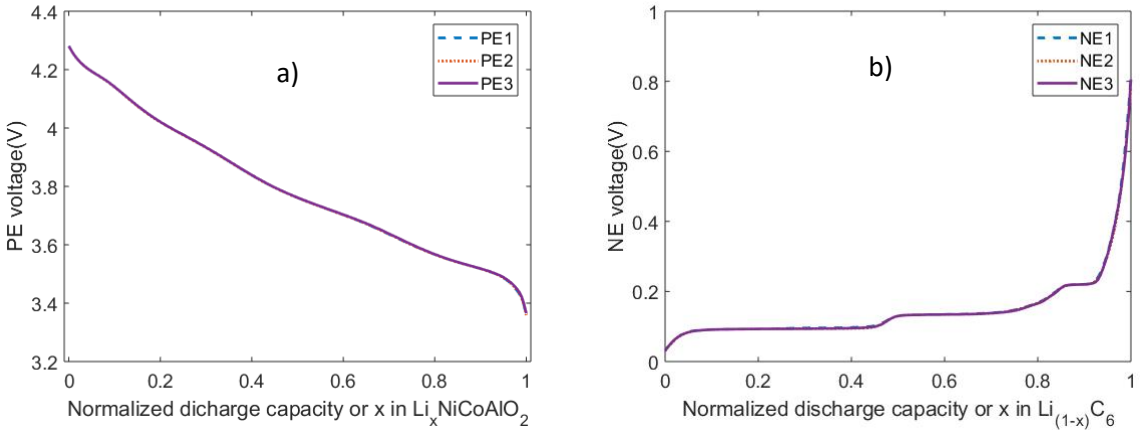

Figure 5.4: OCV as a function of the capacity and lithiation level of a) PE half-cells b) NE half-cells

The normalized capacity of an electrode can be expressed as the lithiation level (ratio of occupied to available lattice sites in a host structure, ranging from 0 to 1) since the capacity delivered by the electrode is proportional to its lithiation level [85]. As discussed within [27], to enable the degradation diagnostics, tested capacity range (or lithiation range) of the electrodes is normalized between 0 and 1. The relationship between half-cell OCVs and lithiation level can be described as shown in Figure 5.4 where x refers to the lithiation and delithiation levels of the PE and NE respectively.

5.4 Quantification procedure of LAM and LLI

LAM at an electrode reduces the available material for lithium intercalation and deintercalation, and thus decreases the electrode capacity [52, 55]. LLI due to parasitic reactions, such as SEI growth, lithium plating, etc. reduces the lithium inventory in a cell; accordingly, lowers the cyclable lithium between the electrodes. LLI or LAM affects the lithiation levels of the electrodes at the EoC and EoD and the capacity delivered between the EoC and EoD. This study presents the extensions of the previous work [27, 55] and quantifies the LAM and LLI from the lithiation levels of the electrodes rather than the lithiation level offsets.

For the quantification of LAM and LLI, the electrochemical behaviour of the electrode is assumed to be unchanged during the cell ageing, i.e., the OCV vs lithiation of the electrode remains the same.

Similar assumptions have been made within [21, 55]. With this assumption, the OCV profiles of the electrodes are captured by using the harvested electrodes from a new full-cell.

To quantify LLI and LAM between two ageing levels of a cell, identification of each electrode's lithiation range used at each ageing level is necessary. An approach to identify the used lithiation range by fitting the OCV of the full cell from the OCVs of the two electrodes is presented in Section 5.4.1. Next, the proposed quantification procedure of LAM and LLI using the identified lithiation use ranges of the electrodes is described in Section 5.4.2.

5.4.1 Cell OCV fitting

5.4.1.1 Identify the Cell OCV fitting range

The full cells are characterized, in terms of OCV between 4.2 and 2.5 V. However, in this work, the cell OCV range used for the degradation analysis is limited within 4.2 and 3.3 V. As shown in Figure 5.5a, the relaxation behaviour of the cell voltage is analysed by tracking its variation towards the end of the relaxation period to verify whether the selected one-hour relaxation period is sufficient for the battery to equilibrate resulting in the correct OCV measurements. When the OCV is above 3.3 V, the cell voltage changes in the last fifteen minutes of the rest period are well below 1 mV. This indicates that the battery has reached equilibrium and the OCV measurements are reliable. For OCV voltages below 3.3 V, the battery voltage change is still noticeable in the last 15 minutes of the 1-hour relaxation period, and thus the OCV measurement is less reliable. The reason for the insufficient 1 h relaxation time at lower SOCs can be explained by the anode overhang effect that deals with the lithium transfer between the active and passive parts of the anode as discussed within [102, 103]. Further, improved relaxation at lower SOCs for the aged cell compared to the new cell (Figure 5.5a) indicates that the effect of anode overhang reduces as the cell ages [104].

Considering the relaxation behaviour, cell voltage levels corresponding to the EoC and EoD are redefined as 4.2 and 3.3 V. Figure 5.5b shows that capacities delivered between these two limits for a cell (3.045 Ah against the total capacity of 3.196 Ah before the ageing tests and 2.46 Ah against the total capacity of 2.53 Ah after the ageing tests) represent more than 95% of the of total capacity.

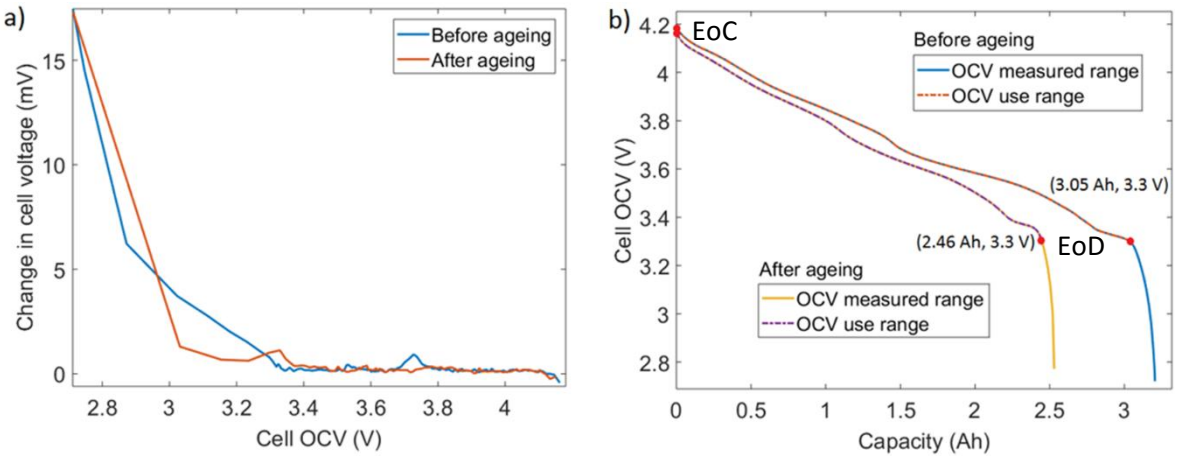

Figure 5.5: Full-cell OCV range selection: a) Change in cell voltage in the last fifteen minutes of the one-hour relaxation during OCV characterization; b) Cell OCV vs delivered capacity and the selected voltage range (between the two red dots) for cell A1.

The OCV profile against the delivered capacity between the EoC and EoD must be identified. At the full-cell level, OCV is measured (defined as E_{cell_meas}) in 120 equal intervals of capacity delivered (Q_{meas}), as shown earlier in Figure 5.1. Full cell capacity (Q_{max}) is the capacity delivered by the cell when discharged from 4.2V to 2.5V. The measured capacity vector and its corresponding OCV vector is represented as:

$$Q_{meas} = 0: Q_{max}/120: Qmax$$

$$E_{cell\_meas} = E_{cell\_meas,1}, E_{cell\_meas,2}\ldots., E_{cell\_meas,121}$$

where $E_{cell\_meas,i}$ is the OCV of the full cell at the measured capacity level $Q_{meas,i}$, i=1,2,…,121.

A curve fitting method based on Root Mean Square Error (RMSE) and spline is applied to this measurement to represent E_{cell_meas} as a function of Q_{meas} as shown in equation (5.1). The fitness using this function is less than 0.1 mV.

$$E_{cell\_meas} = f_1(Q_{meas}) \quad (5.1)$$

Since the OCV profiles between 4.2 and 3.3V are of interest for the analysis in this work, the capacity delivered (Q_{max_use}) by the time the cell OCV reduced to 3.3 V is identified using equation (5.2).

$$Q_{max\_use} = f_1^{-1}(3.3) \quad (5.2)$$

Next, the delivered capacity within 4.2 and 3.3 V is normalized to define the SOC_{use} ranging from 1 to 0. From equations (5.1) and (5.2), the OCV profile within 4.2 and 3.3 V (referred to as E_{cell} where $E_{cell} \subseteq E_{cell\_meas}$) can be then expressed as a function of SOC_{use} as:

$$E_{cell} = f_1((1- SOC_{use})* Q_{max\_use}) \quad (5.3)$$

5.4.1.2 Identification of electrode OCV use range

For the full-cell OCV profile between the EoC and EoD limits, OCV profile range and lithiation limits for each electrode are identified to enable the degradation analysis. As detailed in Section 5.3, OCV of the PE is measured (tagged E_{PE}) between 4.3 and 2.8V at 120 steps of lithiation level (X_{PE}) ranging from 0 to 1. Similarly, OCV of the NE is measured (tagged E_{NE}) between 0 and 1 V in 120 steps of lithiation level (X_{NE}) ranging from 1 to 0. The measured OCV profiles and lithiation levels are represented as:

$$X_{PE} = 0: 1/120:1$$

$$X_{NE} = 1: -1/120:0$$

$$E_H = E_{H,1}, E_{H,1}, \ldots\ldots E_{H,121}$$

where H stands for PE or NE and $E_{H,i}$ is the OCV of the PE or NE at the lithiation level, $X_{H,i}\mathrm{X_{H,i}}$.. The curve fitting approach used on the full cell OCV is applied to the vectors E_H and X_H to develop a fit function f_H as represented by:

$$E_H = f_H(X_H) \tag{5.4}$$

For the selected full cell OCV range, lithiation level of each electrode at the EoC and the EoD is defined as $X_{H,EoC}$ and $X_{H,EoD}$ respectively where H stands for NE or PE. The following iterative procedure (IP) is applied to obtain these four unknown lithiation levels from the multiple combinations within their range of 0 to 1.

IP Step 1: For a selected combination of lithiation limits and using equation (5.4), OCV of each electrode (tagged as $\hat{E}_H$) as a function of cell level SOC_{use} is generated by:

$$\hat{E}_{H,SOC} = f_H(X_{H,EoC} + (X_{H,EoD} - X_{H,EoC})*(1-SOC_{use})) \tag{5.5}$$

$$\text{Here, } SOC_{use} = 1: -0.01: 0$$

IP Step 2: The OCV of the full cell ($\hat{E}_{cell}$) is subsequently calculated based on the OCVs of the PE and the NE between their identified lithiation limits according to:

$$\hat{E}_{cell,SOC} = \hat{E}_{PE,SOC} - \hat{E}_{NE,SOC} \tag{5.6}$$

IP Step 3: The measured cell voltage and calculated voltage over the SOC_{use} range are compared using the RMSE:

$$RMSE = \sqrt{\frac{\sum_{soc=1}^{0}(\hat{E}_{cell,soc} - E_{cell,soc})^2}{101}} \tag{5.7}$$

The RSME depends on the four-lithiation levels, i.e., $X_{PE,EoC}$, $X_{PE,EoD}$ $X_{NE,EoC}$ and $X_{NE,EoD}$. To identify the combination of lithiation limits that produces the least RMSE value, all the possible combinations of

lithiation limits with a resolution of 0.001 between 0 and 1 are verified by repeating the IP steps one to three. Figure 5.6 summarizes the procedure to identify the lithiation limits of the electrodes.

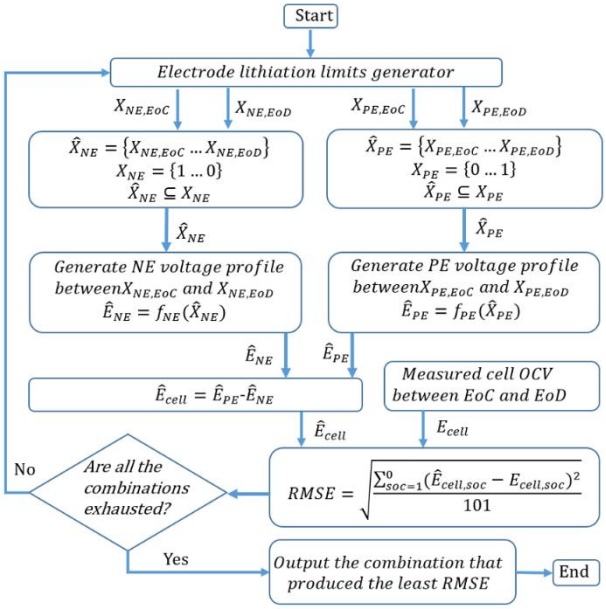

Figure 5.6: A flow chart for the identification of electrode utilization ranges

5.4.2 Quantification of LAM and LLI

A simplified diagnostic method to quantify the degradation modes using lithiation utilization ranges of the electrodes at two different ageing levels of a cell is developed for the quantification of LAM and LLI as explained in this section.

5.4.2.1 LLI calculation

Lithium inventory (LI) of a cell at a working point is the sum of the lithium amounts at the PE (LI_{PE}) and NE (LI_{NE}):

$$LI = LI_{PE} + LI_{NE} \tag{5.8}$$

LI of an electrode is calculated using its current lithiation level and the capacity delivered by the electrode between its lithiation use range limits.

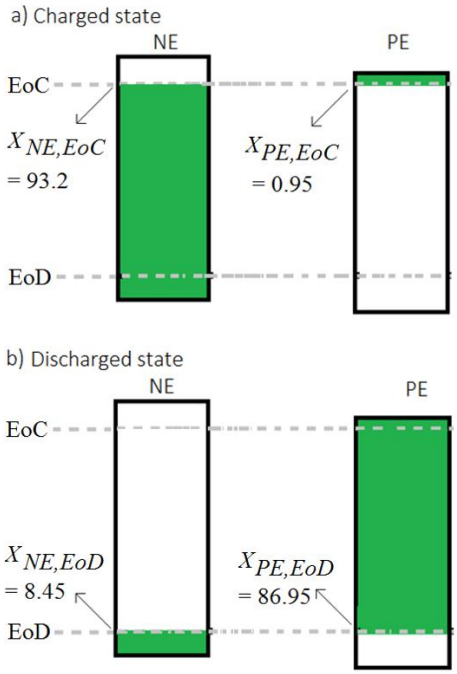

Figure 5.7: Lithiation levels of PE and NE for Cell A1 at: a) charged state (EoC) and b) discharged state (EoD)

Figure 5.7a shows the $X_{NE,EoC}$ and $X_{PE,EoC}$ at EoC while Figure 5.7b shows the $X_{NE,EoD}$ and $X_{PE,EoD}$ at EoD for a cell before the ageing tests using the procedure presented in Section 5.4.1.2. Here, the capacity delivered by the cell before the ageing is 2.91 Ah, which is normalized to 1 unit of lithium transfer (L_{tr}) between the electrodes. The *LI* level of an electrode (LI_A where A stands for PE or NE)at a working point can be then derived as:

$$LI_A = x_{A,EoC} * \left(\frac{L_{tr}}{x_{A,EoC} - x_{A,EoD}}\right) \quad (5.9)$$

$$L_{tr} = \frac{C_{curr}}{C_{pre}} \quad (5.10)$$

where, C_{curr} and C_{pre} are the capacities delivered by the cell at the current ageing level and before ageing tests, respectively.

Using equation (5.9), LI_{PE} and LI_{NE} of Cell A1 are obtained as 0.029 and 1.103 respectively at the EoC. Then, the LI of the cell is calculated as 1.132 units using equation (5.8). Application of this procedure to find the LI at the EoD also results in the same value at a given cell ageing level since the transfer of lithium from one electrode to the other does not change the total lithium present in the cell.

By comparing the full-cell LI levels at two different ageing conditions, the LLI can be derived as:

$$LLI = 1 - \frac{LI_{post}}{LI_{pre}} \tag{5.11}$$

where, LI_{post} and LI_{pre} denote the full-cell LI levels after and before ageing, respectively.

5.4.2.2 LAM calculation

LAM indicates the percentage of active material lost between two different ageing levels of a cell. This can be defined as:

$$LAM_A = \frac{m_{A\_pre} - m_{A\_post}}{m_{A\_pre}} * 100\% \tag{5.12}$$

where m_{A_pre} and m_{A_post} are the masses of an electrode before and after ageing, respectively. Here, A stands for NE or PE. Here, the mass considered for the electrode refers to the active electrode material that is in contact with the current collector and excludes any residues of electrolyte or depositions of the SEI layer. Since the mass of active electrode material is proportional to the capacity it can deliver, equation (5.12) can be represented as:

$$LAM_A = \frac{C_{A\_pre,max} - C_{A\_post,max}}{C_{A\_pre,max}} * 100\% \tag{5.13}$$

Where $C_{A\_pre,max}$ and $C_{A\_post,max}$ are the maximum capacities delivered by the electrode NE or PE before and after ageing, respectively. Since capacity supported by an electrode is in linear relation with its lithiation level, this maximum-capacity can be computed as:

$$C_{A\_max} = \frac{\Delta C_A}{\Delta x_A} * X_{A\_max} \tag{5.14}$$

here, X_{A_max} is the maximum lithiation level of the electrode and ΔC_A is the capacity delivered by the electrode NE or PE for a lithiation change of ΔX_A. Thus, equation (5.13) can be converted into a new form:

$$LAM_A = \frac{\frac{\Delta C_{A\_pre}}{\Delta X_{A\_pre}} - \frac{\Delta C_{A\_post}}{\Delta X_{A\_post}}}{\frac{\Delta C_{A\_pre}}{\Delta X_{A\_pre}}} * 100\% \tag{5.15}$$

where, ΔC_{A_pre} and ΔC_{A_post} are the capacities delivered by the electrode before and after ageing for a lithiation range utilization of ΔX_{A_pre} and ΔX_{A_post}, respectively.

Here, factor ΔC is the capacity delivered by the full-cell between the EoC and EoD and ΔX is obtained from the identified lithiation limits of the electrodes for the full-cell OCV profile between the EoC and EoD. Consequently, the LAM levels at the PE and NE are derived using equation (5.15).

5.5 Degradation analysis: Results and discussion

5.5.1. Identification of electrode utilization range

Following the procedure described in Section 5.4.1, useable ranges of the electrodes are identified for all the full-cells before and after their ageing tests. For example, $X_{PE,EoC}$, $X_{PE,EoD}$ $X_{NE,EoC}$ and $X_{NE,EoD}$ values of cell A1 before the ageing test are identified as 0.95, 93.2, 86.95 and 8.45%, respectively. From this identified lithiation use ranges of the electrodes, the LR that indicates the electrode balance is calculated as 1.015 (N/P = 86/84.8). This value is about 7% lower than the LR value identified from the electrode level capacities as discussed in Section 5.3.2. Results published by Birkl et al. [85] as well show this mismatch that shows an LR value of 1.02 from the matching results for a new cell against the LR value of 1.15 (or 3.18 Ah/2.78 Ah) from the half-cell capacities. This mismatch may originate from two sources. First, at the cell level, the electrodes can have different surface areas because of the differences in their lengths and widths [55]. While both the half-cells are prepared with the same surface areas in this work. Second, both PE and NE half-cells are not tested for their respective entire voltage ranges to capture the actual capacity levels.

Figure 5.8a shows the comparison between the measured (dotted blue line) and the estimated result (green line) of the OCV and useable range of the electrodes (between the star points of the red line for the NE and purple line for the PE) of that Set A's cell. Further, to verify the quality of fitness, DV curves are compared (Figure 5.8b) for the measured and estimated cell voltages that show a close fit.

DV curve at the cell level is compared with the DV curves of the electrodes to understand whether the cell-level DV can reveal the electrode-level degradation modes. Conventional degradation analysis using cell level DV or IC curves relies on the position and magnitude of local peaks and valleys of the curves. As can be seen from the DV curves in Figure 5.8b, two significant peaks from the NE DV curve marked as N1 and N2 are aligned with the cell level DV peaks C2 and C3. Meanwhile, only the peak P1 from the PE DV curve is aligned with the peak C1 of the cell DV curve. Other peaks P2 and P3 of the PE are not observable at the cell level DV curves due to the strong influence of NE peaks N1 and N2 (as per Figure 5.8b).

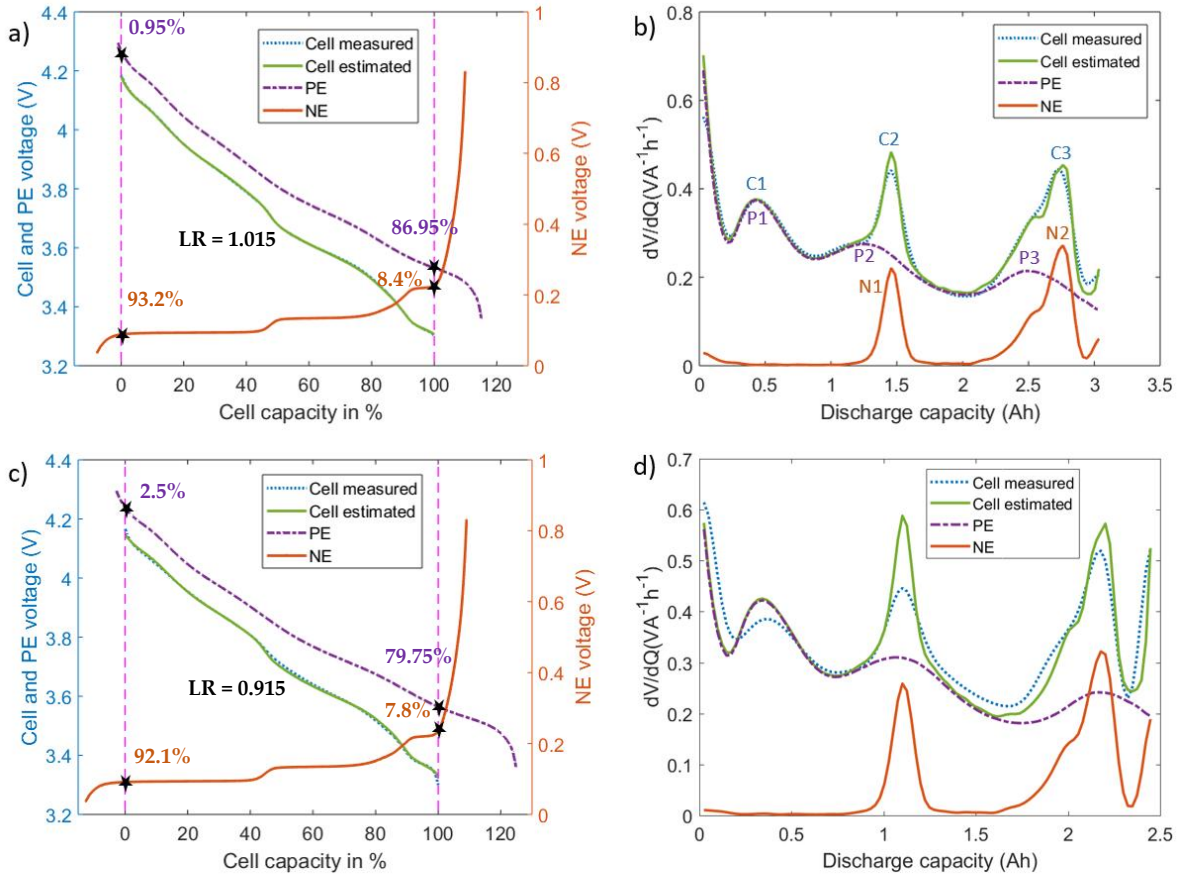

Figure 5.8: Results of electrode capacity range fitting on Cell A1: a) Voltage and b) DV matching prior to the ageing; c) Voltage and b) DV matching after the ageing. The start marks with values indicate the electrode lithiation levels at the EoC and EoD.

As discussed within [105], while using the cell level DV curve, at least two peaks for each electrode are necessary to quantify the degradation of the corresponding electrode. Since the position of the NE peaks (N1 and N2) can be identified with the full cell DV curves from the peaks C2 and C3, LAM at NE can be quantified (discussed in section 5.5.2) using the DV curves at the cell level without the need for electrode level information. On the contrary, only one peak of the PE can be identified from the full cell DV curve. Hence, it is not possible to quantify the LAM at PE with the full cell DV curves alone. As a result, LLI quantification is also deemed to be not possible if LAM at PE occurs in the lithiated state.

Changes in the magnitude of a particular electrode peak cannot be identified from the corresponding cell level peak although their positions are aligned. For example, the magnitude of the peak C2 that corresponds to peak N1 is the sum of the DV magnitudes of PE and NE at that position. Taking a simple case of a certain amount of LLI at the NE, the peak N1 whose magnitude is similar in both the ageing levels can now occur at a different DV level of the PE. This can result in the change of peak C2 level although the magnitude of peak N1 is unchanged. Therefore, the changes in the magnitude of a peak at cell level DV curve as the cell ages can not be attributed to the corresponding electrode peak when

both the electrodes have a dynamic DV profile. These drawbacks of the cell IC or DV curves is addressed by including the OCV profiles and lithiation limits of the electrodes.

Meanwhile, Figure 5.8c and d show the voltage and DV curves with the fit data for the same cell after it lost 20% capacity through cycling. The results highlight that compared to the new cell (RMSE=1.60 mV), the OCV fitting on the aged cell is less accurate (RMSE=4.7 mV). Such results are seen across the cells as shown in Table 5.2. Similarly, the mismatch in terms of DV curves between the measured and estimated cell voltages is significantly higher in the aged state (as seen in Figure 5.8d) compared to its unused state (as seen in Figure 5.8b).

Table 5.2: Cell OCV fitting errors using the OCVs of the electrodes

Test case	SOH (%)	Cell number	RMSE (mV)	Max Error (mV)
Set A (Aggressive charge profile)	100	1	1.60	5.3
	100	2	1.81	6.0
	100	3	1.81	6.0
	78.86	1	4.70	17.8
	84.39	2	3.80	12.2
	78.41	3	4.20	15.1
Set C (Less aggressive charge profile)	100	1	1.89	5.5
	100	2	1.71	5.7
	100	3	1.51	5.6
	93.94	1	2.01	7.9
	94.71	2	1.81	8.4
	93.76	3	1.99	7.2

One potential reason for the error increase for the aged cells is the changes in the electrochemical behaviour of the electrodes. For the PE, the active electrode material NCA is a compound of Nickel, Cobalt, Aluminum and Oxygen. With the dissolution of Ni at the higher voltage levels of PE (>4.2 V) [106], the structure of the electrode can change over the battery ageing. This can modify the PE OCV profile. On the other hand, activation of passivated lithium depositions at the NE may influence its OCV profile. As per [103], a portion of the lithium dispositions that are electrically disconnected but mechanically connected to the electrode may slowly establish electrical contact with the electrode after the fast-charging tests. This may influence the OCV profile measured immediately after the fast charge cycling since the GITT procedure with a low C-rate (C/20) discharge coupled with rest periods

takes more than 120 hours. Therefore, the negative electrode OCV vs lithiation map may differ from the pristine NE electrode.

When fitting full-cell OCV of the aged cells, the half-cell OCVs collected on the electrodes harvested from a new cell are still used, and therefore it does not account for the changes occurring to the electrodes. This may explain why the OCV fitting for the aged cells can have higher levels of fitting errors.

On the other hand, through the cycle ageing, a drop in the lithiation use range of the PE (from 86% to 77.25) or the LR level (from 1.015 to 0.915) is observed as seen from Figure 5.8a and c for cell A1. This indicates that the cell has experienced LAM at the NE [55], although it does not allow quantifying the LAM directly.

5.5.2. Application of the degradation diagnostics

The selected cells are aged under two different conditions as presented in Section 5.3.1. Set A cells are cycled under the plating induced conditions where the VRP method is used to confirm the occurrence of lithium plating. Set C cells are cycled with the less aggressive charge profile where plating is not detected. Levels of degradation in terms of LLI, LAM_{NE} and LAM_{PE} for Set A and Set C cells are calculated as described in Section 5.4.2 and their values are shown in Figure 5.9a and Figure 5.9b respectively. Following observations have been obtained from that result:

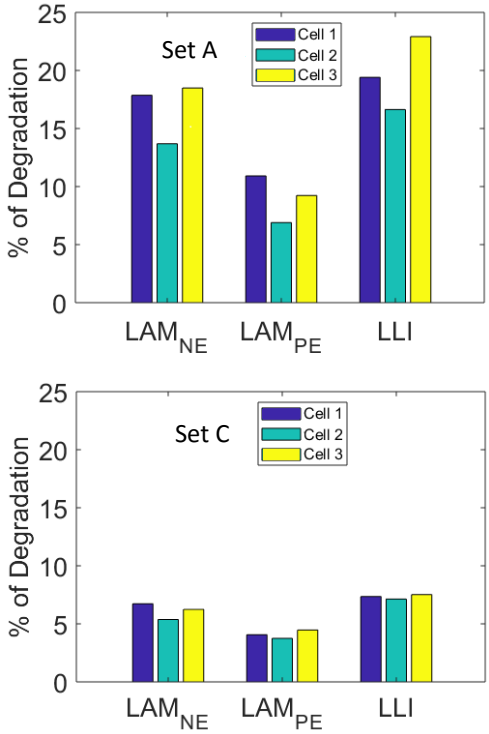

Figure 5.9: LAM and LLI levels: a) Set A cells; b) Set C cells

1. Higher levels of LLI (circa 19.4%) are observed for Set A cells compared to Set C cells (circa 7.3%) as shown in Figure 5.9. This could be explained through the following reasons. First, Set A cells had higher levels of lithium plating (see Figure 4.5). Part of the plated lithium becomes irreversible, leading to LLI. Secondly, the increased LAM could raise the LLI level since LAM could occur in the lithiated state. Third, the plated lithium could crack the SEI layer, resulting in further growth of the SEI layer consuming cyclable lithium [76]. Given that the usual growth of the SEI layer slows down with time after preconditioning of cells [107] and these cells are cycled only 52 times against their rated life of circa 800 cycles, it is reasonable to assume that lithium plating is leading to accelerated LLI levels.

2. Increased levels of LAM at the NE are observed under lithium plating. The LAM levels at NE of Set A cells are significantly higher (an average of 16.2 %, Figure 5.9a) than those of Set C cells (an average of 6.1%, Figure 5.9b). Although relatively low, the LAM levels in Set C indicates that there could be some amount of lithium plating that is below the detectable level. As discussed within [28], the VRP method fails to detect lithium plating levels lower than 2.5%. Visual inspection of the electrodes (Figure 4.6) as detailed in Section 4.5 also indicate relatively lower levels of lithium metal depositions in Set C cells compared to that of Set A cells.

The LAM difference between the two sets indicates that lithium plating dominates the LAM levels at the NE for two reasons. First, Set A cells are charged with an aggressive current profile and found with much higher levels of lithium depositions compared to Set C cell (see Figure 4.6). Second, other possible ageing mechanisms such as binder decomposition and graphite exfoliation at the NE [51, 108] that cause LAM might not induce such high levels of LAM given these cells are only tested for 52 cycles [26].

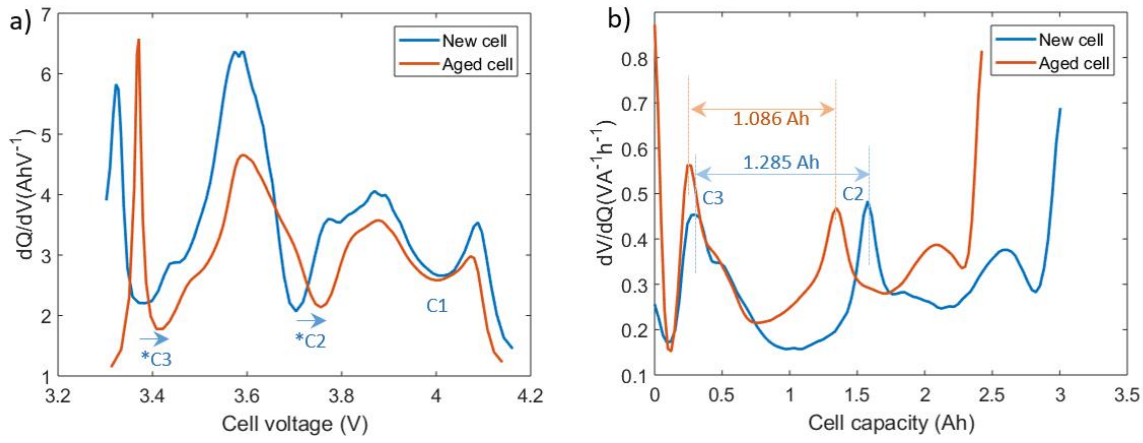

Figure 5.10: a) IC and b) DV curves of the first cell in Set A at two different ageing levels

In addition to the quantification of degradation modes using the proposed electrodes OCV profiles, IC-DV curves are also compared for degradation analysis. Figure 5.10a and b show the evolution of IC and DV curves respectively for cell A1. In the DV curves, the cell capacity delivered between the peaks C2 and C3 is equal to the capacity delivered by the NE electrode between the peaks N1 and N2. Therefore, the percentage of capacity reduction between these peaks can be used to indicate the percentage of LAM_{NE}. As seen from the figure, the capacity between the peaks C2 and C3 has dropped by 15.6% (1.086 Ah compared to 1.285 Ah) which suggests that LAM_{NE} is 15.6%. On the other hand, LAM_{NE} estimated for the same cell using the electrode OCV profiles is 17.8%. The large levels of LAM_{NE} calculated from both techniques highlights that mechanical stress has increased under lithium plating.

Increased levels of LAM under the influence of lithium plating can originate from two possible sources. One, as discussed earlier, volume expansion due to the lithium metal depositions in the early cycles can raise the mechanical stresses within the cell and lead to LAM in the first moment. Second, as discussed within [66], the formation of localized layers due to passivated lithium depositions or electrically isolated LAM in the early cycles may further increase the mechanical stresses locally which in turn can raise the LAM further.

3. LAM_{NE} is higher than LAM_{PE} for each cell in Set A (as per Figure 5.9) and the average LAM_{NE} across Set A cells is 16.2% while the average LAM_{PE} is only 8.9%. Since lithium plating occurs at the NE and metal depositions could stay between the NE and the separator, it can be reasonably assumed that the NE experiences higher levels of mechanical stresses compared to the PE ([2, 17]). Therefore, it follows that mechanical stresses impact on the NE could be higher than the PE.

4. The results also highlight that LAM_{NE} levels are comparable to the LLI levels in the aged cells. For example, cell number one from set A lost 17.8% LAM_{NE} and 19.4% LLI. LAM can occur in lithiated condition, which means LLI along with it, or in the delithiated state. Since lithium plating occurs towards the end of charging or near to full lithiation of the electrode, mechanical stresses could rise in the lithiated state of NE. This could result in higher levels of LAM in the lithiated state (LAM_{liNE}). As discussed within [109], the shift of valley points in the IC curve (*C2 and *C3) that correspond to the peaks C2 and C3 in the DV curve (or the peaks N1 and N2 of the NE) towards higher cell voltages (as seen from Figure 5.10a) as well indicates the dominance of LAM_{liNE}. Therefore, significant levels of LLI may come from LAM_{liNE} and the contribution of irreversible lithium plating to the total LLI can be much lower than the LLI from the LAM. This analysis indicates that the majority of lithium plating can become reversible and LAM_{liNE} can be a major result of lithium plating. However, this initial conclusion needs further study to quantify the LLI from LAM.

In summary, LLI and LAM_{NE} are significant in the cells with lithium plating. These important findings help to confirm the theoretical understanding of increased mechanical stresses under lithium plating. Unlike the previous studies [2, 26] indicating that LLI is the dominant outcome of lithium plating, this study demonstrates that LAM_{liNE} is the most critical degradation mode under the influence of lithium plating. This observation is useful in improving the knowledge about lithium plating and its influence on battery ageing and consequently helpful in deriving fast charging strategies.

5.6 Implications for fast-charge strategies development

The degradation modes of batteries aged under the influence of lithium plating indicate that LAM is increasing with lithium plating levels. This improved knowledge of lithium plating influence on the battery helps in developing charging strategies in two ways. First, this knowledge useful for deriving charging strategies for EVs. Allowing few fast charging events that could cause lithium plating for an EV will be detrimental to its battery life, as there exist short term and long term negative impacts. Lithium depositions from previous charge events that remain in the battery contribute to mechanical stresses. Therefore, to maximize battery life, lithium plating needs to be completely avoided even in fast charging events. In cases where a trade-off is performed between fast charging and battery life, EV manufacturers need to consider both short-term and long-term implications of few fast charging events.

Second, batteries that faced lithium plating in their first use may be avoided for second life use as the presence of higher volume-occupying lithium metal depositions increases mechanical stresses. Alternatively, increased volume of the batteries from their unused condition can be measured and considered in selecting the operating conditions such as DOD use range, charge currents to limit the volume expansion during charge.

5.7 Limitations and future work

5.7.1 Impact of electrode degradation

As the battery degrades the RMSE of OCV fitting started rising. There is a possibility of electrochemical changes in the electrodes that could affect the results because the method depends on the OCV measurements using the electrodes harvested from a new cell. The electrochemical changes such as structural changes in the electrode can modify their OCV profiles that might be affecting the fitting results. In addition, these electrochemical changes may affect the accuracy of the degradation modes estimation. To confirm the reason behind the increased fitting errors for the aged cells and to assess

the influence of electrochemical changes on the quantification accuracy of the degradation modes, a further half-cell OCV comparative study on both new and aged cells is needed.

5.7.2 Impact of lithium metal depositions

This work found that material cracking in the form of LAM at the NE increases under lithium plating. Based on this principle, it is assumed that previous lithium plating occurrence could continue to cause damage to the battery. However, further study is needed to confirm whether lithium plating has a long-lasting impact on battery degradation.

5.7.3 Loading ratio mismatch

As mentioned in Section 5.5.1, there is a mismatch between the LR values identified from the electrode level capacities and matching results. Identifying and accounting for the sources that contribute to the mismatch will help to affirm the matching procedure employed. Further study is required to quantify the surface areas and capacities of both the electrodes in a full cell and include the LR factor in the matching procedure accordingly.

5.8 Conclusions

This study has proposed a two-stage procedure to quantify the degradation modes of Li-ion battery. First, using the OCV profiles of a cell and its electrodes, utilization of the voltage range of each electrode are identified. This procedure is applied to the cell at two different ageing levels. Second, quantification of degradation modes is carried out based on the identified electrode utilization ranges and the capacities delivered at two different ageing levels. LLI is calculated based on the changes to the lithium inventory present in the cell. On the other hand, LAM at each electrode is derived using its scaling effect on the electrode utilization range. The presented diagnostic technique has the potential for applications to other lithium-ion cells using different chemistries.

The proposed procedure of quantifying the degradation modes using the OCV measurements and capacities is applied to a cell aged under lithium plating. Previously, LLI is considered a dominant degradation mode under lithium plating. However, the results in this study highlight that lithium plating results in significant LAM_{NE} in addition to the LLI. This confirms that lithium plating raises the mechanical stresses in the cell. This study, therefore, underpins a better understanding of lithium plating, supporting the future development of optimal charging protocols to minimize battery degradation.

6 Study 4- A New On-line Method for Lithium Plating Detection in Lithium-ion Batteries

6.1 Introduction

Detecting the onset of lithium plating during a charging event is essential to minimize the amount of lithium plating and to track the lithium plating tendency over the battery lifetime [26]. As discussed in Chapter 2, although there exist multiple approaches to detect lithium plating, none of them detects the onset of plating during charge. Therefore, the challenge of determining the onset of lithium plating during charge remains prominent for many battery applications. The objective of this study (or research objective 3 of this IR as discussed in Chapter 2) is to develop and validate an in-situ method for detecting the onset of lithium plating in a commercial cell during charge using standard battery health monitoring signals (e.g. voltage and current) for real-time use. The research hypothesis is to detect lithium plating by tracking battery impedance during a charge event. Concentration gradients in the electrodes and electrolytes, SEI layer, Ohmic resistance of the current collectors and CTL at the electrode interface collectively contribute to the value of battery impedance. It is assumed that a new process introduced by lithium plating in the form of lithium metal depositions at the NE will modify the battery impedance profile. It is therefore believed that lithium plating shall be identifiable by tracking the impedance profile during charge.

The remainder of this chapter is structured as follows. The theoretical background for the consideration of impedance for plating detection is detailed in Section 6.3. Section 6.4 discusses the experimental framework and methodology. Section 6.5 presents the experimental results to highlight the potential of the proposed method. The application and limitations of the study within the context of EV are discussed in Sections 6.6 and 6.7, respectively. Overall conclusions of this research are given in the final section.

6.2 Objective of this study

To detect and control lithium plating in real-time applications, the following objective is defined:

- To develop and validate a new method for BMS use that can identify the onset of plating within a charging event and is implementable in real-time applications.

6.3 Methodology

This section presents the theoretical background of the proposed impedance-based lithium plating detection method. First, multiple processes internal to the battery that underpin the measure of impedance to the charge flow are discussed along with the use of electrochemical impedance spectroscopy (EIS) techniques for their quantification. Second, the potential influence of lithium plating on the impedance of a subset of processes are discussed. Next, a method to detect this change to the impedance profile to identify lithium plating is presented.

6.3.1 Battery impedance

Lithium exchange between the electrodes in a lithium-ion battery comprises of a series of multiple processes including lithium-ion diffusion in the electrolyte, migration through the SEI layer, charge transfer through the electrode/electrolyte interface, solid-state diffusion in the bulk of active material and electron transfer external to the battery via the current collectors [110, 111]. During charge/discharge events, these processes introduce impedance to the charge flow and cause a voltage drop between the two electrodes. As discussed within [111], these processes can be individually identified by using EIS since each of them has a different time constant or frequency range of excitation.

Commercially available 18650-type lithium-ion cells with a rated capacity of 3.1Ah are used in this study. Figure 6.1a shows the EIS plot of a new cell of the selected cell type at 50% SOC after it has been allowed to equilibrate for 4 hours at room temperature (25 ^{o}C). As discussed within [112], voltage changes or impedance changes are not significant beyond the first 4 h of the relaxation after the SOC adjustment performed with 1C discharge rate. Several publications such as [110, 113] describe in detail how to interpret the EIS plot and so this information will not be repeated here. However, for completeness, a summary is provided below. As discussed within [111], the high-frequency region (≥761 Hz) is caused by the ionic conduction through the electrolyte and electronic conduction through the current collectors whose impedances are represented by Z_{EL} and Z_{Ω} respectively. The mid-frequency region (between 761 and 0.67 Hz) represents the CTL at the electrode-electrolyte interfaces and the ion migration through the SEI layer whose impedances are represented by Z_{CTL} and Z_{SEI} respectively. The low-frequency part (<0.67 Hz), usually characterised by a 45° slope, is introduced by the SDL in the electrodes. Figure 6.1b shows the equivalent circuit of a lithium-ion battery by this network of impedance values. In the Figure, the impedance due to SDL (referred as $Z_{SDL,NE}$ or $Z_{SDL,PE}$) at each electrode is hidden under the electrode surface potential represented by $V_{NE,S}$ or $V_{PE,S}$ that is different from OCV due to the potential drop introduced by the SDL.

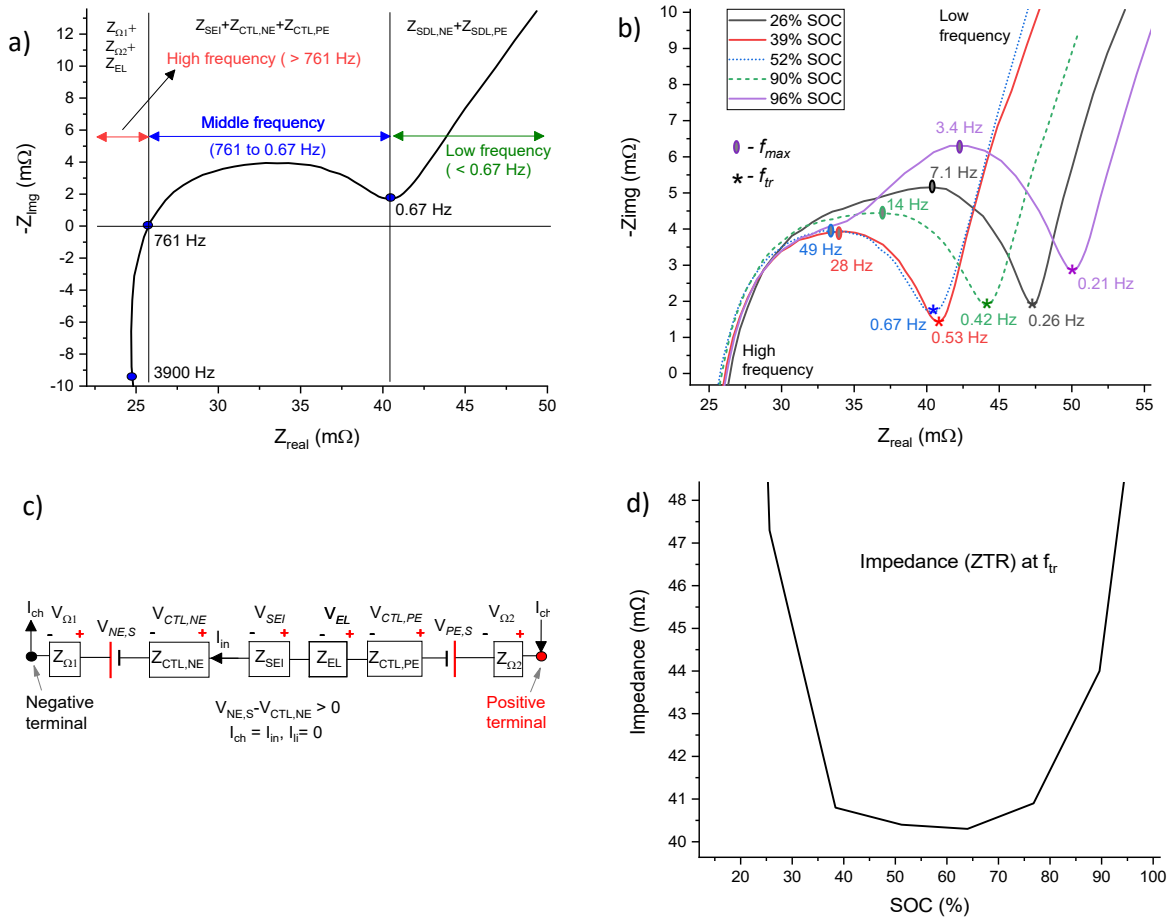

Figure 6.1: Battery impedance: a) EIS plot at 50% SOC, b) EIS plots at different SOC levels, c) Equivalent electrical circuit diagram representation of the battery impedance, and d) impedance and resistance at the transition frequency f_{tr} to track mid to high frequency impedance with SOC

Figure 6.1c shows the EIS plots of the same cell at different SOC levels. As it can be observed and as reported within [111], the impedance in the mid-frequency range varies with SOC. Since Z_{CTL} and Z_{SEI} contribute to this range and since no significant change in the SEI layer thickness is expected in a single charge/discharge cycle [30, 114], the mid-frequency impedance variations can be attributed largely to the Z_{CTL}. The electrochemical models that describe the CTL through the Butler-Volmer equation [90, 115] also support this rationale. According to their presented analysis, Z_{CTL} at an electrode varies according to the electrode surface lithiation level. At low (near to 0 %) and high lithiation levels (near to 100%), Z_{CTL} is high and reduces as the lithiation level moves towards 50%. Therefore, the impedance changes in the mid-frequency region come mainly from the Z_{CTL} and tracking the battery impedance should indicate the way Z_{CTL} is changing while the battery is being charged or discharged. The influence of lithium plating on the value of Z_{CTL} and detection of onset of lithium plating with the help of Z_{CTL} are detailed in section 6.3.3.

The impedance measured at the transition frequency (referred to as f_{tr} which is marked with "*" in Figure 6.1c) at which impedance changes to 45° slope allows quantifying the total impedance from

both the high and the mid-frequency regions. Since the impedance from the high-frequency region is nearly constant (as seen from Figure 6.1c), tracking the impedance at the f_{tr} (referred to as ZTR) allows tracking the mid-frequency impedance changes and thus Z_{CTL}. ZTR measured at the f_{tr} can be estimated as:

$$ZTR = Z_{\Omega} + Z_{CTL} + Z_{SEI} + Z_{El} \quad (6.1)$$

$$where \quad Z_{\Omega} = Z_{\Omega 1} + Z_{\Omega 2} \; and \; Z_{CTL} = Z_{CTL,NE} + Z_{CTL,PE}$$

Here, $Z_{\Omega 1}\ and\ Z_{\Omega 2}$ are Ohmic resistances at the NE and PE respectively; $Z_{CTL,NE}$ and $Z_{CTL,PE}$ are impedance due to CTL at the electrodes NE and PE respectively. Figure 6.1d presents the ZTR profile against the battery SOC where ZTR drops initially as battery SOC raises from 0% and reaches a near flat level in the mid-SOC range before rising again as SOC goes further towards 100%.

6.3.2 Impedance tracking with EIS

The approach taken to track the ZTR and thus Z_{CTL} while charging/discharging without the use of laboratory equipment requires interrupting the current or creating a step change to the current similar to the hybrid pulse power characterization (HPPC) test often used in developing equivalent circuit models [116, 117]. In this work, charge current is interrupted every 1% SOC increase for a predefined period. The step-change in the current and the associated voltage change during the interruption is used to calculate the real part of ZTR (referred to as RTR) based on Ohms law. To understand how RTR enables ZTR tracking, the following discussion is provided.

As seen from Figure 6.1c, the imaginary part of the impedance or reactance at f_{tr} is significantly lower than the resistive part (RTR) irrespective of the SOC level. Table 6.1 shows the ZTR (or impedance at f_{tr}) and its real part along with the reactance at different SOC levels. Here, RTR is found to be within 1% of the total value of ZTR irrespective of the SOC level. Therefore, variations in the mid-frequency impedance or the ZTR can be tracked using the calculated RTR value.

Table 6.1: Impedance and its reactive and resistive parts at f_{tr}

SOC (%)	f_{tr} (Hz)	RTR (mΩ)	Img (ZTR) (mΩ)	ZTR (mΩ)	RTR/ZTR*100
26	0.21	47.3	1.89	47.33	99.94
39	0.54	40.8	1.43	40.82	99.95
52	0.67	40.5	1.69	40.53	99.93
78	0.67	40.9	1.61	40.93	99.93
96	0.16	50.2	2.86	50.28	99.84

To identify the charge interruption period, as discussed within [111], the time constant (τ) of an equivalent RC network that produces the semi-circle in the mid-frequency region can be used. The value of τ is calculated with the frequency (referred to as f_{max}) which is marked with circles in Figure 6.1C at which the imaginary part of the impedance attains a maximum level in the mid-frequency region using $\tau = (2\pi f_{max})^{-1}$. An interruption time of 2τ s shall recover the voltage drop due to the RC network by 87% of the maximum value [111].

6.3.3 Impedance under lithium plating

While charging at low C-rates or during high ambient temperatures, due to the improved diffusion in the electrodes, differences between the lithiation levels of the electrode surface (referred to as Li_{NES} and Li_{PES} for the NE and PE respectively) and the bulk are known to reduce [90, 115]. Therefore, charging conditions that allow Li_{NES} and Li_{PES} closer to their average electrode lithiation levels can produce a ZTR profile similar to the ZTR profile obtained from the EIS measurements taken at different SOC levels (as seen from Figure 6.1d) where the lithiation differences in the electrode particles are deemed to be negligible. Conversely, at high C-rates of charging or at low temperatures, the rate of Li_{NES} rise in line with SOC increases because of increased SDL or reduced diffusion in the electrodes. Therefore, the Z_{CTL} that depends on the Li_{NES} can reach the lower levels at a lower SOC level compared to charging at low C-rates or high temperatures. With further charging, Li_{NES} tends to raise towards a full lithiation level as $V_{NE,S}$ comes closer to Li reference potential much before the battery reaches 100% SOC. The potential drop due to CTL (referred to as V_{CTL}) that increases with increasing C-rate or decreasing temperature when combined with the lower potential of $V_{NE,S}$ can push the NE potential below the Li reference where lithium plating commences. Once lithium plating begins, the rate of electrode lithiation rise is reduced and accordingly the Z_{CTL} rise is reduced since the charging current (referred to as I_{ch}) is now divided into intercalating current (referred to as I_{in}) and lithium plating current (referred as I_{li}). Additionally, as discussed within [56, 61], the lithium plating reaction at the NE also follows the Butler-Volmer equation that introduces a new branch of impedance in parallel to the existing $Z_{CTL,NE}$ as shown in Figure 6.6.2. Similar to the intercalating current that faces $Z_{CTL,NE}$, lithium plating current faces an impedance referred to here as $Z_{CTL,Li}$. As a result, the overall impedance at the NE drops compared to $Z_{CTL,NE}$ after the onset of lithium plating. On this basis, it is hypothesised that tracking the ZTR will allow detecting the onset of lithium plating during the charging event.

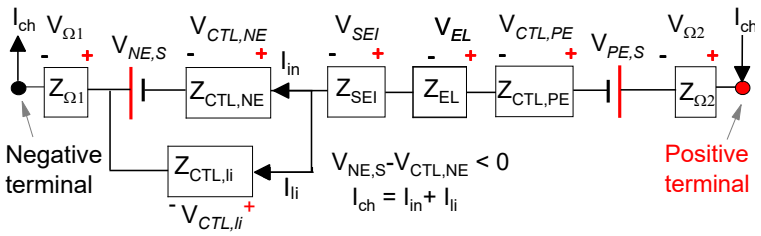

Figure 6.6.2: Equivalent circuit representation of a battery impedance after the onset of lithium plating

The hypothesis to detect lithium plating can be further explained as follows. In the case of a charging event without lithium plating, ZTR (or Z_{CTL}) follows the curve from Figure 6.1d where ZTR faces continuously decreasing reduction at lower SOC levels to reach a near flat level in the mid-SOC range and then increases as SOC rises towards 100%. In the case of a charging event with lithium plating, ZTR faces a second downtrend after the onset of lithium plating because of the introduction of parallel impedance ($Z_{CTL,li}$) across the existing $Z_{CTL,NE}$. Detecting this second downward trend by tracking the ZTR shall, therefore, indicate the onset of lithium plating.

6.3.4 Impedance tracking in real-time

To track ZTR using a charge interruption technique while the battery is undergoing a charge event, f_{max} that varies with SOC, temperature and ageing must be known priori. As seen from Figure 6.1c, f_{max} and f_{tr} levels vary from circa 3.4 to 49 Hz and 0.21 to 0.67 Hz respectively with SOC for the new cell selected while testing at 25°C. As per [111], the values of f_{max} and f_{tr} can reduce as low as in turn to 100 mHz and 10 mHz for a comparative aged cell while testing at 0 °C temperature although these numbers vary between cell type according to the cell format and chemistry [118]. Since it is difficult to identify f_{max} or f_{tr} in real-time applications to track impedance of the mid-frequency region, a fixed frequency approach is adopted in this work. Implications of using a fixed frequency against the variable f_{tr} on ZTR tracking is analysed using the EIS data.

Selecting a frequency level that falls in the low-frequency region and that is below the f_{tr} range shall not only facilitate tracking of the impedance from the mid-frequency region but also some portion of low-frequency region as well. For the observed f_{tr} range of 0.67 and 0.21 Hz, the impact of fixing the frequency of AC excitation at 0.1 Hz and 0.05 Hz is analysed to better understand whether the Z_{CTL} can be adequately quantified while employing this assumption. Figure 6.6.3a shows EIS plots marked with f_{tr}, 0.1 Hz and 0.05 Hz at 50 and 96% SOC levels. The impedance at 0.1 Hz and 0.05 Hz from the EIS measurements are plotted against the SOC as shown in Figure 6.6.3b and Figure 6.6.3c respectively along with that value of the f_{tr}. The impedance profile at 0.1 Hz is found with some offset compared to the ZTR profile obtained at f_{tr}. Impedance from the low-frequency region (termed Z_{low}) at 0.1 Hz is

combined with that of ZTR to produce an offset as seen from Figure 6.6.3b. The impedance at 0.1 Hz can produce a profile similar to that of the ZTR for two reasons.

- First, the contribution of the low-frequency region to the overall impedance value at 0.1 Hz is less than 5% of the overall ZTR value. As seen from Figure 6.6.3b, the minimum level of ZTR (or impedance at f_{tr}) and the maximum level of the Z_{low} are circa 40 and 1.8 mΩ respectively.
- Second, the rate of impedance change experienced by the ZTR is much higher than that of the Z_{low}. For example, an increment in the value of ZTR and decrement in the value of Z_{low} are in turn 9.1 and 0.8 mΩ while SOC is rising from 78 to 96%. As a result, the impedance at 0.1 Hz is still able to maintain the initial drop and final rise and able to produce a profile similar to that of ZTR. Similar results are observed for the impedance profile at 0.05 Hz (Figure 6.6.3c). To summarise, the ZTR profile can be tracked with a chosen frequency that is below the f_{tr} range.

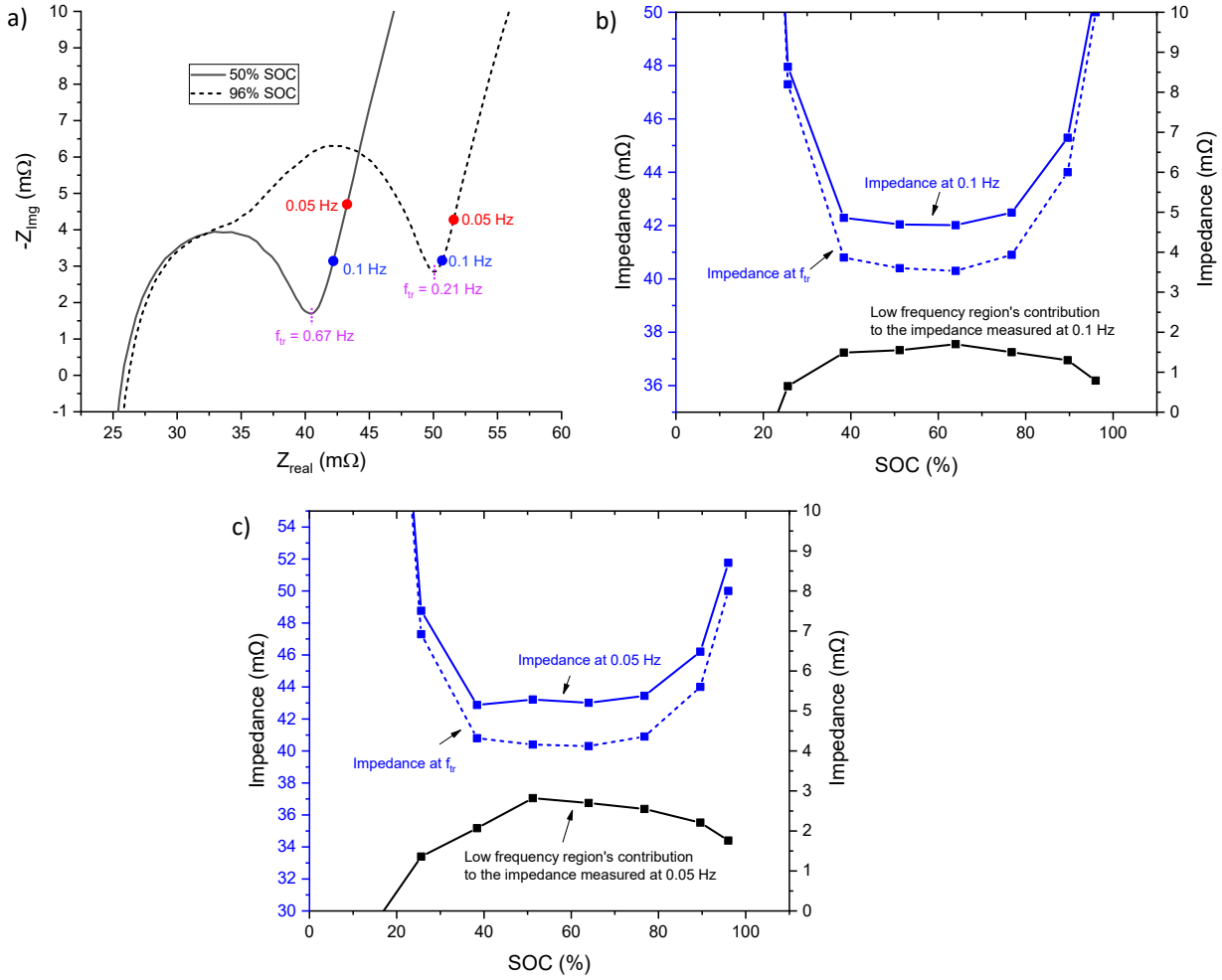

Figure 6.6.3: Battery impedance: a) EIS plots marked frequencies f_{tr}, 0.1 and 0.05 Hz; b) impedance profile at 0.1 Hz in comparison with that of f_{tr} along with the impedance from the low-frequency region at 0.1 Hz and c) impedance profile at 0.05 Hz in comparison with that of f_{tr} along with the impedance from the low-frequency region at 0.05 Hz

Similarly, the value of charge interruption time derived from a frequency that is below the f_{max} range can ensure tracking of the impedance from the mid-frequency region in all operating conditions. Since the minimum level of f_{max} for the new cell is observed at 3.4 Hz and it can decrease further with reducing temperatures and increasing ageing levels [111], a minimum f_{max} level of 100 mHz is considered to derive the rest period. At the identified reference frequency (f_{max}), τ is 1.59 s ($\tau = (2\pi f_{max})^{-1}$) and measuring the voltage response in 3 s allows us to measure 85% of the total change expected. As a result, to study lithium plating by tracking the impedance, charge currents are interrupted for 3 s, every 1% SOC increase. As discussed within [84], pulsed charging by interrupting the charge current frequently can reduce the concentration gradients within the electrodes and thus reduce the potential drops at the electrode. Therefore, the charge interruption procedure benefits indirectly by reducing the lithium-plating occurrence although the magnitude of reduction depends upon the length of the interruption time [10]. Within this work, the study is limited to tracking the impedance while using the charge interruption procedure. The experimental procedures to track ZTR using the intermittent charge interruption are detailed in section 6.4.

6.4 Results and discussions

To track the value of ZTR during different charging events that include potentially non-plating and plating conditions, experiments at different ambient temperatures (10, 20 and 30 ^{o}C) and C-rates (0.2, 0.5, 0.75, 1 and 1.25C) are performed. For the selected cell type, the recommended maximum charge C-rate is 0.42 C (or 1.25 A) and a charge temperature range defined as 10 to 45 ^{o}C. Therefore, charge C-rates higher than 0.42C may be deemed “abusive” and could potentially cause lithium plating even within the recommended temperature range [26, 58]. A detailed description of the experimental setup and test procedure are presented in the following sections.

6.4.1 Test case definition

Four test cases employing four sets of cells are employed for experimentation. For each test case, as shown in Table 6.6.2, three cells are selected for reproducibility and to minimize the influence of cell-to-cell variations on the experimental results. Among them, test cases A1, B1 and C1 are performed at 10, 20 and 30^{o}C respectively to study the ZTR profile at different C-rates at each temperature with active cell surface cooling. In addition, test case D1 is included in the experimental programme to analyse the impact of temperature rise during the charge on the ZTR profile where the cells are operated without active cell surface cooling.

Table 6.6.2: Cell level test case

Test case	Temperature	charge C-rates
Set A1: 3 cells	10^{o}C with active cooling	0.2C, 0.5C, 0.75C, 1C, 1.25C
Set B1: 3 cells	20^{o}C with active cooling	0.2C, 0.5C, 0.75C, 1C, 1.25C
Set C1: 3 cells	30^{o}C with active cooling	0.2C, 0.5C, 0.75C, 1C, 1.25C
Set D1: 3 cells	20^{o}C without active cooling	0.2C, 0.5C, 0.75C, 1C, 1.25C

6.4.2 Experimental setup

In this work, the selected cells are placed on a Perspex plate fixture through which the cells are connected to a Maccor cell cycler (Model: Series 4200). To keep the cell temperature as close as possible to the desired temperature (except for case D1), liquid (Kryo 51 silicon oil) cooling over the cell surface is used with the support of a LAUDA (Model: Proline RP 845 C) temperature Controller. In the case of test case D1, cells are evaluated in an environment maintained at 20^{o}C without any active cooling to allow the usual rise of temperature during charge. For the analysis, the Maccor unit enables data recording of the cell voltage and current with ±0.1 mV and ± 0.03 mA resolutions, respectively. Furthermore, a Maccor probe using T-type thermocouples with an accuracy of ±1 °C is placed at the centre of the cell in the axial direction to measure temperatures on the cell surfaces. The test parameters including the measurement accuracies and sample rates are summarised in *Table 6.6.3*.

Table 6.6.3: Measurement parameters and their range and accuracies

Measuring parameter	Operating range	Measurement accuracy	Resolution	Sampling time
Cell voltage	2.7 to 4.2 V	± 1 mV	0.1 mV	20 ms
Cell current	+4.8 to -1 A	± 1 mA%	0.030 mA	20 ms
Cell temperature	0 to 30 ^{o}C	± 1 ^{o}C	0.01 ^{o}C	1 s

6.4.3 Experimental procedure

All the cells prior to the impedance tests are preconditioned for six cycles at 25°C temperature with C/3 constant current (CC) charge/discharge rates and C/40 constant voltage (CV) cut-off current between the voltage limits of 4.2 and 2.7 V. The SEI layer over the NE grows largely during the initial few cycles after which the rate of growth reduces as its layer thickness increases [119]. As a result, impedances due to the SEI layer attain stable levels after the preconditioning cycles as discussed further within [54]. The number of preconditioning cycles required to stabilize a cell may vary according to its chemistry and format. As presented in section 4.5.1.1, the selected cell type could reach stable capacity levels within the first 6 cycles of preconditioning. After the preconditioning stage, the impedance tests in each test case are performed at their selected temperature while charging. The test procedures are presented through a flow chart as shown in Figure 6.6.4a.

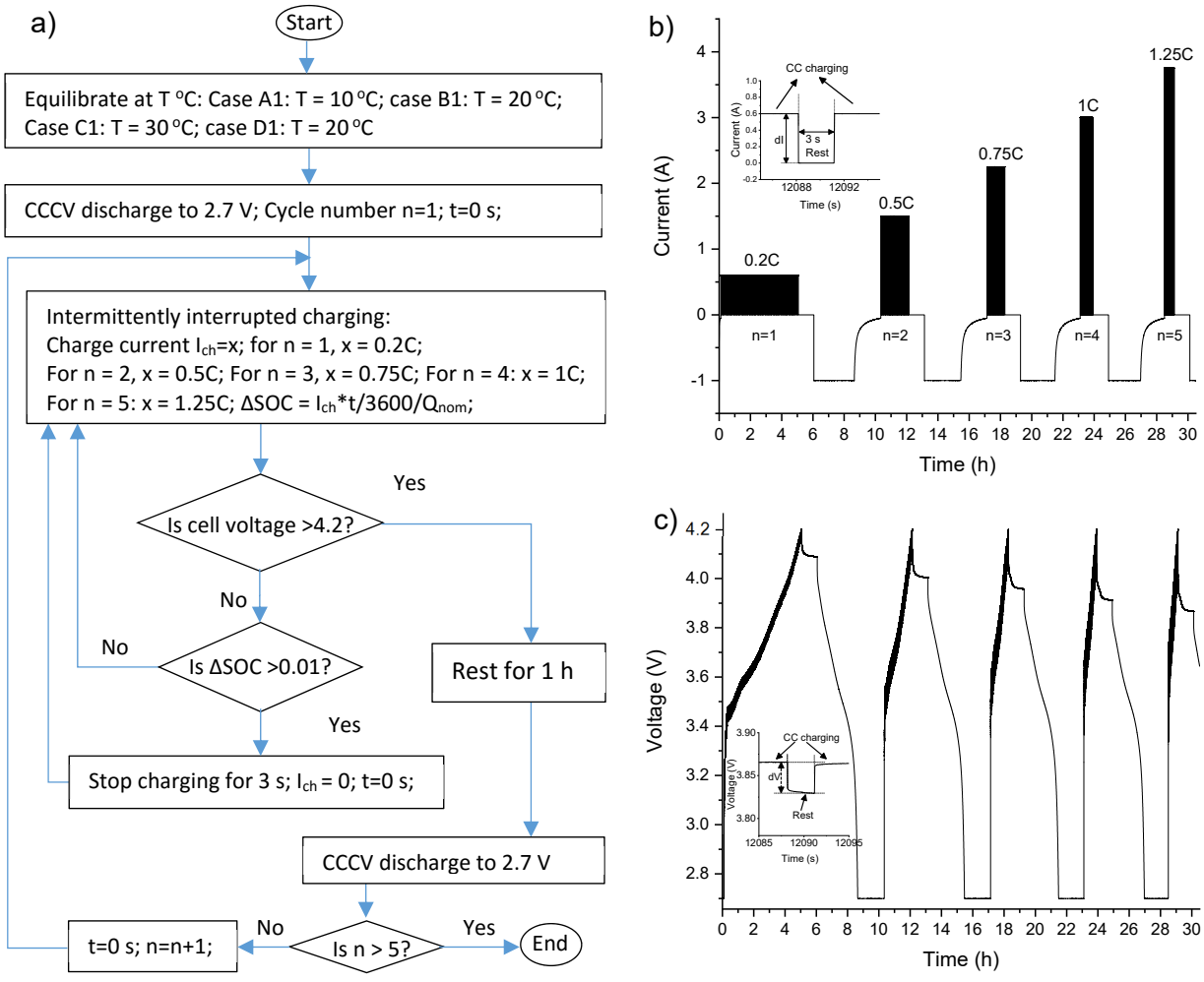

Figure 6.6.4: Experimental procedure: a) flow chart, b) current and c) voltage profiles in charge interruption tests

In each case, the cells are cycled five times with different charge rates in each cycle starting from 0.2C in the first cycle to 1.25C in the last cycle as shown in Figure 6.6.4a. Prior to each charge test, the cells are discharged to 2.7 V with a CC-CV profile using a C-rate of C/3 in the CC phase and a CV cut-off

current of C/40 in the CV phase. Then, the cells are charged with the modified CC charge (intermittent charge interruption) to estimate the values of ZTR in real-time. Since the focus of this research is to detect lithium plating that occurs during charge as detailed in Chapter 2, the application of the modified current profile is limited to charging events.

To track the profile of ZTR, the cells are charged incrementally, in steps of 1/100 of the nominal capacity ($Q = Q_{nom}/100$), by applying selected C-rate of charge and subsequently allowing the cell voltage to relax for 3 s as discussed in section 6.3.4. Here Q_{nom} of the cell refers to the *discharge capacity* measured in the 6^{th} cycle of preconditioning. Figure 6.6.4b and c show cell voltage and charge currents where positive and negative levels of cell current refer to charge and discharge respectively. The cell voltage recovery by the end of each rest period (referred to as dV) and the current difference created (referred as dI) from the CC charge to the 3 s rest are recorded to calculate the resistance ZTR using Ohms law.

6.5 Results & Discussion

6.5.1 Charge at low C-rate

During charge, lithium is transferred from the PE to the NE. The lithiation level of the PE drops and that of NE rises as the charging event progresses. The ZTR that is influenced by the electrode lithiation levels is tracked as the charge progresses. For different current C-rates at 10 ^{o}C, Figure 6.5a shows the ZTR profiles plotted against the battery SOC. For the case of 0.2C charge rate, the ZTR reduced in the initial period of charging and then attained minimum levels in the mid-SOC band and then started to rise once again towards the end of charging. This profile is similar to the original ZTR profile (Figure 6.1d) obtained with the EIS data that is measured under non-plating conditions. Since the potential drops in the battery are expected to be significantly low while charging at a C-rate of 0.2C, the NEP could stay above the Li reference value for the entire charging period and thus, lithium plating is not expected in this low C-rate charging scenario [70]. The absence of lithium plating is further confirmed with the VRP method that infers lithium plating using post-charge voltage relaxation profiles. Figure 6.5b and c show the voltage relaxation profiles and its differential respectively. As per the VRP method, the single-stage relaxation of the voltage or its differential without a valley and peak for the 0.2C charge indicates the absence of plating.

6.5.2 Charge at high C-rates

To observe the ZTR profiles at high charge C-rates and at a temperature of 10 °C where lithium plating could potentially occur, charge C-rates 0.5C, 0.75C, 1C and 1.25C are applied in a sequence where the fully discharged battery is charged at the selected C-rate to 4.2V with the proposed charge interruption procedure. The ZTR profiles (as seen from Figure 6.5a) for charge rates ≥0.5C show an unusual trend compared to that of 0.2C or the ZTR trend derived from the EIS data (Figure 6.1d). After reaching near flat levels in the middle of charging, the ZTR profile of 0.2C shows a continuous rise until the end of CC charging. Conversely, the ZTR profiles for charges rates ≥0.5C have shown a negative trend until the end of CC charging period. The SOC level at which this trend begins (referred to as SOC_{tr} that is marked with vertical lines in Figure 6.5a) reduces with increasing C-rate which is in line with the general understanding, reported in the literature, that increasing C-rates reduce the SOC level at which lithium plating commences [5, 120]. As it can be seen from Figure 6.5a, SOC_{tr} is dropped from 79% at 0.5C charge rate to 35% at 1.25C charge rate.

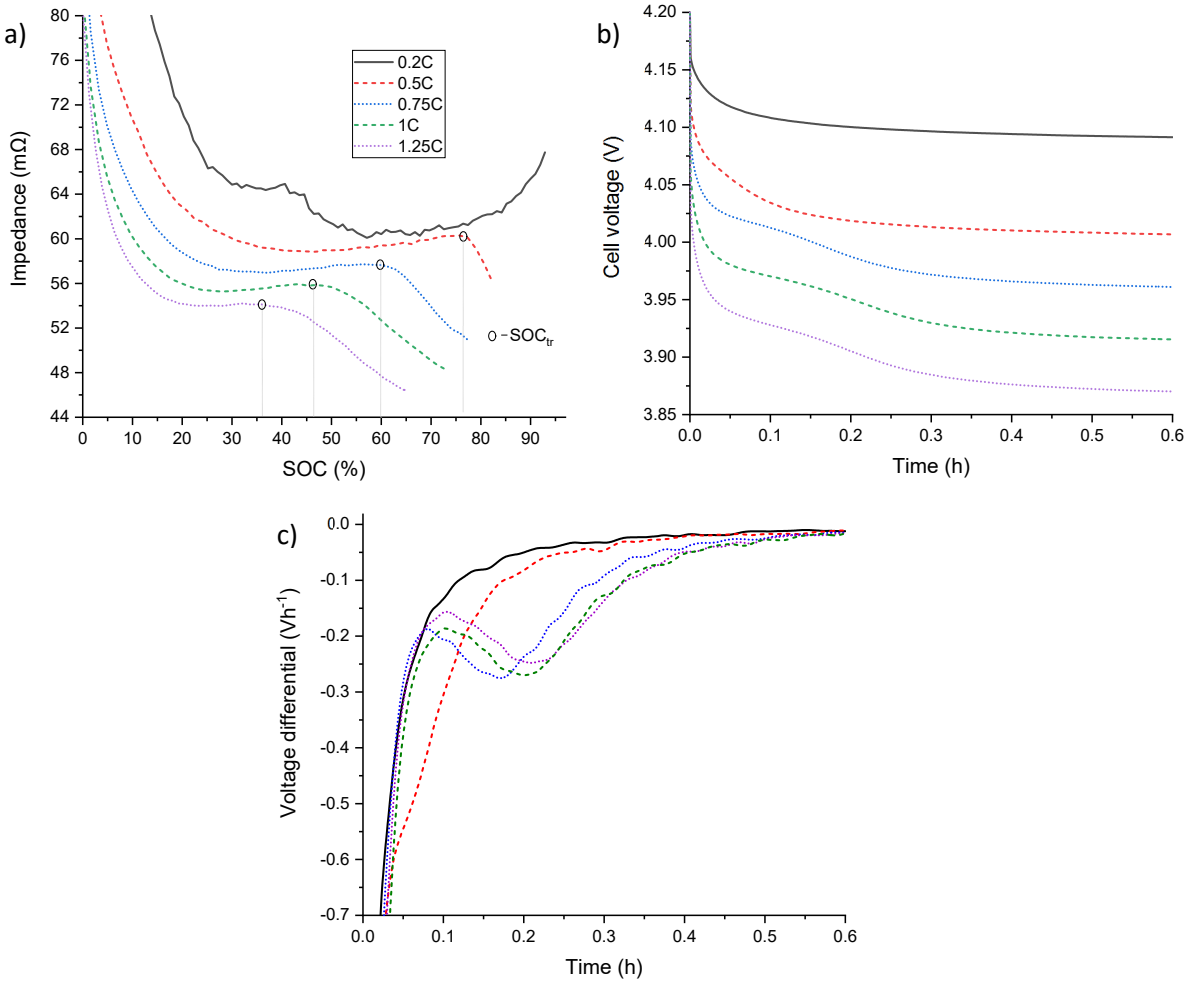

Figure 6.5: a) ZTR profiles of a cell in test case A1 (10 °C) at different C-rates (dotted vertical lines indicate the SOC level at which ZTR shows unusual trend. b) Post-charge voltage relaxation profiles and c) their differentials at different C-rates.

As discussed in section 6.3, the onset of lithium plating could affect the ZTR to produce such a negative trend. As discussed within [24] and described earlier, increasing charge C-rates raises the potential drops due to various internal mechanisms and lithium plating begins if the NEP drops below the Li reference level. The occurrence of lithium plating is confirmed with the VRP method. As shown in Figure 6.5c, the cell voltages in the post-charge relaxation period exhibit a two-stage recovery and their differentials with peaks and valleys indicate the occurrence of lithium plating for the charge rates greater than 0.75C. In the case of 0.5C charge rate, the voltage differential (Figure 6.5c) shows a profile that neither indicates the absence (as in the case of 0.2C) or occurrence of plating (as in the case of 0.75C) potentially because of smaller levels of lithium plating that are not detectable using this method. Therefore, as validated by the VRP method and supported by the theory described in section 6.3, it is believed that the ZTR profiles can be used to detect the occurrence of lithium plating. Once lithium plating begins, the intercalating current drops that reduce the rate of Li_{NES} raise. Since ZTR or Z_{CTL} are strongly associated with the Li_{NES}, the Z_{CTL} increase is reduced. Further, with the introduction of a parallel reaction in the form of lithium plating at the NE surface, the value of Z_{CTL} comes in parallel with the plating induced impedance at the NE interface as described in section 6.3.3. As a result, the impedance at the NE surface drops compared to the Z_{CTL}. Therefore, the SOC_{tr} at which ZTR trend changes shall indicate the onset of plating.

6.5.3 Charge at high temperatures

Similar to test case A1 performed at 10 ^{o}C, the value of ZTR is tracked at high temperatures (20 and 30 ^{o}C) at different C-rates with the charge interruption procedure to verify the proposed method's effectiveness at higher ambient temperatures. Figure 6.6a, b and c show the ZTR trends, post-charge voltage relaxation profiles and their differentials respectively at 20 ^{o}C for the test case B1. As it can be seen from Figure 6.6a, for charge currents ≥0.75C, the ZTR profile shows a negative trend towards the end of CC charging. For these charge rates, differentials of the post-charge voltage relaxation profiles (Figure 6.6c) also show peak and valleys indicating a 2-stage recovery and thus confirming lithium-plating occurrence. Figure 6.6d, e and f show the ZTR trends, post-charge voltage relaxation profiles and their differentials respectively at an ambient temperature of 30 ^{o}C for the test case C1. From the ZTR profiles, it can be seen that lithium plating is occurring for the charge C-rates ≥ 1C. While the VRP method failed to indicate the occurrence of lithium plating for these charge rates.

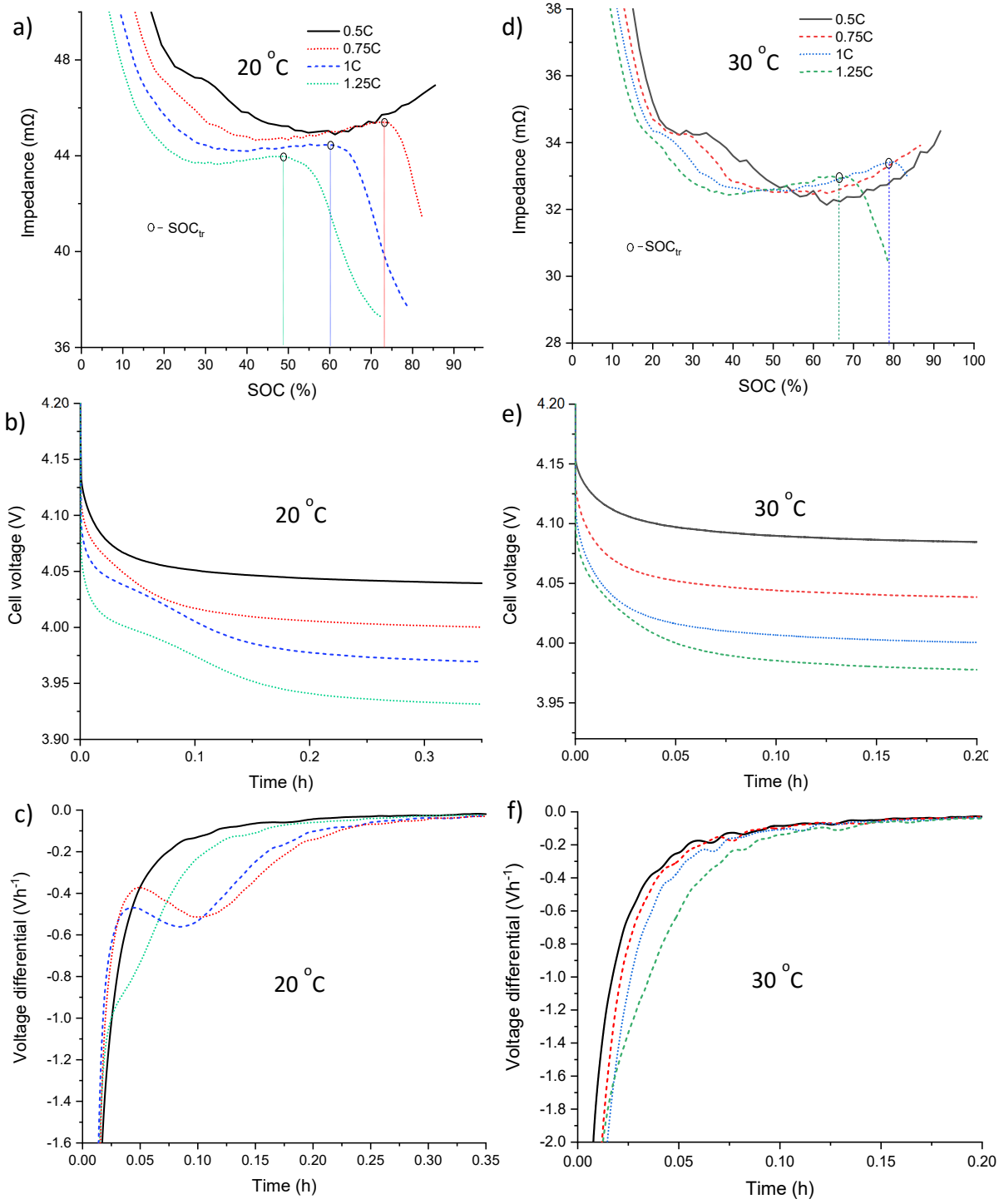

Figure 6.6: ZTR trends at different C-rates at a) 20 °C in test case B1 and d) 30 °C in test case C1; Corresponding post-charge voltage relaxation profiles at b) 20 °C and e) 30 °C and c) and their differentials at c) 20 °C and f) 30 °C

The possible limitation of the VRP method within this context is discussed further within [38] and summarised below. There are two potential reasons for the VRP method's failure to indicate plating at high temperatures. First, as discussed within [13, 70], lithium plating levels reduce with increasing temperature and second, lithium-stripping rate increases with increasing temperature. The combined effect of decreasing lithium plating levels and increasing stripping rate reduces the stripping time. As discussed in section 2.3.4 and within [28], the VRP method often fails to detect plating when the

lithium plating levels are below 2.5% of the battery capacity because it can become difficult to identify the 2-stage recovery in the time domain. However, the proposed ZTR based method validated at low 10 ^{o}C with the VRP method can detect the onset of plating even when the VRP method failed at an ambient 30 ^{o}C temperature. This indicates that the proposed method is highly sensitive compared to the VRP method while having the ability to detect the onset of plating for a broader range of environmental conditions.

6.5.4 Sensitivity to Interruption time

For inclusion within the BMS, influence of the length of the rest period in tracking the ZTR is analysed to better define whether a reduced interruption time is still able to capture the ZTR profiles accurately. By extracting the voltages recovered in 0.25 s, 0.5 s, 1 s and 2 s of the 3 s recovery period, the ZTR is calculated at these intervals of recovery and shown graphically in Figure 6.7a (at 0.2C) and b (at 1C) in comparison with the 3 s data for the test case A1. As it can be seen, the ZTR profiles appear similar albeit with some offset (circa 5 mΩ between the profiles observed at 3 and 0.25 s).

The reason for the ZTR profiles with offsets is analysed here. The selected reference f_{max} (0.1 Hz) is sufficiently lower than the actual f_{max} (> 3.4 Hz as can be seen from Figure 6.1c) of the new cells and therefore the impedance tracking approach captures not only the mid-frequency region but also a portion of the impedance from the low-frequency region. As the rest period is reduced from 3 s to 0.25 s, the contribution of the low-frequency region's impedance to the overall ZTR estimated value is equally reduced. Therefore, the ability to track the impedance from the mid-frequency region and thus detect the onset of lithium plating is still valid with the reduction of the rest period by 12 times.

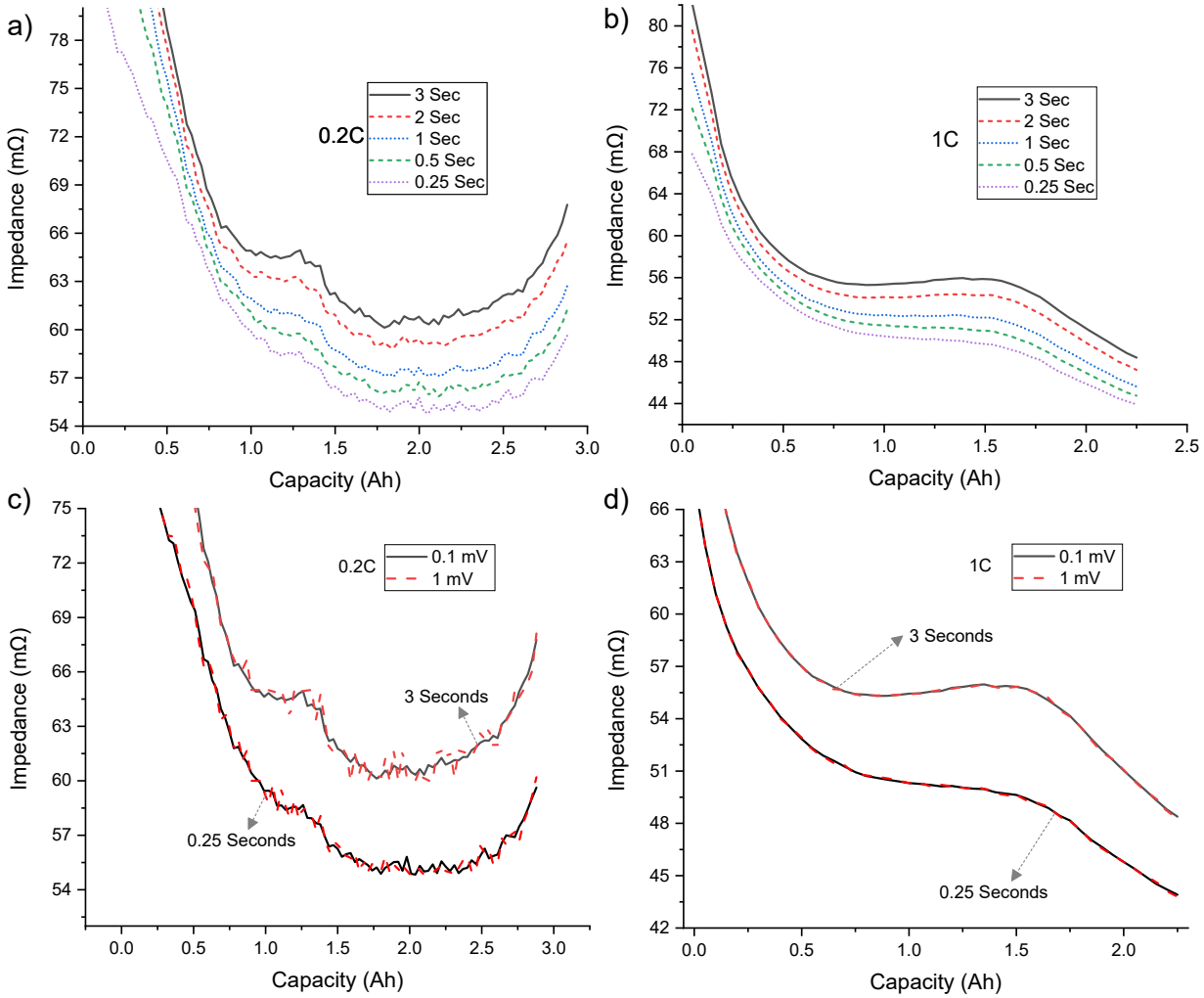

Figure 6.7: Impedance measurement sensitivity: a) Pulse period and b) Voltage resolution influence at 0.2C; c) Pulse and d) Voltage resolution influence at 1C

6.5.5 Sensitivity to voltage measurement resolution

Although the Maccor cell cycler enables voltage measurement with a resolution of 0.1 mV, it may be difficult to obtain such a high resolution in practical applications using typical BMS hardware. A 12 bit analogue to digital converter (ADC) that is found in a microcontroller can measure the voltage with the resolution of circa 1 mV (= 4200/2^12). The current generation of BMS ICs, for example, LTC 6812 from Analog Devices with 16 bit ADC can measure the cell voltage with less than 1 mV resolution with their 12 or higher bit ADCs. To verify the proposed method's ability to track ZTR and detect lithium plating under practical scenarios where voltage resolution is limited by the ADCs, measured voltages are quantised to 1 mV. Figure 6.7c and d show the ZTR profiles at 0.2C and 1C respectively at both resolution levels. ZTR calculated with 1 mV resolution at 0.2C in both 3 s and 0.25 s rest periods is similar to the 0.1 mV but with some additional noise added to the measurement. In the case of 1C, ZTR profiles are similar irrespective of the lower voltage resolution. Therefore, the reduced voltage

resolution may not hinder the ZTR profile tracking methodology and thus detecting lithium plating in real-time applications.

6.5.6 Impact of minimal cooling

The EIS plots at different SOCs (Figure 6.1b) and ZTR profiles in test cases A1, B1 and C1 are taken at constant ambient temperatures in which impedances from Ohmic, SEI layer and electrolyte are assumed to remain constant. However, in practical applications, temperature rise during a charging event is inevitable which can increase the Ohmic resistance and decrease the impedances due to the electrolyte, CTL and the SEI layer [111, 121]. Tracking the Z_{CTL} and thus detecting lithium plating may, therefore, become difficult if all the processes within the mid to high-frequency region are affected by temperature variations. To track the ZTR under the scenarios of minimal cooling, the cells from test case D1 are charged in a large room maintained at 20 ± 2 °C, but with no active thermal management. In each charge event, different C-rates are applied with pulse interruption procedure starting from 0.2C to 1.25C.

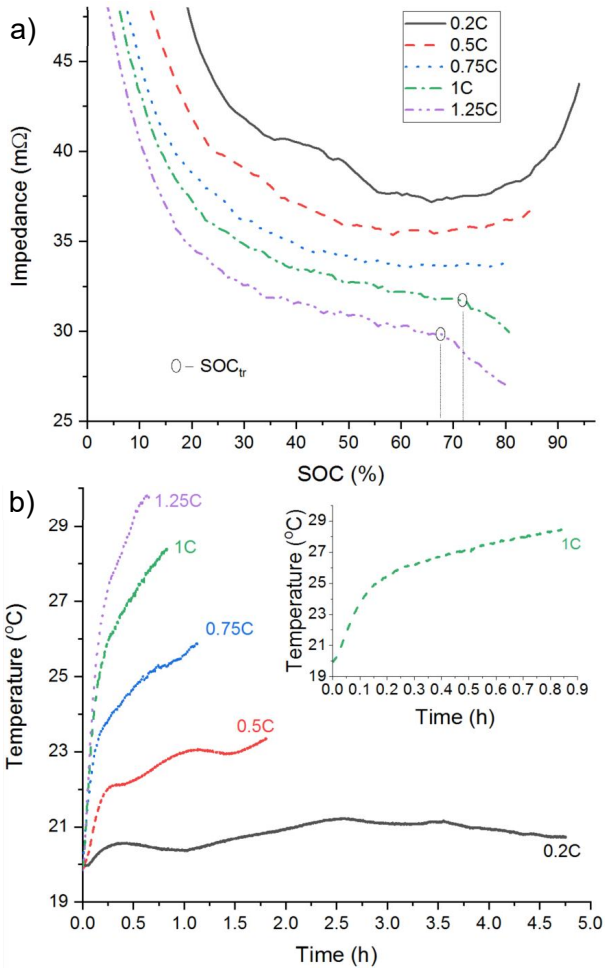

Figure 6.8: ZTR profiles without thermal cooling: a) ZTR profiles at different C-rates and b) temperature profiles measured on the cell surface

Figure 6.a and b show the ZTR profiles and cell surface temperature variations on a cell at different charging C-rates. The ZTR profile at 0.2C where the temperature rise is within +1 ^{o}C is similar to the ZTR profiles observed with active cooling. With the increase of C-rate, lithium plating induced trend change in the ZTR profiles is observed even with a temperature rise higher than 8 ^{o}C for charge rates ≥ 1C.

The ability to detect lithium plating using the ZTR profiles while the temperature is also changing can be explained as follows. As seen from the inset plot in Figure 6.b for 1C charge rate, the majority of the temperature rise (circa 5 ^{o}C rise of the total 8.2 ^{o}C) occurred during the first 10 minutes of the charging process and then the rate of temperature increase is reduced to 3.2 ^{o}C rise over the next 39 minutes. Since lithium plating typically occurs towards the end of CC charging where temperature changes are not assumed to be significant, temperature influence on the internal processes may be limited. Therefore, for the selected cell type and C-rates, lithium-plating detection using the ZTR profiles is possible even under environmental conditions where the temperature is increased during the charging process

6.6 Implications for fast-charge strategies development

Detection of lithium plating in real-time applications is essential to minimize its occurrence and track it over the cycles. Some of the existing approaches such as neutron diffraction and CE are not suitable for real-time use although they allow deriving offline profiles for new cells. While few other methods such as the VRP and DVC fail to detect lithium plating at high temperatures (> 20 ^{o}C) although they are suitable for online use. The proposed impedance-based approach of detection presented in this study overcomes many of these challenges faced by the existing methods. First, it is implementable in BMS given its dependency on the cell voltage and current. Second, it can detect the onset of lithium plating during charge. Finally, it works at ambient temperature. Therefore, it is viable that this method will be implementable in BMS to derive charging strategies that can minimize lithium plating levels and are adaptable to battery ageing.

6.7 Limitations and future work

6.7.1 Optimization of the proposed method

As observed in this work, the shape of the ZTR profile indicates the presence or absence of lithium plating during a charging event. A reduction of interruption pulse length from 3 s to 0.25 can track the ZTR profile shape and identify the onset of lithium plating. Since the interruption procedure can influence the overall charging time, further study is required to optimize the charge interruption

interval to minimize undesirable increases in overall charge time whilst maintaining the ability to track the ZTR profile.

6.7.2 ZTR tracking in aged cells

Within this work, an initial study of a new concept to detect lithium plating is introduced and validated on new cells. The selected 3 s interruption period can track the ZTR profile for a new cell at different C-rates and ambient temperatures effectively. However, as discussed within [111], the f_{tr} and f_{max} reduce as the battery ages and thus the interruption time needs to be re-estimated and adjusted in line with battery ageing to track the ZTR. The impedance levels of the internal processes within the battery are known to change as it degrades. Therefore, further work is required to study the robustness of the proposed method while cycling the cell as it loses capacity and its impedance characteristics change. Within such a study, to further validate the proposed method, the presence of lithium metal depositions can be verified by ex-situ means such as ICP-OES or NMR using the electrodes separated from the cycled cells.

6.7.3 Validation in different working conditions

As discussed in Section 4.7, the proposed method can detect lithium plating in cases where active cooling is not employed. A small variation in the cell surface temperature (for example, circa 3 ^{o}C rise in the last 50% of capacity addition at 1C rate) might have limited the contribution of temperature changes to the impedance variation. However, the cell surface temperature can significantly change and influence the impedance while charging in environments with varying temperature. To study the method's sensitivity to variations in ambient temperature, further study is required.

6.7.4 Implementation within a BMS

Given the proposed method's dependency on the voltage and current measurements, it can be implemented in real-time applications. For this, control algorithms suitable for a BMS to detect and limit lithium-plating need to be developed and evaluated. Within such a study, its ability to detect plating under different battery ageing levels can be included. Besides, when cells are in parallel, the method's ability to detect plating needs to be evaluated. As discussed in Section 2.3.1 and 2.3.3, lithium-plating occurrence follows non-homogeneous behaviour within a cell and non-invasive methods applied at the cell level pick up the average cell behaviour. When it comes to cells in a parallel bunch, the differences between cells such as capacity variations and temperature gradients may extend this non-homogeneous plating behaviour to the parallel bunch. Since the method monitors the voltage of the bunch, it will track the average impedance of the bunch and thus lithium plating similar to that of a single cell. However, as the number of cells in a parallel bunch rise, the ability to

pick up plating in a weaker cell may fade as the average behaviour of the bunch can be dominated by the remaining cells. Therefore, the application of the proposed method for detecting and developing charging strategies and its integration within a BMS needs to be explored.

6.7.5 Validation on different cell types

In this study, NCA/Graphite based 18650 cells are used to demonstrate the impedance-based lithium plating detection strategy. Since lithium plating is a phenomenon that occurs at the graphite electrode, the suggested method should work for all graphite-based lithium-ion cells. However, as discussed within [122] cell construction and chemistry can influence the internal processes and thus their impedance values. Since the method depends on tracking the impedance, further study is required to verify the transferability of the method to different cell formats and chemistries.

6.8 Conclusions

To meet research objective 3 defined in chapter 2, a new method of lithium plating detection is proposed in this study. Since lithium plating diverts a portion of the charging current at the negative electrode, it introduces an effective parallel reaction across the NE intercalation and modifies the battery impedance. Experimental results highlight that tracking the impedance of the cell can be used to detect the onset of lithium plating. During charge at high C-rates, the ZTR impedance has been shown to deviate from the usual profile at a defined SOC threshold, indicating the onset of lithium plating, with a further reduction in impedance as the value of SOC progress towards 100%. Using the established VRP method as a benchmark, this technique has been proven to accurately detect the onset of lithium plating at different C-rates and ambient temperatures. This fact coupled with practical considerations such as the resolution of the voltage measurement and duration of the current interval implies that it is suitable to underpin the derivation of optimised charging strategies and for inclusion in a real-world BMS. Unlike the previously available lithium-plating detection methods that detect lithium plating after completion of the charging process, the proposed in situ impedance (ZTR) based lithium-plating detection method can detect the onset of lithium plating during charge itself. Besides, its ability to detect lithium plating at room temperatures will be useful to study the limitations of fast charging more accurately at practical environmental operating conditions. These advantages are useful particularly for EVs since they will underpin the development of new innovative fast-charging profiles. Further work from this research is therefore focused on the derivation of novel charging strategies that optimise the trade-off between minimal degradation and charge time.

7 Study 5- Development of optimal charging strategies to prevent lithium plating in lithium-ion batteries at room temperature

7.1 Introduction

As discussed in Chapter 2 and 4, the existing approaches of lithium plating detection still face many challenges in their application for online use. For example, the CE approach is not suitable for online use as it needs high accuracy in current measurement and full charge/discharge to estimate capacity changes. While the VRP method fails to detect lithium plating at room temperatures limiting its application to the low-temperature conditions as detailed in Chapter 4. As presented in Chapter 6, in contrast to the existing detection methods of lithium plating, it is shown that the IT method can detect the onset of lithium plating while the battery is still in charge and works at practical environmental operating conditions.

To meet the research objective 5 defined in Chapter 2, this study presents a procedure to derive an online charging strategy based on the IT method. An offline charge profile is derived for use cases where the online implementation is difficult. For the offline one, a pre characterization procedure is employed to identify the charge profile. The identified charge profile is then applied to a set of cells in cycling. For the online method, a procedure to define the self-regulating charge current in real-time is detailed. The online approach is implemented and verified on a microcontroller-based evaluation board to evaluate its applicability for real-time use. The impact of the modified charge profiles on the charging performance and battery life are evaluated against the standard CC-CV charge profile. The IT method as discussed in Chapter 6 was studied on the selected cell type in its unused condition and not verified in the case of aged cells. Therefore in the current study, the method is also evaluated as the cells undergo degradation.

This study is structured as follows: In section 7.3, the experimental plan and test setup are discussed. Section 7.4 presents the procedure to derive the charge profiles. Test results and analysis are discussed in Section 7.5. The application and limitations of the study within the context of EV are discussed in Sections 7.6 and 7.7, respectively. Overall conclusions of this research are given in the final section.

7.2 Objectives of this study

To control lithium plating in real-time applications, the following objective is defined:

- To develop and validate a charging strategy for an online application using the IT method

Within this study, an offline charge profile is derived and the IT method is studied at different ageing levels of the battery.

7.3 Experimental

The commercial 18650 cells are characterized and cycled inside a climate chamber (Binder 9020-0385) along with a liquid cooling system (LAUDA) providing a stable ambient temperature (20 °C) with an accuracy of ±1 ^{o}C. In this study, three types of charging profiles at 20 °C are studied with three cells are used for each profile:

Set A2: Cycling with standard CC-CV protocol

Set B2: Cycling with offline optimized charging profile

Set C2: Cycling with online optimized charging profile

In case of the CC-CV charge profile, the cells are charged at a constant current of 3 A (1C) until a cell voltage of 4.2 V is reached, followed by a CV phase until the current reduces below 1 A (1/3 C). To reduce the test duration and to be able to detect lithium plating using the VRP method, the CV phase cut-off current during the charge is kept at such a high level. As discussed in section 3.4.2, the use of low CV cut-off currents (< C/6) reduces lithium plating available for detection in the post-charge conditions as lithium stripping begins in the CV phase itself.

For the offline and online charge profiles (Set B2 and C2), the CC phase is replaced by a multi-stage CC profile where the charge begins with a rate of 1.5C and then the charge rate reduces gradually to a value of 0.5C in steps of 0.25C. Offline and online charge strategies use different approaches as described in the latter part of this section to identify the cell voltages (V_1 to V_4) corresponding to these transition points in charge current. Charge profile in the proposed (online and offline) strategies along with that of the CC-CV are described in Table 7.1. Irrespective of the charge profile, all the cells during cycling are discharged with a 1C current to a value of 2.7 V followed by a CV phase at 2.7V with a 0.1 A cut-off current. Such a low CV cut-off current reduces the influence of impedance on reaching the EoC.

Table 7.1: Charge parameters for cycling experiments with the proposed and CC-CV charging protocols. All the cells are discharged with a 1C rate current to 2.7 V followed by a CV phase at 2.7V with a 0.1 A cut-off current.

Cell Set	Protocol name	Number of cells	Test case/Objective
Set A2	CC-CV	3	CC charge (1C) until 4.2V ›› CV charge until I < 1 A
Set B2	Offline	3	CC charge (1.5C) until V_1 ›› charge (1.25C) until V_2 ›› charge (1C) until V_3 ›› charge (0.75C) until V_4 ›› charge (0.5C) until 4.2 V ›› CV charge until I < 1 A
Set C2	Online	3	

In the case of CC-CV and Offline protocols (for Set A2 and Set B2 cells), a predefined charge profile is written to the cell cycler (Maccor, Model: Series 4000) for cycling the cells. For the offline protocol, the fixed-voltage levels (or transition voltages, V_1 to V_4 defined in Table 7.1) at which the charge rate is reduced are identified with an iterative pre characterization procedure using a separate five sets of new cells (referred to as OFF1, OFF2, OFF3, OFF4 and OFF5 sets). Here, for every CC stage, one set of cells is used to identify its terminating voltage level at that CC stage.

Table 7.2 shows the experimental parameters and objectives for the pre characterization tests which are conducted with the Maccor and the Lauda system. To derive the impedance profile during charge and to identify the onset of lithium plating, all cells in the pre-characterization tests are interrupted for 0.5 s every 1% SOC increase during the CC charge phase. The reasons for selecting the time as 0.5 s and its ability to track the impedance from the charge transfer limitations and thus detect the onset of lithium plating can be found in detail in Section 6.5.4. The procedure to identify the transition voltage levels in sequence and their application to the next set of cells are detailed in section 7.4.2.

Table 7.2: Offline characterisation test cases

Test sequence	charge Conditions	Test case	Objective
1	CC Charge(1.5C) to 4.2V	Set OFF1: 3 cells	To identify V_1
2	CC charge (1.5C) until V_1 ››› charge (1.25C) until 4.2 V	Set OFF2: 3 cells	To identify V_2
3	CC charge (1.5C) until V_1 ››› charge (1.25C) until V_2 ››› charge (1C) until 4.2 V	Set OFF3: 3 cells	To identify V_3
4	CC charge (1.5C) until V_1 ››› charge (1.25C) until V_2 ››› charge (1C) until V_3 ››› charge (0.75C) until 4.2 V	Set OFF4: 3 cells	To identify V_4
5	CC charge (1.5C) until V_1 ››› charge (1.25C) until V_2 ››› charge (1C) until V_3 ››› charge (0.75C) until V_4 charge (0.5C) until 4.2 V	Set OFF5: 3 cells	To verify that the derived charge profile avoids/minimizes plating

The online profile, applied to set C2 cells, tracks the impedance using the 0.5 s charge interruption for every 1% SOC increase and determines the plating onset and thus transitions between voltage levels (V_1 to V_4) in real-time. A microcontroller-based electronic system (TI evaluation board: C2000 Launchpad) with a cycle time of 10 ms is designed to track the impedance and to determine the voltage levels (V1 to V4) with the support of monitored cell voltages. Cell voltage signals of the cells in the online protocol are input to the TI board through voltage isolator evaluation modules (ISO224EVM) to maintain electrical isolation between the cells. The algorithms in the TI board tracks the cell voltage changes during the charge interruption periods to calculate the impedance for each 1% SOC increment and identifies the onset of lithium plating from the impedance profile. The procedures to calculate the impedance and identify the onset of lithium plating is detailed in section 7.4.3. Once the onset of plating is identified at each CC stage from the impedance values collected so far in that CC stage, the TI board communicates with the cell cycler through a Controlled Area Network (CAN) bus to initiate the charge rate reduction to the next CC level. For comparison and debugging, cell voltages measured and impedances estimated by the TI board are communicated via the CAN bus and recorded in a computer with a CAN bus analyser. Table 7.3 defines the CAN communication from the TI controller. Offline profile derivation and online control algorithm are presented in detail in Section

7.4. To minimize the influence of charge interruptions on the comparison of degradation and to track lithium plating tendency over the cycle ageing, the 0.5 s charge interruption for every 1% SOC increment in the cc phase is applied to the cells in the CC-CV protocol as well.

Table 7.3: CAN communication specifications

Message	**Sample rate**	**Data size**	**Data rate**	**Source**	**Target**
Cell voltage	50 ms	16 bit	500 kbps	TI controller	Computer
Impedance	For every 1% SOC rise	16 bit	500 kbps	TI controller	Computer
Charge control	1 s	8 bit	500 kbps	TI controller	Maccor cycler

To compare the capacity change during cycling, ageing is interrupted once every twenty cycles. During these capacity tests at 20 ^{o}C, CC-CV charging and discharging at 0.5C with a 50 mA cut-off current at the CV stage is performed to quantify comparable values of capacities across all the cells under test. The same ambient temperature for cycle ageing and capacity tests are applied to reduce the test time as a soaking time of up to 4 h is typically employed when the ambient temperature is changed to ensure the cells have reached thermal equilibrium [112].

The schematic diagram of the experimental setup for the cycling experiments is presented in Figure 7.1. The Maccor unit enables the measurement of the cell voltage and current with an accuracy of ± 1mv and ± 1 mA respectively. K-type thermocouples with an accuracy of ± 1°C are attached to the axial surface of each cell to measure the cell surface temperature. Cells are installed within a manifold and liquid surface cooling used to maintain cell temperature at the desired value of 20 ^{o}C using a LAUDA controller (Model: Proline RP 845 C) with the ability to regulate temperature to an accuracy of ± 0.1^{o}C.

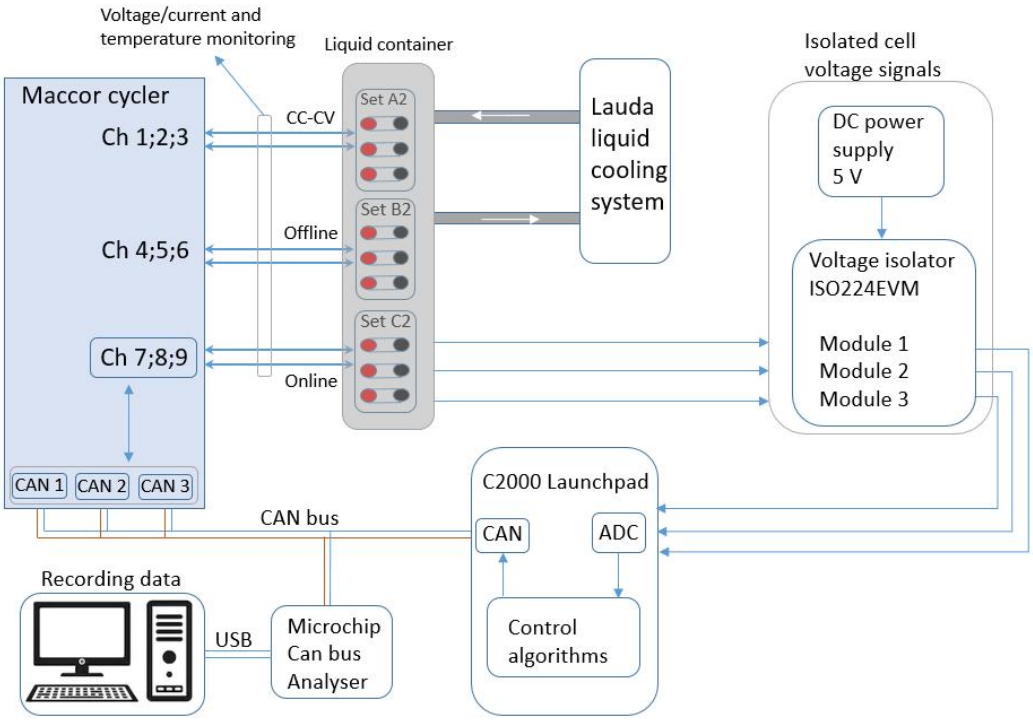

Figure 7.1: A single line diagram of the cycling experiments with the three charge protocols

7.4 Derivation of charge profiles

7.4.1 Impedance profile in the absence of plating

Before the 1.5C characterization, the cells in the OFF1 group are characterized for the impedance profile during the charge at 0.5C that is within the manufacturer recommended charge limits to identify the impedance profile under a plating free charge rate. Figure 7.2a shows the cell voltage and current during charge with the 0.5 s charge interruption every 1% SOC increase. As shown in the inset figure, the voltage difference (dV) between the cell voltage levels recorded before and at the end of an interruption is used for calculating the impedance (Z=dV/dI where dI represents the change in the current level, for example, dI is 1.5 A at 0.5C charge rate). The calculated impedance and its differential are shown in Figure 7.2b. During charge at 0.5C rate, the impedance in the early part of charging is found to reduce until it reaches a minimum level in the mid-SOC levels before it begins to rise in the latter part of charging. Corresponding impedance differential shows a reducing negative rate until it reaches zero level and then rising positive rates as the charge progresses. As discussed in section 6.5.1, such an impedance profile indicates the absence of lithium plating. At higher charge rates such as 1C that can cause lithium plating, the impedance profile shows a second negative trend in the latter part of charging in addition to the one in the early part of the charging process as detailed in the next section.

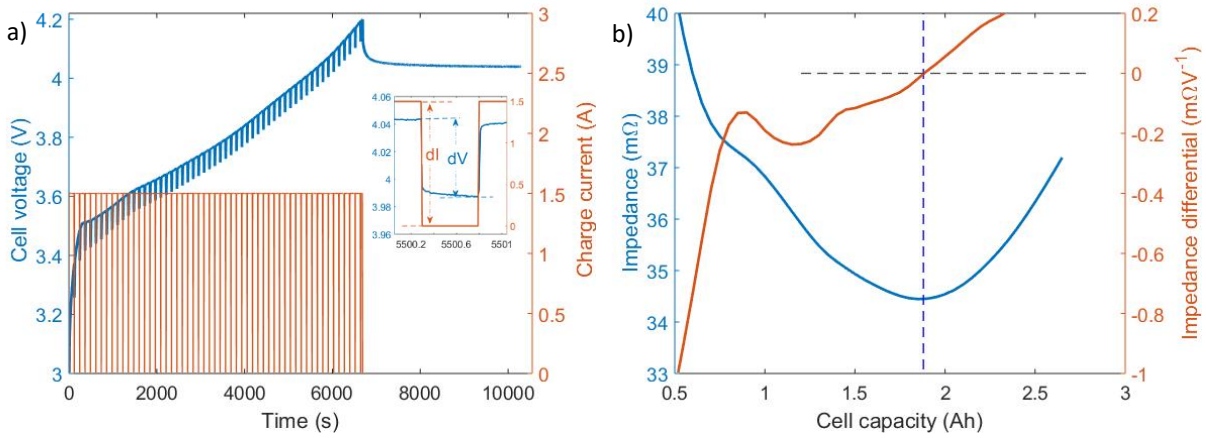

Figure 7.2: Charging at 0.5C rate: a) cell voltage and charge current and b) Impedance and its differential

7.4.2 Identification of Offline charge profile

In the proposed Offline charging protocol, the multi-stage CC with monotonic decreasing charge C-rates (1.5C, 1.25C, 1C, 0.75C and 0.5C) is applied. To identify the cell voltage levels corresponding to these transitions, a sequential characterization procedure is employed using the IT approach.

First, the fully discharged cells in the OFF1 set charged with a charge rate of 1.5C until the cell voltage reached 4.2 V with a 0.5 s charge interruption for every 1% SOC increase as presented in

Table 7.2. Figure 7.3a shows the cell voltage and current profiles during the charge. Figure 7.3b shows the corresponding calculated impedance and its differential. The impedance profile shows a second negative trend after the charge level has increased beyond 1.4 Ah similar to the one at the start of the charging. As discussed within [35], under the influence of lithium plating, the impedance profile that deviates from the usual “bathtub” profile and shows a second negative trend indicates the occurrence of lithium plating and can be used be to identify the onset of plating. The impedance differential is used to identify the cell voltage where the second negative trend begins that infers the onset of lithium plating. At the cell voltage level of 3.936 V for a cell in OFF1 set, the impedance differential reached a minimum level (-0.021 mΩ/V) and then it started to rise once again in the negative direction, unlike the raising positive rate of change as in the case of 0.5C charge rate. For the other two cells, these levels are identified as 3.941 and 3.943 V, respectively. Therefore, an average level of 3.94 V is taken as the plating onset voltage (V_1) at the 1.5C charge rate.

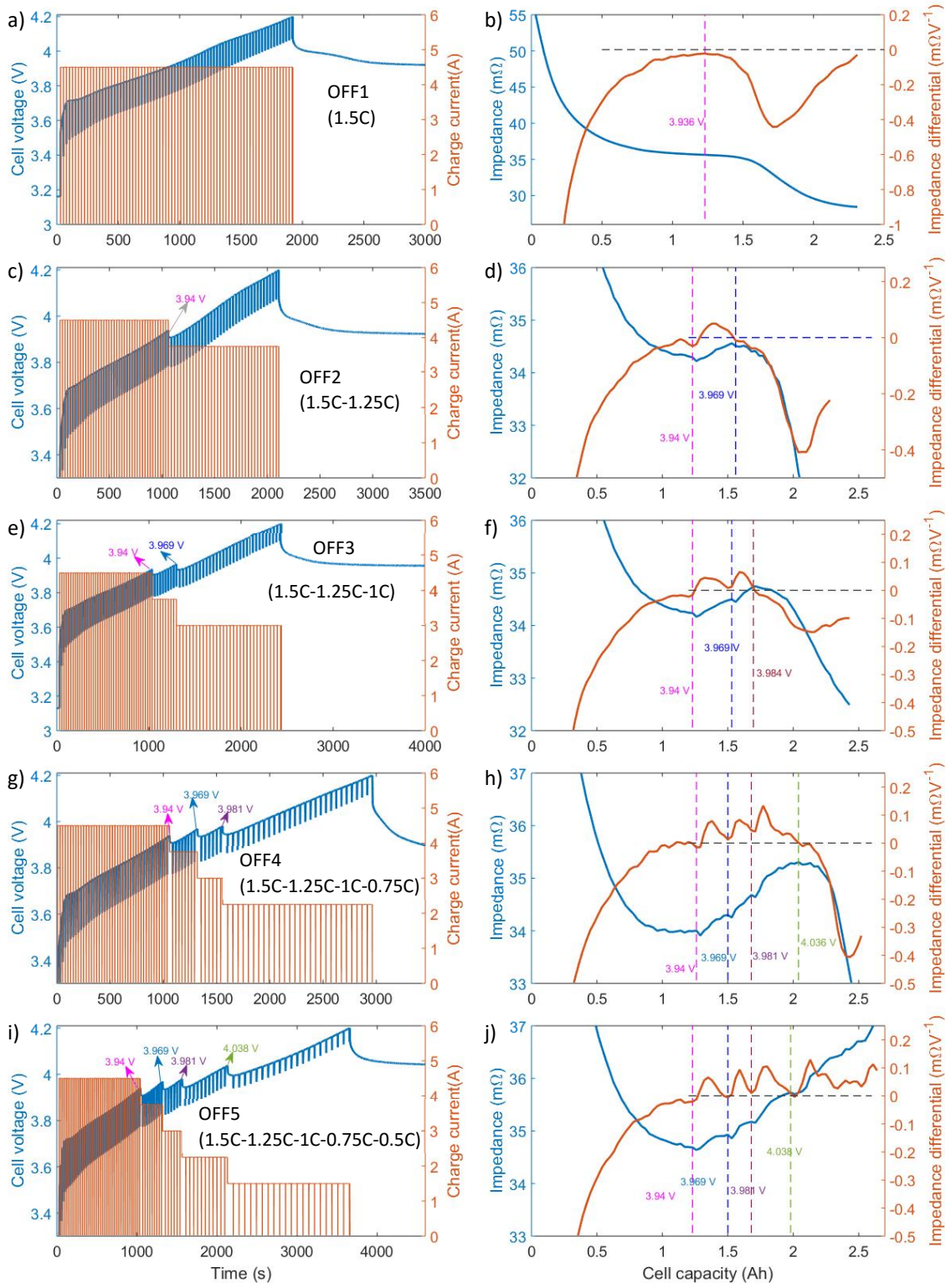

Figure 7.3: Offline charge profile development: Cell voltage and charge currents for different charge profiles and their corresponding impedance profiles and its differentials

Next, with the identified V_1 from the OFF1 cells, the fully discharged OFF2 cells are charged with a 1.5C charge rate until the cell voltage reached 3.94 V and then a 1.25C charge rate is applied for further

charging until 4.2 V as shown in Figure 7.3c. Corresponding Impedance and its differential profiles are shown in Figure 7.3d. After reducing the current at 3.94 V by 0.25C, the impedance started to rise thus leading to levels of a positive rate of impedance differential in the initial phase of the second stage CC. The arrest of the negative trend and its rise as the charge progresses at the reduced CC rate indicates plating onset is avoided at 3.94 V. As the charge continues towards 4.2 V at the reduced 1.25C rate, the impedance profile once again turned to a negative trend indicating the onset of plating. Cell voltage level corresponding to the zero levels of impedance differential and beyond which the impedance differential is negative is identified as 3.969 V. An average level of 3.969 V from the three cells (3.969, 3.972 and 3.967 V) is taken as the plating onset voltage (V_2) at 1.25C charge rate.

Further, with the previously identified V_1 and V_2, a three-stage CC charging (1.5C until 3.94 V- 1.25C until 3.969 V -1C until 4.2 V) is applied to the cells in OFF3 set as shown for a cell in Figure 7.3e. Corresponding impedance and its differential can be found in Figure 7.3f that show the onset of plating at a later stage. From the three cells in OFF3 set, the average value for V_3 is found as 3.981 V similar to the procedure mentioned for 1.5C-1.25C.

The results from the OFF3 are then used to define a 4 stage CC (1.5C-1.25C-1C-0.75C) with V_3 as the transition voltage for reducing the charge rate from 1C to 0.75C as shown in Figure 7.3g. The delayed plating onset voltage is now identified at a cell voltage level (V_4) of 4.038 V from the OFF4 cells using the impedance and its differential as shown for a cell in Figure 7.3h. Therefore V_4 marks the transition of charge rate to 0.5C from 0.75C.

A five-stage CC charge profile with the identified transition levels at V_1, V_2, V_3 and V_4 (as seen from Figure 7.3i) is then applied to the cells in the OFF5 set to verify whether the derived profile can avoid lithium plating. The impedance and its differential as seen from Figure 7.3j show no further negative trend. This charging profile is summarized in Table 7.4 and is used for ageing experiments of the cells in Offline protocol.

Table 7.4: Offline profile: Identified voltage thresholds

CC stage	Charge rate	Terminating voltage (V)
1	1.5C	3.94
2	1.25C	3.969
3	1C	3.981
4	0.75C	4.038
5	0.5C	4.2

7.4.3 Online charge procedure

Similar to the offline profile, charging in the online procedure commences at 1.5C rate and then reduces to 0.5C in steps with a step size of 0.25C. At each CC stage, C-rate reduction is initiated when the onset of plating is detected. To identify the plating onset and reduce the charge C-rate online in a charging event, the impedance values acquired by the TI board so far in that charging event are used. A simple flow chart to describe the algorithm developed for the microcontroller is presented in Figure 7.4 and described in the following sections.

7.4.3.1 Impedance calculation

The cell voltage is monitored every 10 ms and is the single input for the TI board from which the impedance is calculated in multiple steps. First, during charge, the algorithm checks for the charge interruptions as the cell voltage rise from 2.75 V to 4.195 V. Since these cells have an Ohmic resistance of circa 25 mΩ, charge interruptions with a current of 1.5 A (or 0.5C) or more shall produce a minimum instantaneous voltage drop of more than 37.5 mV. To measure the voltage, the inbuilt 16 bit analogue to digital converter (ADC) of the TI controller is used which measures the cell voltage within ±0.4 mV accuracy and with a resolution of 68 µV. For each voltage measurement (v_i) an average of thirty-two samples are taken to further reduce the noise to ±0.05 mV. Here, i defines the control loop or the algorithm execution cycle counter that increases by one once in 10 ms. When a minimum voltage drop of 30 mV is detected from the last two voltage measurements (v_{i-1}-v_i), the charge interruption is detected. The voltage levels taken before the interruption (V_P) and at the end of 0.5 s interruption (V_L) are then recorded. Next, the impedance is calculated. With the known current change (dI) and the measured voltage change ($dV=V_P-V_L$), the impedance Z_n is calculated where n denotes the impedance count in the current charging event. Since the charge rate in each cycle begins with 1.5C as per the test program written to the Maccor and a transition executed by the Maccor to the next lower C-rate at any CC stage is controlled by the TI board, the current C-rate and change in the charge current dI is assumed to be known and is not monitored by the TI board for simplicity. In real-time applications, both dV and dI can be directly calculated as the BMS typically monitors the cell voltage and cell current. However, it is noteworthy that for many applications these values do not define the voltage and current for an individual cell, but rather the parameters across a single parallel connection of cells within the module or pack. With a minimum voltage difference of 50 mV and a current change of 1.5 A observed at 0.5C, error in the impedance calculation is expected to be within 0.22 % (±0.1 mV error for the voltage difference of 50 mV and ±1 mA accuracy maintained by the Maccor for charge currents up to 5 A) of the actual value. Figure 7.5 shows the comparison of impedance profiles obtained from the Maccor data and that calculated by the TI board while performing OFF5 characterization on a cell

where the TI data is found to be within ±0.07 mΩ (< ±0.2%) of the Maccor data throughout the multi CC charging profile.

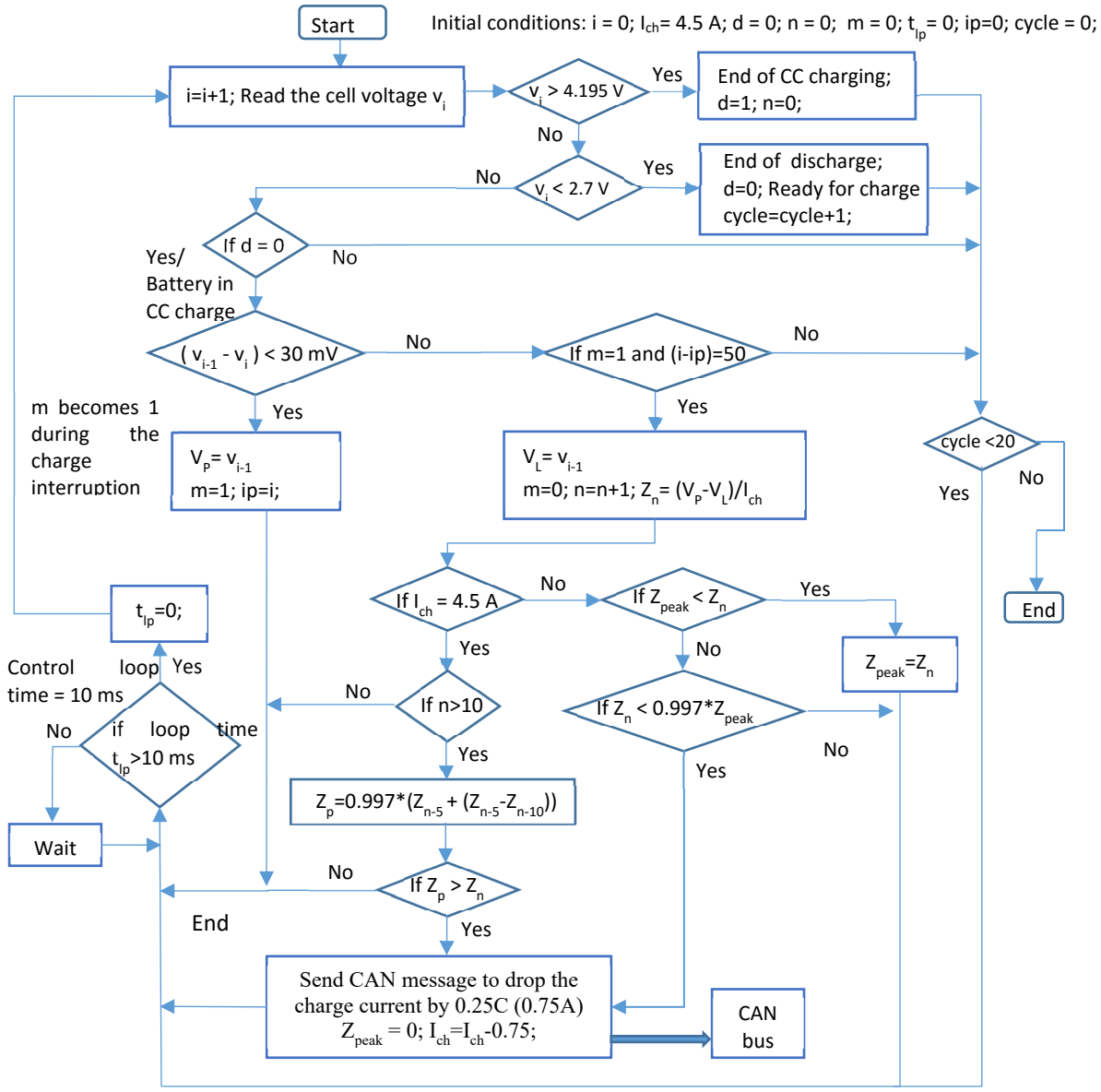

Figure 7.4: Flow chart representation of the online control algorithm

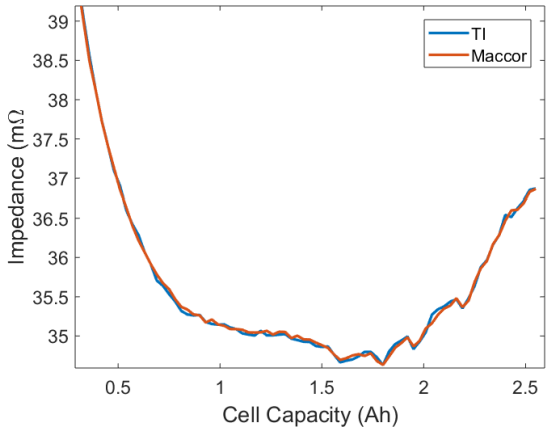

Figure 7.5: Impedance profiles obtained from the Maccor data and calculated by the TI controller

7.4.3.2 Detection of lithium plating onset

A closed-loop algorithm is designed to detect the onset of lithium plating during charge with the impedance values acquired so far within that charging event. Two different detection procedures are employed, one for the first CC stage (1.5C) and the other one for the remaining CC rates (<=1.25C) as described here. Once the SOC rises beyond 10% (or n>10, where n defines the number of SOC measurement points) at the initial charge rate of 1.5C, the past ten impedance values are used to verify the onset. Since the impedance has a reducing negative rate of change in the absence of plating, extrapolating the impedance using the past data (see eq 7.1) and their rate of change to predict the current impedance value (ZP_n) at any point of charge shall always produce a value which is lower than the actual value (Z_n). Once lithium plating commences, the Z_n value that drops from its plating free level goes blow the ZP_n value. Considering the impedance accuracy of 0.22%, a 0.3% margin is provided when comparing the predicted and actual values as shown here:

$$Plating\ is\ onset\ if\ ZP_n > Z_n \qquad (7.1)$$

$$here, ZP_n = 0.997 * (Z_{n-5} + (Z_{n-5} - Z_{n-10}))$$

Within a real-world application, this value may form one of the calibrations variables within the charging strategy. Application of this detection approach to detect plating onset is demonstrated with the data acquired from a cell in the OFF1 characterization as shown in Figure 7.6a. Once the plating onset is detected (marked with T1), the controller sends a CAN message to the Maccor to reduce the charge rate to 1.25C.

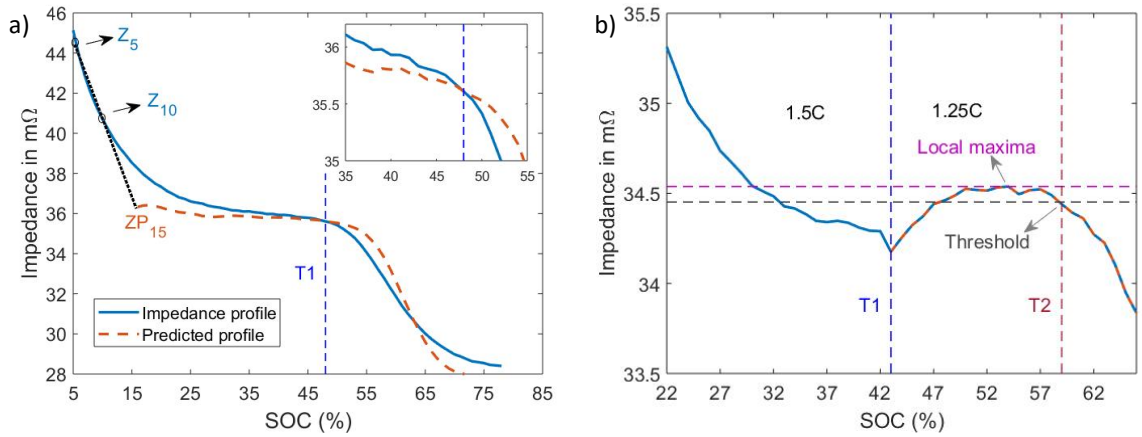

Figure 7.6: Online detection of plating onset: a) Onset is marked with T1 at 1.5C and b) T2 at 1.25C

After the first charge rate drop from 1.5C to 1.25C, a different approach is used to detect the onset of plating as the number of impedance values acquired at the early part of new CC stage (≤ 1.25C) are not sufficient enough to apply the prediction. The peak level of the impedance is recorded as the impedance starts to rise and plating onset is identified if the current impedance level drops by more than 0.3% from the peak. Figure 7.6b shows how this approach works when applied to the impedance data collected at the 1.25C CC stage of an OFF2 cell. As seen from the figure, impedance increased in the initial phase of the 1.25CC stage to reach a peak level of 34.57 mΩ before it started to drop. When a drop of 0.3% (to 34.4 mΩ) from the peak is detected, the negative trend is detected and a transition to the next lower CC rate (marked as T2) is issued. This approach is followed similarly for all other lower CC stages in the Online approach until the cell voltage reached 4.2 V.

7.5 Results and Discussion

7.5.1 Performance of the proposed charge profiles

Optimized charging profiles are required to simultaneously minimize charging time and the level degradation associated with fast charging. The use of a high current to reduce the charge time with the standard CC-CV profile can lead to lithium plating and therefore accelerated ageing. The SOC level at which plating commences can vary according to the operating temperature, charge rate and ageing level. The onset of plating can be identified from the impedance profiles as described in the offline pre-characterization procedure which can be used as a trigger to initiate a charge current transition from a higher to a lower level.

The Offline profile with the multi-stage CC protocol is derived from the pre-characterization procedure that identified the transition voltages for each CC stage (section 7.4.2). For the Online profile, the transitions are identified as the charge progresses for each CC charge stage. These charge profiles (Online and Offline) are evaluated while cycling the cells and compared with the standard CC-CV

charging profile. The results of the cycle ageing test with the charging protocols at 20°C are summarized in Figure 7.7. The standard CC-CV protocol with a 1C charge rate is found to result in the highest level of degradation. Figure 7.7a and b show the SOH as a function of cycle number and Ah throughput, respectively. The proposed multi-stage CC charging procedures show significantly higher charge throughputs compared to the respective standard CC-CV charging protocol. The Online and Offline approaches allow total throughputs for the used 18650 cells for 340 and 635 Ah, respectively while staying above 80% SOH. In contrast, the standard CC-CV charging protocol at 1C leads to a total charge throughput of only 194 Ah by the time it reaches 80% SOH.

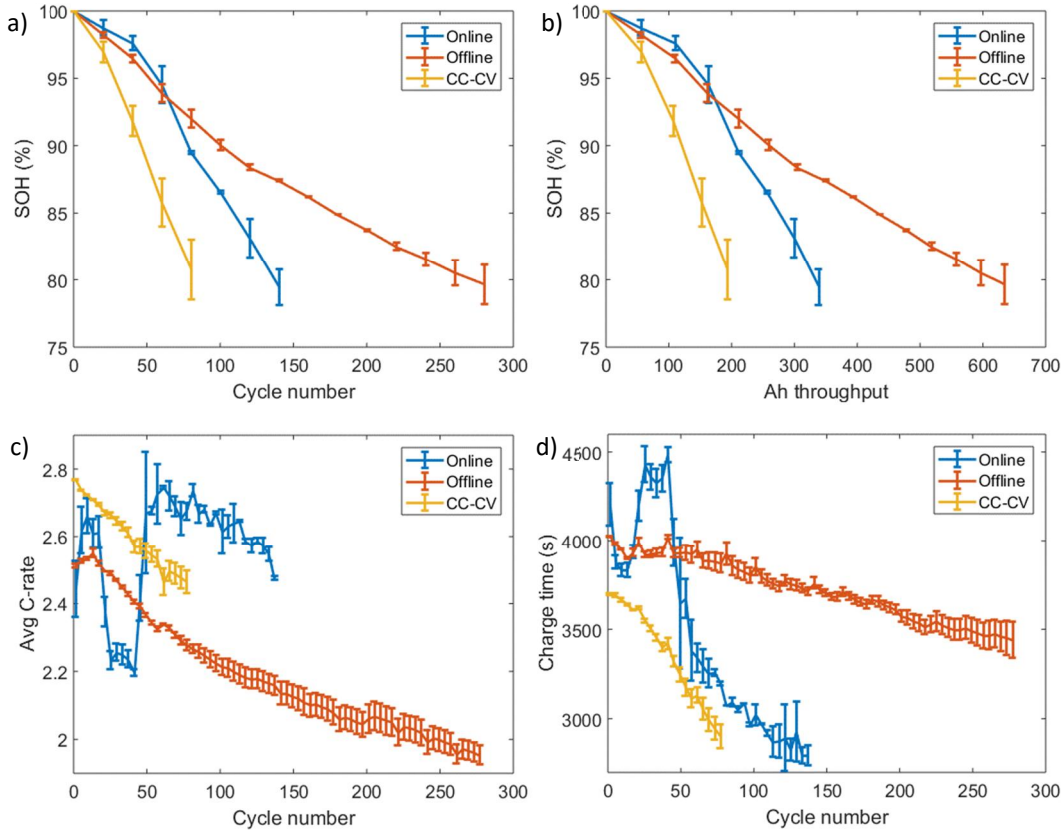

Figure 7.7: Comparison of different charging strategies: SOH as a function of a) cycle number and b) Ah throughput; c) average charging C-rate and d) charging time as a function of cycle number.

While comparing the charging speed, increased charging time or reduced average charge C-rate up to 20% is observed for the proposed charge profiles compared to that of the CC-CV protocol as shown in Figure 7.7c and d. The Offline profile compared to the CC-CV took circa 8.5% longer charging time (4025 s against 3711 s) at cycle number one which gradually increased to a 19% difference (3450 s 2900 s) by the time they reached their respective 80% SOH levels. The cells in the Online profile experienced similar levels of charging speed at the start of the cycling that reduced by nearly 10% in middle (cycle number 40) before finally it becomes circa 20% faster in the end compared to the Offline protocol. The reason for this is that the online approach adapts to the changes occurring as the battery

ages whereas the Offline method uses fixed voltage levels for the charge rate transitions. Between 20 and 45 cycles, the charging speed reduced in the online approach because of the shorter mid CC stages (e.g. 1.25 to 0.75C). After 45 cycles, the charging speed started to rise as the charge addition in the mid CC stages increased.

To make the comparison more understandable, given that charging time and SOH are changing with cycle number, the average charging time and cycle number (for a capacity reduction of 20%) are shown in Table 7.5. At the cost of circa 4% higher charging time, the online profile could extend the cycles by 75% compared to that of the CC-CV profile. Whereas the cell with the offline profile took an average 13% longer charging time while prolonging the cycle life by 250% compared to that of the cells with the CC-CV profile.

Table 7.5: Comparison of three charge profiles

Profile	Average charge time (s)	Number of cycles to lose 20% capacity
CC-CV	3310	80
Online	3440	140
Offline	3750	280

Figure 7.8a to c show the impedance profiles of the charging profiles at different cycle numbers. The star marks in the figures indicate the charge rate transitions for the proposed charge profiles. As seen from Figure 7.8a, at the 1C stage, charge capacity addition is increased from circa 0.3 Ah in the 21st cycle to 0.75 Ah in the 61st cycle. Therefore, with the increased capacity addition at high C-rates, overall charging time is reduced. Increased time between the actual onset (where the impedance rise slows down) to the detectable level (where the impedance drops by 0.3% from the peak level) at mid CC stages could extend the mid-CC stages. Lithium plating rising to the detectable level after the onset may reduce as the battery ages if the influence of degradation on the plating reactions is higher than the intercalation reactions. However, such a conclusion needs further study to understand the impact of previous lithium plating influence on the competing reactions in the form of lithium plating and lithium intercalation into the graphite.

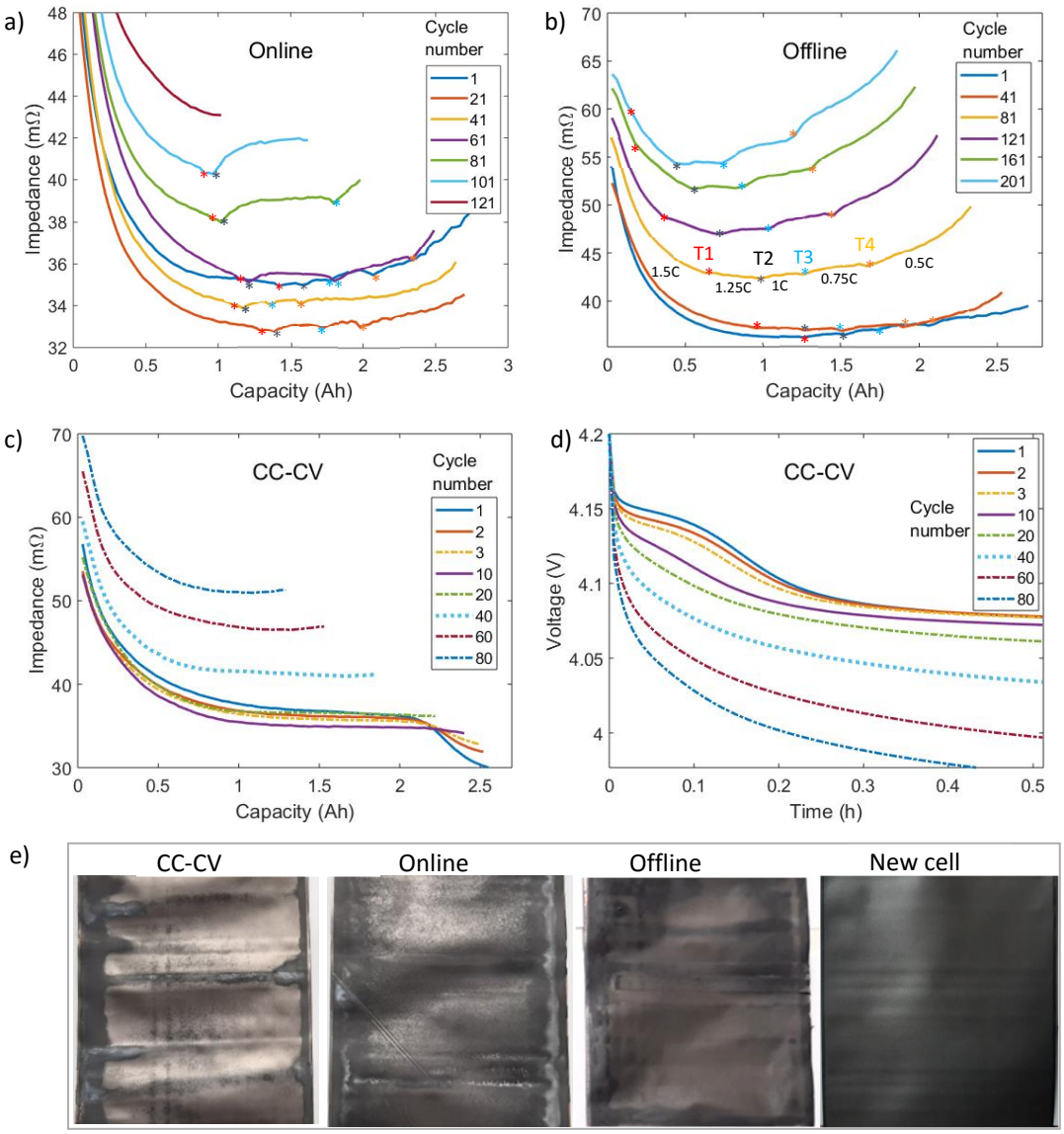

Figure 7.8: Comparison of charging strategies: Impedance profiles of a) Online, b) Offline and c) CC-CV protocols as function of charge capacity, d) voltage relaxation profiles of the CC-CV protocol and e) visual inspection of electrodes separated from aged cells under different protocols and a new cell.

The improvement in the cycle life in both Offline and Online approaches compared to the CC-CV profile can be explained through the impedance profiles derived in each charging event. As seen from Figure 7.8a and b, the impedance profiles in the proposed strategies avoid large second negative trends that, in turn, reduce lithium plating amounts. While Figure 7.8c shows the impedance profiles for a cell using the traditional CC-CV profile that shows a second negative trend inferring large amounts of lithium plating particularly up to the first 20 cycles. Figure 7.8d shows the post-charge voltage relaxation profiles for the same cell that exhibited a two-stage relaxation in the first twenty cycles. None of the cell voltage profiles in post-charge relaxations is found with a two-stage relaxation for both the proposed protocols indicate lithium plating levels are below the detectable levels (approximately <2.5%). Therefore, impedance and VRP methods together indicate higher levels of

lithium plating with the CC-CV protocol. Avoiding large negative trends (as seen from Figure 7.8a and b) both in offline and online approaches could minimize the plating depositions and result in improved battery life.

7.5.2 Cell inspection

One cell from each protocol was randomly selected to open to visually inspect metallic depositions on the graphite electrode surface. For comparison, a new cell is also dismantled. The cells were opened in an argon-filled glove box and electrodes are inspected visually for metallic depositions [58]. Figure 7.8e shows images of the graphite electrodes of the new cell and the cells selected from the CC-CV, Online, and Offline protocols. The graphite electrode of the new cell appears mostly black, as expected for a functional fully discharged graphite-based electrode [20]. A few areas exhibiting silvery depositions are found on the graphite electrode of the Offline cell. Meanwhile, much larger and distinguished areas with silver colour depositions are observed for the online cell. On the other hand, the NE of the CC-CV cell exhibits relatively highest dense silver colour depositions compared to other cells. As discussed in section 4.5.1.2, these depositions can be attributed to lithium plating. It is asserted therefore that proposed charge protocols are able to reduce the lithium plating levels when compared to the CC-CV protocol. Between the proposed protocols, lithium plating depositions are found to be higher with the online protocol compared to the Offline approach.

The approach adopted in the derivation of proposed charge profiles cannot completely avoid lithium plating. After the first transition to 1.25C as shown in Figure 2.3b, the impedance starts to rise in this initial stage and then the rate of increase starts to slow down towards zero before turning to negative levels. The rate of Impedance rise slowing could occur due to the onset of plating. In this case, there could be a small amount of plating by the time rate of change in the impedance becomes zero and some more with as the impedance starts to drop. The use of a zero rate of change or negative rate of change can cause a small amount of plating. In the Offline approach, the cell voltage corresponding to the impedance rate reaching the zero level is defined as the transition point. While the Online approach identifies the transition when the impedance drops from the peak level by 0.3% where the impedance rate of change is already turned to negative from the zero levels. Therefore, a small amount of plating could occur in each cycle in the proposed charge protocols with the Online procedure having higher levels compared to the Offline one. This also explains why the cells with offline charge profile have shown higher cycle life (see Figure 7.7) compared to that of the Online procedure.

7.5.3 Online control in partial charge events

To understand the transferability of the online control approach to real-world applications, the control procedure detailed in Section 7.4.3 is verified in cases where cells are not fully discharged. Before the partial charge events, a set of new cells that are fully discharged to 2.5 V are charged at C/3 to different

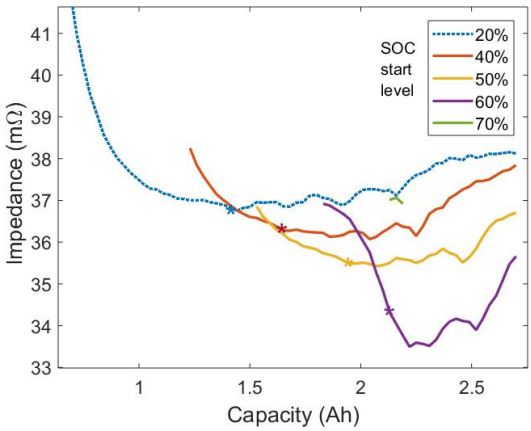

Figure 7.9: Impedance profiles at different partial charge events. Star marks indicate the first transition from 1.5C to 1.25C.

starting SOC levels (e.g. 20, 40, 50, 60 and 70%) and then allowed to rest for 4 h. After this, the cells are charged with the online charge control (beginning with 1.5C) to understand the online control behaviour under partial charge events. Figure 7.9 shows the impedance profiles for these charging events.

According to the online procedure, a minimum of 10% capacity addition or the previous ten impedance values is needed for detecting the onset. For the case of 60% SOC level at the start point, the impedance started to drop as soon as the charge initiated and the drop accelerated significantly after the first 5% capacity addition. As seen from Figure 7.9, the 0.42 mΩ drop in the first 5% SOC rise is increased to circa 1.9 mΩ in the next 5% SOC rise. The accelerated reduction in the impedance level as against the usual decelerated drop indicates the presence of lithium plating. However, as the designed algorithm begins to verify the onset of plating after a minimum of 10% SOC increase irrespective of the SOC level at the beginning of the charge, the onset is identified after the SOC is reached 70%. The delayed detection of the onset could result in increased levels of lithium plating. While for the SOC start levels 50% or lower, the impedance-based control can minimize negative drop and could control the profile with the identified transition points. In the case of 70% as the SOC start level, the cell reached 4.2V in less than 2 minutes with the 1.5C charge rate. Therefore, the results indicate that the online procedure may fail to limit lithium plating levels in partial charge events and, as discussed in section 7.7.4, needs further refinement.

7.5.4 Lithium plating occurrence as cell ages

As seen from Figure 7.8c, the impedance profiles of the CC-CV charge have shown the second negative trend until the first 20 cycles although the magnitude of the impedance reduction in the second negative trend is reducing with cycle number. From circa 7 mΩ or 20% drop in the first cycle, the impedance drop in the second negative trend is reduced nearly to zero by the 20^{th} cycle and no negative trend is observed thereafter. The reason for the undetected lithium plating occurrence beyond 20 cyles can originate from one of two reasons. First, as discussed within [31], there is a possibility of reducing lithium plating levels with the cycle number and then no significant levels of plating in further cycles. With the large levels of lithium plating in the initial cycles as detected with the impedance profiles and VRP method (see Figure 7.8c and d), plating tendency may reduce in the later cycles. The loss of cyclable lithium to the plating depositions and subsequent SEI layer growth in the presence of metallic lithium depositions can reduce the SOC level and the lithiation levels of the NE towards the end of the CC charge. As seen from Figure 7.8c, the SOC level towards the end of CC charging has reduced from 84% (2.52 Ah against the total capacity of 3.12 Ah) in the first cycle to 52% (1.29 Ah against 2.48 Ah) in the 80^{th} cycle. The increased potential drops could raise the cell voltage to 4.2 V in the CC phase at a much a lower SOC level than that of a new cell because of the reduced kinetics associated with battery degradation in the current collectors, electrodes, electrolyte, SEI layer and charge transfer limitations at the electrode surface. Therefore, although lithium plating could begin, reduced levels of charge in the CC stage may not allow lithium plating levels to rise to the detectable level (> 2.5%).

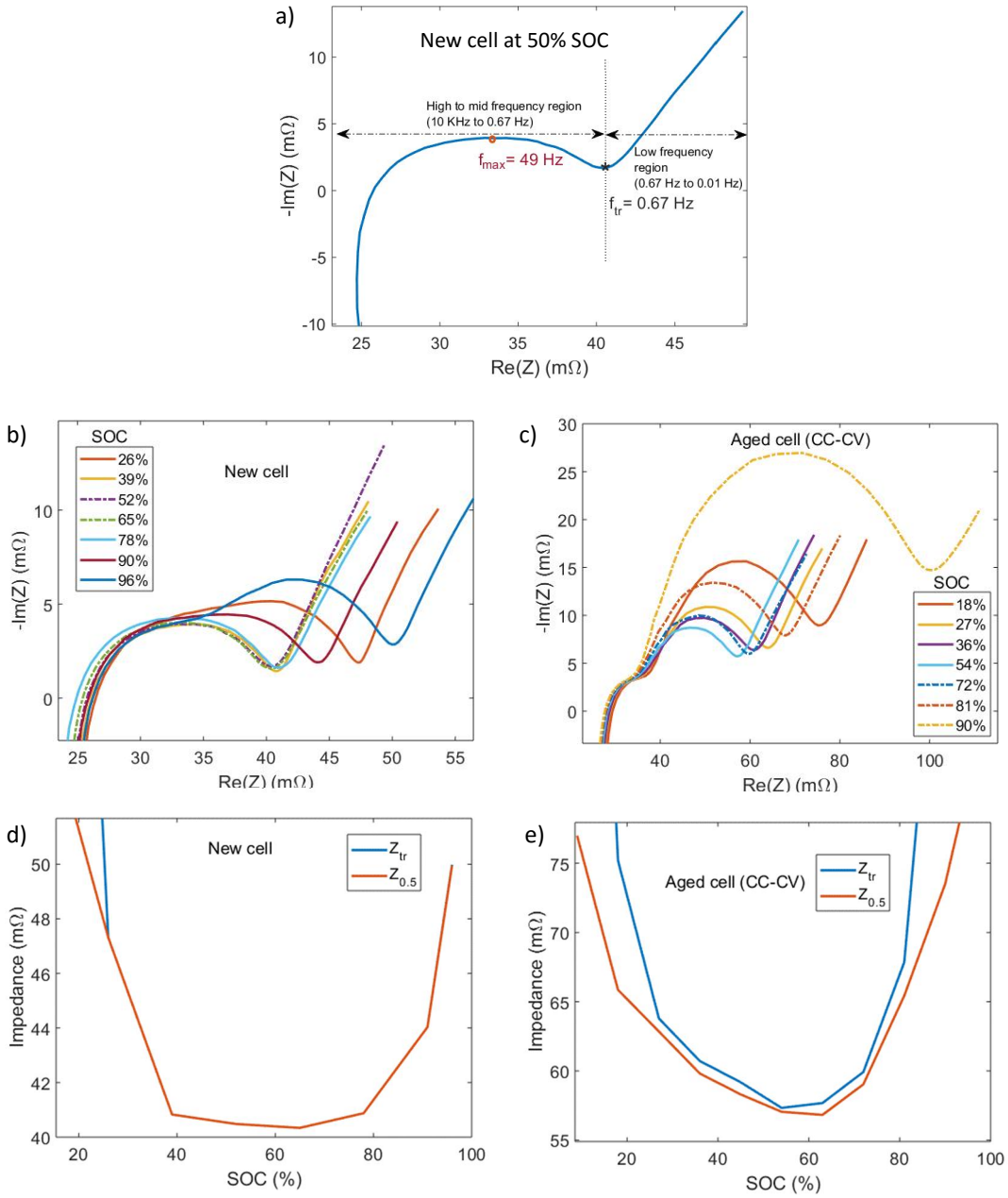

Figure 7.10: Impedance analysis with the EIS plots: a) EIS plot of a new cell at 50% SOC marked with f_{max} and f_{tr}, EIS plots at different SOC levels for b) a new cell and c) an aged cell; Impedance calculated with 0.5 s interruption and at f_{tr} for b) the new cell and c) the aged cell.

Second, there is a possibility of the impedance method failing to detect plating as the battery ages. The fixed interruption period of 0.5 s derived using new cells may fail to track the impedance as the battery ages. EIS plots at different SOC levels of a new cell and a cell aged under the CC-CV protocol are analyzed to study the influence of the interruption time on the impedance profile tracking. The IT method tracks the impedance at the transition frequency (f_{tr}) where impedance due to diffusion with a slope of 45° begins. To identify the impedance corresponding to f_{tr} with the interruption procedure, the frequency (f_{max}) at which reactance (imaginary part of the impedance) attains a maximum level in

the semicircle region is used. Figure 7.10a shows the EIS plot of a new cell at 50% SOC level marked with f_{max} and f_{tr}. As discussed within [111], from the f_{max}, the time constant ($\tau = (2\pi f_{max})^{-1}$) of the equivalent RC network that produces a semicircle impedance plot can be identified. Although f_{max} is varying with SOC, a constant period of 0.5 s is considered based on the previous study of a fresh cell since it was able to produce an impedance profile similar to the one captured at the f_{tr}. Since f_{max} reduces and thus τ rises as the cell ages compared to that of a new cell, the impact of constant charge interruption period on the ability to capture the impedance profile is analyzed. An interruption time of 4τ shall produce a voltage recovery of circa 98% of the total recovery. Use of an interruption time smaller than 4τ only allows a portion of total voltage recovery and therefore the impedance calculated (Z_t) shall also indicate a portion of the total impedance (Z_{tr}) as shown here:

$$Z_t = Z_{tr} * (1 - e^{-t/\tau}) \qquad (7.2)$$

Figure 7.10b and c show the EIS plots at different SOCs for a new cell and a cell that reached 80% SOH levels with the CC-CV protocol, respectively. From these EIS plots, Z_{tr} and $Z_{0.5\ s}$ profiles for these cells are plotted as shown in Figure 5.9d and e. For the new cell, Z with 0.5 s interruption is sufficient to track the Z_{tr} (Figure 7.10d). On the other hand, for the aged cell, the 0.5 s interruption can capture the Z_{tr} profile with up to 20% lower values. However, as discussed in Chapter 6, tracking the Z_{tr} profile is sufficient to detect the occurrence of lithium plating. Therefore, the 0.5 s interruption time used for tracking the Z_{tr} may not be the reason behind the non-observation of plating with the impedance method and indicates that lithium plating is reducing with the cycle number.

The reason for continued capacity loss after the first twenty cycles where lithium plating is not detected can occur because of the previously deposited lithium metal. As discussed in section 5.5.2, the lithium metal depositions could raise the mechanical stresses locally. As a result, active material cracking and subsequent growth of the SEI layer may continue to occur as long as the metal depositions remain in the cell. This indicates that lithium plating may have a long-lasting impact on battery degradation.

In summary, the analysis presented here indicates that lithium plating is reducing as the cell degrades under the influence of lithium plating in the previous cycles and therefore plating could not be detected with the impedance method in the later part of cycling. Further, small amounts of plating in each cycle combined with the effect of previous lithium metal depositions and their effect on the SEI layer may continue to degrade the battery.

7.6 Implications for fast-charge strategies development

The online charge protocol using the IT method is implementable within BMS given it relies on the measurement of cell voltage and current. By monitoring the impedance during charge, the online strategy modifies the charge current to control lithium plating. Therefore, unlike other approaches, the online protocol adapts to battery operating conditions including its ageing over several cycles. Unlike the CE or VRP approach that needs numerous testing to identify optimal charge profiles, the online approach using the IT method can select the charge profile within a single charging event. Therefore, while deriving the charge profile, this approach causes significantly lower levels of lithium plating compared to the approaches based on the CE or VRP method.

The offline protocol that uses a predefined charge profile show an improved performance compared to the online protocol as the online protocol relies on the occurrence and detection of lithium plating in every charging event. To maintain the benefits of the offline protocol and adapt it to battery ageing conditions, the offline profile can be derived and applied to the BMS at regular intervals such as EV service intervals. Since the offline characterization takes up to few cycles depending on the number of CC stages (for example, 5 stage CC charge profile needs at least five full charge events), the online procedure that needs a single charging event can be utilized to derive the charge profile at the service centres.

7.7 Limitations and future work

7.7.1 Improvement of the proposed strategies

The proposed strategies although they significantly extended the battery life can be further improved concerning the identification of the transition cell voltage levels that correspond to the potential onset of lithium plating. For example, the offline approach infers the onset point to the impedance differential when it reaches zero before it becomes negative. However, as discussed in section 7.5.2, the actual onset of plating could begin earlier somewhere close to the point where impedance rise starts to slow down. The approach used for identifying the transition could allow small amounts of plating. Such small levels of plating over several cycles may increase battery degradation compared to a low C-rate charge event. Since the Low C-rate shows a continuously rising impedance differential, initiating the transition as soon as impedance rise starts slows down may bring down the lithium plating amounts further. Therefore, further work is required to improve the plating onset identification accuracy and its impact on battery performance in terms of life and charging speed.

7.7.2 Charging strategy selection

The experimental work presented indicates that the offline protocol is better in extending the battery life while the online is superior for improving the charging speed. The predefined charge profile used in the offline approach could cause small amounts of lithium plating in the early cycle as discussed in 7.7.1 and avoid lithium plating completely in later cycles as lithium plating tendency drops with cycles as detailed in Section 7.5.4. Conversely, the online approach that modifies the charge profile when it detects lithium plating could induce a small amount of lithium plating in every cycle thus apply a high CC charge for a longer time and lose the capacity faster compared to the offline approach. To improve charging speed and battery life, both approaches can be incorporated into a charging strategy to adapt the offline profile to battery ageing. Therefore, further study is needed in these areas to facilitate the future deployment of fast charge algorithms.

7.7.3 The long-lasting impact of the plating

As observed in this work, the cells with the CC-CV charge protocol have experienced large levels of lithium plating which are then reduced with the increasing cycle number. However, the cells experienced higher levels of degradation in the later cycles where plating is not detected. One possibility is that depositions from the lithium plating in the early cycles might impact the battery kinetics and capacity fade. In such a context, lithium plating occurrence in the batteries needs to be completely avoided to eliminate the long-lasting negative impact of previous lithium depositions. To study whether plating has a long-lasting impact on battery degradation, further work is needed.

7.7.4 Charging strategy for partial charge events

The current derivative of the online approach is failing to detect and limit the plating occurrence when the starting SOC level is already high. Since even small amounts of plating in a few charging events may cause considerable degradation, Online control in the first 10% SOC rise needs an improved control method. For example, a comparison of the rate of change as SOC rises may provide further information in addition to the extrapolation of impedance profile. Further, SOC or voltages levels identified for each transition in full charge events can be recorded and used in partial charge events as hard limits in case of no sufficient data in the current charging event is available. Further work is required to improve Online control.

7.8 Conclusions

In this study, to meet research objective five, the impedance-based lithium plating detection method is utilized in developing an online charging strategy for BMS implementation. Besides, an offline charge profile is derived for comparison and for applications where the online procedure is not feasible. First, a procedure to derive charging profiles is detailed using the impedance profiles. The onset of lithium plating is inferred when a second negative trend in the impedance profile is observed and the cell voltage at which this occurs is then utilized to reduce the charge current by a predefined level. After the transition, the impedance profile recovery indicates the ceasing of further lithium plating. A pre characterization experiments are conducted to derive an offline charging profile with a multi-stage CC charge protocol. On the other hand, an online control algorithm is developed for a TI controller to detect and reduce the charge current in the online strategy.

Next, the charging performance of the proposed charging protocols along with that of a standard CC-CV protocol is verified on the selected cells during their cycle ageing at 20^{o}C. The significant improvement in battery life along with the inspection of electrodes after the ageing tests indicates that proposed charge profiles do reduce lithium plating when compared to the CC-CV protocols. The online and offline approaches with up to 20% increase in the charging time can extend the battery life by circa 75% and 250%, respectively compared to the CC-CV protocol before losing a 20% capacity. Further work from this research will be focussed on fine-tuning the developed charging strategies and their implementation in an EV BMS.

8 Discussion

This Chapter presents a reflective review of the research portfolio. The research has resulted in four innovations highlighted in Table 8.1. For each innovation, the contribution to knowledge and the impact to TVS motor Company is discussed. Section 8.6 outlines the opportunities for further work from this research.

8.1 Innovation 1: Improving the non-invasive lithium plating detection methods

8.1.1 Contribution to the knowledge

As detailed in section 2.3, none of the existing plating detection methods could detect the onset of plating within a charging event. Besides, they fail to detect lithium plating when plating levels are below 2.5%. Development of a new method of lithium plating detection to overcome these challenges is achieved through two separate studies generating one supporting and one primary innovation as presented in Table 8.1. The first study aimed at improving the existing non-invasive methods proposes a procedure to minimize the influence of the CV phase of charging on the reversible plating after the charge is terminated. The proposed procedure and experimental results in this study are published in the International Journal of Smart Grid and Clean Energy [37].

The second study (study 4) proposes a new method of lithium plating detection and evaluated it with the support of the improved existing non-invasive method. As presented in Chapter 6, the proposed IT method by tracking the impedance profile during charge allows detecting the onset of plating in real-time within a charging event, unlike any other approach of lithium plating detection. Further, its dependency on the measurement of the standard battery parameters such as cell voltage and current make it suitable for BMS use. The method and its experimental validation from this study are published in the Journal of Power Sources [35]. It is believed that academics would benefit from this method in lithium plating studies as it has many advantages compared to existing approaches.

Table 8.1: Summary of innovations

Serial number	Research Objective	Innovation	Contribution to academia	Impact to TVS	Chapter in IR
1	Research and develop a new approach to lithium plating detection that is implementable in real-time use and that detects the onset of plating during charge	A new method that is implementable in a BMS is developed to detect the onset of plating within a charging event and to improve the detection sensitivity	Published in [35]	Improved plating detection helps in developing optimal fast charging strategies to reduce charging time and thus range anxiety The effectiveness of a charge profile in avoiding lithium plating can be validated within a charge/discharge cycle	6
		Secondary innovation: A procedure to minimize the influence of the CV phase of charging on the existing non-invasive lithium-plating detection methods is developed	Published in [37]	Helps in validating a fast charging profile, particularly at low-temperature use cases	3
2	Develop a systematic procedure to develop a charging strategy for offline use	Procedures to derive charge profiles with the CE and IT methods	The CE based approach published in [38] Submitted to Journal of Energy Storage [39]	These procedures allow derivation of optimal charge profiles to maximize charging speed without negatively impacting the battery life Suitable for offline use	4 and 7
3	Develop a simplified degradation mode quantification procedure and identify the degradation modes of Li-ion battery aged under fast charge cycling	A procedure to quantify the degradation modes of Li-ion cells is developed Degradation modes of lithium plating are quantified	Published in [36]	Helps in minimizing the capacity fade in fast charging by taking the long-lasting negative impacts of plating into consideration	5
4	Explore a more practical solution that can derive optimal charging profile irrespective of the battery ageing conditions and be implemented in online mode	A procedure to derive an online charging strategy using the IT method.	Submitted to Journal of Energy Storage [39]	Battery life can be extended or the warranty period can be increased by adapting the charge profile to operating conditions and battery ageing. Developed algorithms are Implementable in TVS BMS	7

8.1.2 Impact to the sponsoring company

To improve the charging speed of the EV battery while limiting its negative impact on battery life, lithium-plating detection is crucial. As the proposed detection method is more sensitive and allows detection of lithium plating onset during charge, it will benefit TVS to study lithium plating in real-time in two ways. First, the developed method helps to evaluate a charging strategy without the need for long-term battery life tests as it can confirm the presence or absence of lithium plating within a charging event (reducing development time and the need for costly experimental facilities). Second, the new method of lithium plating can be used to develop improved fast charging strategies as presented in Study 5. Its potential application for online use allows the sponsoring company to adapt the charging strategies to battery ageing. Previous to this study, lithium plating studies were not included in the development of fast charging strategies at TVS because of a lack of knowledge and practical means of lithium plating detection. Since the new method relies on the measurement of cell voltage and current, works at practical working conditions and is superior to the existing approaches, TVS can employ it for studying and developing fast charging strategies to reduce charging time and thus to reduce range anxiety.

8.2 Innovation 2: Development of offline charging strategies for EV applications

8.2.1 Contribution to the knowledge

As detailed in Section 2.4, a systematic procedure to derive an optimal charge profile by considering lithium plating needs to be developed. Within this EngD, two new approaches of offline charge profile derivation are proposed. The first one employs the CE method as presented in study 2 (Chapter 4). Influence of lithium plating on the CE is used to identify the onset of plating iteratively and thus to derive multi-stage charge profiles. It is noteworthy that the CE approach needs extensive testing to identify the onset of lithium plating at each CC stage and thus to refine a charge profile as presented in Chapter 4. The proposed charging strategy and its experimental validation from this study are published in the Journal of Energy Storage [38].

The second one employs the IT method that identifies the onset of lithium plating within a single charging event at each CC stage of charging. Therefore, this reduces the testing required to refine the charging profile compared to the CE approach. However, unlike the CE approach, the IT method cannot minimize the overall level of battery ageing as its control is limited to lithium plating. Derivation and validation of the offline charge profile using the IT method are submitted to the Journal of Energy

Storage for publication [39]. It is believed that academics would benefit from these charging strategies as they allow developing offline charge profiles and minimizing the lithium plating in Li-ion battery packs.

8.2.2 Impact to the sponsoring company

Finding a strategy to minimize the degradation associated with the fast charging of Li-ion batteries represents a key research activity of TVS Motor Company. As lithium plating is known to occur at high C-rates of charging, it is essential to avoid lithium plating while developing a fast charge profile. Within this EngD, two different approaches to derive multi-stage charge profiles using the CE and IT method are proposed for EV applications. Using these approaches, Study 2 and 5 provide TVS the knowledge and procedure to derive offline charging profiles. Previous to this study, charge profile identification at TVS was limited to the standard CC-CV profile. The findings from this research provide better alternative approaches to TVS to derive improved fast charging strategies. Currently, TVS is developing a battery charger with a controllable current so that the developed charging strategies can be evaluated and implemented for their future EV projects. With the proposed procedures, TVS can optimize charging profiles to improve the charging speed without negatively affecting the battery life.

8.3 Innovation 3: Understanding the influence of lithium plating on battery degradation

8.3.1 Contribution to the knowledge

Lithium plating is considered to cause loss of lithium inventory (LLI) and thus capacity fade [31]. However, as discussed in Section 2.2, it is not understood whether plating induces loss of active material (LAM) as well. The study presented in Chapter 5 proposes a simplified procedure to quantify the degradation modes of li-ion battery and analyses the degradation in fast charging. The results indicate that lithium plating also results in significant levels of LAM at the NE. High volume-occupying lithium metal depositions could locally increase mechanical stresses and thus lead to or accelerate a LAM within the electrode. This finding is significant as lithium metal depositions from a previous charging event can potentially induce mechanical stresses as long as they are present in the cell. The degradation quantification procedure and its application to the cells aged under lithium plating from this study are published in the Journal of Energies [36]. It is believed that academics would benefit from this method in lithium plating studies as it has broadened the knowledge of lithium plating.

8.3.2 Impact to the sponsoring company

The knowledge generated and the procedure developed for quantifying the degradation modes help TVS in identifying the underlying damage happening to the battery as it loses capacity and in defining the limits for battery operating conditions such as depth of discharge (DOD) and temperature range to minimize such damages or maximize Ah throughput. In this study, the quantification procedure is applied to cells that lost capacity in fast-charge cycling. The findings from this study indicate that lithium plating raises LAM levels. High volume-occupying lithium metal depositions can result in increased mechanical stresses in Li-ion battery. As discussed within [2], the irreversible part of lithium plating that gets electrically isolated from the electrode can remain in the cell. Such high volume-occupying depositions may continue to maintain increased mechanical stresses and thus may produce a long-lasting negative impact on the battery life not limiting to the charge events that experience lithium metal depositions. Although further study is required to validate the long-lasting impacts of lithium plating, the analysis from the study suggests TVS avoid lithium plating completely to maximise its battery life. Improved battery life allows TVS to offer a higher warranty period for its EV battery.

8.4 Innovation 4: Development of online charging strategies for EV applications

8.4.1 Contribution to the knowledge

As discussed in section 2.4.5, the existing charging strategies have many limitations in their online use and adaption to operating conditions. An online procedure to derive a self-regulating charging strategy using the IT method is developed for real-time use as detailed in Chapter 7. Once the onset of lithium plating is detected at a particular CC charge, the charge rate is reduced to a next lower predefined CC level. In this way, a multi-stage CC charge profile is derived while minimizing lithium plating. This novel approach that optimizes the charge profile is suitable for real-time use and is adaptable to operating conditions including battery ageing level. The developed charging strategy and its experimental evaluation from this study are submitted to the Journal of Energy Storage for publication [39]. It is believed that academics will benefit from this approach of lithium plating control as it allows real-time use and adapts to operating conditions.

8.4.2 Impact to the sponsoring company

For EV applications, adapting charging strategies to the battery operating conditions is essential to optimise the charging performance in terms of maximizing charging speed and battery life. Existing charging strategies that aim to minimize lithium plating have many challenges in their implementation

for real-time use and adaption to operating conditions as discussed in Chapters 2 and 4. As an alternative, by employing the IT method that detects the onset of lithium plating in real-time, an experimental based approach of a new online charging strategy is proposed for the EV (Chapter 7). Unlike the other approaches such as those based on the CE, the developed charging strategy based on the IT method can be implemented in real-time applications and adapts to different operating conditions. The real-time implementation of this approach is demonstrated with the help of a TI based evaluation board. Therefore, this proposed approach would benefit the sponsoring company to derive online charging strategies and adapt them to different ageing levels of the battery while minimizing lithium plating. Therefore, by optimizing the charging profile throughout the battery life, TVS can extend the battery life further and thus offer a longer warranty period. Previous to this study, charge profile adaption to the operating conditions were not part of the TVS charging strategies. The knowledge and procedures developed from this research allow TVS to develop improved charging strategies for its future EV products.

8.5 Opportunities for further work

Table 8.2 summarises the research outcomes from this EngD and further work required for each research area at the research and application level. The concepts or procedures developed from this research can be validated and applied to a cell or a battery. The research within the Portfolio is limited to cell level because this is the most convenient direction taking into account the available resources. For instance, validating a developed procedure at a battery pack level requires high voltage and high power handling testing equipment and preparing a pack with mechanical and thermal considerations. The procedures developed could be proved and applied at pack level irrespective of the number of series connections given they can be applied to every parallel collection of cells. However, the influence of the cell to cell differences among the cells in parallel connection on the proposed concepts needs to be studied in further work. Further work specific to each research area at the research and application level is discussed in greater detail in the following subsections.

Table 8.2: Summary of innovations and areas for further investigation.

Research area	Research outcomes from this EngD	Further work at the research level	Further work for EV implementation
Understanding the influence of lithium plating on battery degradation	**A new procedure to quantify the degradation modes is developed** LAM quantification procedure is validated	**LLI quantification procedure needs validation** The long-lasting negative impact of lithium plating needs to be studied	**Optimisation of the quantification procedure for BMS implementation** Developing guidelines based on further research work for charging strategies

	Lithium plating raises LAM levels		based on the research outcomes
Improvement of lithium plating detection methods	**Development of a new method of lithium plating detection for real-time use** Validation and verification of the method at the cell level at different temperatures, C-rates and ageing levels **Method implementation in an embedded controller**	**Refining the impedance tracking procedure** Validation of the method at the battery pack level **Verification of the transferability of the method to different cell formats** Quantifying the accuracy level of the plating onset detection	**Optimization of the developed algorithms** Implementation of the method in an EV BMS
Development charging strategies to minimize lithium plating	**Development and validation of Offline charge profiles using the CE and IT methods at the cell level** Development and validation of Online charging strategy using the IT method at the cell level **Implementation of the Online strategy in an embedded controller**	**Extending the offline profiles derived to different temperatures and ageing levels** Refining the online charge strategy **Extending the online strategy to partial charge events** Validation of the proposed profiles at the battery pack level	**Optimization of algorithms developed for the online strategy** Implementation of the charge strategies in an EV BMS.

8.5.1 Research area 1: Understanding the influence of lithium plating on battery degradation

The proposed procedure for quantifying the degradation modes as presented in chapter 5 is partly validated with the IC-DV curves that allowed the comparison of LAM levels in both these approaches. However, the LLI levels estimated needs further validation to study the robustness of the proposed quantification procedure. The quantification procedure can be optimized for BMS use to keep track of changes occurring to the battery during its service.

Application of the quantification procedure to the cells aged in fast-charge cycling indicates lithium plating increases LAM levels and suggests degradation due to lithium plating is not limited to the charge events that experience lithium plating. To verify whether lithium plating has a long-lasting negative impact on the battery as isolated lithium metal depositions from previous lithium plating events can remain in the cell, further research is required. The outcome of such research will be useful to guide future charging strategies.

8.5.2 Research area 2: plating detection

In this study, the proposed IT method tracks the cell impedance using the charge interruption procedure. Since the interruption procedure can influence the overall charging time, further study is required to optimize the impedance tracking procedure to minimize undesirable increases in overall charge time whilst maintaining the ability to track the ZTR profile.

Accuracy in detecting the onset of lithium plating needs to be quantified. Since there exists no other experimental approach that could identify the onset. Further research is required to evaluate the accuracy of detection using the IT method.

The IT method is verified on the selected cell type and shall work for all graphite-based lithium-ion cells. However, as cell construction and chemistry can influence the internal processes and thus their impedance values, further work is required to verify the transferability of the method to different cell formats and chemistries.

Real-time implementation of the IT method is performed at cell level with the support of a TI evaluation board and Maccor cycler as discussed in Chapter 7. While implementing the same in battery modules in an EV that operates with large charge currents, further work is required in multiple areas. First, compared to that of the Maccor cycler used in the laboratory, a typical BMS measures voltages and currents with relatively lower accuracies. Second, while interrupting or initiating large charge currents at the battery module level, the slew rate of a charger can be lower than that of the Maccor operated with cell level currents. Third, depending upon the battery module, the number of cells in parallel can vary. Since the IT method tracks the average behaviour of a cell or cells in parallel, a higher number of cells in a parallel connection may make the plating detection difficult if plating occurs non-uniformly across these cells. Therefore, further work is required to study the influence of these factors on the impedance tracking method in real-time systems.

For the charge interruption procedure, as an alternative to the controllable charging system, it is possible to create a step-change to the charge current with the usual cell balancing circuits embedded in the BMS. Since impedance is tracked by creating step changes to the current, use of cell balancing currents during charge may allow tracking the impedance. Therefore, further work is required to evaluate the use of balancing currents for the IT method.

8.5.3 Research area 3: plating control

Within this work, offline and online charging strategies are proposed. The offline charge protocol derivation at a temperature and C-rate using the CE and IT method can be extended to different

temperatures and C-rates to enable the selection of a charge profile according to operating conditions. Towards this, further work is required. The IT-based procedure can be refined to optimize the charge profile which needs a separate study. At the pack level, further research is required in selecting a charge profile given there can be cell to cell variations such as temperature gradients. Similarly, BMS implementation of the offline profiles and their evaluation in an EV needs to be performed in future work.

The online charging strategy using the IT method can be improved by refining the procedure in detecting the onset of lithium plating in real-time. The online charge strategy is implemented in a real-time controller in this study to evaluate its practical use. The systematic procedure developed in deriving the online charging strategy is not computationally intensive and hence, it should be feasible to implement in a BMS. However, further study is required to look into the further refinement of the algorithm developed to optimize the code in terms of minimizing execution time and memory need. The IT method employs frequent charge interruption periods for a minimum of 0.5 s for a one per cent SOC increase. To apply a multi-stage CC profile with such interruptions, hardware and software of the BMS and battery charger need to be modified to implement the method. Therefore, further work is required for BMS implementation to utilize the proposed method in an EV.

Given TVS is working on controllable chargers, both offline and online charging strategies can be implemented in TVS EVs. Optimizing the charging performance in terms of charging speed and battery life will help TVS to reduce range anxiety and/or increase battery life. Further work is required to implement and evaluate the developed procedures in TVS EVs to realise and quantify the benefits specific to TVS needs.

9 Conclusions

This research programme started with the objective of deriving fast charging strategies by controlling lithium plating, within the context of a real-time embedded control application (BMS), to improve the performance of a future EV in terms of charging speed and battery life. After reviewing the relevant literature and understanding the requirements of the sponsoring company, three research areas have been identified: 1. Understanding the influence of lithium plating on battery degradation; 2. Detection of lithium plating occurrence; and 3. Control of lithium plating.

The influence of lithium plating on battery degradation (research area 1) is studied by proposing a new procedure to quantify the degradation modes and applying it to cells aged under fast-charge cycling. To quantify degradation modes, first, the utilization voltage range of each electrode is identified using the OCV profiles of a cell and its electrodes. This procedure is applied to the cell at two different ageing levels. Quantification of degradation modes is then carried out based on the identified electrode utilization ranges and the capacities delivered at two different ageing levels. LLI is calculated based on the changes to the lithium inventory present in the cell. On the other hand, LAM at each electrode is derived using its scaling effect on the electrode utilization range. The proposed procedure of quantifying the degradation modes using the OCV measurements and capacities when applied to cells aged under lithium plating highlight that lithium plating results in significant LAM_{NE} in addition to the LLI. Previously, LLI is considered a dominant degradation mode under lithium plating. This confirms that lithium plating raises the mechanical stresses in the cell and indicates potential long-term negative impacts of lithium plating. This study as presented in Chapter 5, therefore, underpins a better understanding of lithium plating, supporting the future development of optimal charging protocols to minimize battery degradation.

Studies involving improving the detection of lithium plating occurrence (research area 2) are conducted in two stages. First, research was focused on improving the existing approaches of lithium plating detection. Previous studies suggest different methods to detect plating in a non-invasive manner [2, 28]. However, they fail to detect the occurrence in some cases as they do not consider the impact of the cut-off current level at the CV phase of charging. To improve the detection sensitivity, Study 1 (refer to Chapter 3) proposes a procedure to identify the critical cut-off current. The results revealed that terminating the charge at the identified cut-off current level increases the plating detection ability. Further, this study suggests a procedure to distinguish the plating induced 2-stage

voltage relaxation from that of graphite phase changes for the VRP method. These outcomes improved plating detection sensitivity.

At the second stage, the research is focused on developing a new method of lithium plating detection as the existing methods still face many challenges such as they fail to detect the onset of lithium plating during charge. To overcome these challenges, Study 4 proposes a new method that use cell voltage and current measurements to track the impedance profile by causing a disturbance to charge current once for every 1% SOC rise. Verification and validation of the method at different temperatures and charge rates indicate its superiority over other non-invasive methods that barely detect lithium plating at near operating conditions. Therefore, the proposed technique provides the advantage of applying to real-world applications straightforwardly. The impact of this research provides new knowledge and capabilities to TVS regarding the detection of lithium plating in fast charging.

Similar to the studies involving lithium plating detection, charging strategies to control lithium plating (research area 3) are studied in two stages. First, charge profiles were derived with the support of existing approaches of lithium plating detection. Study 2 (refer to Chapter 4) applies the improved non-invasive plating detection method and CE approach for identifying the onset of plating to derive a three-stage (CC-CV-CC) charge profile for online and offline use, respectively. This experimental validation of the charge profile against the standard CC-CV profile show improved performance. However, the results also indicate the need for detecting the onset of lithium plating within a charging event as uncontrolled plating even in few charging events cause significant damage to the battery.

At the second stage of research involving plating control, charging strategies are developed using the developed IT method as the charging strategies derived with the existing approaches still face many challenges. The CE approach is not suitable for online use as it needs high accuracy in current measurement and full charge/discharge to estimate capacity changes and requires numerous tests to derive an offline profile. While the VRP method fails to detect lithium plating at room temperatures limiting its application to the low-temperature conditions as detailed in Chapter 4. To overcome these drawbacks, using the IT method, improved charging strategies for Online and Offline use are derived (Study 5 as presented in Chapter 7). The onset of lithium plating is inferred when a second negative trend in the impedance profile is observed and the cell voltage at which this occurs is then utilized to reduce the charge current by a predefined level. The Offline strategy used a pre characterization procedure to identify the charge profile while the Online approach tracks the impedance as the charge progresses, identifies the onset and modifies the charge current. Applying these charging strategies

shows that impedance-based charge control reduces lithium plating and improves battery life while minimizing the charging time. This outcome suggests that proposed charging strategies are suitable for implementation in BMS. Further, the potential scope for improvement of the derived strategies is identified for future work. For TVS, proposed charging strategies can be used to improve the charging performance, increasing the charging speed while minimizing its influence on the battery life to support the development of future battery designs.

In summary, the research presented in this thesis provides new knowledge, improved lithium plating detection and control methods and experimental data that allow manufacturers and researchers to better manage fast charging of batteries within onboard vehicle applications (e.g., BMS). Research yields a significant impact by providing a transferable procedure to detect and control lithium plating in fast charging.

References

1. McKinsey, *Urbanization in India.* URL: https://www.mckinsey.com/featured-insights/urbanization/indias-urbanization-a-closer-look accessed on 18 April 2020.
2. Uhlmann, C., J. Illig, M. Ender, R. Schuster, and E. Ivers-Tiffée, *In situ detection of lithium metal plating on graphite in experimental cells.* Journal of Power Sources, 2015. **279**: p. 428-438.
3. ICCT, *India BS6 emission norms.* URL: https://theicct.org/sites/default/files/publications/India%20BS%20VI%20Policy%20Update%20vF.pdf accessed on 20 April 2020.
4. McKinsey, *The Global EV market.* URL: https://www.mckinsey.com/industries/automotive-and-assembly/our-insights/the-global-electric-vehicle-market-is-amped-up-and-on-the-rise accessed on 15 April 2020.
5. Waldmann, T., M. Kasper, and M. Wohlfahrt-Mehrens, *Optimization of Charging Strategy by Prevention of Lithium Deposition on Anodes in high-energy Lithium-ion Batteries – Electrochemical Experiments.* Electrochimica Acta, 2015. **178**: p. 525-532.
6. Anseán, D., M. González, J.C. Viera, V.M. García, C. Blanco, and M. Valledor, *Fast charging technique for high power lithium iron phosphate batteries: A cycle life analysis.* Journal of Power Sources, 2013. **239**: p. 9-15.
7. Motors, T., *Cars portfolio.* URL: https://cars.tatamotors.com/ accessed on 15 April 2020.
8. Boomberg, *Battery price trends.* URL: https://about.bnef.com/blog/behind-scenes-take-lithium-ion-battery-prices accessed on 15 April 2020, 2020.
9. NITI, *EV report.* URL: https://niti.gov.in/writereaddata/files/document_publication/EV_report.pdf accessed on 1 May 2020.
10. Keil, P. and A. Jossen, *Charging protocols for lithium-ion batteries and their impact on cycle life—An experimental study with different 18650 high-power cells.* Journal of Energy Storage, 2016. **6**: p. 125-141.
11. Nitta, N., F. Wu, J.T. Lee, and G. Yushin, *Li-ion battery materials: present and future.* Materials Today, 2015. **18**(5): p. 252-264.
12. Wang, Q., B. Jiang, B. Li, and Y. Yan, *A critical review of thermal management models and solutions of lithium-ion batteries for the development of pure electric vehicles.* Renewable and Sustainable Energy Reviews, 2016. **64**: p. 106-128.
13. Waldmann, T., B.-I. Hogg, M. Kasper, S. Grolleau, C.G. Couceiro, K. Trad, B.P. Matadi, and M. Wohlfahrt-Mehrens, *Interplay of Operational Parameters on Lithium Deposition in Lithium-Ion Cells: Systematic Measurements with Reconstructed 3-Electrode Pouch Full Cells.* Journal of The Electrochemical Society, 2016. **163**(7): p. A1232-A1238.
14. Schuster, S.F., T. Bach, E. Fleder, J. Müller, M. Brand, G. Sextl, and A. Jossen, *Nonlinear aging characteristics of lithium-ion cells under different operational conditions.* Journal of Energy Storage, 2015. **1**: p. 44-53.
15. Motors, T., *Tata Nexon EV.* URL: https://nexonev.tatamotors.com/ accessed on 25 April 2020.
16. Bussiness Insider UK, *Battery price.* http://uk.businessinsider.com/tesla-electric-car-vehicle-battery-cost-chart-2017-1 (Accessed 21 Apr 2017).
17. Legrand, N., B. Knosp, P. Desprez, F. Lapicque, and S. Raël, *Physical characterization of the charging process of a Li-ion battery and prediction of Li plating by electrochemical modelling.* Journal of Power Sources, 2014. **245**: p. 208-216.
18. Cicconi, P., L. Postacchini, E. Pallotta, A. Monteriù, M. Prist, M. Bevilacqua, and M. Germani, *A life cycle costing of compacted lithium titanium oxide batteries for industrial applications.* Journal of Power Sources, 2019. **436**.
19. Zhang, Q., M.G. Verde, J.K. Seo, X. Li, and Y.S. Meng, *Structural and electrochemical properties of Gd-doped Li4Ti5O12 as anode material with improved rate capability for lithium-ion batteries.* Journal of Power Sources, 2015. **280**: p. 355-362.

20. Gallagher, K.G., D.W. Dees, A.N. Jansen, D.P. Abraham, and S.H. Kang, *A Volume Averaged Approach to the Numerical Modeling of Phase-Transition Intercalation Electrodes Presented for LixC6.* Journal of the Electrochemical Society, 2012. **159**(12): p. A2029-A2037.
21. Lu, T., Y. Luo, Y. Zhang, W. Luo, L. Yan, and J. Xie, *Degradation Analysis of Commercial Lithium-Ion Battery in Long-Term Storage.* Journal of The Electrochemical Society, 2017. **164**(4): p. A775-A784.
22. Smart, M.C. and B.V. Ratnakumar, *Effects of Electrolyte Composition on Lithium Plating in Lithium-Ion Cells.* Journal of The Electrochemical Society, 2011. **158**(4): p. A379.
23. Guo, Z., B.Y. Liaw, X. Qiu, L. Gao, and C. Zhang, *Optimal charging method for lithium ion batteries using a universal voltage protocol accommodating aging.* Journal of Power Sources, 2015. **274**: p. 957-964.
24. Bitzer, B. and A. Gruhle, *A new method for detecting lithium plating by measuring the cell thickness.* Journal of Power Sources, 2014. **262**: p. 297-302.
25. Vetter, J., P. Novák, M.R. Wagner, C. Veit, K.C. Möller, J.O. Besenhard, M. Winter, M. Wohlfahrt-Mehrens, C. Vogler, and A. Hammouche, *Ageing mechanisms in lithium-ion batteries.* Journal of Power Sources, 2005. **147**(1-2): p. 269-281.
26. Anseán, D., M. Dubarry, A. Devie, B.Y. Liaw, V.M. García, J.C. Viera, and M. González, *Operando lithium plating quantification and early detection of a commercial LiFePO 4 cell cycled under dynamic driving schedule.* Journal of Power Sources, 2017. **356**: p. 36-46.
27. Birkl, C.R., M.R. Roberts, E. McTurk, P.G. Bruce, and D.A. Howey, *Degradation diagnostics for lithium ion cells.* Journal of Power Sources, 2017. **341**: p. 373-386.
28. von Lüders, C., V. Zinth, S.V. Erhard, P.J. Osswald, M. Hofmann, R. Gilles, and A. Jossen, *Lithium plating in lithium-ion batteries investigated by voltage relaxation and in situ neutron diffraction.* Journal of Power Sources, 2017. **342**: p. 17-23.
29. Arora, P., *Capacity Fade Mechanisms and Side Reactions in Lithium-Ion Batteries.* Journal of The Electrochemical Society, 1998. **145**(10): p. 3647.
30. Pinson, M.B. and M.Z. Bazant, *Theory of SEI Formation in Rechargeable Batteries: Capacity Fade, Accelerated Aging and Lifetime Prediction.* Journal of the Electrochemical Society, 2012. **160**(2): p. A243-A250.
31. Petzl, M., M. Kasper, and M.A. Danzer, *Lithium plating in a commercial lithium-ion battery – A low-temperature aging study.* Journal of Power Sources, 2015. **275**: p. 799-807.
32. Waldmann, T., B.-I. Hogg, and M. Wohlfahrt-Mehrens, *Li plating as unwanted side reaction in commercial Li-ion cells – A review.* Journal of Power Sources, 2018. **384**: p. 107-124.
33. TVS, *About us.* URL: https://www.tvsmotor.com/About-Us/Overview accessed on 6th May 2020.
34. TVS, *TVS iQube.* URL: https://www.tvsmotor.com/iqube accessed on 5 May 2020.
35. Koleti, U.R., T.Q. Dinh, and J. Marco, *A new on-line method for lithium plating detection in lithium-ion batteries.* Journal of Power Sources, 2020. **451**.
36. Koleti, U.R., A. Rajan, C. Tan, S. Moharana, T.Q. Dinh, and J. Marco, *A Study on the Influence of Lithium Plating on Battery Degradation.* Energies, 2020. **13**(13).
37. Koleti, U.R., C. Zhang, T.Q. Dinh, J. Marco, T. Amietszajew, and R. Malik, *A new concept to improve the lithium plating detection sensitivity in lithium-ion batteries* International Journal of Smart Grid and Clean Energy 2019. **vol. 8, no. 5**: p. 505-516.
38. Koleti, U.R., C. Zhang, R. Malik, T.Q. Dinh, and J. Marco, *The development of optimal charging strategies for lithium-ion batteries to prevent the onset of lithium plating at low ambient temperatures.* Journal of Energy Storage, 2019. **24**.
39. Koleti, U.R., T.M. Ngoc, T.Q. Dinh, and J. Marco, *Development of optimal charging strategies to prevent lithium plating in lithium-ion batteries at room temperature.* Journal of Energy Storage, 2020. **Sumitted in September 2020.**

40. Koleti, U.R., T.Q. Dinh, and J. Marco, *Submission-1: Research on Lithium plating control techniques to reduce ageing and extend battery life: literature survey report.* EngD internal submission, Tech. rep., WMG, The University of Warwick, 2017.
41. Koleti, U.R., T.Q. Dinh, and J. Marco, *Submission-2: Improving lithium plating detection sensitivity.* EngD internal submission, Tech. rep., WMG, The University of Warwick.
42. Koleti, U.R., T.Q. Dinh, and J. Marco, *Submission-4: Degradation diagnostics of plating induced ageing.* EngD internal submission, Tech. rep., WMG, The University of Warwick, 2019.
43. Koleti, U.R., T.Q. Dinh, and J. Marco, *Submission-5: Study of Voltage Relaxation Profiles for lithium plating detection in Lithium-ion batteries at half-cell level.* EngD internal submission, Tech. rep., WMG, The University of Warwick, 2019.
44. Koleti, U.R., T.Q. Dinh, and J. Marco, *Submission-6: A new on-line method for lithium plating detection in Lithium-ion batteries.* EngD internal submission, Tech. rep., WMG, The University of Warwick, 2019.
45. Koleti, U.R., T.Q. Dinh, and J. Marco, *Submission-7: Development of optimal charging strategies to prevent lithium plating in lithium-ion batteries at room temperature.* EngD internal submission, Tech. rep., WMG, The University of Warwick, 2020.
46. Koleti, U.R., T.Q. Dinh, and J. Marco, *Submission-3: Reversible lithium plating detection based plating control.* EngD internal submission, Tech. rep., WMG, The University of Warwick, 2018.
47. Sarasketa-Zabala, E., F. Aguesse, I. Villarreal, L.M. Rodriguez-Martinez, C.M. López, and P. Kubiak, *Understanding Lithium Inventory Loss and Sudden Performance Fade in Cylindrical Cells during Cycling with Deep-Discharge Steps.* The Journal of Physical Chemistry C, 2014. **119**(2): p. 896-906.
48. Park, H., T. Yoon, Y. Kim, J.G. Lee, J. Kim, H.s. Kim, J.H. Ryu, J.J. Kim, and S.M. Oh, *Thermal Behavior of Solid Electrolyte Interphase Films Deposited on Graphite Electrodes with Different States-of-Charge.* Journal of the Electrochemical Society, 2015. **162**(6): p. A892-A896.
49. Collins, J., G. Gourdin, M. Foster, and D. Qu, *Carbon surface functionalities and SEI formation during Li intercalation.* Carbon, 2015. **92**: p. 193-244.
50. Dubarry, M., C. Truchot, B.Y. Liaw, K. Gering, S. Sazhin, D. Jamison, and C. Michelbacher, *Evaluation of commercial lithium-ion cells based on composite positive electrode for plug-in hybrid electric vehicle applications. Part II. Degradation mechanism under 2C cycle aging.* Journal of Power Sources, 2011. **196**(23): p. 10336-10343.
51. Sethuraman, V.A., N. Van Winkle, D.P. Abraham, A.F. Bower, and P.R. Guduru, *Real-time stress measurements in lithium-ion battery negative-electrodes.* Journal of Power Sources, 2012. **206**: p. 334-342.
52. Dubarry, M. and B.Y. Liaw, *Identify capacity fading mechanism in a commercial LiFePO4 cell.* Journal of Power Sources, 2009. **194**(1): p. 541-549.
53. Smith, A.J. and J.R. Dahn, *Delta Differential Capacity Analysis.* Journal of The Electrochemical Society, 2012. **159 (3) A290-A293**
54. Dubarry, M., C. Truchot, M. Cugnet, B.Y. Liaw, K. Gering, S. Sazhin, D. Jamison, and C. Michelbacher, *Evaluation of commercial lithium-ion cells based on composite positive electrode for plug-in hybrid electric vehicle applications. Part I: Initial characterizations.* Journal of Power Sources, 2011. **196**(23): p. 10328-10335.
55. Dubarry, M., C. Truchot, and B.Y. Liaw, *Synthesize battery degradation modes via a diagnostic and prognostic model.* Journal of Power Sources, 2012. **219**: p. 204-216.
56. Ge, H., T. Aoki, N. Ikeda, S. Suga, T. Isobe, Z. Li, Y. Tabuchi, and J. Zhang, *Investigating Lithium Plating in Lithium-Ion Batteries at Low Temperatures Using Electrochemical Model with NMR Assisted Parameterization.* Journal of The Electrochemical Society, 2017. **164**(6): p. A1050-A1060.
57. Zhang, Y., X. Li, L. Su, and Z. Li, *Lithium Plating Detection and Quantification in Li-Ion Cells from Degradation Behaviors.* ECS Transactions, 2017. **75 (23) 37-50**.

58. Bach, T.C., S.F. Schuster, E. Fleder, J. Müller, M.J. Brand, H. Lorrmann, A. Jossen, and G. Sextl, *Nonlinear aging of cylindrical lithium-ion cells linked to heterogeneous compression.* Journal of Energy Storage, 2016. **5**: p. 212-223.
59. Eckera, M., P.S. Sabeta, and D.U. Sauer, *Influence of operational condition on lithium plating for commercial lithium-ion batteries – Electrochemical experiments and post-mortemanalysis.* Applied Energy. **206**: p. 934-946.
60. Klett, M., R. Eriksson, J. Groot, P. Svens, K. Ciosek Högström, R.W. Lindström, H. Berg, T. Gustafson, G. Lindbergh, and K. Edström, *Non-uniform aging of cycled commercial LiFePO4//graphite cylindrical cells revealed by post-mortem analysis.* Journal of Power Sources, 2014. **257**: p. 126-137.
61. Ren, D., K. Smith, D. Guo, X. Han, X. Feng, L. Lu, M. Ouyang, and J. Li, *Investigation of Lithium Plating-Stripping Process in Li-Ion Batteries at Low Temperature Using an Electrochemical Model.* Journal of The E lectrochemical Society, 2018. **165 (10) A2167-A2178**
62. Ye, Y., Y. Shi, L.H. Saw, and A.A.O. Tay, *Simulation and evaluation of capacity recovery methods for spiral-wound lithium ion batteries.* Journal of Power Sources, 2013. **243**: p. 779-789.
63. Moura, S.J., F.B. Argomedo, R. Klein, A. Mirtabatabaei, and M. Krstic, *Battery State Estimation for a Single Particle Model With Electrolyte Dynamics.* IEEE Transactions on Control Systems Technology 2017. **Volume: 25 , Issue: 2**.
64. Broussely, M., P. Biensan, F. Bonhomme, P. Blanchard, S. Herreyre, K. Nechev, and R.J. Staniewicz, *Main aging mechanisms in Li ion batteries.* Journal of Power Sources, 2005. **146**(1-2): p. 90-96.
65. Leung, P.K., C. Moreno, I. Masters, S. Hazra, B. Conde, M.R. Mohamed, R.J. Dashwood, and R. Bhagat, *Real-time displacement and strain mappings of lithium-ion batteries using three-dimensional digital image correlation.* Journal of Power Sources, 2014. **271**: p. 82-86.
66. Lewerenz, M., A. Warnecke, and D.U. Sauer, *Post-mortem analysis on LiFePO 4 |Graphite cells describing the evolution & composition of covering layer on anode and their impact on cell performance.* Journal of Power Sources, 2017. **369**: p. 122-132.
67. Frisco, S., A. Kumar, J.F. Whitacre, and S. Litster, *Understanding Li-Ion Battery Anode Degradation and Pore Morphological Changes through Nano-Resolution X-ray Computed Tomography.* Journal of The Electrochemical Society, 2016. **163**(13): p. A2636-A2640.
68. Bhardwaj, R.C., T. Hwang, and R.M. Mank, *Modulated, temperature-based multi-CC CVcharging technique for Li-ion/Li-Polymer batteries.* US patent 8816648 B2, 2014.
69. Downie, L.E., L.J. Krause, J.C. Burns, L.D. Jensen, V.L. Chevrier, and J.R. Dahn, *In Situ Detection of Lithium Plating on Graphite Electrodes by Electrochemical Calorimetry.* Journal of the Electrochemical Society, 2013. **160**(4): p. A588-A594.
70. Burns, J.C., D.A. Stevens, and J.R. Dahn, *In-Situ Detection of Lithium Plating Using High Precision Coulometry.* Journal of the Electrochemical Society, 2015. **162**(6): p. A959-A964.
71. Smith, A.J., J.C. Burns, S. Trussler, and J.R. Dahn, *Precision Measurements of the Coulombic Efficiency of Lithium-Ion Batteries and of Electrode Materials for Lithium-Ion Batteries.* Journal of The Electrochemical Society, 2010. **157**(2): p. A196.
72. Smart, B.V.R.a.M.C., *Lithium Plating Behavior in Lithium-ion Cells.* ECS Transactions, 25 (36) 241-252 (2010).
73. Zinth, V., C. von Lüders, M. Hofmann, J. Hattendorff, I. Buchberger, S. Erhard, J. Rebelo-Kornmeier, A. Jossen, and R. Gilles, *Lithium plating in lithium-ion batteries at sub-ambient temperatures investigated by in situ neutron diffraction.* Journal of Power Sources, 2014. **271**: p. 152-159.
74. Schindler, S., M. Bauer, M. Petzl, and M.A. Danzer, *Voltage relaxation and impedance spectroscopy as in-operando methods for the detection of lithium plating on graphitic anodes in commercial lithium-ion cells.* Journal of Power Sources, 2016. **304**: p. 170-180.

75. Yang, X.-G., Y. Leng, G. Zhang, S. Ge, and C.-Y. Wang, *Modeling of lithium plating induced aging of lithium-ion batteries: Transition from linear to nonlinear aging.* Journal of Power Sources, 2017. **360**: p. 28-40.
76. Petzl, M. and M.A. Danzer, *Nondestructive detection, characterization, and quantification of lithium plating in commercial lithium-ion batteries.* Journal of Power Sources, 2014. **254**: p. 80-87.
77. Omar, N., M.A. Monem, Y. Firouz, J. Salminen, J. Smekens, O. Hegazy, H. Gaulous, G. Mulder, P. Van den Bossche, T. Coosemans, and J. Van Mierlo, *Lithium iron phosphate based battery – Assessment of the aging parameters and development of cycle life model.* Applied Energy, 2014. **113**: p. 1575-1585.
78. Liu, Y.-H., C.-H. Hsieh, and Y.-F. Luo, *Search for an Optimal Five-Step Charging Pattern for Li-Ion Batteries Using Consecutive Orthogonal Arrays.* IEEE Trans. Energy Convers. 26 (2011) 654–661.
79. Schuster, S.F., M.J. Brand, P. Berg, M. Gleissenberger, and A. Jossen, *Lithium-ion cell-to-cell variation during battery electric vehicle operation.* Journal of Power Sources, 2015. **297**: p. 242-251.
80. McTurk, E., T. Amietszajew, J. Fleming, and R. Bhagat, *Thermo-electrochemical instrumentation of cylindrical Li-ion cells.* Journal of Power Sources, 2018. **379**: p. 309-316.
81. Raccichini, R., M. Amores, and G. Hinds, *Critical Review of the Use of Reference Electrodes in Li-Ion Batteries: A Diagnostic Perspective.* Batteries, 2019. **5**(1).
82. Liu, K., T.R. Ashwin, X. Hu, M. Lucu, and W.D. Widanage, *An evaluation study of different modelling techniques for calendar ageing prediction of Lithium-ion batteries.* Renewable and Sustainable Energy Reviews, 2020.
83. Liu, Y.-H., C.-H. Hsieh, and Y.-F. Luo, *Search for an Optimal Five-Step Charging Pattern for Li-Ion Batteries Using Consecutive Orthogonal Arrays.* IEEE Transactions on Energy Conversion, 2011. **26**(2): p. 654-661.
84. Savoye, F., P. Venet, M. Millet, and J. Groot, *Impact of Periodic Current Pulses on Li-Ion Battery Performance.* IEEE Transactions on Industrial Electronics, 2012. **59**(9): p. 3481-3488.
85. Birkl, C.R., E. McTurk, M.R. Roberts, P.G. Bruce, and D.A. Howey, *A Parametric Open Circuit Voltage Model for Lithium Ion Batteries.* Journal of The Electrochemical Society, 2015. **162**(12): p. A2271-A2280.
86. HyupJeon, D., *Wettability in electrodes and its impact on the performanceof lithium-ion batteries.* Energy Storage Materials 2019. **18**: p. 139-147.
87. Smith, K. and C.-Y. Wang, *Solid-state diffusion limitations on pulse operation of a lithium ion cell for hybrid electric vehicles.* Journal of Power Sources, 2006. **161**(1): p. 628-639.
88. Ji, Y., Y. Zhang, and C.Y. Wang, *Li-Ion Cell Operation at Low Temperatures.* Journal of the Electrochemical Society, 2013. **160**(4): p. A636-A649.
89. Keil, P. and A. Jossen, *Calendar Aging of NCA Lithium-Ion Batteries Investigated by Differential Voltage Analysis and Coulomb Tracking.* Journal of The Electrochemical Society, 2016. **164**(1): p. A6066-A6074.
90. von Srbik, M.-T., M. Marinescu, R.F. Martinez-Botas, and G.J. Offer, *A physically meaningful equivalent circuit network model of a lithium-ion battery accounting for local electrochemical and thermal behaviour, variable double layer capacitance and degradation.* Journal of Power Sources, 2016. **325**: p. 171-184.
91. Bird, J., *Electrical Circuit Theory and Technology.* Routledge; 4 edition, 2010.
92. Lewerenz, M., A. Warnecke, and D.U. Sauer, *Introduction of capacity difference analysis (CDA) for analyzing lateral lithium-ion flow to determine the state of covering layer evolution.* Journal of Power Sources. **354**: p. 157-166.
93. Lewerenz, M., G. Fuchs, L. Becker, and D.U. Sauer, *Irreversible calendar aging and quantification of the reversible capacity loss caused by anode overhang.* Journal of Energy Storage, 2018. **18**: p. 149-159.

94. Lewerenz, M., J. Münnix, J. Schmalstieg, S. Käbitz, M. Knips, and D.U. Sauer, *Systematic aging of commercial LiFePO 4 |Graphite cylindrical cells including a theory explaining rise of capacity during aging.* Journal of Power Sources, 2017. **345**: p. 254-263.
95. Schmalstieg, J., S. Käbitz, M. Ecker, and D.U. Sauer, *A holistic aging model for Li(NiMnCo)O2 based 18650 lithium-ion batteries.* Journal of Power Sources, 2014. **257**: p. 325-334.
96. Troxler, Y., B. Wu, M. Marinescu, V. Yufit, Y. Patel, A.J. Marquis, N.P. Brandon, and G.J. Offer, *The effect of thermal gradients on the performance of lithium-ion batteries.* Journal of Power Sources, 2014. **247**: p. 1018-1025.
97. Lewerenz, M., P. Dechent, and D.U. Sauer, *Investigation of capacity recovery during rest period at different states-of-charge after cycle life test for prismatic Li(Ni1/3Mn1/3Co1/3)O2-graphite cells.* Journal of Energy Storage, 2019. **21**: p. 680-690.
98. Koleti, U.R., C. Zhang, R. Malik, T. Amietszajew, T.Q. Dinh, and J. Marco, *A new concept to improve the lithium plating detection sensitivity in lithium-ion batteries.* International Journal of Smart grid and Clean Energy, 2019. **Accepted for publication**.
99. Waldmann, T., M. Wilka, M. Kasper, M. Fleischhammer, and M. Wohlfahrt-Mehrens, *Temperature dependent ageing mechanisms in Lithium-ion batteries – A Post-Mortem study.* Journal of Power Sources, 2014. **262**: p. 129-135.
100. Yang, X.-G., S. Ge, T. Liu, Y. Leng, and C.-Y. Wang, *A look into the voltage plateau signal for detection and quantification oflithium plating in lithium-ion cells.* Journal of Power Sources, 2018. **395**: p. 251-261.
101. Stiaszny, B., J.C. Ziegler, E.E. Krauß, M. Zhang, J.P. Schmidt, and E. Ivers-Tiffée, *Electrochemical characterization and post-mortem analysis of aged LiMn2O4–NMC/graphite lithium ion batteries part II: Calendar aging.* Journal of Power Sources, 2014. **258**: p. 61-75.
102. Lewerenz, M., A. Warnecke, and D.U. Sauer, *Introduction of capacity difference analysis (CDA) for analyzing lateral lithium-ion flow to determine the state of covering layer evolution.* Journal of Power Sources, 2017. **354**: p. 157-166.
103. Epding, B., B. Rumberg, H. Jahnke, I. Stradtmann, and A. Kwade, *Investigation of significant capacity recovery effects due to long rest periods during high current cyclic aging tests in automotive lithium ion cells and their influence on lifetime.* Journal of Energy Storage, 2019. **22**: p. 249-256.
104. Wilhelm, J., S. Seidlmayer, P. Keil, J. Schuster, A. Kriele, R. Gilles, and A. Jossen, *Cycling capacity recovery effect: A coulombic efficiency and post-mortem study.* Journal of Power Sources, 2017. **365**: p. 327-338.
105. Han, X., M. Ouyang, L. Lu, J. Li, Y. Zheng, and Z. Li, *A comparative study of commercial lithium ion battery cycle life in electrical vehicle: Aging mechanism identification.* Journal of Power Sources, 2014. **251**: p. 38-54.
106. Mohanty, D., K. Dahlberg, D.M. King, L.A. David, A.S. Sefat, D.L. Wood, C. Daniel, S. Dhar, V. Mahajan, M. Lee, and F. Albano, *Modification of Ni-Rich FCG NMC and NCA Cathodes by Atomic Layer Deposition: Preventing Surface Phase Transitions for High-Voltage Lithium-Ion Batteries.* Sci Rep, 2016. **6**: p. 26532.
107. Kassem, M. and C. Delacourt, *Postmortem analysis of calendar-aged graphite/LiFePO4 cells.* Journal of Power Sources, 2013. **235**: p. 159-171.
108. Choi, J., M.-H. Ryou, B. Son, J. Song, J.-K. Park, K.Y. Cho, and Y.M. Lee, *Improved high-temperature performance of lithium-ion batteries through use of a thermally stable co-polyimide-based cathode binder.* Journal of Power Sources, 2014. **252**: p. 138-143.
109. Marongiu, A., N. Nlandi, Y. Rong, and D.U. Sauer, *On-board capacity estimation of lithium iron phosphate batteries by means of half-cell curves.* Journal of Power Sources, 2016. **324**: p. 158-169.
110. Singh, M., J. Kaiser, and H. Hahn, *Effect of Porosity on the Thick Electrodes for High Energy Density Lithium Ion Batteries for Stationary Applications.* Batteries, 2016. **2**(4): p. 35.

111. Waag, W., S. Käbitz, and D.U. Sauer, *Experimental investigation of the lithium-ion battery impedance characteristic at various conditions and aging states and its influence on the application.* Applied Energy, 2013. **102**: p. 885-897.
112. Barai, A., G.H. Chouchelamane, Y. Guo, A. McGordon, and P. Jennings, *A study on the impact of lithium-ion cell relaxation on electrochemical impedance spectroscopy.* Journal of Power Sources, 2015. **280**: p. 74-80.
113. Itagaki, M., K. Honda, Y. Hoshi, and I. Shitanda, *In-situ EIS to determine impedance spectra of lithium-ion rechargeable batteries during charge and discharge cycle.* Journal of Electroanalytical Chemistry, 2015. **737**: p. 78-84.
114. Kassem, M., J. Bernard, R. Revel, S. Pélissier, F. Duclaud, and C. Delacourt, *Calendar aging of a graphite/LiFePO4 cell.* Journal of Power Sources, 2012. **208**: p. 296-305.
115. Lundgren, H., P. Svens, H. Ekström, C. Tengstedt, J. Lindström, M. Behm, and G. Lindbergh, *Thermal Management of Large-Format Prismatic Lithium-Ion Battery in PHEV Application.* Journal of The Electrochemical Society, 2015. **163**(2): p. A309-A317.
116. Hariharan, K.S. and V. Senthil Kumar, *A nonlinear equivalent circuit model for lithium ion cells.* Journal of Power Sources, 2013. **222**: p. 210-217.
117. Cho, S., H. Jeong, C. Han, S. Jin, J.H. Lim, and J. Oh, *State-of-charge estimation for lithium-ion batteries under various operating conditions using an equivalent circuit model.* Computers & Chemical Engineering, 2012. **41**: p. 1-9.
118. Gordon, I.J., S. Genies, G. Si Larbi, A. Boulineau, L. Daniel, and M. Alias, *Original implementation of Electrochemical Impedance Spectroscopy (EIS) in symmetric cells: Evaluation of post-mortem protocols applied to characterize electrode materials for Li-ion batteries.* Journal of Power Sources, 2016. **307**: p. 788-795.
119. Stroe, D.-I., M. Swierczynski, A.-I. Stroe, and S. Knudsen Kær, *Generalized Characterization Methodology for Performance Modelling of Lithium-Ion Batteries.* Batteries, 2016. **2**(4): p. 37.
120. Chu, Z., X. Feng, L. Lu, J. Li, X. Han, and M. Ouyang, *Non-destructive fast charging algorithm of lithium-ion batteries based on the control-oriented electrochemical model.* Applied Energy, 2017. **204**: p. 1240-1250.
121. Mathew, M., S. Janhunen, M. Rashid, F. Long, and M. Fowler, *Comparative Analysis of Lithium-Ion Battery Resistance Estimation Techniques for Battery Management Systems.* Energies, 2018. **11**(6).
122. Vogel, J.E., M.M. Forouzan, E.E. Hardy, S.T. Crawford, D.R. Wheeler, and B.A. Mazzeo, *Electrode microstructure controls localized electronic impedance in Li-ion batteries.* Electrochimica Acta, 2019. **297**: p. 820-825.